

1 Biotransformations from and to
2 methylated flavonoids

3 Dissertation

4 zur Erlangung des Doktorgrades der
5 Naturwissenschaften
6 (Dr. rer. nat)

7 der

8 Naturwissenschaftlichen Fakultät II
9 Chemie, Physik und Mathematik

10 der Martin-Luther-Universität
11 Halle-Wittenberg

12 vorgelegt von

13 Herr Benjamin Weigel
14 geb. am 06. April 1986 in Bernburg (Saale)

15 Gutachter:

- 16 1. Prof. Dr. Ludger A. Wessjohann (Martin-Luther Universität Halle-Wittenberg)**
- 17 2. zweiter Gutachter**

18 Halle (Saale), October 29, 2015

1

It is what it is. Accept it and move on.

2

– *unknown* –

1 Contents

2	Contents	iii
3	List of Figures	vii
4	List of Tables	xiv
5	List of Schemes	xvii
6	I Preface	1
7	<hr/>	
8	1 Abstracts	2
9	1.1 English Abstract	2
10	1.2 Deutsche Zusammenfassung	3
11	2 List of Publications	5
12	II Thesis	6
13	<hr/>	
14	3 Introduction and Motivation	7
15	3.1 Flavonoids	7
16	3.1.1 Overview	7
17	3.1.2 The phenyl propanoid pathway	9
18	3.1.3 Biological activity	10
19	3.2 Methyl transferases (MTs)	11
20	3.2.1 Overview	11
21	3.2.2 S-Adenosyl-L-methionine	13
22	3.2.3 Methyl transferase mechanisms	16
23	3.2.4 Plant O-methyl transferases (O-MTs)	18

1	3.3 Alkylations and biotransformations	20
2	3.3.1 Overview	20
3	3.3.2 Methyl transferases for industrial use	21
4	3.3.3 Artificial SAM analogues.	23
5	3.4 Motivation	24
6	4 Material And Methods	26
7	4.1 Materials	26
8	4.1.1 Chemicals	26
9	4.1.2 Commonly used solutions and buffers	26
10	4.1.3 Culture media used to grow bacteria	27
11	4.1.4 Bacterial strains	28
12	4.1.5 Plasmids	29
13	4.1.6 Oligonucleotides and synthetic genes	30
14	4.1.7 Instruments	30
15	4.1.8 Software	31
16	4.2 Molecular Biology	31
17	4.2.1 Golden Gate Cloning	32
18	4.2.2 Subcloning of genes	32
19	4.2.3 Transformation of electrocompetent <i>Agrobacterium tumefaciens</i> cells.	33
20	4.3 Treatment of plant material	34
21	4.3.1 Infiltration of <i>Nicotiana benthamiana</i>	34
22	4.3.2 Plant material harvest	34
23	4.3.3 Extraction of flavonoids from <i>N. benthamiana</i> leaves	35
24	4.4 Protein biochemistry	35
25	4.4.1 Determination of protein concentration	35
26	4.4.2 Protein production test (expression test)	36
27	4.4.3 Protein subfractionation	36
28	4.4.4 Protein sample concentration by TCA precipitation	37
29	4.4.5 Preparation of periplasmic protein	38
30	4.4.6 Discontinuous SDS-polyacrylamide gel electrophoresis (SDS-PAGE)	38
31	4.4.7 Buffer change of protein samples	39
32	4.4.8 Production of recombinant protein	39
33	4.4.9 Preparation of inlusion bodies (IBs).	40
34	4.4.10 Purification of His-tagged proteins using immobilized metal affinity chromatography (IMAC)	41
35	4.4.11 Refolding of SOMT-2 on a micro scale using design of experiments (DoE)	42

1	4.4.12 Enzymatic production of SAM and SAE	44
2	4.5 Crystallographic Procedures	45
3	4.5.1 Crystallization of proteins	45
4	4.5.2 Data collection and processing	46
5	4.5.3 Structure solution.	47
6	4.5.4 Model building, refinement and validation.	47
7	4.5.5 <i>In silico</i> substrate docking	48
8	4.6 Analytics	48
9	4.6.1 Recording of growth curves	48
10	4.6.2 <i>In vitro</i> determination of glucose	49
11	4.6.3 <i>In vitro</i> O-methyl transferase (O-MT) assay	49
12	4.6.4 Photospectrometric assay for the methylation of catecholic moi- 13 ties.	52
14	4.6.5 Concentration of SOMT-2 using hydrophobic interaction chro- 15 matography (HIC)	53
16	4.6.6 Analytical gel filtration.	53
17	4.6.7 Binding experiments using Isothermal Titration Calorimetry 18 (ITC)	53
19	4.6.8 High-performance liquid chromatography (HPLC) analytics .	54
20	4.6.9 Liquid chromatography-tandem mass spectrometry (LC- 21 MS/MS) measurements.	55
22	5 Engineering of phenylpropanoid and flavonoid O-methyl trans- 23 ferase (PFOMT)	56
24	5.1 Introduction	57
25	5.2 Crystallization of PFOMT	59
26	5.3 Substrate binding studies using ITC.	63
27	5.4 Study of variants for long-chain alkylations	66
28	5.5 Conclusion/Discussion	68
29	5.6 Contributions	70
30	6 Tandem mass-spectrometry studies of flavonoids	71
31	6.1 Introduction	72
32	6.2 Fragmentation of flavanones	75
33	6.3 Fragmentation of flavones	79
34	6.4 Fragmentation of flavonols	84
35	6.5 Conclusions	89
36	6.6 Contributions	90
37	7 Enzymatic methylation of non-catechols	91
38	7.1 Introduction	92

1	7.2 SOMT-2	93
2	7.2.1 <i>In vivo</i> biotransformation in <i>Nicotiana benthamiana</i>	94
3	7.2.2 <i>In vivo</i> biotransformation in <i>E. coli</i>	96
4	7.2.3 <i>In vitro</i> studies using recombinantly produced SOMT-2	99
5	7.3 PFOMT	107
6	7.3.1 Phenolic hydroxyls	107
7	7.3.2 PFOMT pH-profiles are influenced by Mg ²⁺	109
8	7.3.3 Methylation of different chemical motifs.	113
9	7.4 Conclusion	119
10	8 Summary	121
11	9 Acknowledgements	123
12	10 Affidavit	124
13	III Appendix	125
14	<hr/>	
15	A Engineering of PFOMT	126
16	B Tandem mass-spectrometry studies of flavonoids	129
17	C Enzymatic methylation of non-catechols	133
18	C.1 SOMT expression studies.	133
19	C.2 Conversion of non-catechols by PFOMT	138
20	C.2.1 Modelling and shrinkage of catechols subset (pH profile)	138
21	C.3 Identification of products from conversion of non-catechols by PFOMT	140
22	C.3.1 <i>p</i> -Coumaric acid methylester	140
23	C.3.2 iso-Ferulic acid esters and caffeic acid dimethylether	140
24	C.3.3 3',4'-dimethyl eriodictyol.	141
25	C.3.4 3',4'-dimethyl luteolin	142
26	D Additional information	145
27	Bibliography	168
28	Acronyms	169
29	Glossary	174

1 List of Figures

2	3.1 The central feature of the flavonoids is the chromane ring. The names	
3	of the different groups of flavonoids are derived from the substitution	
4	of this moiety. From a biosynthetic point of view, flavonoids are built	
5	up from phenylpropanoid (blue) and acetate derived moieties (orange).	8
6	3.2 General pathways in the biosynthesis of flavonoids. PAL – pheny-	
7	lalanin ammonia lyase, C4H – cinnamate-4-hydroxylase, 4CL – 4-	
8	coumarate:CoA ligase, CHS – chalcone synthase, CHI – chalcone iso-	
9	merase, F3H – flavanone-3-hydroxylase, FLS – flavonol synthase, FNS	
10	– flavone synthase, IFS – isoflavone synthase.	10
11	3.3 Topology plots of the five major structural classes of methyl transferases	
12	and radical SAM methyl transferases (RSMTs) (modified and extended	
13	from Schubert <i>et al.</i> [174]). Helices are depicted as circles and β -strands	
14	as triangles. The SAM binding site is depicted as a flag. Radical SAM	
15	methyl transferases all share a common “radical SAM”-domain, which	
16	cotains the iron sulfur cluster (red checker). The individual radical	
17	SAM methyl transferase classes are differentiated according to the	
18	other domains they contain.	12
19	3.4 Reactions catalyzed by methyl transferases (MTs). Different shades of	
20	gray were used to differentiate between different groups of compounds	
21	and methyl transferases. In contrast to other methyl transferases, the	
22	group of radical SAM methyl transferases also requires additional co-	
23	factors to SAM.	14

1	3.5 Mechanism of the methyl transfer reaction catalyzed by methyl trans-	16
2	ferases. Non-radical <i>S</i> -adenosyl-L-methionine dependent methyl trans-	
3	ferases catalyze the nucleophilic transfer of a methyl group from the	
4	donor <i>S</i> -adenosyl-L-methionine to a nucleophile (Nu; e.g. O,N,C,S). A	
5	proton (H^+) is usually abstracted through a general base (B), to achieve	
6	activation of the nucleophile. The proton is later transferred to the	
7	aqueous medium. The S_N2 reaction proceeds via a single transition	
8	state, during which the methyl-carbon is sp^2 hybridized. After transfer	
9	of the methyl to the nucleophile the carbon's configuration is inverted.	
10	3.6 Bioenzymatic synthesis of chiral acetate, the precursor for the syn-	17
11	thesis of SAM carrying an assymetrical methyl, as used by Woodward	
12	<i>et al.</i> [223]. Ring hydroxyls of hexoses and pentoses are omitted for	
13	easier reading. HK – hexokinase, PGI – phosphoglucose isomerase,	
14	PFK – phosphofructokinase, ALD – aldolase, TIM –triose phosphate	
15	isomerase, G3PDH – glycerinaldehyde-3-phosphate dehydrogenase,	
16	PGM – phosphoglycerate mutase, ENO – enolase, Glu – glucose, F1,6BP	
17	– fructose-1,6-bisphosphate, 3PG – 3-phosphoglycerate, PEP – phos-	
18	phoenol pyruvate	
19	3.7 Natural products synthesized with the help of methyl trans-	22
20	ferases. <i>O</i> -methyl transferases were used for the synthesis of er-	
21	manine (1), 7- <i>O</i> -methyl-aromadendrin (2) and 3,5-dimethoxy-4'-	
22	fluorostilbene (3). <i>N</i> -MT catalyze the production of epinephrine (4)	
23	and <i>N</i> -methyltetrahydroisoquinoline (5), whereas 3-(benzoylamino)-	
24	8-methylumbelliferone (6) and furfuryl-methyl-sulfide (7) can be	
25	produced by <i>C</i> -methyl transferase (C-MT) and <i>S</i> -methyl transferase	
26	(<i>S</i> -MT)	
27	3.8 Labelling of macromolecules by using a combination of novel alkine-	24
28	derivatized <i>S</i> -adenosyl-L-methionine analogues and Cu ^I -catalyzed	
29	azide-alkyne 1,3-dipolar cycloaddition (CuAAC). Depending on the	
30	type of label used, it can be employed for detection (e.g. through	
31	fluorophores, coupled assays) or affinity purification (e.g. biotin). This	
32	technique might also be also feasable for use in activity based protein	
33	profiling (ABPP) approaches.	
34	4.1 Golden Gate cloning scheme for SOMT-2	33
35	4.2 Pruned <i>N. benthamiana</i> plant, with two bottom and one top leaf, ready	35
36	to be infiltrated.	

1	4.3 Oxidation of the reporter substrate <i>o</i> -dianisidine. Consecutive		
2	one-electron transfers lead to the fully oxidized diimine form of		
3	<i>o</i> -dianisidine. The first electron transfer is believed to produce a charge		
4	transfer complex intermediate. [31, 91]	50	
5	5.1 Some crystal and pseudo-crystal shapes that were observed during the		
6	crytsallization screen. a – high $(\text{NH}_4)_2\text{SO}_4$, b-c – CaCl_2 , PEG-4000, e –		
7	LiCl , PEG-6000	60	
8	5.2 An overview of the features in the <i>apo</i> -PFOMT structure. a – The assy-		
9	metric unit of <i>apo</i> -PFOMT consists of two homodimers (4 monomers).		
10	Individual monomers are rainbow colored from N- (blue) to C-terminus		
11	(red). b – Comparison of 3C3Y (steelblue) and <i>apo</i> -PFOMT (green). The		
12	N-terminus of <i>apo</i> -PFOMT was resolved up to the N-terminus (red) and		
13	even the His-tag (red, transparent) was partly resolved. The N-terminus		
14	fits into a cleft on the surface of the 3C3Y structure, shown as a sur-		
15	face model on the right. SAH (white ball-and-sticks) and Ca^{2+} (green		
16	sphere) are featured in the published structure, whereas a sulphate ion		
17	(red/yellow spheres) was bound in the newly solved structure.	62	
18	5.3 Positional differences between the individual residues of the solved <i>apo</i> -		
19	PFOMT and the structure with bound SAH (pdb: 3C3Y). The diffraction		
20	precision indicator [46] (DPI) of the structures was (0.137 and 0.064) Å		
21	respectively. The overall rmsd amounted to 0.9034 Å. The secondary		
22	structure of apo-PFOMT is displayed at the top. Helices are displayed		
23	as rectangles and sheets are shown as arrows. Graphical background		
24	annotations are used to display the binding sites of SAH (green) and		
25	the metal ion (plum). The orange bars indicate regions, where much		
26	movement seems to happen upon binding or release of the co-substrate.		
27	The blue bar shows the region that was annotated as "insertion loop"		
28	in previous studies [109].	63	
29	5.4 The binding of different SAM analogues was measured via ITC.	64	
30	5.5 ITC measurements of PFOMT:effector binding. a – Binding of SAH,		
31	SAM and SAE to PFOMT. b – SAH is injected into a PFOMT solution,		
32	with (red) or without (black) addition of Mg^{2+} and caffeic acid. When		
33	Mg^{2+} and caffeic acid were already present, the binding process seems		
34	to happen quicker, but is less enthalpic. c – Upon addition of caffeic		
35	acid to the protein heat is produced, however no sensible binding curve		
36	could be obtained.	65	

1	5.6 The active site of PFOMT (pdb: 3C3Y). The outline of the protein 2 backbone is displayed, with active site residues portrayed as colored 3 sticks (cyan – F103, red – F80, turquoise – M52, yellow – Y51, white – 4 F198, blue – W184, orange – N202, grey – as labelled). The co-substrate 5 SAM (ball-and-stick model) was docked into the structure.	67
6	5.7 Activities of different PFOMT variants towards caffeic acid methylation. 7 Colorations correspond to the ones used in Figure 5.6.	68
8	5.8 Comparison of the active sites of a – the solved <i>apo</i> -structure (green) 9 and b – the ligand-bound structure (steelblue; pdb: 3C3Y). Waters are 10 represented as small red spheres, calcium as a green sphere (complexing 11 bonds are dashed) and SAH is displayed as a white ball-and-stick model. 12 A possible hydrogen bond network (blue lines) for the ligand-bound 13 state is displayed.	69
14	6.1 Comparison of CID and HCD MS ² spectra of eriodictyol (2). A – CID at 15 45 % NCE. B – HCD at 75 % NCE. C – HCD at 100 % NCE. Four different 16 prominent peaks are annotated in each spectrum. D – The shift to 17 smaller masses in HCD spectra and with increasing NCE is illustrated 18 by the boxplot of the distribution of peaks with relative intensities 19 above 1 % in each of the above spectra. E – Relationship between 20 the activation method and the intensity of four fragments (\bullet ^{1,3} A ⁺ , 21 \blacktriangle ^(1,4) B ⁺ -2H), \blacksquare ^(1,4) B ⁺ -2H-CO), + C ₇ H ₅ ⁺) of different flavanones. .	78
22	6.2 Comparison of CID and HCD MS ² spectra of chrysoeriol (10). A – 23 CID at 45 % NCE. B – HCD at 75 % NCE. C – HCD at 100 % NCE. Four different 24 prominent peaks are annotated in each spectrum. D – The shift to smaller masses in HCD spectra and with increasing NCE is 25 illustrated by the boxplot of the distribution of peaks with relative 26 intensities above 1 % in each of the above spectra.	81
27	6.3 Comparison of CID and HCD MS ² spectra of isorhamnetin (15). A – 28 CID at 45 % NCE. B – HCD at 75 % NCE. C – HCD at 100 % NCE. 29 Four different prominent peaks are annotated in each spectrum. D – 30 The shift to smaller masses in HCD spectra and with increasing NCE is 31 illustrated by the boxplot of the distribution of peaks with relative 32 intensities above 1 % in each of the above spectra.	87

1	7.8 CD-spectrum of refolded SOMT-2 (black) compared to the spectrum	
2	that was calculated (red) by the K2D3 web service (http://cbdm-01.zdv.uni-mainz.de/~andrade/k2d3//index.html) from the SOMT-2 sequence.	
3	Secondary structure estimates from the measured spectrum are 12.39 %	
4	α -helix and 32.51 % β -sheet.	106
5		
6	7.9 Specific activity/pH-profiles for the conversion of three different sub-	
7	strates (● caffeoic acid, ▲ eriodictyol, ■ iso-ferulic acid) by PFOMT.	
8	The specific activity for the non-catecholic substrate iso-ferulic acid	
9	was much lower than the specific activity for the catecholic substrates.	
10	When magnesium is omitted, the activity is increased by increasing the	
11	pH	109
12	7.10 pH-profiles of substrate conversion along with predicted data. Predicted	
13	data from the linear regression models (blue, dashed lines) grasp the	
14	general trend of the data reasonably well to draw inferences. 95 %	
15	prediction intervals are displayed as shaded areas.	113
16	7.11 Conversion of multiple different substrates, catecholic and non-	
17	catecholic, by PFOMT wild-type (a) and the 4'-specific variant Y51R	
18	N202W (b). Every individual box represents one substrate <i>p</i> -coumaric	
19	acid (A.1), . . . , chrysoeriol (C.4). pH/Mg ²⁺ -conditions are color coded	
20	from light to dark: ✘/✗, ✘/✓, ↗/✗, ↗/✓. — ✘(low pH), ↗(high pH), ✗(no	
21	Mg ²⁺), ✓(yes, Mg ²⁺)	116
22	A.1 Differences in the dihedrals ψ (red) and φ (black) of the solved <i>apo</i> -	
23	PFOMT and the structure with bound SAH (pdb: 3C3Y). The secondary	
24	structure is displayed at the top. Helices are displayed as rectangles	
25	and sheets are shown as arrows. Graphical background annotations	
26	are used to display the binding sites of SAH (green) and the metal ion	
27	(plum). The orange bars indicate regions, where much movement seems	
28	to happen upon binding or release of the co-substrate. The blue bar	
29	shows the region that was annotated as "insertion loop" in previous	
30	studies.	127
31	A.2 Differences in the regioselectivity of some PFOMT variants. The prod-	
32	ucts observed in HPLC and LC/MS measurements switched from 3'-	
33	methylated (dark grey) to 4'-methylated (light grey) for the displayed	
34	variants. The height of the bars corresponds to the total conversion of	
35	substrate.	128

1	C.1 Additional scatterplots of the PCA of HPLC data obtained from 2 <i>N. benthamiana</i> leaves infiltrated by <i>A. tumefaciens</i> harbouring differ- 3 ent constructs. A – samples colored by leaf position (top: red; bottom: 4 cyan), B – samples colored by plant (plant 1: red; plant 2: green; plant 5 3: blue)	133
6	C.2 Growth curve of <i>E. coli</i> BL21(DE3) expressing soy O-methyl transferase 7 (SOMT-2) at 37 °C. Glucose is depleted about 5 hours into growth, at 8 which point the start of SOMT-2 expression is expected. The OD ₆₀₀ 9 after inoculation was about 0.1.	134
10	C.3 SDS-PAGE gel of samples acquired during growth curve measurements. 11 The arrow indicates the band that could correspond to the GST-tagged 12 SOMT-2 protein.	135
13	C.4 Graphical representation of a SOMT-2 model obtained from the 14 PHYRE2 web portal (http://www.sbg.bio.ic.ac.uk/phyre2/html/page.cgi?id=index) [98]. Cysteines are shown as sticks. The distance be- 15 tween neighboring cysteines that could be oxidized to disulfide bridges 16 is shown in orange.	136
18	C.5 Chromatogram of the gel filtration analysis of refolded SOMT-2 (blue). 19 Gel-filtrations standards (red) were used to assess the size of the SOMT- 20 2 protein. The estimated molecular weights for the eluting peaks were 21 165 kDa (12.47 ml) and 65.5 kDa (14.26 ml). Protein standard: 9.15 ml 22 – thyroglobulin (670 kDa), 12.62 ml – γ-globulin (158 kDa), 15.43 ml – 23 ovalbumin (44 kDa), 17.63 ml – myoglobin (17 kDa), 21.11 ml – vitamin 24 B12 (1.35 kDa)	137
25	C.6 MS ² spectra of (1) and (3). (a) negative mode MS ² of (1). (b) positive 26 mode MS ² of (1). (c) positive mode MS ² of (3).	141
27	C.7 MS ² spectra of 3'4'-dimethyl eriodictyol (4). (a) positive mode MS ² CID 28 spectrum of (4). (b) positive mode MS ² HCD spectrum of (4).	142
29	C.8 MS ² spectra of 3'4'-dimethyl luteolin (5). (a) positive mode MS ² CID 30 spectrum of (5). (b) positive mode MS ² HCD spectrum of (5).	143
31	C.9 Product composition after conversion of flavones with PFOMT. Bar 32 chart of the peak heights of the unidentified (black) and (3' or 4')- 33 O-methylated products (gray) in the selected ion chromatograms (HCD 34 at 100 % NCE). The conversion experiments were conducted with the 35 wild-type PFOMT at pH 8.6 with 10 mM Mg ²⁺ added.	144

1 List of Tables

2	3.1 Defining motifs of plant O-MTs as described by Joshi <i>et al.</i> [92].	19
3	4.1 Natural deep eutectic solvent (NADES)-mixtures used within this work.	27
4	4.2 Plasmids used in this work.	29
5	4.3 Primers used in this work. Recognition sites for endonucleases are 6 underlined. Positions used for site directed mutagenesis are in lower 7 case font.	30
8	4.4 Calculated extinction coefficients of proteins used in this work..	36
9	4.5 Factors and their high and low levels (+/-) used in the construction of 10 the fractional factorial design (FrFD).	42
11	4.6 Experimental design matrix for the FrFD.	43
12	5.1 Results of fitting a simple one-site binding model to the data obtained 13 from ITC experiments.	66
14	7.1 Naringenin and 4'-methylated derivatives that were inquired for in 15 the plant samples via HPLC. The core structure of the compounds is 16 displayed on the left.	95
17	7.2 <i>In vivo</i> biotransformation of different flavonoids, phenylpropanoids and 18 anthraquinones by SOMT-2 in <i>E. coli</i> . Conversion ratios were calculated 19 for samples taken after 30 hours. Multiple substrates containing a 4'- 20 hydroxyl were methylated. Calculation of conversion percentages are 21 only rough estimates, because of the nature of crude medium extracts. 22 Products were determined by LC-MS/MS.	97

1	7.3 pK _a -values of phenolic hydroxyl groups exemplified by <i>p</i> -cresole	
2	derivatives. Substituent positions on the aromatic ring are arbitrary	
3	and do not reflect conventions of the International Union of Pure and	
4	Applied Chemistry (IUPAC)	108
5	7.4 Maximum specific activity for the conversion of three different sub-	
6	strates with and without addition of magnesium. The pH at which the	
7	maximal activity was reached is indicated by the column titled "pH".	110
8	7.5 Coefficients of the model (Equation 7.1) for activity of <i>iso</i> -ferulic acid	
9	methylation. The factor Mg is a categorical variable (addition/no addi-	
10	tion) and can therefore only be 0 or 1.	112
11	7.6 Substrate grid that was tested for methylation with PFOMT. Four dif-	
12	ferent groups of compounds were screened. The groups of flavones,	
13	flavanones and cinnamic acids each contained one representative of	
14	each motif, phenolic, catecholic, 3'-hydroxy-4'-methoxy (3O4M) and	
15	4'-hydroxy-3'-methoxy (4O3M).	114
16	7.7 Conversion of substrates after 16 hours incubation. Only the maximum	
17	conversion is displayed, along with the conditions it was achieved	
18	under.	117
19	7.8 Products of the enzymatic methylation of the studied substrates. The	
20	products were confirmed by authentic standards or via LCMS.	118
21	A.1 Crystallographic data, phasing and refinement statistics.	126
22	B.1 Key ions in the positive mode CID and HCD ESI-MS ² spectra of fla-	
23	vanones.	130
24	B.2 Key ions in the positive mode CID and HCD ESI-MS ² spectra of flavones.	131
25	B.3 Key ions in the positive mode CID and HCD ESI-MS ² spectra of	
26	flavonoles.	132
27	C.1 Results for the ANOVA of the main effects model describing soluble	
28	protein obtained after refolding.	135
29	C.2 Results for the ANOVA of the main effects model describing protein	
30	activity after refolding.	136

1	C.3 Coefficients of the model (C.1) for activity of catechol methylation by 2 PFOMT. The factor Mg is a categorical variable (addition/no addition) 3 and can therefore only be 0 or 1.	138
4	C.4 Coefficients obtained for linear regression model using the catechols 5 subset after shrinkage using the Lasso method and 5-fold cross valida- 6 tion. Only non-zero coefficients (variables actually do have an effect) 7 are retained during the Lasso. Seed was set to 1336.	139
8	D.2 SAM analogues that have been used with MTs. Targets: P – pep- 9 tide/protein, D – DNA, R – RNA, S – small molecule.	145
10	D.1 Overview over the constructs produced for the present thesis. Each step 11 during the production of the construct is given in the workflow steps 12 column. Primers (italic font) or restriction sites used during each step 13 are displayed in parenthesis.	148

¹ List of Schemes

2	6.1 Ion fragment nomenclature of flavonoid aglycones as proposed by Ma 3 <i>et al.</i> , illustrated on naringenin. Ions are labelled according to the ring 4 they contain and the positions of the C ring that were broken. Thus 5 $^{1,3}\text{A}^+$, contains the ring A and bonds 1 and 3 of the C ring were broken.	74
6	6.2 Major fragmentation pathways of flavanones. Activation using CID 7 conditions at 45 % NCE mainly results in neutral losses of H_2O and 8 ketene ($\text{C}_2\text{H}_2\text{O}$) from the molecular ion $[\text{M}+\text{H}]^+$ (bold frame). These 9 neutral losses are scarcely observed when HCD with a NCE of 75 % or 10 100 % is used for activation. Here, C-ring cleavages followed by neutral 11 losses from the cleavage fragments are dominant.	76
12	6.3 Proposed MS^2 fragmentation of $^{1,3}\text{A}^+$ after HCD activation. In high 13 energy MS^2 experiments, $^{1,3}\text{A}^+$ might lose two CO followed by an 14 unusual C_2H_4 . A single loss of ketene ($\text{C}_2\text{H}_2\text{O}$) to afford m/z 111 is also 15 sensible.	77
16	6.4 Major fragmentation pathways of non-methylated and methylated 17 flavones. Multiple neutral losses of small molecules (e.g. CO, water 18 or ketene) and 0/4 and 1/3 C ring cleavages are predominant in the 19 MS^2 spectra of non-methylated flavones. Methylated flavones loose a 20 methyl group in CID experiments, but only in HCD experiments do 21 other fragmentation reaction become obvious.	80
22	6.5 Stability of the $[\text{M}+\text{H}-\text{CH}_3]^+$ ion of flavones. The $[\text{M}+\text{H}-\text{CH}_3]^+$ ion of 23 methylated flavones like diosmetin is highly stabilized by resonance, 24 explaining the high intensity of the corresponding peak and limiting 25 its fragmentation at low activation energies.	82

1	6.6 Proposed pathway of fragmentation of (10) after HCD activation. Losses		
2	of CH ₃ [·] and CH ₄ , followed by loss of CO are the major fragmentations		
3	observed in the corresponding MS spectra. However, multiple losses of		
4	CO only occur after a loss of methane (CH ₄), possibly due to the relative		
5	stability of the benzochromenylium radical cation (iii). At 100 % NCE		
6	even higher order fragmentations were observed.		83
7	6.7 Major fragmentation pathways of flavonoles. Unlike flavones, methylated		
8	and non-methylated flavonoles share common fragmentations,		
9	albeit signals corresponding to small molecule losses are typically small		
10	for methylated analogues. Ring fragments observed typically corre-		
11	spond to the cleavage along bonds 0/3 or 0/2. Methylated flavonols		
12	shared common fragments with the methylated flavones. However, loss		
13	of methanol and a couple CO was also observed. n/o – not observed		
14	(relative intensity <1 %).		85
15	6.8 Proposed pathways of fragmentation of isorhamnetin (15). Isorham-		
16	netin might loose methyl, methane or methanol upon activation. A sim-		
17	ilar fragmnetation pathway was proposed for the analogous chrysoe-		
18	riol (Scheme 6.6). Some fragmentations were observed in HCD mode		
19	only (box).		88



1

2

Preface

1 Abstracts

1.1 English Abstract

The present study outlines the useability of two plant *O*-methyl transferases (*O*-MTs), phenylpropanoid and flavonoid *O*-methyl transferase (PFOMT) and soy *O*-methyl transferase (SOMT-2), of classes I and II for the biocatalytic methylation of common structural motifs encountered throughout the group of plant polyphenolic compounds. Class I plant *O*-MTs, such as PFOMT, are magnesium-dependent caffeoyl CoA dependent *O*-methyltransferase (CCoAOMT)-like enzymes comprising 200 to 280 amino acids, generally with a limited substrate scope. Class II plant *O*-MTs (i.e. SOMT-2) are metal-ion independent, 340 to 390 amino acids in length and generally more promiscuous than class I representatives.

Biophysical characterization of PFOMT using Isothermal Titration Calorimetry demonstrated its ability to bind the biosynthetically obtained *S*-adenosyl-L-methionine analogue *S*-adenosyl-L-ethionine (SAE). However, although numerous variants were characterized, conversion of SAE by PFOMT was not observed. Nonetheless, a novel crystal structure of the *apo*-form of PFOMT obtained during the present study gives new insights into the movements and domains involved in substrate binding.

A systematic grid of 15 flavonoids (i.e. flavanones, flavones and flavonoles) with different substitutions at the B-ring was characterized by tandem mass-spectrometry (MS/MS) studies in positive mode. Thereby, the fragmentation patterns produced by activation via collision induced dissociation (CID) and higher-energy collisional dissociation (HCD) were compared. Fragmentation, especially the appearance of characteristic C-ring cleavage fragments such as $^{1,3}\text{A}^+$, of methyl-

lated members of flavones and flavonoles was easily achieved in HCD experiments. The results obtained demonstrate the complementary nature of both activation methods and the importance of HCD spectra for the identification of methylated flavones and flavonols.

In vivo studies using SOMT-2 showed its capability to methylate flavonoids and stilbenes at the 4'-position. Design of experiments and fractional factorial design were used successfully to optimize *in vitro* refolding conditions for SOMT-2. However, sufficiently active enzyme could not be obtained. Moreover, using PFOMT it was demonstrated, that the activity of this class I plant *O*-MT could be modulated by high a pH and magnesium concentration to achieve previously unobserved methylations of non-catecholic moieties such as 3'-hydroxy-4'-methoxy and 4'-hydroxy-3'-methoxy. This resulted in the production of e.g. 3',4'-dimethyl eriodictyol and 3',4'-dimethyl luteolin by PFOMT from hesperetin and diosmetin respectively. The knowledge obtained from the MS/MS studies was crucial in identifying these products.

1.2 Deutsche Zusammenfassung

Die vorliegende Arbeit umreißt die Verwertbarkeit zweier pflanzlicher *O*-Methyltransferasen (*O*-MTs), PFOMT und SOMT-2, der Klassen I and II für die biokatalytische Methylierung in polyphenolischen Verbindungen verbreiteter Strukturmotive. Klasse I Planzen *O*-MTs, wie PFOMT, sind magnesiumabhängige Kaffeoyl CoA-abhängige *O*-Methyltransferase (CCoAOMT)-ähnliche Enzyme von 200 bis 280 Aminosäuren und einem gemeinhin limitierten Substratumsfang. Vertreter der Klasse II (d.h. SOMT-2) sind metallionen-unabhängig, 340 bis 390 Aminosäuren lang und im Allgemeinen promiskuitiver im Substratspektrum denn Vertreter der Klasse I.

Die biophysikalische Charakterisierung der PFOMT mittels isothermaler Titrationskalorimetrie zeigte die Bindung von *S*-Adenosyl-L-ethionin (SAE), ein biosynthetisch gewonnenes *S*-Adenosyl-L-methionin-Derivat, an das Enzym. Eine Umsetzung von SAE durch PFOMT konnte jedoch nicht gezeigt werden, obgleich mehrere Enzymvarianten untersucht wurden. Nichtsdestotrotz wurde eine neue Kristall-

1 struktur des *apo*-Enzyms gelöst, welche neuerliche Einblicke in die Bewegungen
2 innerhalb des Enzyms und an der Substratbindung involvierter Domänen liefert.
3 Fünfzehn Flavonoide (d.h. Flavanone, Flavone und Flavonole) mit un-
4 terschiedlichen Substitutionsmustern am B-Ring wurden mittels Tandem-
5 Massenspektrometrie (MS/MS) im positiven Modus charakterisiert. Dabei wurden
6 zwei Aktivierungsmethoden, *collision induced dissociation* (HCD) und *higher-energy*
7 *collisional dissociation* (CID), verglichen. HCD erleichterte die Fragmentierung,
8 besonders das Erscheinen durch C-Ring-Spaltung enstandener Fragmente (z.B.
9 $^{1,3}\text{A}^+$), methylierter Vertreter von Flavonen und Flavolonen. Die erhaltenen
10 Ergebnisse demonstrieren die Komplementarität beider Aktivierungsmethoden
11 und die Bedeutung von HCD-Spektren für die Identifizierung methylierter Flavone
12 und Flavonole.

13 *In vivo* Studien der SOMT-2 zeigten die Methylierung von Flavonoiden und
14 Stilbenen an der 4'-Position. Statistische Versuchplanung und ein Teilstudioplan
15 wurden erfolgreich verwendet, um die Rückfaltungsausbeuten der *in vitro* Rück-
16 faltung der SOMT-2 zu optimieren. Jedoch konnten nur ungenügende Mengen
17 an aktivem Protein erhalten werden. Es wurde weiterhin gezeigt, dass die Aktiv-
18 ität der PFOMT durch Variation von pH und Magnesium so weit moduliert wer-
19 den konnte vorher unbeschriebene Methylierungen von 3'-Hydroxy-4'-methoxy
20 und 4'-Hydroxy-3'-methoxy-Motiven zu erreichen. So konnten unter anderem
21 3',4'-Dimethyleriodictyol und 3',4'-Dimethyluteolin durch Umsetzung von Hes-
22 peritin und Diosmetin mittels PFOMT produziert werden. Für die Identifizierung
23 der genannten Produkte wurde unter anderem auf das in den MS/MS-Studien
24 gewonnene Wissen zurückgegriffen.

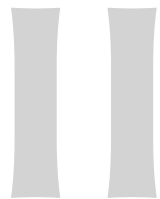
1 2 List of Publications

2 Part of this work have been published:

- 3 1.** Wessjohann, L. A., Keim, J., Weigel, B., & Dippe, M. (2013). Alkylating enzymes.
4 Current Opinion in Chemical Biology, 17(2), 229–235. *http://doi.org/10.1016/j.cbpa.2013.02.016*
- 5 2.** Dippe, M., Weigel, B., Heinke, R., Vogt, T., & Wessjohann, L. A. (2015). Engineering of a Mg²⁺-dependent O-methyltransferase towards novel regiospecificity.
6Manuscript to be submitted.
7
- 8**

9 Publications that are not part of this work:

- 10 1.** Landgraf, R., Smolka, U., Altmann, S., Eschen-Lippold, L., Senning, M., Sonnewald, S., Weigel, B., ... Rosahl, S. (2014). The ABC Transporter ABCG1 Is Required for Suberin Formation in Potato Tuber Periderm. *The Plant Cell*, **13**(August), 3403–3415. *http://doi.org/10.1105/tpc.114.124776*



1

2

Thesis

3 Introduction and Motivation

Secondary metabolites comprise a vast collection of organic compounds produced in nature, that do not directly parttake in the growth and development of an organism. Many functions of these natural products are unknown and remain to be elucidated, but it has been shown that they can be used for gene regulation, defense against biotic and abiotic stresses, (pollinator) attractant, communication and others. Natural compounds can be quite complex and show remarkable biological activities. The major classes of secondary compounds are terpenoids, alkaloids, phenylpropanoids including lignans/lignins, flavonoids and polyketides. This work is largely concerned about phenyl propanoids and flavonoids, as well as their modification, and will therefore mainly focus on these compounds.

3.1 Flavonoids

3.1.1 Overview

Plant phenolic compounds account for more than 40 % of the organic carbon in the biosphere and are essential for the survival of vascular plants. They are largely derived from the *phenylpropanoid* and relating pathways and take on various structural (e.g. cell walls) and non-structural roles (e.g. plant defense, flower color) [39]. The name *phenylpropanoid* describes the aromatic phenyl connected to a three-carbon chain, which biosynthetically originates from phenylalanine. Flavonoids, from the Latin *flavus* (yellow), are a diverse subclass of these phenolic compounds comprising more than 4500 different compounds described thus far and their main structural feature is the central chromane (benzodihydropyran) moiety (Figure 3.1).

- 1 They consist of three rings named A, B and C. Ring A and B are of acetate and
- 2 phenylpropanoid origin respectively, whereas ring C is a result of the condensation of the former. Different types of flavonoids are named depending on the substitution

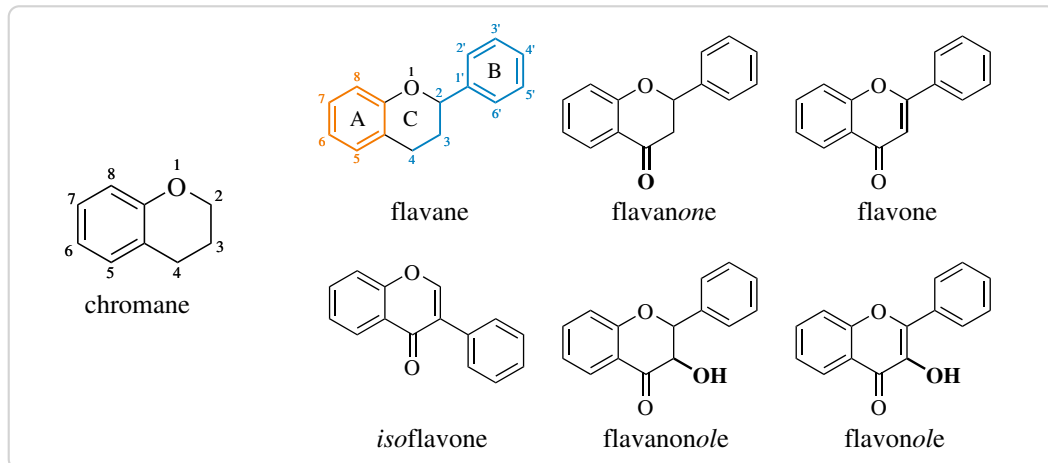


Figure 3.1.: The central feature of the flavonoids is the chromane ring. The names of the different groups of flavonoids are derived from the substitution of this moiety. From a biosynthetic point of view, flavonoids are built up from phenylpropanoid (blue) and acetate derived moieties (orange).

3 pattern of the chromane ring (Figure 3.1). For example, a phenyl group at C-2 or C-3
 4 gives flavonoids or isoflavonoids respectively, an unsubstituted C-4 means flavane,
 5 whereas a carbonyl group at C-4 indicates flavanones *et cetera*. Flavonoids are
 6 usually poly-hydroxylated, but can also carry multiple other different substitutions.
 7 *O*-methylations are common at all hydroxyl positions, but flavonoids can also be
 8 *C*-methylated [10]. Other common derivatizations are (*O* or *C*)-prenylation, (*O* or
 9 *C*)-glycosylation, methylene-dioxy bridges (C-3'/C-4' or C-6/C-7) and various (*O*
 10 or *C*)-acylations (aliphatic and aromatic acids) [42, 76, 183, 221].

11 In plants flavonoids are usually produced to combat biotic or abiotic stresses.
 12 They can absorb highly energetic ultra violet (UV) light, suppress the formation
 13 of, or scavenge reactive oxygen species (ROS) [2]. Furthermore, flavonoids can act
 14 as regulators during plant development [191]. A growing interest in flavonoids
 15 for the use in medicinal and nutritional applications has been spiked by their
 16 beneficial effects on health. Flavonoids possess a high antioxidant activity and
 17 also show protective effects against age-related ailments, such as cardiovascular

1 diseases and cancers. Furthermore, they show anti-inflammatory, hepatoprotective,
2 antimicrobial and antiviral activities [111].

3 A number of flavonoids are produced by the valorization of wastes and by-
4 products of the food industry. Citrus and olive processing byproducts are especially
5 rich in polyphenols [72, 151, 155]. However, many flavonoids are scarce in nature
6 and/or the production from by-products is not enough to saturate the market
7 demand, thus requiring different approaches for production. Recent developments
8 in the field of metabolic engineering allowed for the high-level production of many
9 flavonoids in microbial hosts, such as *Escherichia coli* or *Saccharomyces cerevisiae*
10 [198, 211]. For example, eriodictyol was produced from tyrosine in metabolically
11 engineered *E. coli* at levels of up to 107 mg/ml [234], whereas naringenin was
12 produced in *S. cerevisiae* from glucose at levels of 109 mg/ml [108].

13 3.1.2 The phenyl propanoid pathway

14 Biosynthesis of flavonoids via the phenylpropanoid pathway starts from phenyl-
15 lalanine, which is non-oxidatively deaminated by phenylalanine ammonia-lyase
16 (PAL) to yield cinnamic acid (Figure 3.2) [74, 125]. Cinnamate-4-hydroxylase (C4H),
17 a P450 monooxygenase, hydroxylates the cinnamic acid at the *para*-position and
18 4-coumarate:CoA ligase (4CL) converts the *p*-coumaric acid to its corresponding
19 coenzyme A (CoA)-ester [80, 201]. Chalcone synthase (CHS) uses 3 molecules of
20 malonyl-CoA (produced from acetyl-CoA by acetyl-CoA carboxylase) to produce
21 naringenin chalcone from *p*-coumaryl-CoA [59]. Next, the linear chalcone can
22 cyclize spontaneously or catalyzed by a chalcone isomerase (CHI) via a MICHAEL-
23 type addition to afford the flavanone naringenin [88]. Naringenin can serve as
24 substrate for numerous enzymes such as flavanone-3-hydroxylase (F3H), flavone
25 synthase (FNS) or isoflavone synthase (IFS) to afford dihydroflavonols, flavones or
26 2-hydroxyisoflavones respectively [69]. Dihydroflavonols are again precursors for
27 the biosynthesis flavonols, flavanols and anthocyanidines.

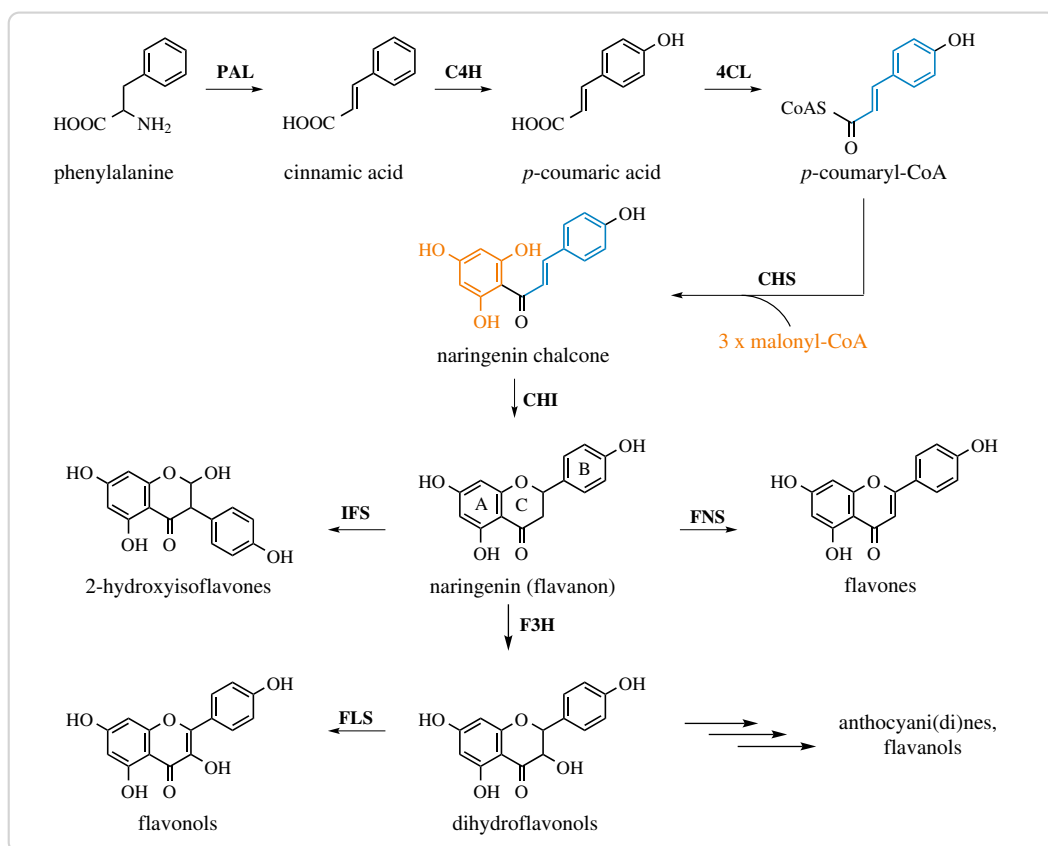


Figure 3.2.: General pathways in the biosynthesis of flavonoids. PAL – phenylalanine ammonia lyase, C4H – cinnamate-4-hydroxylase, 4CL – 4-coumarate:CoA ligase, CHS – chalcone synthase, CHI – chalcone isomerase, F3H – flavanone-3-hydroxylase, FLS – flavonol synthase, FNS – flavone synthase, IFS – isoflavone synthase.

1 3.1.3 Biological activity

- 2 Flavonoids possess many properties associated with a healthy diet. They act as
 3 antioxidants and can help reduce oxidative stress. Several mechanisms that might
 4 be involved in the antioxidant activity of flavonoids are currently discussed. They
 5 can act as scavengers for free ROS or mask metal ions by chelation to suppress the
 6 production of radicals [27, 119]. The substitution pattern plays an important role in
 7 the antioxidant activity. Generally, the more free hydroxyls are present, the stronger
 8 the antioxidant activity of the flavonoid [27]. Hydroxyls can donate an electron, or
 9 a hydrogen atom to free ROS to inactive such molecules. The resulting flavonoid

1 radicals are stabilized by resonance, however possess prooxidant properties [144].
2 Numerous flavonoids possess antimicrobial activities [40]. For example, cate-
3 chins from green and black teas have been shown to be effective against *Bacillus*
4 *cereus* at nanomolar concentrations [64]. The mechanisms of action for the antimicro-
5 bial activity can be the inactivation of enzymes, binding of adhesins, membrane
6 disruption or cell wall complexation [36].

7 **3.2 Methyl transferases (MTs)**

8 **3.2.1 Overview**

9 S-adenosyl-L-methionine (SAM)-dependent methyl transferases (MTs) (EC 2.1.1.x)
10 transfer the methyl group of SAM to an activated atom of an acceptor molecule, via
11 an S_N2 displacement mechanism. SAM is converted to S-adenosyl-L-homocysteine
12 (SAH), the co-product of the reaction, in the process. There are currently over
13 300 manually annotated MTs, each catalyzing a different reaction, included in the
14 UniProtKB/Swiss-Prot database (<http://www.uniprot.org>). Transfer of the methyl
15 group to oxygen and nitrogen atoms is most common, but carbon, sulfur, selenium,
16 arsenic atoms and even halide ions can be methylated too (Figure 3.4) [171, 193].
17 Acceptor molecules are diverse and range from relatively small natural products (e.g.
18 flavonoids) to bio-macromolecules such as nucleic acids or proteins. In fact, MTs
19 are key-tailoring enzymes for many natural products of all groups (e.g. flavonoids,
20 alkaloids or non-ribosomal peptides) [100, 109, 188, 211]. These small molecule
21 methyl transferases (smMTs) account for a significant part of the diversity present
22 in natural products.

23 Other MTs, such as protein methyl transferases (P-MTs), DNA methyl trans-
24 ferases (DNA-MTs) and RNA methyl transferases (RNA-MTs) methylate proteins
25 and nucleic acids respectively. In eukaryotes, DNA-MTs and P-MTs play important
26 roles in the epigenetic regulation of gene expression and have been associated with
27 a number of cancers and other diseases [34, 162, 163]. In bacteria, DNA-MTs are an
28 essential part of the restriction modification system [140].

According to their structure, MTs can be classified into five main groups (I–V) (Figure 3.3)[174]. Class I MTs are the largest group of MTs and are characterized by a central Rossmann-like $\alpha\beta\alpha$ sandwich, consisting of a seven-stranded β -sheet flanked by α -helices. Most smMTs, DNA-MTs and some P-MTs belong to class I. Even though some of the enzymes belonging to class I share as little as 10 % sequence similarity, there is a pronounced structural conservation [174]. Class II MTs comprise a long anti-parallel β -sheet encompassed by numerous α -helices [50]. In class III MTs the SAM binding site is located between two $\alpha\beta\alpha$ domains [173]. A knot structure at the C-terminus contributes to SAM binding in the *SpoU*-TrmD (SPOUT) family of class IV RNA-MTs [145]. Protein lysine MTs make up the largest part of P-MTs and structurally belong to class V MTs containing a suvar3-9, enhancer-of-zeste, trithorax (SET) domain [224]. Interestingly, a recent study of the

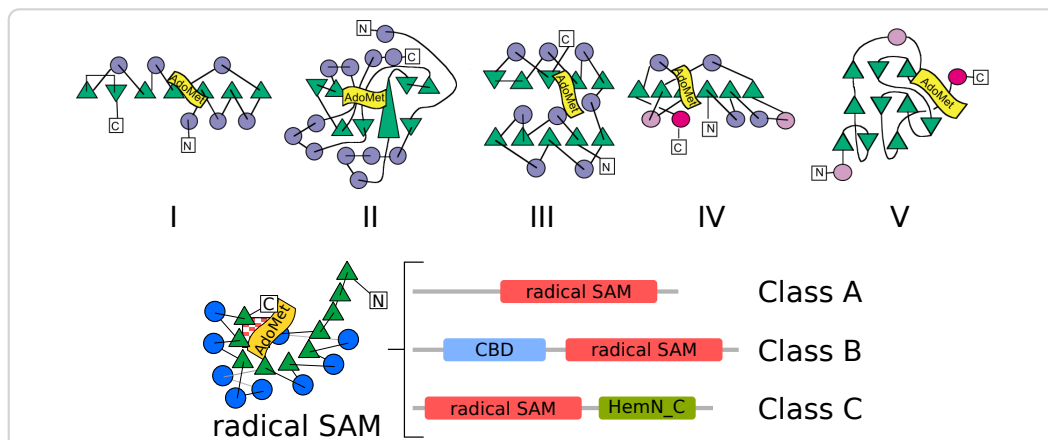


Figure 3.3.: Topology plots of the five major structural classes of methyl transferases and radical SAM methyl transferases (RSMTs) (modified and extended from Schubert *et al.* [174]). Helices are depicted as circles and β -strands as triangles. The SAM binding site is depicted as a flag. Radical SAM methyl transferases all share a common “radical SAM”-domain, which contains the iron sulfur cluster (red checker). The individual radical SAM methyl transferase classes are differentiated according to the other domains they contain.

methyltransferome of baker’s yeast (*S. cerevisiae*) argues, that there are four more classes of MTs [218]. Opposite to the studies by Schubert *et al.*, this work mainly relied on bioinformatical methods for structural information. 83 out of 86 MT structures in total were homology-modelled. It was shown, that two thirds of the

1 reviewed yeast MTs belonged to class I. However, four new folding architectures,
2 namely SSo0622-like, all- β , all- α (RNA/DNA 3-helical bundle) and transmembrane,
3 were postulated.

4 Radical SAM methyl transferases (RSMTs) comprise another class of recently
5 discovered MTs that contain an iron-sulfur ([4Fe-4S])-cluster coordinated by a three
6 cysteine CxxxCxxC motif. RSMTs methylate unreactive centers through a radical
7 mechanism [210]. Structural evidence suggests, that the mechanism is initiated by
8 reductive cleavage of SAM into a reactive 5'-deoxyadenosyl (dAdo) radical by the
9 [4Fe-4S] cluster [13, 24]. Three distinct classes (A, B, C) with distinct structural
10 and mechanistic characteristics have been recognized within the RSMTs [231].
11 The centerpiece of RSMTs is the *radical SAM* domain, whose structure was first
12 described in the ribosomal ribonucleic acid (rRNA) methyl transferase RlmN of
13 *E. coli* [13]. This domain consists of an α_6/β_6 partial barrel and contains the [4Fe-
14 4S] cluster, as well as the SAM binding site (Figure 3.3). Class A only contains the
15 radical SAM domain and mainly comprises rRNA methyl transferases. In addition
16 to the radical SAM domain, an N-terminal cobalamin binding domain (CBD) is
17 proposed to be contained in RSMTs of class B. Class B RSMTs methylate numerous
18 substrates at unreactive sp^3 carbon centers, heterocycles and phosphinates. Class C
19 RSMTs most likely contain a C-terminal domain related to the coproporphyrinogen
20 III oxidase HemN in addition to the radical SAM domain [115]. Class C enzymes
21 methylate aromatic heterocycles.

22 Radical SAM chemistry within enzymes is not confined to just methyl transfer.
23 Instead, it has been shown that this type of chemistry is important for a number of
24 rearrangement, cyclization, dehydrogenation, bond-formation and bond-cleavage
25 reactions in nature [24].

26 3.2.2 **S-Adenosyl-L-methionine**

27 S-adenosyl-L-methionine (SAM), first described in 1953 [26], is the universal co-
28 substrate for all SAM dependent methyl transferases. However, it is not only
29 involved in methyl transfer, but is essential for a myriad of other reactions [24]. This

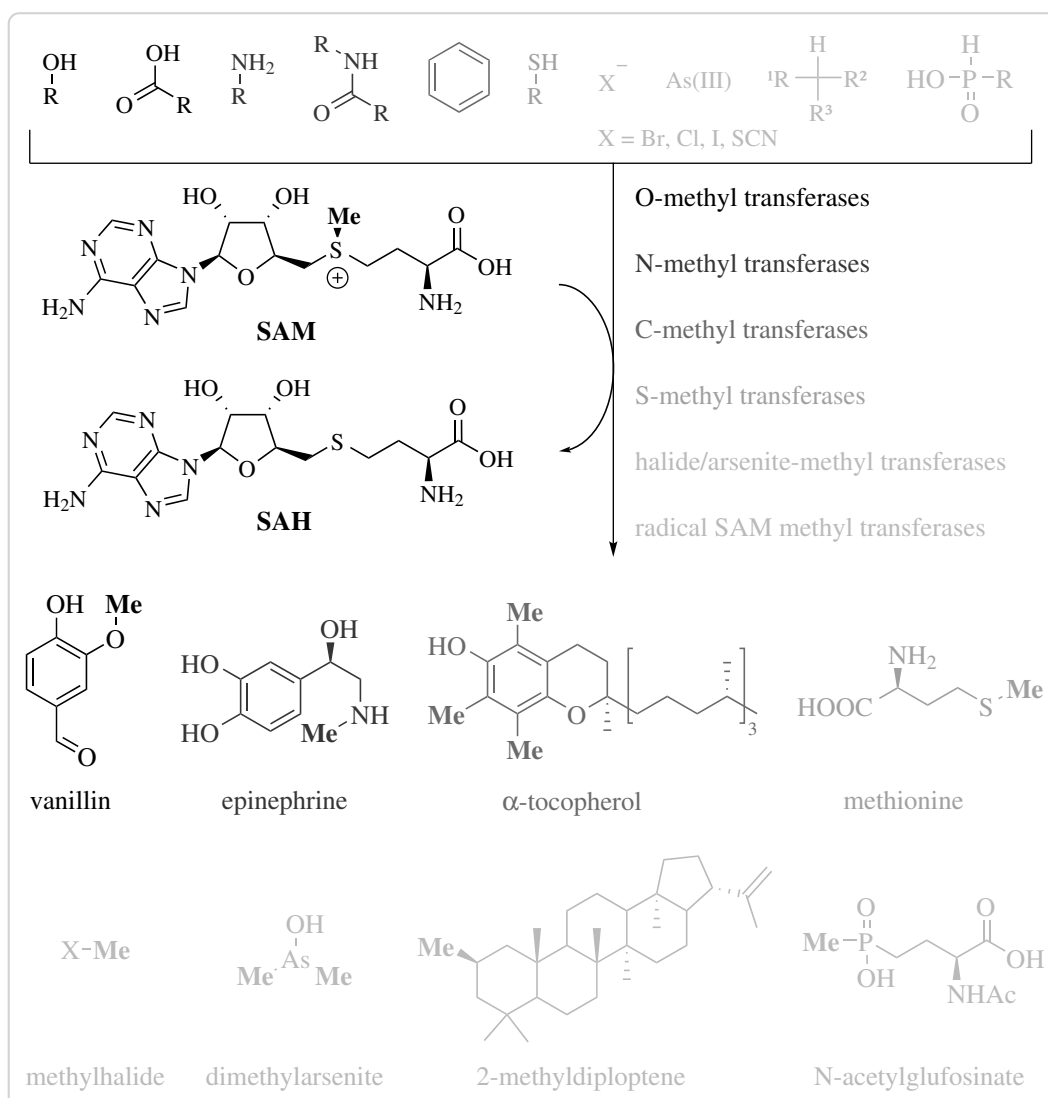


Figure 3.4.: Reactions catalyzed by methyl transferases (MTs). Different shades of gray were used to differentiate between different groups of compounds and methyl transferases. In contrast to other methyl transferases, the group of radical SAM methyl transferases also requires additional co-factors to SAM.

1 makes SAM the second most ubiquitous co-substrate after adenosine triphosphate
2 (ATP).

3 The methyl group of SAM is partially positively charged due to its position at
4 the sulfonium center and is in consequence highly activated. The increased elec-
5 trophilicity of the methyl group makes it a strong alkylation agent. Demethylated
6 SAM is called *S*-adenosyl-L-homocysteine (SAH), which is a good leaving group.
7 Therefore, nucleophilic transfer of the methyl group of SAM is thermodynamically
8 highly favoured ($\Delta G^0 \approx -70$ kJ/mol for SAM + homocysteine \rightarrow SAH + methion-
9 ine) and allows the rapid and selective methylation of a range of substrates [174].
10 The fact that the methyl group is the least sterically hindered of all transferable
11 carbon groups makes a methyl transfer the kinetically most favourable S_N2 reaction
12 (disregarding nucleophile and leaving group). Despite its apparent reactivity,
13 SAM is still quite stable at physiological conditions compared to other sulfonium
14 species like the trimethylsulfonium ion, which quickly reacts with nucleophiles
15 and is often used for derivatization prior to GC analytics [25]. Meanwhile, SAM
16 is readily cleaved into adenine and *S*-ribosylmethionine under alkaline conditions
17 [16] and other deteriorating processes such as racemization and intramolecular
18 cleavage are to be reckoned with [77].

19 SAM is produced by the enzyme SAM synthetase (EC 2.5.1.6) from methionine
20 and ATP in a two step reaction [190]. At first SAM is formed and the triphosphate
21 group of ATP is cleaved off. Then, the inorganic triphosphate is hydrolyzed to
22 monophosphate and diphosphate after which the products are released. SAH is a
23 common side product of all SAM dependent MTs and can be further cleaved by
24 SAH hydrolase (EC 3.3.1.1) to afford homocysteine and adenosine [127]. The cobal-
25 amine (vitamin B₁₂) dependent methionine synthase (EC 2.1.1.13) can remethylate
26 homocysteine to methionine using N⁵-methyltetrahydrofolate as a methyl donor
27 [9]. Taken together, reactions leading from and to SAM are commonly called the
28 activated methyl cycle.

3.2.3 Methyl transferase mechanisms

- Non-radical SAM-dependent MTs catalyze the transfer of the methyl group of SAM to an activated nucleophile. The methylation reaction proceeds via a single displacement S_N2 mechanism, through an sp^2 hybridized transition state and results in the inversion of configuration (Figure 3.5). The S_N2 mechanism was proposed as

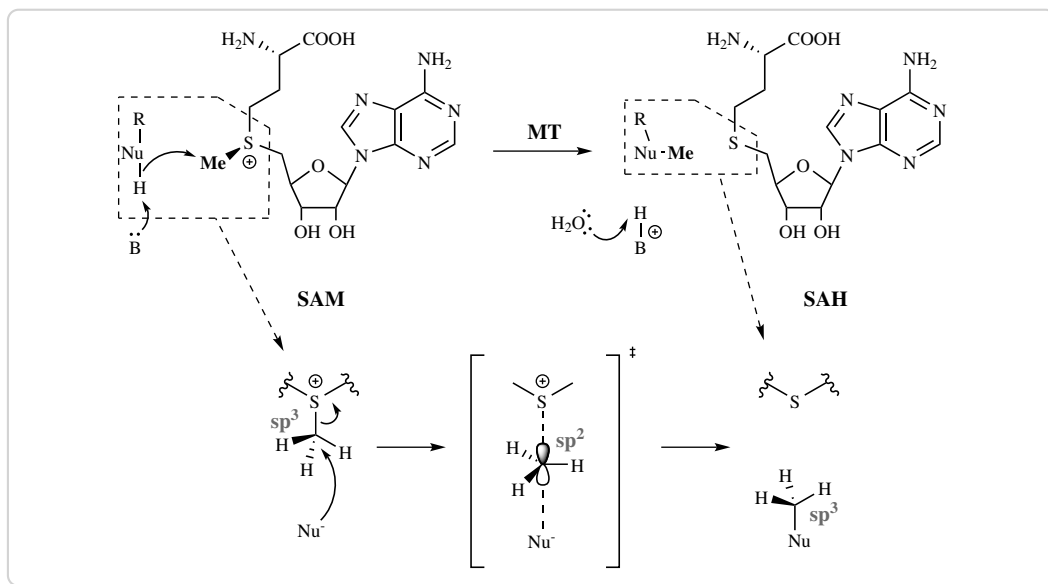


Figure 3.5: Mechanism of the methyl transfer reaction catalyzed by methyl transferases. Non-radical *S*-adenosyl-*L*-methionine dependent methyl transferases catalyze the nucleophilic transfer of a methyl group from the donor *S*-adenosyl-*L*-methionine to a nucleophile (Nu ; e.g. $\text{O}, \text{N}, \text{C}, \text{S}$). A proton (H^\oplus) is usually abstracted through a general base (B), to achieve activation of the nucleophile. The proton is later transferred to the aqueous medium. The S_N2 reaction proceeds via a single transition state, during which the methyl-carbon is sp^2 hybridized. After transfer of the methyl to the nucleophile the carbon's configuration is inverted.

- early as 1979 [73, 146], but only with the development of the chiral methyl group methodology (Figure 3.6) extended mechanistic studies were made possible [61, 62]. An elegant method for the synthesis of chiral acetate made use of glycolytic enzymes to convert $[1-{}^3\text{H}]\text{-glucose}$ via its glycolysis intermediates to $[3-{}^2\text{H}, {}^3\text{H}]\text{-lactate}$, which is subsequently oxidized by chromiumtrioxide (Figure 3.6) [223]. The chirality of the resulting acetate can be controlled by the solvents (D_2O or

- 1 H_2O) used during the enzymatic reactions. The chiral acetate can be used for the synthesis of e.g. [*methyl*- ^2H , ^3H]-methionine.

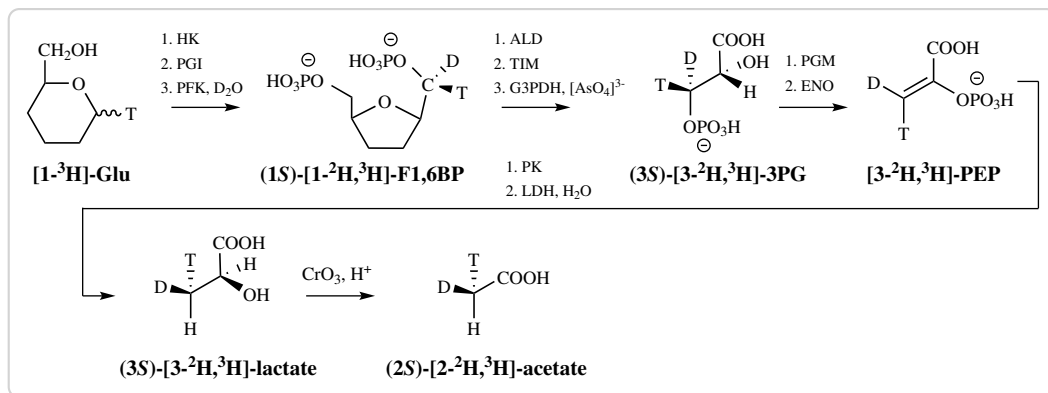


Figure 3.6.: Bioenzymatic synthesis of chiral acetate, the precursor for the synthesis of SAM carrying an assymetrical methyl, as used by Woodward *et al.* [223]. Ring hydroxyls of hexoses and pentoses are omitted for easier reading. HK – hexokinase, PGI – phosphoglucose isomerase, PFK – phosphofructokinase, ALD – aldolase, TIM – triose phosphate isomerase, G3PDH – glycerinaldehyde-3-phosphate dehydrogenase, PGM – phosphoglycerate mutase, ENO – enolase, Glu – glucose, F1,6BP – fructose-1,6-bisphosphate, 3PG – 3-phosphoglycerate, PEP – phosphoenol pyruvate

2
3 In 1980, Woodward *et al.* fed *R*- and *S*-methionine containing an assymetrical
4 methyl group to cultures of *Streptomyces griseus*. They found, that the enzymatic
5 transfer of two methyl groups (*N* and *C*-methylation) during the indolmycin
6 biosynthesis proceeded with inversion of the configuration, strongly implying an
7 $\text{S}_{\text{N}}2$ mechanism [223]. This experiment also demonstrated that, *in vivo*, [*methyl*-
8 ^2H , ^3H]-methionine is converted to [*methyl*- ^2H , ^3H]-SAM before the methyl group
9 is transferred by a MT. *In vitro* experiments conducted using catechol O-methyl
10 transferase (COMT) further supported the hypothesis of an $\text{S}_{\text{N}}2$ mechanism [222].

The nucleophile attacking the methyl group of SAM is usually activated by abstraction of a proton through a general base (e.g. histidine, lysine) [22, 235, 236] and/or with the help of a lewis acid such as complexed Mg^{2+} [109, 204]. In a bimolecular reaction, the rate is highly dependent on the concentration of both compounds:

$$\text{rate} = k[A][B].$$

1 Low concentrations of either result in a low rate. Thus, bimolecular reactions
2 are entropically disfavoured (concentration and entropy are inversely correlated).
3 MTs (and enzymes in general) strongly increase the effective concentration of
4 each reactant and thereby decrease entropy, because methyl donor and acceptor
5 are bound (“immobilized”) in close proximity to each other in the active site [60].
6 The right positioning of the substrates is a major factor for efficient catalysis and
7 enzymes go through great lengths to achieve optimal alignment of substrates. One
8 remarkable example are DNA-MTs, which can flip the target nucleotide out of the
9 DNA-helix to provide the best orientation of SAM and the acceptor nucleophile
10 [104].

11 Since the reaction catalyzed by MTs is a two substrate reaction, kinetics-driven
12 mechanistic studies have been done on a number of different MTs to show the
13 binding mode of the substrates. It turns out, that the reaction mechanism varies
14 for MTs from different organisms and classes. There is no one mechanism that
15 describes every MT. A random bi-bi binding mechanism is for example exhib-
16 ited by rat liver COMT [37], CheR protein-L-glutamate O-MT from *Salmonella*
17 *typhimurium* [182] and the protoporphyrin IX O-MT of *Rhodobacter capsulatus*
18 [170]. The protoporphyrin IX MT from etiolated wheat *Triticum aestivum* on the
19 other hand shows a ping-pong bi-bi mechanism [226], whereas ordered bi-bi mech-
20 anisms were shown for the cytosine DNA-MT MSPI and isoprenylated P-MT [12,
21 179]. Meanwhile, the enzymes exhibiting ordered bi-bi mechanisms were different
22 in that some bound SAM first and released SAH last [179], whereas the others
23 bound the acceptor molecule first [12]. Competitive product inhibition, especially
24 by SAH, is commonly observed for MTs [8, 12, 179, 182].

25 The mechanisms of RSMTs are outside the scope of this work, but the interested
26 reader is referred to current reviews on the topic [24, 231].

27 **3.2.4 Plant O-methyl transferases (O-MTs)**

28 Plant O-methyl transferases (O-MTs) were the prime interest of this work. Plant O-
29 MTs represent a large group of plant enzymes that catalyze the transfer of a methyl
30 group to a hydroxyl or carboxyl group of phenylpropanoids, flavonoids or alkaloids.

1 *O*-methylation greatly effects the (bio)-chemical properties of a compound and can
 2 have profound influences on reactivity, solubility, bioavailability, antimicrobial or
 3 antioxidant activities.

4 Plant *O*-MTs are subdivided into two groups according to their size and the
 5 spatial relationship between three highly preserved motifs (Table 3.1) [92]. Group I
 6 members, containing caffeoyl CoA dependent *O*-methyltransferase (CCoAOMT)-
 7 like representatives, are usually between 110 and 140 amino acid residues shorter
 than group II members (\approx 340–390 amino acids). The distance between motifs A and

Table 3.1. Defining motifs of plant *O*-MTs as described by Joshi *et al.* [92].

motif	consensus	distance to motif ...		
		...	group I	group II
A	(V,I,L)(V,L)(D,K)(V,I)GGXX(G,A)	B	19	52
B	(V,I,F)(A,P,E)X(A,P,G)DAXXXX(W,Y,F)	C	24	30
C	(A,P,G,S)(L,I,V)(A,P,G,S)XX(A,P,G,S)(K,R)(V,I)(E,I)(L,I,V)			

8
 9 B, and between B and C is also shorter in group I members, than in group II members.
 10 In contrast to group II, group I plant *O*-MTs require Mg²⁺ for activity. Overall, they
 11 are fairly similar to mammalian COMTs [92]. Group II plant *O*-MTs can methylate
 12 a variety of substrates, whereas group I plant *O*-MTs are usually very strict in their
 13 substrate scope utilizing only a couple of substrates. However, some enzymes from
 14 group I are much more relaxed with their acceptance of substrates. For example,
 15 phenylpropanoid and flavonoid *O*-methyl transferase (PFOMT) from the ice-plant
 16 *Mesembryanthemum crystallinum* and an *O*-MT from chickweed *Stellaria longipes*
 17 can utilize several phenyl propanoid derived substrates [85, 232].

18 **Phenylpropanoid and flavonoid *O*-methyl transferase (PFOMT)** is a
 19 Mg²⁺-dependent class I plant *O*-MT from the ice plant *M. crystallinum* and was first
 20 described in 2003 by Ibdah *et al.* [85]. PFOMT was the first class I MT that provided
 21 evidence showing, that methylation of flavonoids is not only restricted to class II
 22 plant *O*-MTs. It belongs to a subgroup of class I plant *O*-MTs, that is distinguished
 23 from CCoAOMT by a lower sequence homology and a broader substrate promiscuity
 24 and regiospecificity. PFOMT methylates a number of flavonoids and phenyl

1 propanoids at the *meta*-position, provided a catecholic moiety is present. Enzyme
2 purified from its native source *M. crystallinum* is truncated N-terminally by 11
3 amino acids, although there is no known signaling sequence [206]. This truncation
4 has deleterious effects on the catalytic efficiency, especially towards substrates
5 such as caffeoyl glucose and caffeoyl-CoA, but also influences the regioselectivity.
6 There is only speculation as to the purpose of this N-terminal truncation *in vivo*,
7 but metabolic regulation is plausible.

8 PFOMT is a biological dimer, as the three dimensional structure of PFOMT shows
9 (pdb: 3C3Y) [109]. Each monomer exhibits a Rossmann α/β -fold consisting of 8
10 α -helices and 8 β -strands. The catalytically important N-terminus is not resolved
11 in the structure. SAH and Ca^{2+} were cocrystallized and appear bound in the active
12 site. Ca^{2+} is complexed by two aspartate and one asparagine residues with the rest
13 of the coordination spaces occupied by waters.

14 **Soy O-methyl transferase (SOMT-2)** has been described in the literature to
15 methylate multiple flavonoids at the 4'-position of the B-ring [99, 102, 103]. It
16 has the highest activity towards naringenin, to produce ponciretin (also known
17 as isosakuranetin). No structural data of soy O-methyl transferase (SOMT-2) or
18 *in vitro* activity studies have been published to date. Enzymes like SOMT-2, that
19 methylate a *para*-monohydroxylated B ring of flavonoids, either seem to be a rare
20 occurrence or fairly inactive, since descriptions of characterized representatives are
21 scarce in the literature and are only limited to a couple of enzymes [47, 172].

22 3.3 Alkylation and biotransformations

23 3.3.1 Overview

24 Alkylation reactions are a crucial factor helping nature create highly diverse natural
25 products from a limited number of precursors and as such, these reactions are
26 becoming more and more important in biocatalysis. Methylation, prenylation and
27 glycosylation constitute the major alkylation reactions in nature and can largely
28 influence the (bio)chemical characteristics of a compound. Intra- and intermolecular

1 prenylation is achieved by prenyl transferases, which employ mono- and oligo-
2 prenyl diphosphates and are mainly responsible for the over 70 000 terpenoids
3 described today [23]. Glycosyl transferases catalyze the formation of a glycosidic
4 bond using nucleotide- or lipid phospho-sugars (e.g. uridine diphosphate (UDP)-
5 glucose, dolichol phosphate oligosaccharides) as sugar donating substrates [113].
6 Methylation reactions are catalyzed by MTs using SAM as methyl donor and will
7 be the focus of this section.

8 The introduction of a methyl group ($V \approx 20 \text{ \AA}^3$) for a hydrogen ($V \approx 5 \text{ \AA}^3$) can have
9 different effects, chemically and biologically. Polar groups (e.g. hydroxyl, amine,
10 carboxyl) are masked by methylation, which majorly alters their chemistry. Possible
11 hydrogen donors are lost and the lipophilicity is increased. The methylation can
12 act as a molecular signal, which might be specifically recognized by other enzymes
13 than the original more polar, hydrogen donating group. This can in turn have
14 dramatic physiological consequences in an organism.

15 3.3.2 Methyl transferases for industrial use

16 The industrial potential of MTshas been demonstrated by several studies [211]. Li
17 and Frost [122] presented an environmentally friendly method to produce vanillin
18 from glucose by genetically modified *E. coli* cells. During the fermentation, methyl
19 transfer was achieved by recombinantly expressed COMT. Recent developments
20 mainly focus on the synthesis of structurally more complex and highly valuable
21 compounds, especially flavonoids, due to their manifold biological effects (Figure 3.7). For example, ermanine (1) with a claimed anti-inflammatory and antiviral
22 activity, can be synthesized from its inactive precursor kaempferol (5,7-dihydroxy-
23 3,4'-dimethoxyflavone) by whole-cell biotransformation [15]. Sequential introduc-
24 tion of the two methyl groups was performed by OMT-9 from rice (ROMT-9)
25 and OMT-2 from soybean and resulted in almost quantitative conversion of the
26 substrate. Similarly, transformation of kaempferol and quercetin by an engineered
27 variant of the OMT-7 from *Populus deltoides* gave the 3,7-di-O-methyl products
28 in 58 % and 70 % yield, respectively [89]. The conversion of naringenin (4',5,7-
29 trihydroxyflavanone) to 3-O-methylkaempferol was performed as an enzymatic

- 1 two-step process involving initial oxidation by flavonol synthase and methylation
- 2 of the intermediate by ROMT-9 [101].

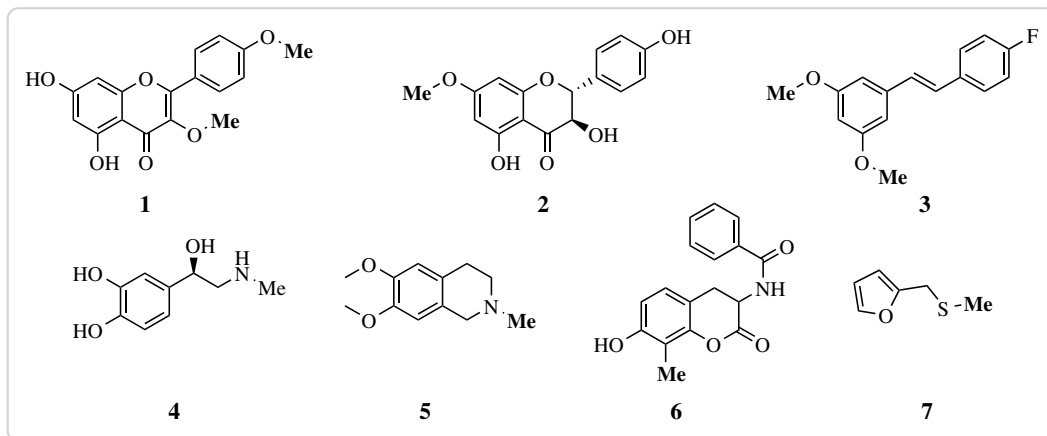


Figure 3.7.: Natural products synthesized with the help of methyl transferases. *O*-methyl transferases were used for the synthesis of ermanine (**1**), 7-*O*-methyl-aromadendrin (**2**) and 3,5-dimethoxy-4'-fluorostilbene (**3**). *N*-methyl transferase (*N*-MT) catalyze the production of epinephrine (**4**) and *N*-methyltetrahydroisoquinoline (**5**), whereas 3-(benzoylamino)-8-methylumbelliferone (**6**) and furfuryl-methyl-sulfide (**7**) can be produced by *C*-methyl transferase (*C*-MT) and *S*-methyl transferase (*S*-MT)

- 3 The most promising approach for the chemoenzymatic production of flavonoids
- 4 remains the *de novo* synthesis from inexpensive biosynthetic precursors such as
- 5 *p*-coumaric acid, which is initially processed into non-methylated flavonoids and
- 6 subsequently modified by *O*-MT reactions. This way, 7-*O*-methyl-aromadendrin (**2**)
- 7 and the corresponding flavone genkwanin were obtained from recombinant *E. coli* in
- 8 yields of 2.7 mg/l and 0.2 mg/l, respectively [118, 134]. Similarly, several non-natural
- 9 (e.g. fluorinated) cinnamic acids can be converted to mono- and dimethylated
- 10 stilbenes such as 3,5-dimethoxy-4'-fluorostilbene (**3**) using a reconstructed plant
- 11 pathway in *E. coli*.
- 12 *N*-, *C*- and *S*-methyl transferases have also been successfully used in bio-
- 13 catalytical applications. For example, epinephrine (**4**) and *N*-methyltetrahydro-
- 14 isoquinoline (**5**) were obtained by *in vitro* and *in vivo* biotransformations of their
- 15 respective precursors [138, 148]. Furthermore, a number of studies describe the
- 16 production of several other *N*-methylated alkaloid and non-alkaloid compounds
- 17 [156, 161, 230]. *C*-methyl transferases (*C*-MTs) have been used biocatalytically to

1 modify different phenols [38] and coumarin derivatives, to obtain compounds such
2 as 3-(benzoylamino)-8-methylumbelliferone (**6**) [187]. Also, the composition of the
3 main tocopherol species in plants could be tuned by the introduction of bacterial
4 C-MTs [84]. S-methyl transferases (S-MTs) have only seen a limited number of
5 biocatalytic applications, but a candidate from *Catharanthus roseus* shows some
6 promiscuous activity towards small aliphatic and aromatic thiols and can produce
7 molecules such as furfuryl-methyl-sulfide (**7**) [32].

8 *In vivo* biotransformations for the high-yield methylation of compounds is a
9 feasable method, especially since SAM is a rather expensive cofactor (3000 to 15 000
10 €/g). However, SAM cannot be easily substituted for artificial analogues *in vivo*.

11 3.3.3 Artificial SAM analogues

12 SAM analogues have shown tremendous potential in *in vitro* biocatalytic applica-
13 tions. The first description of novel synthetic SAM analogues with extended carbon
14 chains, including S-adenosyl-L-ethionine (SAE), allyl and propargyl derivatives, that
15 were also shown to be useful in modifying DNA via the action of several DNA-MTs
16 was provided by Dalhoff, *et al.* [44, 45]. A whole variety of allyl derivatives was
17 examined by different researchers and site-specific introductions of allyl, pent-2-
18 en-4-ynyl and even 4-propargyloxy-but-2-enyl moieties into proteins (i.e. histones)
19 was demonstrated using P-MTs [158, 209]. However, the larger substrate analogues
20 were not neccesarily accomodated by the native P-MTs making engineering efforts
21 for the accomodation of larger substrates inevitable [209]. The specific introduction
22 of alkine functionalized groups made it then possible to use click chemistry for
23 further functionalization and/or detection of the labelled proteins, DNA or RNA
24 (Figure 3.8) [150, 158, 175, 209, 215].

25 In 2012 Bothwell and Luo even described the exchange of the sulfonium with a
26 selenonium center, which afforded Se-adenosyl selenomethionine (SeAM) analogues
27 that have since then been described as substrates for several P-MTs [18, 19]. SeAM
28 analogues have the advantage of being more resistant to chemical decomposition
29 than their sulfur counterparts, but also show enhanced transmethylation reactivity
30 [18]. There have been some reports on the use of SAM analogues by small molecule

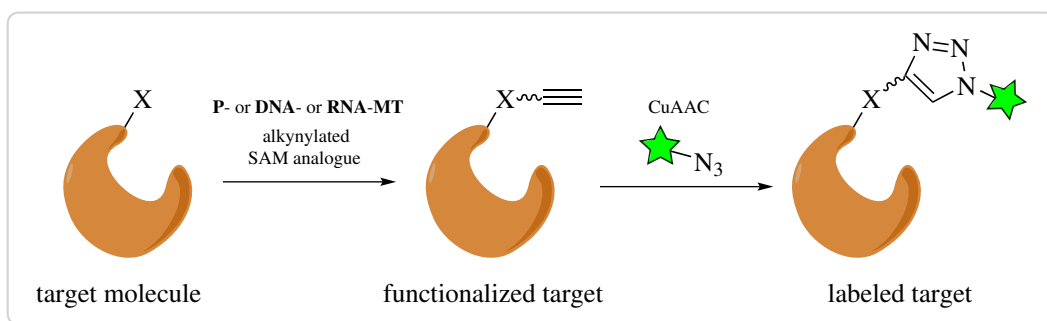


Figure 3.8: Labelling of macromolecules by using a combination of novel alkyne-derivatized S-adenosyl-L-methionine analogues and Cu^I-catalyzed azide-alkyne 1,3-dipolar cycloaddition (CuAAC). Depending on the type of label used, it can be employed for detection (e.g. through fluorophores, coupled assays) or affinity purification (e.g. biotin). This technique might also be also feasable for use in activity based protein profiling (ABPP) approaches.

1 MTs. In 2009 Stecher *et al.* reported the use of the C-MTs NovO and CouO along
 2 with synthetic SAM analogues to accomplish biocatalytic Friedel-Crafts alkylations
 3 of some aminocoumarine antibiotics [187]. Lee *et al.* were the first ones to describe
 4 the transfer of a keto-group from an SAM derivative by means of the small molecule
 5 MTs catechol O-methyl transferase (EC 2.1.1.6) and thiopurine S-methyl transferase
 6 (EC 2.1.1.67) [116]. Furthermore the work done on the O-MTs RebM and RapM,
 7 which modify the antitumor active natural products rebeccamycin and rapamycin
 8 respectively, shows the general feasibility of using SAM analogues in combination
 9 with MTs to modify small molecules [114, 184, 229]. However, no bioactivity
 10 data has been reported that shows the biological activity of the newly produced
 11 compounds.

12 3.4 Motivation

13 The motivation of this work was to assess the useability of plant O-methyl trans-
 14 ferases (O-MTs) for the derivatization and functionalization of phenyl propanoid
 15 derived phenolics, especially flavonoids.

16 Phenylpropanoid and flavonoid O-methyl transferase (PFOMT) from the ice-
 17 plant *Mesembryanthemum crystallinum* was to be used as a model enzyme to study

1 the promiscuity of class I plant *O*-MTs towards the alkyl donor, using the hemisyn-
2 thetically produced *S*-adenosyl-*L*-methionine analogue *S*-adenosyl-*L*-ethionine,
3 (2*S*)-2-amino-4-[(2*S,3S,4R,5R*)-5-(6-aminopurin-9-yl)-3,4-dihydroxyoxolan-2-
4 yl]methyl-ethylsulfonio]butanoat. Biophysical methods such as x-ray crystallog-
5 raphy and Isothermal Titration Calorimetry (ITC) should be used to study the
6 binding of the artificial analogues. The obtained knowledge could be used to aid the
7 development of novel small molecule methyl transferase with desirable catalytic
8 properties.

9 Furthermore, the enzymatic methylation of different structural motifs encoun-
10 tered throughout the phenyl propanoids was to be studied using class I and class
11 II plant *O*-MTs. Soy *O*-methyl transferase (SOMT-2) and PFOMT are examples
12 of both classes and should thus be used in this work. The results should help in
13 understanding the specific catalytic properties of both classes.

14 Furthermore, the analytical power of tandem mass-spectrometry (MS/MS) to
15 study substitutions commonly occurring in 5,7-dihydroxylated flavonoids should
16 be assessed using a distinct set of exemplary compounds. The insights obtained
17 should provide a reliable and fast method to determine structural properties of
18 unknown flavonoids.

4 Material And Methods

Within this section percentages refer to volume per volume (v/v) percentages unless otherwise specified.

4.1 Materials

4.1.1 Chemicals

Enzymes and buffers used for molecular cloning were obtained from Life Technologies (Darmstadt, Germany), unless otherwise noted. Flavonoid HPLC standards were purchased from Extrasynthese (Genay, France). Deuterated solvents were acquired from Deutero GmbH (Kastellaun, Germany). Solvents, purchased from VWR (Poole, England), were distilled in-house before use.

All other chemicals were obtained from either Sigma-Aldrich (Steinheim, Germany), Applichem (Darmstadt, Germany), Carl Roth (Karlsruhe, Germany) or Merck (Darmstadt, Germany).

4.1.2 Commonly used solutions and buffers

50× 5052 binding buffer	25 % glycerol, 2.5 % (w/v) glucose, 10 % (w/v) α -lactose 50 mM Tris/HCl, 500 mM NaCl, 10 % glycerol, 2.5 mM imidazole pH 7
elution buffer	50 mM Tris/HCl, 500 mM NaCl, 10 % glycerol, 250 mM imidazole pH 7

lysis buffer	50 mM Tris/HCl, 500 mM NaCl, 10 % glycerol, 2.5 mM imidazole, 0.2 % Tween-20 pH 7
1 M MMT pH 4 (10×)	26.8 g/l L-malic acid, 78.1 g/l MES, 26.8 g/l Tris, 2.1 % 10 M HCl
1 M MMT pH 9 (10×)	26.8 g/l L-malic acid, 78.1 g/l MES, 26.8 g/l Tris, 6.7 % 10 M NaOH
20× NPS	1 M Na_2HPO_4 , 1 M KH_2PO_4 , 0.5 M $(\text{NH}_4)_2\text{SO}_4$
1 M SSG pH 4 (10×)	14.8 g/l succinic acid, 60.4 g/l $\text{NaH}_2\text{PO}_4 \cdot \text{H}_2\text{O}$, 32.8 g/l glycine, 0.4 % 10 M NaOH
1 M SSG pH 10 (10×)	14.8 g/l succinic acid, 60.4 g/l $\text{NaH}_2\text{PO}_4 \cdot \text{H}_2\text{O}$, 32.8 g/l glycine, 10.3 % 10 M NaOH
5× SDS sample buffer	10 % (w/v) SDS, 10 mM β -mercaptoethanol, 20 % glycerol, 0.2 M Tris/HCl pH 6.8, 0.05 % (w/v) bromophenolblue
1000× trace elements	50 mM FeCl_3 , 20 mM CaCl_2 , 10 mM MnCl_2 , 10 mM ZnSO_4 , 2 mM CoCl_2 , 2 mM CuCl_2 , 2 mM NiCl_2 , 2 mM Na_2MoO_4 , 2 mM Na_2SeO_3 , 2 mM H_3BO_3

1 Preparation of natural deep eutectic solvent (NADES)

- 2 Natural deep eutectic solvent (NADES) were prepared by adding each component in a round-bottom flask with a stirrer and stirring the mixture at 50 °C with
 3 intermittent sonication treatments until a clear solution was obtained.

Table 4.1.: Natural deep eutectic solvent (NADES)-mixtures used within this work.

name	composition	mole ratio	mass fraction (w/w)
PCH	propane-1,2-diol	1:1:1	0.326
	choline chloride		0.597
	water		0.077
GCH	L-glucose	2:5:5	0.314
	choline chloride		0.608
	water		0.078

5 4.1.3 Culture media used to grow bacteria

LB-medium	10 g/l NaCl, 10 g/l tryptone, 5 g/l yeast extract, pH 7.5
LB-agar	LB + 1.5 % (w/v) agar-agar
TB-medium	12 g/l tryptone, 24 g/l yeast extract, 0.4 % glycerol, 72 mM K ₂ HPO ₄ , 17 mM KH ₂ PO ₄
ZY	10 g/l tryptone, 5 g/l yeast extract
ZYP-5052	volume fraction (v/v): 0.928 ZY, 0.05 20× NPS, 0.02 50× 5052, 0.002 1 M MgSO ₄ , 0.0002 1000× trace elements

1 4.1.4 Bacterial strains

2 *E.coli*

BL21(DE3)	F ⁻ <i>ompT hsdSB(r_B⁻,m_B⁻) gal dcm λ(DE3)</i> Invitrogen, Karlsruhe (Germany)
C41(DE3)	F ⁻ <i>ompT hsdSB(r_B⁻,m_B⁻) gal dcm λ(DE3)</i> Lucigen, Wisconsin (USA)
C43(DE3)	F ⁻ <i>ompT hsdSB(r_B⁻,m_B⁻) gal dcm λ(DE3)</i> Lucigen, Wisconsin (USA)
DH5α	F ⁻ Φ80lacZΔM15 Δ(<i>lacZYA-argF</i>) U169 <i>recA1 endA1 hsdR17(r_K⁻m_K⁺) phoA supE44 λ⁻ thi-1 gyrA96 relA1</i> Invitrogen, Karlsruhe (Germany)
JM110	<i>rpsL thr leu thi lacY galK galT ara tonA tsx dam dcm glnV44 Δ(lac-proAB) e14- [F' traD36 proAB⁺ lacI^q lacZΔM15] hsdR17(r_K⁻m_K⁺)</i> Martin-Luther-University Halle-Wittenberg
JW1593 (BW25113 derivative)	<i>rrnB ΔlacZ4787 HsdR514 Δ(arabAD)568 rph-1 ΔydgG</i> (Kan ^R) Keio Collection, National Institute of Genetics (Japan)
MG1655	F ⁻ λ ⁻ <i>ilvG⁻ rfb-50 rph-1</i> DSMZ, Hamburg (Germany)
One Shot TOP10	F ⁻ Φ80lacZΔM15 Δ(<i>mrr-hsdRMS-mcrBC</i>) <i>recA1 endA1 mcrA ΔlacX74 araD139 Δ(ara-leu)7697 galU galK rpsL</i> (Str ^R) λ ⁻ <i>nupG</i> Invitrogen, Karlsruhe (Germany)

Origami(DE3)	$\Delta(ara-leu)7697 \Delta lacX74 \Delta phoA P_{vull} phoR araD139 ahpC galE galK rpsL F'[lac + lacI q pro]$ (DE3) <i>gor522::Tn10 trxB</i> (Kan ^R , Str ^R , Tet ^R)
	Novagen, Wisconsin (USA)
Rosetta(DE3)	F ⁻ <i>ompT hsdSB(r_B⁻,m_B⁻) gal dcm λ</i> (DE3) pRARE (Cam ^R)
	Novagen, Wisconsin (USA)
Rosetta(DE3) pLysS	F ⁻ <i>ompT hsdSB(r_B⁻,m_B⁻) gal dcm λ</i> (DE3) pLysSRARE (Cam ^R)
	Novagen, Wisconsin (USA)
T7 Express	<i>fhuA2 lacZ::T7 gene1 [lon] ompT gal sulA11 R(mcr-73::miniTn10-Tet^S)2 [dcm] R(zgb-210::Tn10-Tet^S) endA1 Δ(mcrC-mrr)114::IS10</i>
	NEB, Massachusetts (USA)

1 *Agrobacterium tumefaciens*

GV3101	chromosomal background: C58, marker gene: <i>rif</i> , Ti-plasmid: cured, opine: nopaline Sylvestre Marillonet, IPB
--------	--

2 4.1.5 Plasmids

Table 4.2: Plasmids used in this work.

name	supplier/source
pACYCDuet-1	Merck, Darmstadt (Germany)
pCDFDuet-1	Merck, Darmstadt (Germany)
pET-20b(+)	Merck, Darmstadt (Germany)
pET-28a(+)	Merck, Darmstadt (Germany)
pET-32a(+)	Merck, Darmstadt (Germany)
pET-41a(+)	Merck, Darmstadt (Germany)
pQE30	QIAGEN, Hilden (Germany)
pUC19	Invitrogen, Karlsruhe (Germany)

1 4.1.6 Oligonucleotides and synthetic genes

2 Oligonucleotides and primers were ordered from Eurofins Genomics (Ebersberg,
 3 Germany). The purity grade was *high purity salt free* (HPSF). Synthetic genes
 4 or gene fragments were obtained from GeneArt® (Life Technologies, Darmstadt,
 5 Germany) or Eurofins Genomics (Ebersberg, Germany).

Table 4.3.: Primers used in this work. Recognition sites for endonucleases are underlined. Positions used for site directed mutagenesis are in lower case font.

name	sequence (5'→3')	cloning site
somt1	TTG AAG ACA AAA TGG CTT CTT CAT TAA ACA ATG GCC G	BpiI
somt2	TTG <u>AAG ACA</u> AGG ACA CCC CAA ATA CTG TGA GAT CTT CC	BpiI
somt3	TTG <u>AAG ACA</u> AGT CCT TAG GAA CAC CTT TCT GGG AC	BpiI
somt4	TTG <u>AAG ACA</u> AAA GCT CAA GGA TAG ATC TCA ATA AGA GAC	BpiI
pfomt1.fw	CAG AGA GGC cTA TGA GAT TGG CTT GC	
pfomt1.rv	GCA AGC CAA TCT CAT AgG CCT CTC TG	
pfomt2.fw	<u>CAT ATG</u> GAT TTT GCT GTG ATG AAG CAG GTC	NdeI
pfomt2.rv	<u>GAA TTC</u> AAT AAA GAC GCC TGC AGA AAG TG	EcoRI
pRha1.fw	CTC TAG <u>CAG ATC</u> TCG GTG AGC ATC ACA TCA CCA CAA TTC	BglII
pRha1.rv	CAA TTG <u>AGG ATC</u> CCC ATT TTA ACC TCC TTA GTG	BamHI
pUC1.fw	GCG TAT TGG Gag aTC TTC CGC TTC CTC	
pUC1.rv	GAG GAA GCG GAA GAT ctC CCA ATA CGC	

6 4.1.7 Instruments

CD-spectrometer	Jasco J-815 (Eaton, USA)
electrophoresis (horizontal)	Biometra Compact XS/S (Göttingen, Germany)
electrophoresis (vertical)	Biometra Compact M (Göttingen, Germany) Biometra Minigel-Twin (Göttingen, Germany)
FPLC	ÄKTA purifier (GE Healthcare, Freiburg, Germany)
GC/MS	GC-MS-QP2010 Ultra (Shimadzu, Duisburg, Germany)
HPLC	VWR-Hitachi LaChrom Elite (VWR, Darmstadt, Germany)
ITC	MicroCal iTC200 (Malvern, Worcestershire, UK)
plate-reader	SpectraMax M5 (Molecular Devices, Biberach, Germany)

NMR-spectrometer	Varian Unity 400 (Agilent, Böblingen, Germany)
	Varian VNMRS 600 (Agilent, Böblingen, Germany)
photospectrometer	Eppendorf Biophotometer Plus (Hamburg, Germany)
	JASCO V-560 (Eaton, USA)
	Colibri Microvolume Spectrometer (Biozym, Hess. Oldendorf, Germany)
centrifuges	Eppendorf 5424 (Hamburg, Germany)
	Hettich Mikro 120 (Kirchlengern, Germany)
	Beckman Avanti J-E, Beckman Allegra X-30R (Krefeld, Germany)
centrifuge rotors	Beckman JA-10, JA-16.250, JS-4.3 (Krefeld, Germany)

1 4.1.8 Software

2 All mathematical and statistical computations and graphics were done with the R
3 software (versions 3.1.X, <http://cran.r-project.org/>) [33]. Visualizations of macro-
4 molecules were arranged using the PyMol Molecular Graphics System, version
5 1.7.0.0 (Schrödinger, New York, USA) or UCSF Chimera version 1.9 (<http://www.cgl.ucsf.edu/chimera>) [159]. Physicochemical calculations and calculations of different
6 molecular descriptors were performed using Marvin Beans 15.4.13.0 (ChemAxon,
7 Budapest, Hungary) and Molecular Operating Environment 2008.10 (Chemical
8 Computing Group, Montreal, Canada). Special software used for X-ray crystal
9 structure solution is discussed separately in the corresponding section (4.5).

11 4.2 Molecular Biology

12 Basic molecular biology methods like polymerase chain reaction (PCR), DNA re-
13 striction/ligation, DNA gel electrophoresis, preparation of competent cells and
14 transformation were performed based on the protocols summarized by Sambrook
15 and Russell [167]. Plasmid DNA was isolated using the QIAprep® Spin Miniprep
16 Kit (QIAGEN, Hilden, Germany) according to the manufacturer's instructions.
17 In vitro site-directed mutagenesis was set-up according to the protocol of the
18 QuikChange™ Site-Directed Mutagenesis kit [3] offered by Agilent Technologies

1 (Santa Clara, USA). Nucleotide fragments obtained by PCR, restriction/ligation
2 procedures or excision from electrophoresis gels were purified and concentrated
3 using the *Nucleospin Gel and PCR Clean-up* kit provided by Machery-Nagel (Düren,
4 Germany) according to the instructions provided by the manufacturer.

5 4.2.1 Golden Gate Cloning

6 The Golden Gate cloning procedure is a one-pot method, meaning the restriction
7 digestion and ligation are carried out in the same reaction vessel at the same time [55,
8 106]. Consequently PCR-fragments, destination vector, restriction endonuclease
9 and ligase are added together in this reaction. The methodology employs type II
10 restriction enzymes, which together with proper design of the fragments allow
11 for a ligation product lacking the original restriction sites. For digestion/ligation
12 reactions of fragments containing BpiI sites, 20 fmol of each fragment or vector,
13 together with 5 U of BpiI and 5 U of T4 ligase were combined in a total volume
14 of 15 µl 1× ligase buffer. For fragments to be cloned via BsaI sites, BpiI in the
15 above reaction was substituted by 5 U BsaI. The reaction mixture was placed in
16 a thermocycler and incubated at 37 °C for 2 min and 16 °C for 5 min. These two
17 first steps were repeated 50 times over. Finally, the temperature was raised to 50 °C
18 (5 min) and 80 °C (10 min) to inactivate the enzymes.

19 The *SOMT2* gene was amplified from pET28a-SOMT using primers *somt1–somt4*
20 (Table 4.3), cloned into vector pICH41308 (level 0) using BpiI and consequently
21 subcloned into the level 1 module pICH75044, alongside 35S promoter and nopaline
22 synthase (nos)-terminator, using BsaI (Figure 4.1). The resulting construct was
23 denoted as pBEW107.

24 4.2.2 Subcloning of genes

25 All subcloning procedures were performed according to section 4.2 and specifically
26 subsection 4.2.1. Specific steps for the subcloning of any genes discussed can be
27 found in the appendix (p.148). The *pfromt* gene was subcloned from the pQE-30
28 vector kindly provided by Thomas Vogt (Leibniz-Institute of Plant Biochemistry
29 (IPB), Halle, Germany) into the pET-28a(+) vector. The *somt-2* gene was subcloned

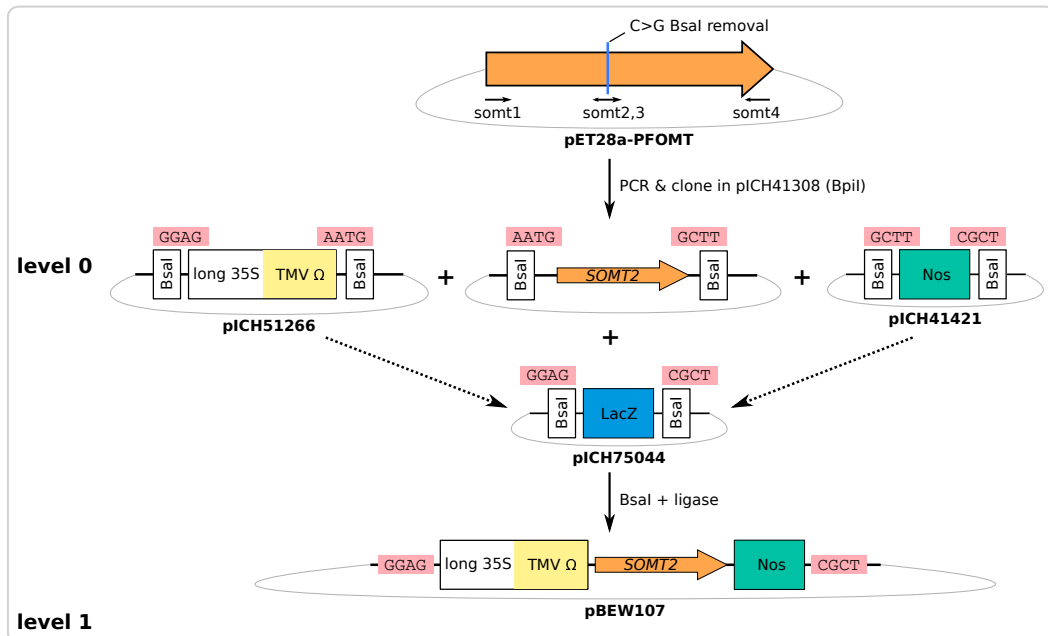


Figure 4.1: Golden Gate cloning scheme for soy *O*-methyl transferase (*SOMT-2*)

- 1 from the pQE-30 vector kindly provided by Martin Dippe (IPB, Halle, Germany)
- 2 into the pET-28-MC vector.

3 4.2.3 Transformation of electrocompetent *Agrobacterium tumefaciens* cells

- 5 A 50 µl aliquot of electrocompetent *A. tumefaciens* cells was thawed on ice. (50 to
- 6 100) ng of plasmid were added, the solution was mixed gently and transferred to a
- 7 pre-cooled electroporation cuvette. After pulsing (2.5 kV, 200 Ω) 1 ml of lysogeny
- 8 broth (LB)-medium was added, the mixture transferred to a 1.5 ml tube and incu-
- 9 bated for (3 to 4) hours at 28 °C. The culture was centrifuged (10 000 × g, 1 min)
- 10 and 900 µl supernatant were discarded. The pellet was resuspended in the remain-
- 11 ing liquid, plated onto LB-agar plates supplemented with 40 µg/ml rifampicin and
- 12 50 µg/ml carbencillin and incubated at 28 °C for (2 to 3) days.

1 4.3 Treatment of plant material

2 4.3.1 Infiltration of *Nicotiana benthamiana*

3 Before infiltration *N. benthamiana* plants were pruned, such that only leaves to
4 be infiltrated remained with the plant (Figure 4.2). 5 ml cultures of transformed
5 *A. tumefaciens* in LB-medium (with 40 µg/ml rifampicin and 50 µg/ml carbencillin)
6 were grown over night at 28 °C and 220 rpm. OD₆₀₀ of the culture was measured
7 and adjusted to 0.2 by dilution with infiltration buffer (10 mM MES/NaOH, 10 mM
8 MgSO₄ pH 5.5). When multiple *A. tumefaciens* transformed with different construct-
9 s/plasmids were used for infiltration, the cultures were mixed and diluted using
10 infiltration buffer, such that OD₆₀₀ of each culture in the mix was 0.2. The solution
11 was infiltrated into the abaxial side of *N. benthamiana* leaves using a plastic syringe.
12 The leaf material was harvested after 7 days.

13 Infiltration of *N. benthamiana* for *in vivo* biotransformation using SOMT- 14 2

15 Both sides of *N. benthamiana* leaves were infiltrated with different samples (Fig-
16 ure 4.2). The left side was infiltrated with *A. tumefaciens* cultures transformed
17 with pAGM10733 (phenylalanine ammonia-lyase (PAL)), pAGM10406 (chalcone
18 synthase (CHS)) and pBEW107 (SOMT-2). For the right side the *A. tumefaciens*
19 culture containing pBEW107 was replaced by a control: *A. tumefaciens* transformed
20 with the empty vector pICH75044.

21 4.3.2 Plant material harvest

22 Infiltrated/Infected areas of *N. benthamiana* leaf material were cut out and grouped
23 by plant number, leaf position (top/bottom) and leaf side (right/left). The grouped
24 clippings were weighed, frozen in liquid nitrogen, ground to a powder, freeze-dried
25 and stored at -80 °C.

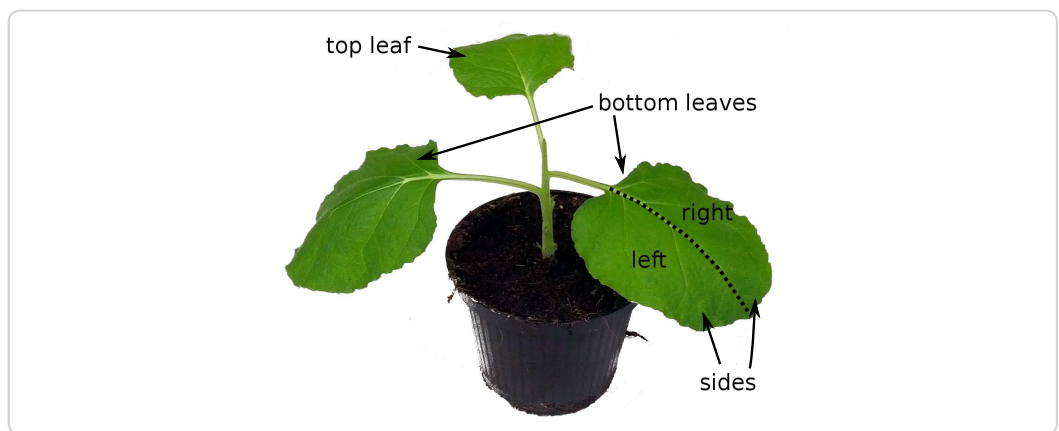


Figure 4.2.: Pruned *N. benthamiana* plant, with two bottom and one top leaf, ready to be infiltrated.

- 1 **4.3.3 Extraction of flavonoids from *N. benthamiana* leaves**
- 2 Two tips of a small spatula of freeze-dried material (≈ 6 mg), were weighed exactly
- 3 and extracted with 500 μ l 75 % aqueous methanol containing 1 mM ascorbic acid,
- 4 0.2 % formic acid and 0.1 mM flavone (internal standard). Therefore the suspension
- 5 was vortexed for 30 s, rotated on an orbital shaker for 10 min and vortexed again for
- 6 30 s. The suspension was centrifuged ($20\,000 \times g$, 4 °C, 10 min) and the supernatant
- 7 transferred to a new tube, to remove the insoluble plant material. The supernatant
- 8 was centrifuged again ($20\,000 \times g$, 4 °C, 10 min) and the resulting supernatant was
- 9 transferred to a HPLC-vial and stored at -20 °C until analysis.

10 **4.4 Protein biochemistry**

- 11 Stock solutions of antibiotics, IPTG or sugars were prepared according to the pET
- 12 System Manual by Novagen [154], unless otherwise noted.

13 **4.4.1 Determination of protein concentration**

- 14 Protein concentrations were estimated using the absorption of protein solutions at
- 15 280 nm, which is mainly dependent on the amino acid composition of the protein

Table 4.4: Calculated extinction coefficients of proteins used in this work.

protein/enzyme	$\varepsilon_{280\text{nm}}^{1\text{ g/l}}$ in ml mg $^{-1}$ cm $^{-1}$
PFOMT (reduced)	0.714
PFOMT Y51K N202W (reduced)	0.852
SOMT-2 (oxidized)	1.263
SOMT-2 (reduced)	1.247

1 studied [70]. Extinction coefficients of proteins were calculated from the amino
 2 acid sequence using the ExpPASy servers's ProtParam tool [66].

3 4.4.2 Protein production test (expression test)

4 The heterologous production of proteins in *E. coli* was assessed in a small scale
 5 protein production test, henceforth called expression test. Single colonies of *E. coli*
 6 transformed with the constructs to be studied were used to inoculate a 2 ml starter
 7 culture in LB-medium containing the appropriate antibiotics. The working con-
 8 centrations of antibiotics used was as follows: 200 µg/ml ampicillin, 150 µg/ml
 9 kanamycin, 50 µg/ml chloramphenicol, 20 µg/ml tetracycline. The starter culture
 10 was allowed to grow at 37 °C and 200 rpm over night. A 5 ml sampling culture
 11 of the medium to be studied containing the appropriate antibiotics was prepared.
 12 The media tested included LB, terrific broth (TB) and auto-induction media like
 13 ZYP-5052. The sampling culture was inoculated to an OD₆₀₀ of 0.075 using the
 14 starter culture and incubated at different temperatures and 200 rpm in a shaking
 15 incubator. 1 mM isopropyl-D-thiogalactopyranosid (IPTG) was added when the
 16 OD₆₀₀ reached 0.6-0.8, if appropriate for the studied construct. 1 ml samples were
 17 removed after different times of incubation (e.g. 4, 8, 12 hours), subfractionated
 18 (4.4.3) and analyzed via SDS-polyacrylamide gel electrophoresis (PAGE) (4.4.6).

19 4.4.3 Protein subfractionation

20 The protein subfractionation procedure described herein was adapted from the
 21 protocol described in the pET Manual [154]. Overall 5 protein subfractions can be
 22 obtained, including *total cell protein*, *culture supernatant (medium) protein*, *periplas-*

1 *mic protein, soluble cytoplasmic protein and insoluble protein.* The OD₆₀₀ of the cul-
2 ture sample was measured and the cells harvested by centrifugation at 10 000 × g,
3 4 °C for 5 minutes. The protein in the supernatant medium was concentrated by
4 precipitation with trichloro acetic acid (TCA) (4.4.4) for SDS-PAGE analysis. The
5 periplasmic protein was prepared (4.4.5) and also concentrated by TCA precipi-
6 tation for SDS-PAGE. Cells were lysed by resuspending the cell pellet in (OD₆₀₀
7 × V × 50) µl of bacterial protein extraction reagent (B-PER) and vortexing vigor-
8 ously for 30 s. The suspension was incubated at room temperature (RT) for 30 min to
9 assure complete lysis. To separate insoluble protein and cell debris from the soluble
10 cytosolic protein, the suspension was centrifuged at 10 000 × g and 4 °C for 10 min.
11 Soluble cytoplasmic protein was contained in the supernatant, whereas insoluble
12 protein remained in the pellet. For SDS-PAGE analysis of the insoluble protein,
13 the pellet was resuspended in the same volume of B-PER. To obtain only the total
14 cell protein fraction, the preparation of periplasmic and soluble cytosolic protein
15 was omitted. Sample volumes of 10 µl of each fraction were used for SDS-PAGE
16 analysis.

17 4.4.4 Protein sample concentration by TCA precipitation

18 Diluted protein samples were concentrated by TCA precipitation in microcentrifuge
19 tubes. Therefore 0.1 volume (V) of 100 % (w/v) TCA in water was added to the clar-
20 ified sample, which was then vortexed for 15 s and placed on ice for a minimum of
21 15 min. The sample was centrifuged at 14 000 × g, 4 °C for 15 min. The supernatant
22 was discarded and the pellet was washed twice with 0.2 V ice-cold acetone. The
23 acetone was removed and the pellet set to air-dry in an open tube. After drying, the
24 protein pellet was resuspended in 0.1 V phosphate buffered saline (PBS) containing
25 1 × SDS-sample buffer by heating to 85 °C and vigorous vortexing, to achieve a
26 10 × concentration. After resuspension the sample was analyzed by SDS-PAGE or
27 stored at -20 °C until use.

1 4.4.5 Preparation of periplasmic protein

2 Target proteins may be directed to the periplasmic space by N-terminal signal
3 sequences like *pelB* or *DsbA/C* [133]. The periplasma is, other than the cytosol, an
4 oxidizing environment and often used for the production of proteins containing
5 disulfide linkages. The preparation of periplasmic protein was accomplished by
6 an osmotic shock protocol modified from Current Protocols in Molecular Biology
7 [7]. The cell pellet was resuspended in the same volume as the culture sample of
8 30 mM tris-HCl, 20 % (w/v) sucrose, pH 8 and 1 mM ethylenediaminetetraacetic
9 acid (EDTA) was added. The suspension was stirred for 10 min at RT and the cells
10 were collected by centrifugation at $10\,000 \times g$, 4 °C for 10 min. The supernatant
11 was discarded and the cell pellet was resuspended in the same volume of ice-cold
12 5 mM MgSO₄. The suspension was stirred for 10 min on ice, while the periplasmic
13 proteins were released into the solution. The cells were collected by centrifugation
14 as before. Periplasmic proteins were contained in the supernatant.

**15 4.4.6 Discontinuous SDS-polyacrylamide gel electrophoresis
16 (SDS-PAGE)**

17 The analysis of samples via SDS-PAGE was realized via the discontinuous system
18 first described by Laemmli, which allows separation of proteins based on their
19 electrophoretic mobility, which in turn depends on their size [112]. The SDS-
20 PAGE procedure was carried out according to standard protocols described by
21 Sambrook and Russell [167]. Very dilute and/or samples with high ionic strength
22 were concentrated and/or desalted by the TCA precipitation procedure described in
23 subsection 4.4.4. Generally a 10 % (acrylamide/bisacrylamide) running gel combined
24 with a 4 % stacking gel was used. Reducing SDS-PAGE sample buffer was added to
25 the protein sample to be analyzed, whereafter the sample was heated to 95 °C for
26 5 min, to allow for total unfolding of the protein. After cooling to RT the samples
27 were transferred into the gel pockets for analysis. The *PageRuler™ Prestained*
28 *Protein Ladder* (Life Technologies GmbH, Darmstadt, Germany) was used as a
29 molecular weight (MW) marker and run alongside every analysis as a reference.
30 Gels were stained using a staining solution of 0.25 % Coomassie Brilliant Blue G-

1 250 (w/v) in water:methanol:acetic acid (4:5:1) and destained by treatment with
2 water:methanol:acetic acid (6:3:1).

3 4.4.7 Buffer change of protein samples

4 The buffer in protein samples was exchanged either by dialysis, or by centrifugal
5 filter concentrators (Amicon[®] Ultra Centrifugal Filter; Merck, Darmstadt, Ger-
6 many). Large volumes of highly concentrated protein solutions were preferably
7 dialyzed. Respectively, very dilute samples were concentrated and rebuffed using
8 centrifugal concentrators. Dialysis was carried out at least twice against a mini-
9 mum of 100 times the sample volume. Dialysis steps were carried out at RT for 2
10 hours, or over-night at 4 °C. Centrifugal concentrators were used according to the
11 manufacturers instructions.

12 4.4.8 Production of recombinant protein

13 Heterologous production of PFOMT

14 Phenylpropanoid and flavonoid O-methyl transferase (PFOMT) was produced as a
15 N-terminally (His)₆-tagged fusion protein. A 2 ml starter culture of LB containing
16 100 µg/ml kanamycin was inoculated with a single colony of *E. coli* BL21(DE3)
17 transformed with pET28-pfomt and incubated at 37 °C, 220 rpm for 6 hours. The
18 main culture (N-Z-amino, yeast extract, phosphate (ZYP-5052) containing 200 µg/ml
19 kanamycin) was inoculated with the starter culture such that OD₆₀₀ was 0.05.
20 The culture was incubated in a shaking incubator at 37 °C, 220 rpm over night
21 (~16 h). Due to the autoinducing nature of the ZYP-5052 medium, addition of
22 IPTG was not necessary. Cells were harvested by centrifugation at 10 000 × g, 4 °C
23 for 10 min and the supernatant discarded. The pellet was resuspended in 50 mM
24 Tris/HCl, 500 mM NaCl, 2.5 mM imidazole, 10 % glycerol pH 7 using a volume of
25 ~10 ml/g of cell pellet. The cells were lysed by sonication (70 % amplitude, 1 s on-
26 off-cycle) for 30 seconds, which was repeated twice. The crude lysate was clarified
27 by centrifugation at 15 000 × g, 4 °C for 15 minutes followed by filtration through a
28 0.45 µm filter. Consequently, the His-tagged PFOMT was purified by immobilized

1 metal affinity chromatography (IMAC) (4.4.10). The eluted PFOMT protein was
2 dialyzed (4.4.7) against 25 mM HEPES, 100 mM NaCl, 5 % glycerol pH 7 and stored
3 at -20 °C until use.

4 **Heterologous production of SOMT-2**

5 SOMT-2 was produced as a fusion protein with an N-terminal His-tag. A starter
6 LB-culture (\approx 2 ml) containing 100 μ g/ml kanamycin was inoculated with a single
7 colony of *E. coli* BL21(DE3) transformed with pET28MC-somt and incubated at
8 37 °C, 220 rpm for 6 hours. The starter culture was used to inoculate the main
9 culture (LB-medium containing 100 μ g/ml kanamycin), such that $OD_{600} \approx 0.05$.
10 The culture was incubated at 37 °C, 220 rpm in a shaking incubator until OD_{600}
11 ≈ 0.6 . Expression was induced by addition of 1 mM IPTG. Incubation continued at
12 37 °C, 220 rpm for 6 hours. Cells were harvested by centrifugation ($10\,000 \times g$, 4 °C,
13 10 min) and used, or stored at -20 °C until use. SOMT-2 was produced in inclusion
14 bodies (IBs), which were prepared as laid out in subsection 4.4.9.

15 **4.4.9 Preparation of inlusion bodies (IBs)**

16 Often, when recombinant protein is produced in high levels in *E. coli* it is accu-
17 mulated in so-called inlusion bodies (IBs) [166]. The accumulating IBs consist
18 mainly of the overproduced target protein, which is inherently quite pure already.
19 IBs can be selectively recovered from *E. coli* cell lysates and can consequently be
20 refolded. IBs were prepared according to a modified protocol by Palmer [157].
21 The cells were resuspended in 5 ml/g_{cells} IB lysis buffer (100 mM Tris/HCl, 1 mM
22 EDTA pH 7), 0.5 mM phenylmethylsulfonylfluoride (PMSF) was added as protease
23 inhibitor. The solution was homogenized using a tissue grinder homogenizer (Ultra
24 Turrax®; IKA®-Werke GmbH & Co. KG, Staufen, Germany). 200 μ g/ml lysozyme
25 was added to aid in the breakage of cells and the cells were lysed by sonicating
26 thrice at 70 % amplitude (1 s on-off-cycle) for 30 seconds. DNase I (10 μ g/ml) was
27 added and the solution was incubated on ice for 10 min. The lysate was clarified by
28 centrifuging for 1 h at $20\,000 \times g$, 4 °C. The supernatant was discarded and the pellet
29 was resuspended in 5 ml/g_{cells} IB wash buffer I (20 mM EDTA, 500 mM NaCl, 2 %

1 (w/v) Triton X-100 pH), followed by thorough homogenization. The solution was
2 centrifuged (30 min at 20 000 × g, 4 °C), the supernatant discarded and the pellet
3 was washed twice more. To remove detergent, the pellet was washed twice again
4 with IB washing buffer II (20 mM EDTA, 100 mM Tris/HCl pH 7). The IBs were
5 resuspended in IB solubilization buffer (100 mM Tris/HCl, 5 mM DTT, 6 M GdmCl
6 pH 7), such that the protein concentration was about 25 mg/ml and stored at -20 °C
7 until use.

8 **4.4.10 Purification of His-tagged proteins using immobilized
9 metal affinity chromatography (IMAC)**

10 N- or C-terminal oligo-histidine tags (His-tags) are a common tool to ease purification
11 of recombinantly produced proteins. The free electron pairs of the imidazol
12 nitrogens of histidines can complex divalent cations such as Mg²⁺ or Ni²⁺, which
13 are usually immobilized on a matrix of nitrilo triacetic acid (NTA)-derivatives. The
14 affinity of the His-tag is correlated with its length and tagged proteins can simply
15 be eluted by increasing the concentration of competing molecules (e.g. imidazole).
16 His-tagged protein was purified by fast protein liquid chromatography (FPLC) via
17 Ni²⁺- (HisTrap FF crude) or Co²⁺-NTA (HiTrap Talon FF crude) columns, obtained
18 from GE Healthcare (Freiburg, Germany), following modified suppliers instructions.
19 First the column was equilibrated with 5 column volumes (CV) of binding buffer
20 (50 mM Tris/HCl, 500 mM NaCl, 10 % glycerol, 2.5 mM imidazole pH 7). The sample
21 (generally clarified lysate) was applied to the column using a flow of 0.75 ml/min.
22 Unbound protein was removed by washing with 3 CV binding buffer. Unspecifically
23 bound proteins were washed away by increasing the amount of elution buffer
24 (50 mM Tris/HCl, 500 mM NaCl, 10 % glycerol, 250 mM imidazole pH 7) to 10 %
25 (constant for 3 to 5 CV). Highly enriched and purified target protein was eluted
26 with 6 to 10 CV of 100 % elution buffer.

**1 4.4.11 Refolding of SOMT-2 on a micro scale using design of
2 experiments (DoE)**

3 Design of experiments (DoE) and fractional factorial design (FrFD) have been
4 successfully used to optimize the refolding conditions of several proteins [4, 11,
5 214]. Thus, an approach using fractional factorial design (FrFD) was used to find
6 optimal refolding conditions for SOMT-2. Factors studied were pH (buffer), arginine,
7 glycerol, divalent cations, ionic strength, redox system, cyclodextrin and co-factor
8 addition. The experimental matrix was constructed using the FrF2 package
9 (<http://cran.r-project.org/web/packages/FrF2/index.html>) in the R software.

Table 4.5.: Factors and their high and low levels (+/-) used in the construction of the fractional factorial design (FrFD).

factor	symbol	setting (level)		unit
		-	+	
pH	A	5.5	9.5	-
arginine	B	0	0.5	M
glycerol	C	0	10	% (v/v)
divalent cations [†]	D	no	yes	-
ionic strength [‡]	E	low	high	-
redox state [*]	F	reducing	redox-shuffling	-
α -cyclodextrin	G	0	30	mM
SAH	H	0	0.5	mM

[†]no: 1 mM EDTA; yes: 2 mM CaCl₂, MgCl₂

[‡]low: 10 mM NaCl, 0.5 mM KCl; high: 250 mM NaCl, 10 mM KCl

^{*}reducing: 5 mM DTT; redox-shuffling: 1 mM glutathione (GSH), 0.2 mM glutathione disulfide (GSSG)

10 The buffers were mixed from stock solutions and prepared in 1.5 ml microcen-
11 trifuge tubes immediately prior to the experiment. 50 μ l of solubilized SOMT-2
12 (1 mg/ml) in IB solubilization buffer was added to 1 ml of each buffer followed by a
13 short vortex boost for rapid mixing. The final protein concentration in the refolding
14 reaction was 50 μ g/ml, whereas the remaining GdmCl concentration was \approx 286 mM.
15 The refolding reactions were incubated at RT for 1 hour, followed by an over
16 night incubation at 4 °C. After incubation the refolding reactions were centrifuged
17 (10 000 $\times g$, 4 °C, 10 min) to separate insoluble and soluble protein fractions. The
18 supernatant was transferred to a new tube, whereas the pellet was washed twice

Table 4.6.: Experimental design matrix for the FrFD.

Experiment	A	B	C	D	E	F	G	H
1	+	+	+	-	-	-	-	+
2	-	-	-	-	-	-	-	-
3	+	-	+	+	-	+	+	-
4	-	+	+	-	+	+	+	-
5	+	+	-	-	+	+	-	-
6	-	+	-	+	+	-	+	+
7	+	+	-	+	-	-	+	-
8	-	-	+	-	+	-	+	+
9	+	-	+	+	+	-	-	-
10	-	-	-	-	-	+	+	+
11	+	-	-	+	+	+	-	+
12	-	+	+	+	-	+	-	+

1 with 200 µl acetone and once with 400 µl methanol/acetone (1:1). The pellet was
 2 resuspended in 100 µl PBS with 20 µl SDS-PAGE sample buffer and 10 µl were used
 3 for SDS-PAGE analysis. 100 µl of the supernatant were concentrated using TCA
 4 precipitation (4.4.4) and analyzed by SDS-PAGE. The remaining supernatant was
 5 rebuffered into 50 mM 2-[Bis(2-hydroxyethyl)amino]-2-(hydroxymethyl)propane-
 6 1,3-diol (BisTris) pH 7.5 using Amicon® Ultra 0.5 ml centrifugal filters (Merck, Darm-
 7 stadt, Germany) according to the manufacturers instructions. The pre-weighed
 8 collection tubes were re-weighed after recovery and the volume of recovered liquid
 9 calculated ($\rho \approx 1 \text{ g/cm}^3$). The sample was filled up to 100 µl using 50 mM BisTris
 10 pH 7.5 and the protein concentration was assessed using the Roti®-Quant protein
 11 quantification solution (Carl Roth, Karlsruhe, Germany) according to the manu-
 12 facturers description. 50 µl of each refolded sample was used for an activity test
 13 using naringenin as substrate (4.6.3). The reactions were incubated over night and
 14 stopped by the extraction method. However, before the actual extraction 1 µl of
 15 anthracene-9-carboxylic acid (AC-9) was added as internal standard. The samples
 16 were analyzed by high-performance liquid chromatography (HPLC).

1 Assessment of refolding performance

2 The performance of each buffer on the refolding of SOMT-2 was examined by
3 comparing the SDS-PAGE results, as well as the amount of soluble protein and
4 the conversion of naringenin over night (see subsection 4.6.3). Main effects were
5 analyzed qualitatively using main effects plots [20].

6 Upscaling of refolding reactions

7 Refolding reactions were scaled up to 50 ml. Therefore 2.5 ml solubilized SOMT-2
8 (1 mg/ml) were added over 10 minutes to 50 ml of refolding buffer while stirring at
9 RT. The refolding reaction was allowed to complete over night at 4 °C.

10 4.4.12 Enzymatic production of SAM and SAE

11 S-adenosyl-L-methionine (SAM) and S-adenosyl-L-ethionine (SAE) were prepared
12 according to the method described by Dippe, et. al [49].

13 Preparative reactions (20 ml) were performed in 0.1 M Tris/HCl, 20 mM MgCl₂,
14 200 mM KCl pH 8.0 and contained 7.5 mM adenosine triphosphate (ATP), 10 mM
15 D,L-methionine or D,L-ethionine, for the production of SAM or SAE respectively,
16 and 0.2 U S-adenosylmethionine synthase (SAMS) variant I317V. The reaction was
17 stopped by lowering the pH to 4 using 10 M acetic acid after 18 h of incubation
18 at 30 °C, 60 rpm. After 10 min incubation on ice the solution was centrifuged
19 (15 000 × g, 10 min) to remove insoluble matter. The supernatant was transferred
20 to a round bottom flask, frozen in liquid nitrogen and lyophilized. Crude products
21 were extracted from the pellet using 73 % ethanol and purified using ion exchange
22 chromatography (IEX). IEX was performed on a sulfopropyl sepharose matrix
23 (25 ml) via isocratic elution (500 mM HCl). Before injection, the crude extract was
24 acidified to 0.5 M HCl using concentrated hydrochloric acid. After elution, the
25 product containing fractions were dried via lyophilization. The amount of product
26 was determined by UV/VIS-spectroscopy at 260 nm using the published extinction
27 coefficient of SAM ($\epsilon_0 = 15\,400\text{ M}^{-1}\text{ cm}^{-1}$) after resuspension in water [178].

1 4.5 Crystallographic Procedures

2 4.5.1 Crystallization of proteins

3 Commercially available crystallization screens were used to find initial crystalliza-
4 tion conditions. The tested screens included kits available from Hampton Research
5 (Aliso Viejo, USA) and Jena Bioscience (Jena, Germany). Crystallization screens
6 were processed in 96-well micro-titer plate (MTP)s, where each well possessed
7 4 subwells aligned in a 2×2 matrix. The subwells were divided into 3 shallow
8 wells for sitting drop vapour diffusion experimental setups and a fourth subwell,
9 which was deep enough to act as buffer reservoir. This way the performance of
10 each crystallization buffer could be assessed using three different protein solutions
11 with varying concentrations, effectors etc. A pipetting robot (Cartesian Microsys,
12 Zinsser-Analystik; Frankfurt, Germany) was used to mix 200 nl of each, protein
13 and buffer solution, for a final volume of 400 nl. The crystallization preparations
14 were incubated at 16 °C and the progress of the experiment was documented by
15 an automated imaging-system (Desktop Minstrel UV, Rigaku Europe, Kent, UK).
16 Furthermore, fine screens (e.g. for refinement of crystallization conditions) were
17 set up by hand in 24-well MTPs using the hanging drop vapour diffusion method.

18 PFOMT

19 PFOMT protein was concentrated to (6 to 8) mg/ml and rebuffered to 10 mM
20 Tris/HCl pH 7.5 using Amicon® Ultracel centrifugal concentrators (10 kDa MWCO).
21 The concentrated protein solution was centrifuged at 14 000 × g, 4 °C for 10 min
22 to remove any insoluble material or aggregates. Flavonoids and phenylpropanoid
23 substrates were added to the protein solution from 10 mM stock solution in dimethyl
24 sulfoxide (DMSO). Crystallization screens were set up as described above.
25 apo-PFOMT was crystallized using the following conditions – 2 M (NH₄)₂SO₄,
26 20 %glycerol. The protein solution contained 0.25 mM SAE, 0.25 mM MgCl₂,
27 0.25 mM eriodictyol and 7.53 mg/ml (0.262 mM) PFOMT .

1 Crystallization of proteins using NADES

2 NADES have the potential to be excellent solvents for hydrophobic compounds
3 such as flavonoids or cinnamic acids [43] and in addition they are able to stabilize
4 and activate enzymes [81].

5 Four different model proteins (bovine trypsin, hen-egg white lysozyme, pro-
6 teinase K and *Candida cylindrica* lipase B) were used to assess the capability of
7 NADES for protein crystallization. PCH was tested in a full factorial grid lay-
8 out using PCH concentrations of (20, 30, 40 and 50) % combined with buffers of
9 different pH. The buffers included 0.1 M sodium acetate pH (4.5 and 5.5), 0.1 M
10 sodium citrate pH 6.5, 0.1 M 2-[4-(2-hydroxyethyl)piperazin-1-yl]ethanesulfonic
11 acid (HEPES)/NaOH pH (7 and 7.5) and 0.1 M Tris/HCl pH 8.5. Thus, the full
12 factorial design had a size of $4 \times 6 = 24$ different conditions. Protein solutions
13 were prepared from lyophilized protein and were as follows: 90 mg/ml trypsin in
14 10 mg/ml benzamidine, 3 mM CaCl₂; 75 mg/ml lysozyme in 0.1 M sodium acetate
15 pH 4.6; 24 mg/ml proteinase K in 25 mM Tris/HCl pH 7.5 and 6 mg/ml lipase B in
16 water. For crystallization 2 µl enzyme solution and 1 µl reservoir buffer were mixed
17 and set up in a hanging drop experiment on a 24-well MTP. The experiments were
18 set up at 4 °C.

19 4.5.2 Data collection and processing

20 Crystallographic data were collected at the beamline of the group of Professor
21 Stubbs (MLU, Halle, Germany). The beamline was equipped with a rotating anode
22 X-ray source MicroMax007 (Rigaku/MSC, Tokio, Japan), which had a maximum
23 power of 0.8 kW (40 kV, 20 mA) and supplied monochromatic Cu-K_α-radiation with
24 a wavelength of 1.5418 Å. Diffraction patterns were detected with a Saturn 944+
25 detector (CCD++, Rigaku/MSC, Tokio, Japan).

26 Indexing and integration of the reflexes via Fourier transformation (FT) was
27 accomplished using *XDS* [93, 94, 95] or *MOSFLM* [160]. *Scala* [57], which is inte-
28 grated in the Collaborative Computational Project No. 4 (CCP4)-Suite, was used
29 for scaling of the intensities.

1 4.5.3 Structure solution

2 For the determination of the electron density $\rho(\mathbf{r})$, where \mathbf{r} is the positional vector,
3 from the diffraction images by FT two terms are necessary as coefficients; the
4 *structure factor amplitudes*, $F_{\text{obs}}(\mathbf{h})$ and the *phase angles or phases*, $\alpha(\mathbf{h})$, where \mathbf{h}
5 is the reciprocal index vector. The structure factor amplitudes can be directly
6 determined from the measured and corrected diffraction intensities of each spot.
7 However, the phase information is lost during the detection of the diffracted photons
8 and there is no direct way to determine the phases. This constitutes the so-called
9 *phase problem*. Thus, additional phasing experiments are necessary in order to
10 obtain the phases. A variety of phasing experiments are available, which include
11 *marker atom substructure methods*, *density modification* and *molecular replacement*
12 (*MR*) techniques [197]. Phases of the structures herein were exclusively determined
13 by MR [164, 165]. MR was performed using the software *Phaser* [141, 142], which is
14 included in the CCP4-Suite [216]. A previously published PFOMT structure (PDB-
15 code: 3C3Y [109]) was used as a template during MR procedure for the PFOMT
16 structure solution.

17 4.5.4 Model building, refinement and validation

18 Macromolecular model building and manipulation, as well as real space refinement
19 and Ramachandran idealization were performed using the Crystallographic Object-
20 Oriented Toolkit (*Coot*) software [54]. Structure refinement was done using the
21 software REFMAC5 [152, 202] as part of the CCP4-suite or the Phyton-based
22 Hierachial Environment for Integrated Xtallography (PHENIX) [1]. Validation of
23 the structures was carried out using the web service MolProbity (<http://molprobity.biochem.duke.edu/>) [30]. Structure visualization and the preparation of figures
24 was performed using PyMOL (Schrödinger, New York, USA) and UCSF Chimera
25 (<http://www.cgl.ucsf.edu/chimera>) [159].

1 4.5.5 *In silico* substrate docking

2 *In silico* molecular docking studies were performed using the AutoDock Vina 1.1.2
3 or AutoDock 4.2.6 software in combination with the AutoDockTools-Suite (<http://autodock.scripps.edu/>) [82, 149, 199]. Substrates were docked into the PFOMT
4 structure with the PDB-code 3C3Y. The grid box, which determines the search
5 space, was manually assigned to center at 1.581, 5.196 and 25.718 (x, y, z) and
6 had size of (22, 20 and 25) Å (x, y, z). The exhaustiveness of the global search for
7 AutoDock Vina was set to 25, whereas the rest of the input parameters were kept
8 at their defaults.

10 4.6 Analytics

11 4.6.1 Recording of growth curves

12 Starter cultures (\approx 2 ml) of the transformed *E. coli* cells were prepared in the medium
13 to be studied, containing the appropriate antibiotics. The cultures were incubated
14 at 37 °C, 200 rpm over night and harvested by centrifugation (5000 $\times g$, 4 °C, 5 min).
15 The pellet was resuspended in 15 ml PBS and the suspension centrifuged (5000 $\times g$,
16 4 °C, 5 min). The supernatant was discarded and the washing step repeated once
17 more. The washed pellet was resuspended in 2 ml of the medium to be studied with
18 the appropriate antibiotics and the OD₆₀₀ was measured. Three independent 50 ml
19 cultures of the medium containing the appropriate antibiotics were inoculated such
20 that OD⁶⁰⁰ \approx 0.05 using the washed cell suspension. The cultures were incubated
21 at the conditions to be studied and sampled at appropriate intervals of time (\approx 1 h).
22 One ml samples were kept on ice until all samples were acquired. 100 µl aliquots of
23 the samples were transferred into a clear MTP and the OD₆₀₀ was measured.
24 Green fluorescent protein (GFP) fluorescence was measured accordingly, but the
25 MTP used was opaque. Exitation (λ^{ex}) and emission (λ^{em}) wavelengths were (470
26 and 510) nm respectively.

1 4.6.2 *In vitro* determination of glucose

2 The glucose concentration in clarified, aqueous samples was determined by a mod-
3 ified version of the glucose assay kit procedure provided by Sigma-Aldrich [181].
4 Glucose oxidase (GOD) oxidizes D-glucose to gluconic acid, whereby hydrogen
5 peroxide is produced. The hydrogen peroxide can be detected and quantified by
6 horseradish peroxidase (HRP), which reduces the produced H₂O₂ and thereby oxi-
7 dizes its chromogenic substrate o-dianisidine via consecutive one-electron transfers.
8 The oxidized diimine form of o-dianisidine can then be measured photospectro-
9 metrically [31].

10 The methodology employs a coupled photospectrometric assay using GOD
11 and HRP with o-dianisidine as reporter substrate. The assay was prepared in
12 MTP-format. A reaction solution containing 12.5 U/ml GOD, 2.5 U/ml HRP and
13 0.125 mg/ml o-dianisidine dihydrochloride in 50 mM sodium acetate pH 5.1 was
14 prepared. Sample solutions from culture supernatants were typically diluted in
15 9 volumes of water. The reaction was started, by adding 50 µl reaction solution to
16 25 µl of sample and was incubated at 37 °C and 200 rpm for 30 min in a shaking incu-
17 bator. 50 µl 6 M sulfuric acid was added to stop the reaction and achieve maximum
18 color development (full oxidation of any o-dianisidine charge transfer complexes)
19 (Figure 4.3). The developed pink color was measured at 540 nm in a MTP-reader.
20 A calibration curve of a standard D-glucose solutions (0 to 100 µg/ml), that was
21 always part of the experiments, was used to quantify the sample measurements.

22 4.6.3 *In vitro* O-methyl transferase (O-MT) assay

23 O-methyl transferase (O-MT) assays were conducted in a total volume of (50
24 to 100) µl. The standard assay buffer was 100 mM Tris/HCl, 2.5 µM GSH pH 7.5.
25 1 mM MgCl₂, which was otherwise omitted, was added for reactions using cation
26 dependent O-MTs (e.g. PFOMT). Reactions contained 0.5 mM alkyl donor (e.g. (S,S)-
27 SAM) and 0.4 mM flavonoid or cinnamic acid substrate. Enzymatic reactions were
28 started by addition of enzyme (usually 0.2 mg/ml) and incubated at 30 °C. Reactions
29 were stopped by addition of 500 µl ethyl acetate containing 2 % formic acid and
30 vortexed for 15 s to extract the hydrophobic phenylpropanoids and flavonoids. After

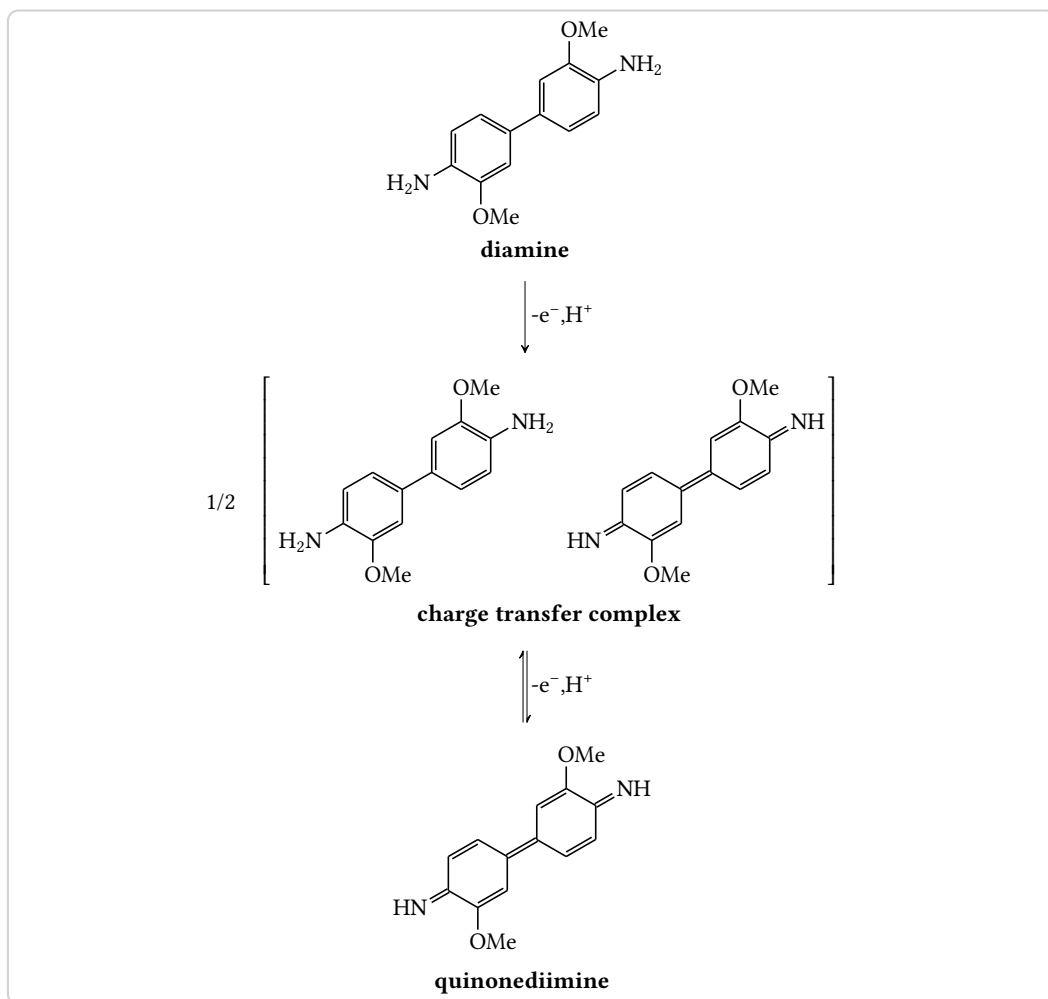


Figure 4.3.: Oxidation of the reporter substrate *o*-dianisidine. Consecutive one-electron transfers lead to the fully oxidized diimine form of *o*-dianisidine. The first electron transfer is believed to produce a charge transfer complex intermediate. [31, 91]

1 centrifugation ($10\,000 \times g$, 4 °C, 10 min) the organic phase was transferred into a new
2 tube. The reaction was extracted once more with 500 µl ethyl acetate, 0.2 % formic
3 acid and the pooled organic phases were evaporated using a vacuum concentrator
4 (Concentrator 5301; eppendorf, Hamburg, Germany). The residue was dissolved
5 in methanol and centrifuged at $10\,000 \times g$ for 10 min to remove unsoluble matter.
6 The supernatant was transferred into a HPLC vial and analyzed by HPLC (4.6.8).
7 When detection of hydrophobic (e.g. flavonoids) and hydrophilic compounds (e.g.
8 SAM, S-adenosyl-L-homocysteine (SAH)) was performed simultaneously reactions
9 were stopped by addition of 0.3 volumes 10 % (w/v) TCA in 50 % acetonitrile. The
10 mixture was vortexed for complete mixing and incubated on ice for at least 30 min.
11 After centrifugation ($10\,000 \times g$, 4 °C, 10 min) the supernatant was transferred into
12 HPLC-sample vials and analyzed (see 4.6.8).

13 **Measurement of activity/pH profiles**

14 Assays to measure activity over larger pH ranges were set up in 50 mM L-malic
15 acid/MES/Tris (MMT)- (pH 4 to 9) or succinate/sodium phosphate/glycine (SSG)-
16 buffer (pH 4 to 10) to keep the concentrations of buffer salts constant for each pH
17 [153]. The protein of interest was first extensively dialyzed against the reaction
18 buffer (e.g. MMT, SSG) at pH 7 with added EDTA (5 mM) and then against the same
19 buffer without EDTA. Standard reaction conditions were 50 mM buffer, 0.4 mM
20 alkyl acceptor (e.g. caffeic acid), 0.5 mM SAM, 2.5 µM GSH and 0.2 mg/ml enyzme.
21 MgCl₂ was either omitted or added at 10 mM to assess influences of divalent cations.
22 Assays were stopped as described in 4.6.3 and analyzed accordingly.

23 **Estimation of product concentration and enzymatic activities**

Product concentrations were estimated from HPLC runs. The automatically integrated peaks of SAM and SAH provided the area under the curve (AUC). From the AUC of both peaks the concentrations were estimated as follows.

Under the assumption, that

$$AUC^{\text{SAH}} + AUC^{\text{SAM}} = 1 \sim c_0^{\text{SAM}},$$

the fraction and concentration of one (e.g. SAH) can be estimated by

$$x^{\text{SAH}} = \frac{AUC^{\text{SAH}}}{AUC^{\text{SAH}} + AUC^{\text{SAM}}}$$

and

$$c^{\text{SAH}} = x^{\text{SAH}} \times c_0^{\text{SAM}}.$$

- 1 The amount n is obtained by multiplying the concentration c by the injection volume
- 2 V . Enzymatic activities (i.e. initial rates) can be calculated from the concentrations
- 3 by standard procedures.

4.6.4 Photospectrometric assay for the methylation of catecholic moieties

- 6 Catecholic moieties can form stable complexes in the presence of heavy metals such
- 7 as copper or iron [143, 176]. Hence, caffeic acid can complex ferric (Fe^{3+}) ions and
- 8 form a colored complex with $\lambda_{\text{max}} = 595 \text{ nm}$ [48]. Since the complex formation is
- 9 specific for caffeic acid and methylated derivatives (i.e. ferulic and iso-ferulic acid)
- 10 cannot complex Fe^{3+} , this can be used as a measure for methylation reactions. *O*-
- 11 MT assays were prepared as before (subsection 4.6.3). However, the reactions were
- 12 stopped by addition of 0.1 volumes 1 M Tris/HCl pH 8, immediately followed by
- 13 0.5 volumes catechol reagent (2 mM FeCl_3 in 10 mM HCl). The complex formation
- 14 reaction was allowed to equilibrate for 5 min at RT and the absorbance at 595 nm
- 15 was measured.

**1 4.6.5 Concentration of SOMT-2 using hydrophobic interac-
2 tion chromatography (HIC)**

3 After refolding using rapid dilution protein samples are very dilute and a con-
4 centration step is required. Refolded SOMT-2 was concentrated directly from the
5 refolding buffer using hydrophobic interaction chromatography (HIC). The am-
6 monium sulfate concentration of the protein sample was brought to 1 M using a
7 2 M $(\text{NH}_4)_2\text{SO}_4$ solution and the pH was adjusted to 7 using 5 M NaOH. The sample
8 was centrifuged ($20\,000 \times g$, 4 °C, 30 min) to remove insoluble material and the
9 clarified supernatant was applied to a 1 ml HiTrap Phenyl FF (Low Sub) (GE Health-
10 care, Freiburg, Germany), which had been equilibrated with high salt buffer (1 M
11 $(\text{NH}_4)_2\text{SO}_4$, 50 mM HEPES pH 7). The target protein was eluted using a stepwise
12 gradient ((1, 0.8, 0.6, 0.4, 0.2 and 0) M $(\text{NH}_4)_2\text{SO}_4$, 50 mM HEPES pH 7; 5 CV each)
13 to remove the ammonium sulfate. The column was washed using 20 % ethanol.
14 Before SDS-PAGE analysis the eluted high salt fractions were desalted using TCA
15 precipitation (4.4.4).

16 4.6.6 Analytical gel filtration

17 Analytical gel filtration was done using a Superdex 200 10/300 GL column (GE
18 Healthcare, Freiburg, Germany) in combination with a FPLC system according to
19 the manufacturers instructions. The column was equilibrated using an appropriate
20 buffer (e.g. 0.1 M Tris/HCl pH 7.5) and 100 µl of sufficiently concentrated ($\geq 1 \text{ mg/ml}$)
21 protein sample were injected. The Gel Filtration Standard by Bio-Rad (München,
22 Germany) was run separately to assess the size of the proteins in the analyzed
23 sample.

**24 4.6.7 Binding experiments using Isothermal Titration Calori-
25 metry (ITC)**

26 Isothermal Titration Calorimetry (ITC) can be used to directly characterize the ther-
27 modynamics of an observed process, be this a binding interaction or an enzymatic
28 reaction [63]. ITC measurements to describe the interaction between PFOMT and

its substrates/effector were performed using a MicroCal iTC200 device (Malvern, Worcestershire, UK). PFOMT protein was extensively dialyzed against 50 mM MMT-buffer pH 7 prior to ITC experiments. The solution was subsequently centrifuged ($14\,000 \times g$, 4 °C, 10 min), to remove insoluble matter and aggregates. The dialysate was stored at 4 °C and used to prepare substrate and effector solutions. Generally 50 µM protein was provided in the ITC cell and the effectors/substrates to be titrated were loaded into the syringe. The substance concentration in the syringe was ten times higher than the protein solution. Experiments were carried out at 20 °C unless otherwise stated. The stirring speed was set to 500 rpm. The injection volume was set to (2 to 4) µl, amounting to a total of 10 to 19 injections.

4.6.8 High-performance liquid chromatography (HPLC) analytics

Due to their aromaticity, methanolic extracts of flavonoids exhibit two major absorption peaks in the UV/VIS region of the light spectrum in the range of (240 to 400) nm [132]. However, even the more simple phenyl propanoids (e.g. cinnamic acids) show absorption of light in the UV/VIS-region. Methanolic extracts of flavonoids and phenyl propanoids were analyzed by HPLC using a photo diode array (PDA)-detector, which was set to record in the range of (200 to 400) nm. HPLC runs were performed on a reverse-phase C-18 end-capped column (YMC-Pack ODS-A; YMC Europe, Dinslaken, Germany) with a pore size of 120 Å. The mobile phase was aqueous acetonitrile supplemented with 0.2 % formic acid. The flow was kept constant at 0.8 ml/min. 10 µl O-MT enzyme assay extract (4.6.3) were injected and analyzed using an acetonitrile gradient starting with 5 % acetonitrile (4 min). The acetonitrile content was increased to 100 % in 21 min and was kept at 100 % for 5 min. Peaks were integrated from the 280 nm trace using the software provided by the manufacturer of the device.

1 4.6.9 Liquid chromatography-tandem mass spectrometry 2 (LC-MS/MS) measurements

3 The positive and negative ion high resolution electrospray ionization (ESI) and
4 collision induced dissociation (CID) MS_n spectra as well as higher-energy colli-
5 sional dissociation (HCD) MS/MS spectra were obtained from an Orbitrap Elite
6 mass spectrometer (Thermo Fisher Scientific, Bremen, Germany) equipped with an
7 heated-electrospray ionization (H-ESI) ion source (positive spray voltage 4.5 kV,
8 negative spray voltage 3.5 kV, capillary temperature 275 °C, source heater temper-
9 ature 250 °C, Fourier transform mass spectrometry (FTMS) resolving power (RP)
10 30 000). Nitrogen was used as sheath and auxiliary gas. The MS system was coupled
11 with an ultra-high performance liquid chromatography (UHPLC) system (Dionex
12 UltiMate 3000, Thermo Fisher Scientific), equipped with a RP-C18 column (particle
13 size 1.9 µm, pore size 175 Å, 50 x 2.1 mm inner diameter, Hypersil GOLD, Thermo
14 Fisher Scientific, column temperature 30 °C) and a photodiode array detector ((190
15 to 400) nm, Thermofisher Scientific). For the UHPLC a gradient system was used
16 starting from H₂O:CH₃CN 95:5 (each containing 0.2 % formic acid) raised to 0:100
17 within 10 min and held at 0:100 for further 3 min. The flow rate was 150 µl/min.

18 The mass spectra (buffer gas: helium) were recorded using normalized collision
19 energies (NCE) of (30 to 45) % and (75 to 100) % for CID and HCD mass spectra
20 respectively (see Appendix). The instrument was externally calibrated using the
21 Pierce® LTQ Velos ESI positive ion calibration solution (product number 88323,
22 Thermofisher Scientific, Rockford, IL, 61105 USA) and the Pierce® LTQ Velos ESI
23 negative ion calibration solution (product number 88324, Thermofisher Scientific,
24 Rockford, IL, 61105 USA) for positive and negative ionization mode respectively.

¹ 5 Engineering of phenylpropanoid
² and flavonoid O-methyl trans-
³ ferase (PFOMT)

1

Evaluation of PFOMT towards the acceptance of long-chain SAM analogues

2 Benjamin Weigel^{1,a}, Martin Dippe, Ludger A. Wessjohann^{1,c}

Contact: bweigel@ipb-halle.de^a, law@ipb-halle.de^c

Affiliation: Leibniz-Institute of Plant Biochemistry, Department of Bioorganic Chemistry¹

Keywords: methyl transferase, pfomt, SAM

3

Abstract

4

The cation dependent phenylpropanoid and flavonoid O-methyl transferase (PFOMT) from the ice plant, *Mesembryanthemum crystallinum*, methylates a number of flavonoids and phenyl propanoids. A newly solved crystal structure of the protein without any bound ligand shows the fully resolved N-terminus, which acts as a lid to close off the active site. Binding of co-substrates (analogues) (e.g. S-adenosyl-L-homocysteine (SAH), S-adenosyl-L-methionine (SAM), S-adenosyl-L-ethionine (SAE)) is more entropically driven as the chain length increases. However, even though the ethyl-analogue of SAM – SAE – was shown to bind to the enzyme, no conversion of the model substrate caffeic acid was observed for the wild-type and several engineered variants.

14

15 5.1 Introduction

16

Small changes to molecules can have profound influences on their chemical, physical and biological properties. For example, butyric acid esters differing only by a few methylene groups already exhibit quite divergent smells. However, not only the macroscopically qualitative properties can differ. The quantifiable psychotomimetic effect of methylated and ethylated lysergic acid amids differ by at least an order of magnitude [78, 180]. There are many more of these so-called structure activity relationship (SAR) and quantitative structure activity relationship (QSAR) studies on any number of compounds [5, 135, 168].

1 Methylation reactions are one of the key tailoring steps during natural product
2 biosynthesis and can in consequence greatly affect a molecules bio- and physico-
3 chemical behavoir [120, 188]. Methyl transferases (MTs) catalyze the transfer of
4 a methyl group from the co-substrate SAM to an activated atom of the acceptor
5 molecule [188].

6 Between the highly complex core structures of natural products, which are
7 produced by a plethora of enzymes (e.g. poly ketide synthases (PKSs), non-
8 ribosomal peptide synthases (NRPSs), terpene cyclases), and the rather simple
9 alkyl-modification introduced by methylation, nature is missing some medium-
10 sized modifaction options that proceed as elegantly as the methylation by MTs.
11 Thus, natural products containing longer chain alkyl modifications like ethyl or
12 propyl moieties on O, N or S-centers have rarely, if ever been observed.¹

13 It has recently been shown however, that a wide array of SAM analogues are
14 used as co-substrates by a variety of MTs [188]. The majority of the work so far has
15 been done on protein methyl transferases (P-MTs) and DNA methyl transferases
16 (DNA-MTs), since epi-genetics and finding regions of gene-regulation is of great
17 interest. However, small molecule methyl transferases (*sm*MTs) have also been
18 shown to accept different SAM analogues [114, 116, 184, 187, 229]. There have been
19 a great many of SAM analogues synthesized, both chemically and enzymatically,
20 that were consequently studied with the help of MTs [44, 184, 188].

21 The *O*-methyl transferase (*O*-MT) PFOMT is a highly promiscuous enzyme with
22 regards to its flavonoid substrates and has extensively been characterized [22, 85,
23 109, 206]. However, the promiscuity towards different SAM analogues has net yet
24 been described. Combination of both, substrate and co-substrate promiscuity in the
25 small molecule MT PFOMT could provide a powerful tool towards the biosynthetic
26 production of novel small molecules with potentially new and promising biological
27 activities. Functionalization/Detection of substrates could furthermore provide a
28 means of finding new compounds/substrates in complex (e.g. biological) samples
29 analogous to activity based protein profiling (ABPP) approaches.

¹Reaxys searches for natural product isolates with a molecular mass between (150 and 1500) containing the substructures methyl, ethyl or propyl connected to a heteroatom return 66759, 2797 and 52 results respectively. However, it stands to note that 70 % of the propyl results were either esters or otherwise activated moieties. [53]

1 In this work we show, that PFOMT binds the co-substrate analogues SAH, SAM
2 and SAE with similar affinities. A newly developed crystal structure of the *apo*-
3 enzyme shows the fully resolved N-terminus is lodged in a cleft atop the active
4 site, closing it off. Although semi-rationally designed enzyme variants could not
5 afford enzymatic ethylation of substrates, the regio-selectivity of the methylation
6 reaction was altered.

7 5.2 Crystallization of PFOMT

8 The crystal structure of PFOMT was published in 2008, however binding of sub-
9 strates could not be accomplished [109]. Nonetheless, the demethylated co-substrate
10 SAH was cocrystallized. The first goal of this study was to crystallize the *apo*-form
11 of the enzyme, to obtain a system that allows for the soaking of substrates. At the
12 same time, PFOMT was to be cocrystallized along with an acceptor substrate and
13 the co-substrate analogs SAE and SAH.

14 At first the already available crystallization procedures were evaluated [109].
15 However, reproduction of these results could not be accomplished and new crys-
16 tallization conditions had to be found.

17 Several commercially available buffer solutions (see section 4.5) were screened
18 in combination with different protein solutions (e.g. solutions containing co-
19 substrates and acceptor substrates or not) to obtain protein crystals co-crystallized
20 with substrates or of the *apo*-form. Crystals were obtained in various wells after
21 a few days. The crystal shape varied from very smooth and almost cubic (high
22 ammonium sulfate) over sphreulites and intergrown crystals (CaCl_2 , PEG-4000) to
23 brittle and ragged needles (LiCl , PEG-6000) (Figure 5.1).

24 Crystals that were large enough ($\geq 50 \mu\text{m}$), where screened for diffraction at
25 the home-source after cryoprotection. A rough estimate of the resolution, cell
26 parameters and the space group was acquired, if the diffraction images could be
27 indexed. The screened crystals all had similar cell parameters and belonged to the
28 same space group, $P2_12_12_1$, as the previously published structure (pdb: 3C3Y)[109].
29 However, the unit cell of crystals that grew out of high ammonium sulfate concen-
30 trations ($\geq 1.8 \text{ M}$) was approximately four times as large as that of the published

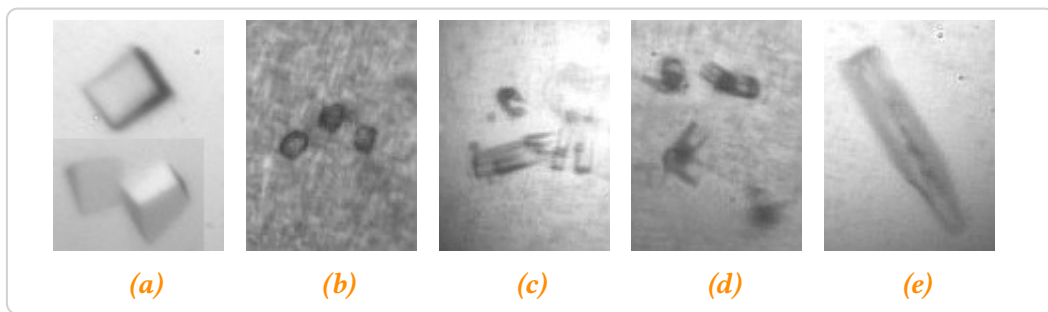


Figure 5.1.: Some crystal and pseudo-crystal shapes that were observed during the crystallization screen. a – high $(\text{NH}_4)_2\text{SO}_4$, b-c – CaCl_2 , PEG-4000, e – LiCl , PEG-6000

1 structure. Several datasets were collected of crystals from high $(\text{NH}_4)_2\text{SO}_4$, since
2 these seemed to be promising candidates to find differences in the bound substrates.
3 Datasets of crystals that grew from other conditions were insufficient for structure
4 solution.

5 **The crystal structure of *apo*-PFOMT**

6 PFOMT crystallized without any bound substrates under conditions of high
7 $(\text{NH}_4)_2\text{SO}_4$. One dataset was solved to completion to obtain a complete structure
8 of this novel *apo*-PFOMT at a resolution of 1.95 Å (Table A.1). The assymetric unit
9 of *apo*-PFOMT contained two homodimers (4 monomers) (Figure 5.2a), rather than
10 just one homodimer (3C3Y). The active site of each monomer was found to be
11 empty except for a sole sulfate ion, which was positioned where the amino- and
12 carboxylate groups of the SAH residue in the 3C3Y structure (Figure 5.2b). Shifts in
13 the structure of some loops were observed and contrary to the previously published
14 structure the entire N-terminus was resolved up to and including the His-tag.

15 The resolved N-terminus contained another N-terminal α -helix, which was
16 positioned in a cleft on the surface, where substrates may be bound [109]. This
17 interaction extends up to the His-tag. Considerable movement was observed in
18 different parts of the protein, when no substrate was bound, some of which can be
19 attributed to SAM and metal ion binding residues (Figure 5.3 and Figure A.1) as is
20 obvious for the loop region between β -sheet 1 and α -helix 4. Nonetheless, most of
21 the movement seemed to be restricted to areas, which are not directly involved in

- 1 the binding of either SAM or metal ions. However, all of the regions that moved
- 2 are located at or near the active site.
- 3 Unfortunately soaking of these “*apo*”-crystals did not afford binding of substrates.

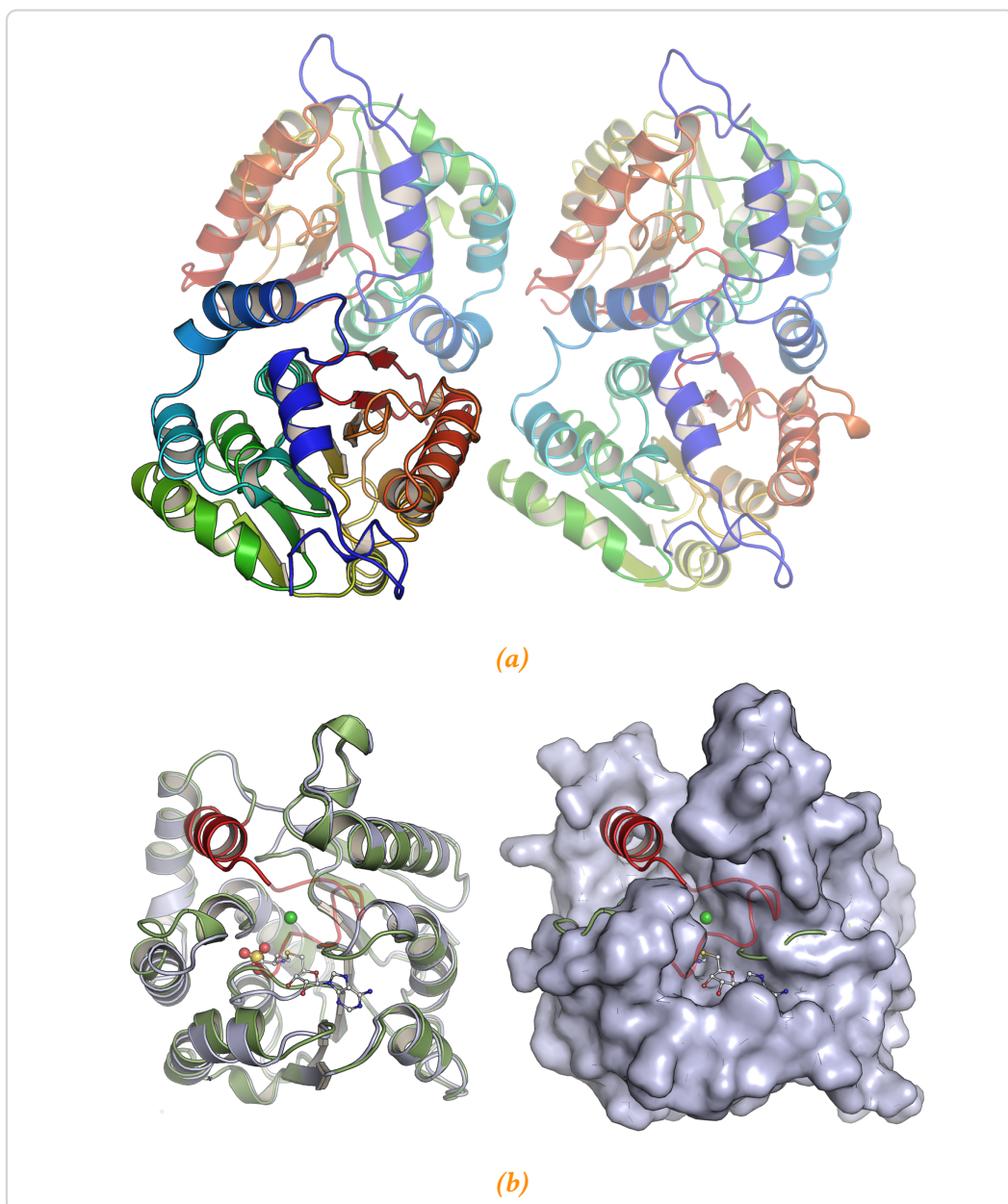


Figure 5.2.: An overview of the features in the apo-PFOMT structure. a – The assymmetric unit of apo-PFOMT consists of two homodimers (4 monomers). Individual monomers are rainbow colored from N- (blue) to C-terminus (red). b – Comparison of 3C3Y (steelblue) and apo-PFOMT (green). The N-terminus of apo-PFOMT was resolved up to the N-terminus (red) and even the His-tag (red, transparent) was partly resolved. The N-terminus fits into a cleft on the surface of the 3C3Y structure, shown as a surface model on the right. SAH (white ball-and-sticks) and Ca²⁺ (green sphere) are featured in the published structure, whereas a sulphate ion (red/yellow spheres) was bound in the newly solved structure.

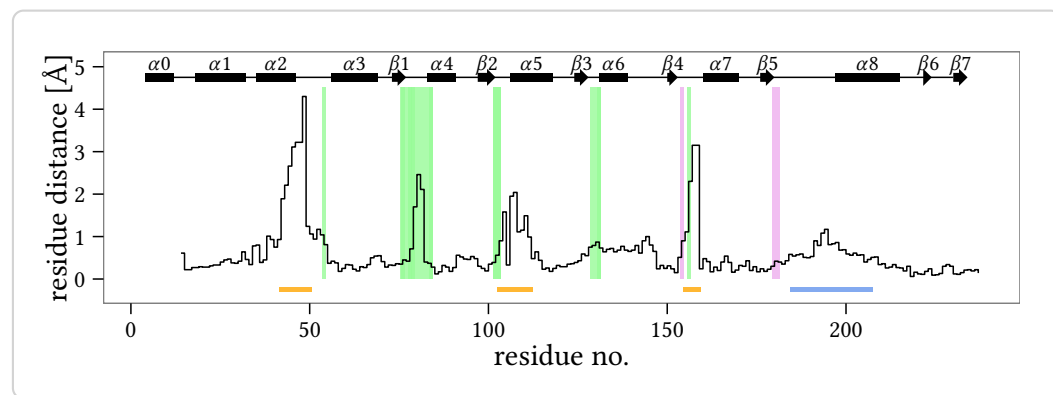


Figure 5.3.: Positional differences between the individual residues of the solved apo-PFOMT and the structure with bound SAH (pdb: 3C3Y). The diffraction precision indicator [46] (DPI) of the structures was (0.137 and 0.064) Å respectively. The overall rmsd amounted to 0.9034 Å. The secondary structure of apo-PFOMT is displayed at the top. Helices are displayed as rectangles and sheets are shown as arrows. Graphical background annotations are used to display the binding sites of SAH (green) and the metal ion (plum). The orange bars indicate regions, where much movement seems to happen upon binding or release of the co-substrate. The blue bar shows the region that was annotated as "insertion loop" in previous studies [109].

5.3 Substrate binding studies using ITC

The binding of different substrates to PFOMT was examined by Isothermal Titration Calorimetry (ITC), to determine whether the enzyme can bind non-natural SAM analogues. The homologues SAH, SAM and SAE were selected to also study the influence of the alkyl chain length on binding (Figure 5.4). Furthermore the binding of the substrate caffeic acid and the influence of Mg²⁺ addition on substrate binding was investigated.

The K_D values of SAH, SAM and SAE were all in the low micromolar range, around 2 μM. However, the binding enthalpy clearly decreased with the length of the aliphatic chain connected to the sulfur atom (Figure 5.5a). The binding of SAH, gave off more heat than the binding of SAM, which in turn gave off more heat than the binding of SAE (Table 5.1). Thus, the entropic influence must get larger with

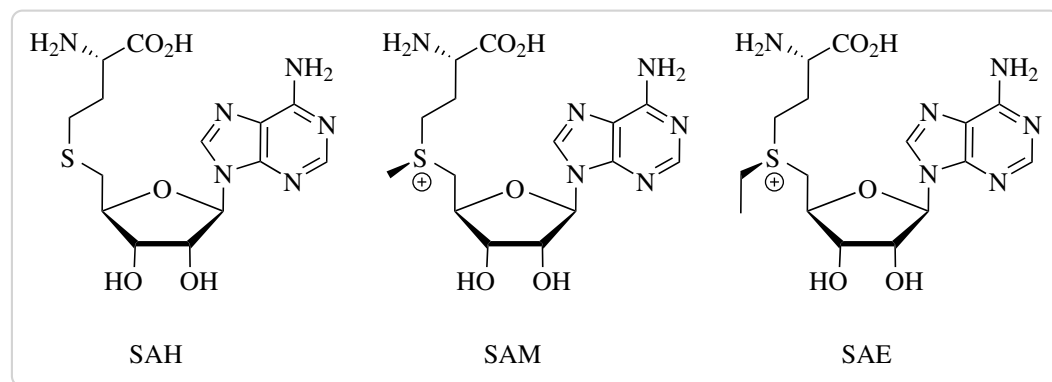


Figure 5.4: The binding of different SAM analogues was measured via ITC.

- 1 increasing chain length in order for equations (5.1) and (5.2) to still hold true.

$$\Delta G = \Delta H - T\Delta S \quad (5.1)$$

2

$$\Delta G = \Delta G^0 - RT \ln K \quad (5.2)$$

3 Indeed, the value for ΔS was negative for binding of SAH, but positive for
 4 the binding of SAM and SAE (Table 5.1). This relationship between the change of
 5 entropy and the change of enthalpy has been found for many biological systems and
 6 is called enthalpy-entropy compensation (EEC) [52, 71, 177]. The stoichiometry
 7 for the binding process is given by the parameter N . For all the ligands SAH, SAM
 8 and SAE this value was found to be about 0.5, which corresponds to one bound
 9 molecule ligand per dimer of PFOMT (Table 5.1).

10 Upon titration of caffeic acid to PFOMT small amounts of released heat were
 11 detected for the system (Figure 5.5c). When the enzyme was incubated with SAH
 12 prior to addition of caffeic acid the released heat was slightly increased. The slope
 13 of the ITC profile also got steeper. However, the data obtained could not be fitted to
 14 afford a sensible solution. When caffeic acid and Mg^{2+} were incubated with PFOMT
 15 prior to addition of SAH, the process of heat production as observed by ITC had a
 16 steeper slope (Figure 5.5b). Nonetheless, the thermodynamic parameters did not
 17 differ significantly. Mg^{2+} , in the form of an $MgCl_2$ solution, titrated to the enzyme
 18 solution did not cause signals during the ITC experiments.

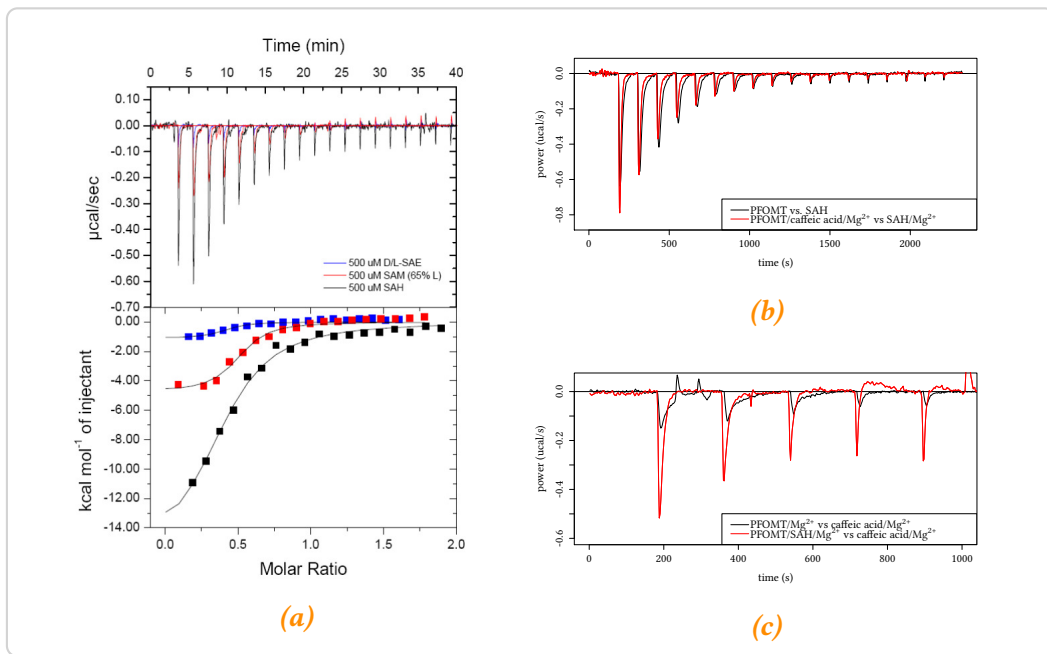


Figure 5.5: ITC measurements of PFOMT:effector binding. **a** – Binding of SAH, SAM and SAE to PFOMT. **b** – SAH is injected into a PFOMT solution, with (red) or without (black) addition of Mg²⁺ and caffeinic acid. When Mg²⁺ and caffeinic acid were already present, the binding process seems to happen quicker, but is less enthalpic. **c** – Upon addition of caffeinic acid to the protein heat is produced, however no sensible binding curve could be obtained.

Table 5.1.: Results of fitting a simple one-site binding model to the data obtained from ITC experiments.

	K_D [μM]	ΔH [cal mol^{-1}]	ΔS [cal $\text{mol}^{-1} \text{K}^{-1}$]	N
SAH	2.06 ± 4.27	$-10\,380 \pm 1025$	-9.41	0.505 ± 0.038
SAM	1.08 ± 3.50	-4606 ± 242	11.6	0.492 ± 0.018
SAE	2.22 ± 3.79	-1338 ± 190	21.3	0.513 ± 0.050

1 5.4 Study of variants for long-chain alkylations

2 Since the ability to bind the elongated analogue SAE was present in wild-type
 3 PFOMT, the activity of the PFOMT protein towards SAE was tested. Activity tests
 4 were performed with caffeic acid as substrate under standard reaction conditions.
 5 Unfortunately no ethylation of the substrate by PFOMT was observed, even after
 6 extended incubation times.

7 Consequently enzyme variants were prepared to achieve a PFOMT variant with
 8 an ethylation activity, since a number of groups were able to accomplish transalky-
 9 lation with larger substrates by expanding the available space in the active site
 10 [209]. The available crystal structures of PFOMT were consulted to select suitable
 11 residues. Residues that were exchanged were selected based upon their position
 12 in the active site and in relation to the substrate(s) (Figure 5.6). The residues were
 13 exchanged to the non-spaceous alanine, as well as amino acids frequently observed
 14 at homologous positions in other class I O-MTs.

15 Over 20 enzyme variants were prepared to assess, whether PFOMT ethylation
 16 activity would improve over the wild-type. However, no ethylation activity was ob-
 17 served for either variant. Some of the new variants however displayed an increased
 18 methylation activity with the substrates caffeic acid and SAM (Figure 5.7). The
 19 methylation activity of some of the variants increased by over 4-fold. Interestingly
 20 most amino acid substitutions proved as beneficial.

21 Methylation activity benifited greatly from the replacement of bulky hydrophobic
 22 residues by smaller and/or charged residues in the vicinity of the acceptor substrates
 23 (Tyr51, Trp184 and Phe198). However, this was not a general trend since the

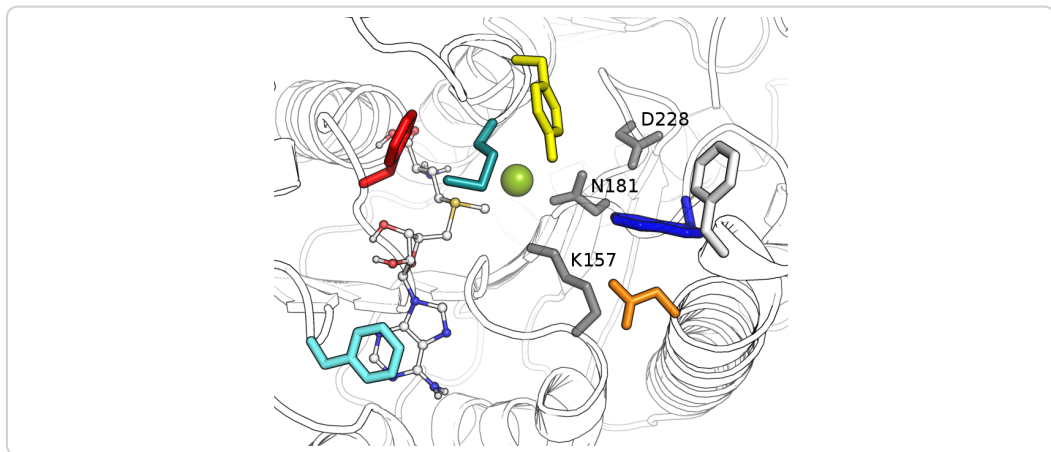


Figure 5.6.: The active site of PFOMT (pdb: 3C3Y). The outline of the protein backbone is displayed, with active site residues portrayed as colored sticks (cyan – F103, red – F80, turquoise – M52, yellow – Y51, white – F198, blue – W184, orange – N202, grey – as labelled). The co-substrate SAM (ball-and-stick model) was docked into the structure.

1 substitutions N202W and Y51W also improved methylation activity. Looking more
2 closely at residue Tyr51, the activity enhancing effect was greatest, when the
3 tyrosine was substituted by the basic amino acids lysine or arginine. In addition to
4 an enhanced activity the selectivity for the hydroxyl position to be methylated was
5 also altered in these variants. This was not apparent, when caffeic acid was used as a
6 substrate. However when a flavonoid, especially eriodictyol, was used not only the
7 3' hydroxyl, but to some extent the 4' hydroxyl was methylated (Figure A.2). This
8 effect was improved in some double variants, where also position 202 was altered.
9 For example the variant Y51R N202W almost exclusively methylated flavonoid
10 substrates at the 4' position. A detailed discussion of the results was published in a
11 peer reviewed journal.

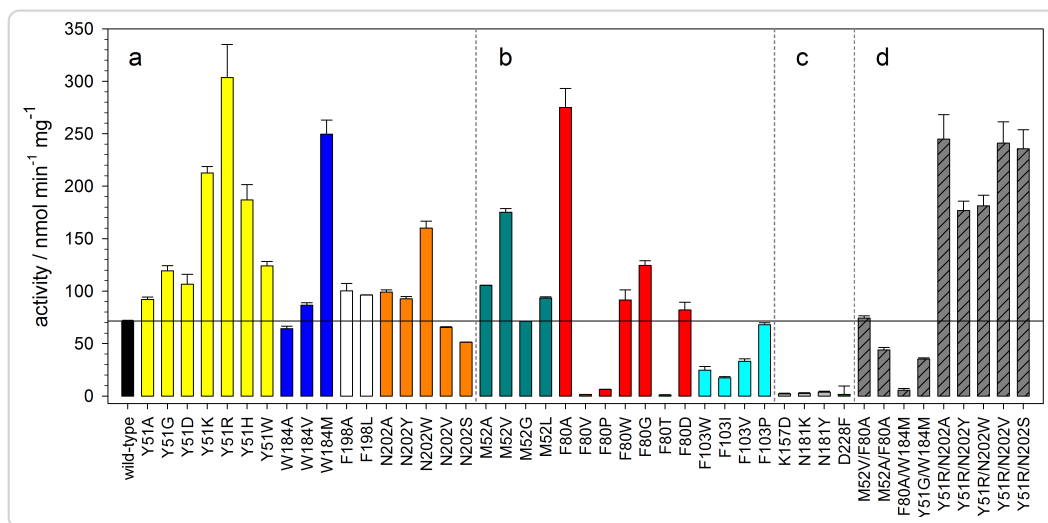


Figure 5.7.: Activities of different PFOMT variants towards caffeic acid methylation. Colorations correspond to the ones used in Figure 5.6.

1 5.5 Conclusion/Discussion

2 Whereas the binding of SAH was solely dependent on the large negative enthalpy,
 3 the binding of SAE was almost entirely driven by entropy, since ΔH was close to 0
 4 (Table 5.1). Entropy gain can be a major driving force for ligand-protein interactions
 5 and in some cases ligand binding can be entirely attributed this gain in entropy
 6 [123]. Displacement of protein-bound water molecules contributes strongly to the
 7 entropic gain. There were some waters present in the active site of PFOMT in
 8 the crystal structure developed herein. However, no metal ion was present in the
 9 active site in the *apo*-PFOMT structure. Furthermore Mg²⁺ titration via ITC did
 10 not afford significant signals, suggesting the notion, that the metal is only bound
 11 along with the co-substrate (Figure 5.8). It has been suggested, that the entropy cost
 12 to transfer one water molecule from bulk to the protein-bound state can be up to
 13 7 cal mol⁻¹ K⁻¹ [51]. The replacement of ordered waters from the active site or from
 14 a hydrated metal ion by a growing aliphatic chain could therefore explain the gain
 15 in entropy, and SAH is positioned in a way to warrant exactly that (Figure 5.8). Also,
 16 the hydrogen and metal complexing bonds consequently lost could explain the less
 17 negative enthalpy. However, this is purely hypothetical since more evident data

is missing. Additional insight might be gained by expanding the ITC experiments to even longer SAM analogues. The limited space in the active site, which forces the growing side chain to expel water and possibly the metal ion might also be the reason for the inactivity of PFOMT towards SAE. If the metal ion is blocked from its complexing moieties, activation of the substrate hydroxyl would be hindered.

Comparison of the novel *apo*-PFOMT and the published structure (pdb: 3C3Y) suggests that the movement (upon ligand binding) along multiple parts of the backbone proximal to the active site pocket is a main contributor to the overall rmsd of 0.9 Å (Figure 5.3).

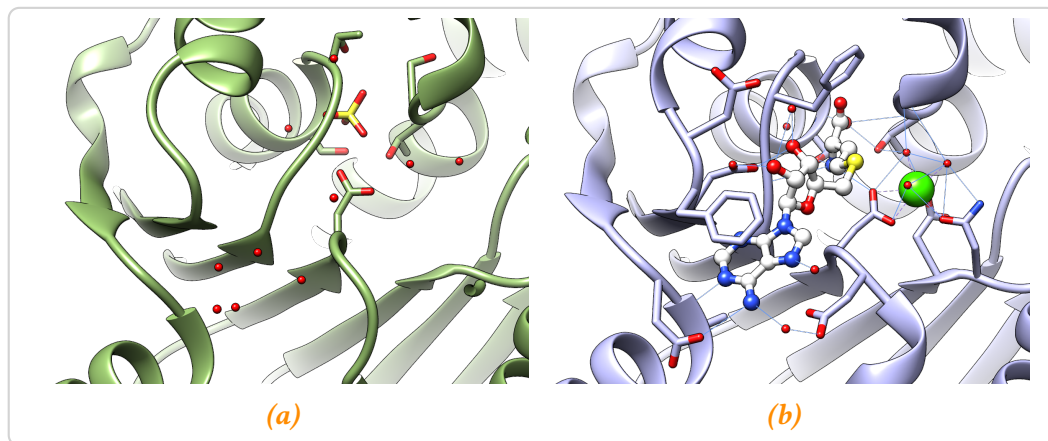


Figure 5.8.: Comparison of the active sites of **a – the solved apo-structure (green) and **b** – the ligand-bound structure (steelblue; pdb: 3C3Y). Waters are represented as small red spheres, calcium as a green sphere (complexing bonds are dashed) and SAH is displayed as a white ball-and-stick model. A possible hydrogen bond network (blue lines) for the ligand-bound state is displayed.**

The N-terminus of PFOMT seems to act as a lid, which is closed in the *apo*-form, but highly flexible and therefore unresolved in the ligand bound form. Furthermore, the native enzyme has been shown to be truncated, starting only at residue 12 and being less catalytically efficient than the full length protein [109, 206]. The work presented here consequently supports the notion that the N-terminus plays an important role on the regulation of the enzymatic activity.

During our studies, transethylation activities could not be observed for any of the prepared PFOMT variants. However, some of the variants showed higher

1 methylation activities towards caffeic acid and even different regioselectivities
2 ($3' \rightarrow 4'$) than the wild-type.

3 Given the fact that only residues in the active site and therefore in direct contact
4 with the substrates were prepared, the laid out findings provide novel hints for
5 indirect proximal regions in the PFOMT structure that might be studied using site-
6 directed mutagenesis, gene-shuffling or similar approaches in order to work towards
7 a variant that can in fact employ SAE for transalkylation reactions. Furthermore
8 variation of these regions might provide variants with altered substrate specificities
9 which are of high interest.

10 **5.6 Contributions**

11 Benjamin Weigel wrote the manuscript, prepared figures, sub-cloned, produced and
12 crystallized PFOMT, solved the *apo*-structure and conducted the ITC experiments.
13 Dr. Martin Dippe prepared most of the PFOMT variants and ethylation activity tests.
14 Dr. Christoph Partier (group of Prof. Dr. Milton T. Stubbs, MLU Halle-Wittenberg)
15 helped collect X-ray datasets.

¹ **6 Tandem mass-spectrometry stud-**
² **ies of flavonoids**

1

Comparative CID and HCD MS/MS studies for the characterization of flavanoid aglycones

Benjamin Weigel^{1,a}, Annegret Laub^{1,b}, Jürgen Schmidt^{1,c}, Ludger A. Wessjohann^{1,d}

Contact: bweigel@ipb-halle.de^a, alaub@ipb-halle.de^b, jschmidt@ipb-halle.de^c, law@ipb-halle.de^d

Affiliation: Leibniz-Institute of Plant Biochemistry, Department of Bioorganic Chemistry¹

Keywords: tandem mass spectrometry, LCMS, flavonoids

3

Abstract

Flavonoids are an important class of natural compounds and make up a large part of the world's biomass. Due to their anti-inflammatory and anti-oxidant properties, many health benefits are associated with flavonoids and there is a growing interest to use flavonoids in medicinal and dietary contexts. The availability of methods that provide for a quick and reliable identification of flavonoids from different sources is therefore essential. In this work a range of flavonoids was studied using liquid chromatography coupled mass-spectrometry (LC/MS). Two modes of activation, namely CID and HCD, were evaluated to study fragmentation of flavonoids from their $[M+H]^+$ molecular ions. It was found, that HCD outperformed CID in the ring-fragmentations of methylated flavonoids. Together, both methods provide complementary information that can be used to distinguish different types of flavonoids.

15

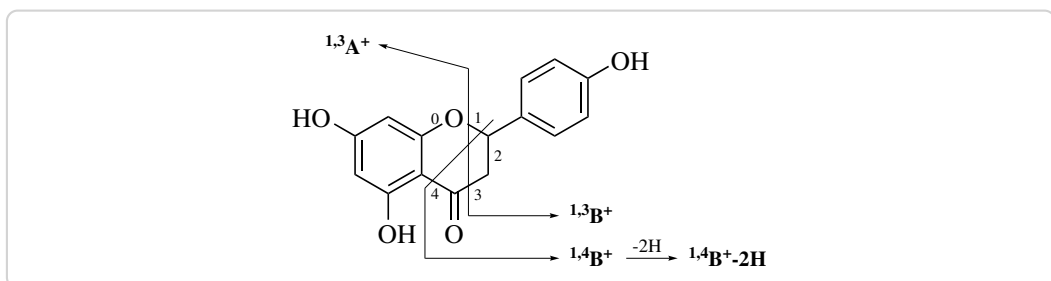
6.1 Introduction

Liquid chromatography-tandem mass spectrometry (LC-MS/MS) has been widely used for the identification of compounds from complex samples, such as crude mixtures from plant or bacterial extracts and is an unexpendable method in the field of metabolomics [56, 124, 128, 169].

1 Ionization of samples in LC-MS/MS instruments is usually achieved by soft
2 methods operating at atmospheric pressure, such as electrospray ionization (ESI)
3 [212] or atmospheric pressure chemical ionisation (APCI) [79]. However, small
4 molecules rarely produce fragment ions under these conditions and usually only the
5 $M+H]^+$ or $M-H]^-$ of the molecular ion is observed. A range of different approaches
6 has been used to circumvent this draw-back. The most direct approach is to use
7 electron ionization (EI), where the analytes are bombarded with electrons, for
8 ionization. However, EI is operating under high-vacuum and the coupling with
9 liquid chromatography (LC)-systems is not trivial [203]. In order to still generate
10 fragments in liquid chromatography coupled mass-spectrometry (LC/MS) MS/MS
11 methods such as collision induced dissociation (CID) or surface-induced dissociation
12 (SID) were developed [185].

13 Flavonoids comprise a huge chemical space, with millions of theoretical structures
14 [213]. Due to their biological activities and associated health benefits, applications to
15 quickly identify and characterize these compounds are of special interest. Already,
16 a number of studies have been published that show how MS/MS-approaches using
17 CID can aid in the structural characterization of flavonoids [28, 41, 58, 67, 83, 117,
18 121, 131, 136, 137]. Researchers have reported that specific patterns of fragmentation
19 along the C-ring can be observed for different classes of flavonoids and can help
20 differentiate between them [41, 131]. However, it was found that the cleavage of the
21 C-ring is less commonly observed for flavonoids methylated at the B-ring, while
22 the loss of small molecules becomes predominant [41, 131].

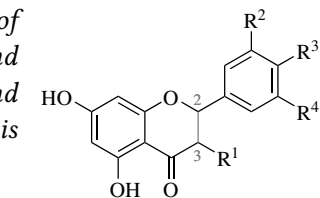
23 Fragments of flavonoid aglycones can be represented by a systematic nomenclature
24 first proposed by Ma *et al.* [131]. The labels i,jA^+ and i,jB^+ refer to fragments
25 containing an intact A or B ring, with the superscripts *i* and *j* denoting the bonds
26 of the C-ring that were broken (Scheme 6.1). Our group currently works with
27 methyl transferases that act on flavonoids. Identifying the site of methylation is a
28 crucial step in identifying the product of an enzymatic methylation. MS/MS has
29 been shown to be a rather quick and reliable method to identify characteristic key
30 ions of flavonoids, that can help identify the localization of different functional
31 groups [41, 58, 110, 130, 131]. In this work the complementarity of two activation
32 methods, CID and higher-energy collisional dissociation (HCD), for the structural



Scheme 6.1: Ion fragment nomenclature of flavonoid aglycones as proposed by Ma et al., illustrated on naringenin. Ions are labelled according to the ring they contain and the positions of the C ring that were broken. Thus $^{1,3}A^+$, contains the ring A and bonds 1 and 3 of the C ring were broken.

- 1 characterization of flavonoids (Table 6.1), especially those methylated at the B-ring,
- 2 in positive ionization mode was evaluated. An specific array of different flavonoids
- 3 (Table 6.1) was studied, to get a holistic impression of the fragmentations of these
- 4 compounds.

Table 6.1: Substrates studied in this work. Three classes of flavonoids were tested: flavanones (**1-5**), flavones (**6-10**) and flavonols (**11-15**). The topology of the bond between C2 and C3 in the C-ring specifying flavanones or flavones/flavonols is denoted with - (single) or = (double), respectively.



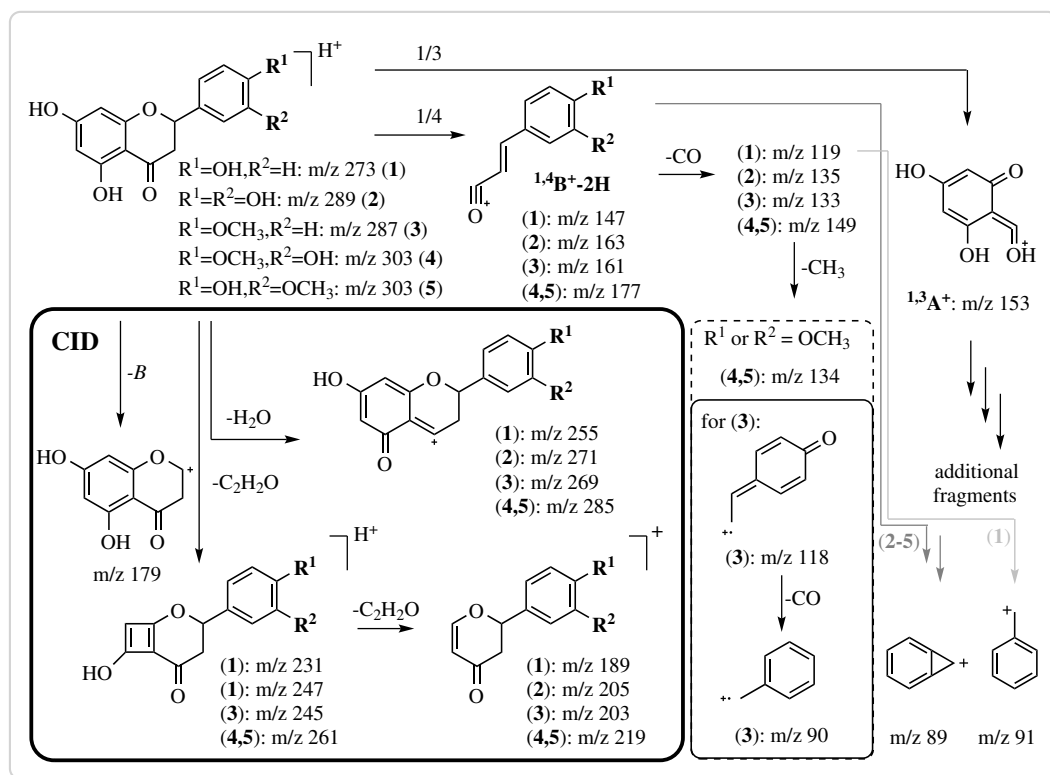
	name	[M+H] ⁺	C2-C3	R ¹	R ²	R ³	R ⁴
1	naringenin	273	-	H	H	OH	H
2	eriodictyol	289	-	H	OH	OH	H
3	ponciretin	287	-	H	H	OCH ₃	H
4	hesperetin	303	-	H	OH	OCH ₃	H
5	homoeriodictyol	303	-	H	OCH ₃	OH	H
6	apigenin	271	=	H	H	OH	H
7	luteolin	287	=	H	OH	OH	H
8	acacetin	285	=	H	H	OCH ₃	H
9	diosmetin	301	=	H	OH	OCH ₃	H
10	chrysoeriol	301	=	H	OCH ₃	OH	H
11	kaempferol	287	=	OH	H	OH	H
12	quercetin	303	=	OH	OH	OH	H
13	myricetin	317	=	OH	OH	OH	OH
14	kaempferide	301	=	OH	H	OCH ₃	H
15	isorhamnetin	317	=	OH	OCH ₃	OH	H

6.2 Fragmentation of flavanones

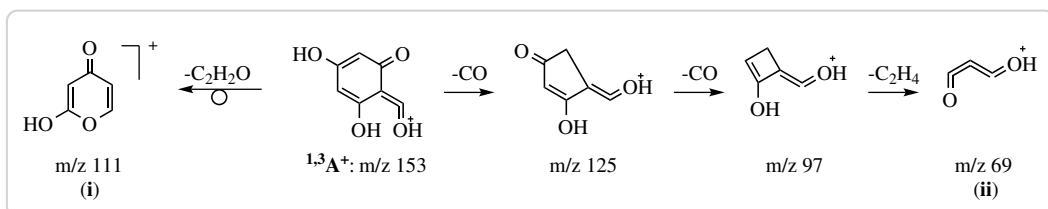
Positive ionization MS² spectra of flavanones (Table B.1) are mostly characterized by a base peak at *m/z* 153, which corresponds to the A-ring fragment ^{1,3}A⁺ of the flavonoid skeleton (Scheme 6.2). In contrast, negative mode MS² spectra of 3,7-dihydroxy flavanones show an *m/z* 151, which correspond to the negatively charged ^{1,3}A⁻ ion [58]. Even when *m/z* 153 was not the base peak, it was still dominant in the spectrum with intensities ranging between 20 % and 77 %. Peaks corresponding to the molecular ions [M+H]⁺ were not observed for any of the flavanones. The structure of the ion ^{1,3}A⁺ corresponding to *m/z* 153 is the same for all compounds (**1**) to (**5**) (Scheme 6.2). Peaks corresponding to mass-to-charge ratio (*m/z*) values of the respective (^{1,4}B⁺-2H) ions are also present in the mass spectra of each flavanone. Apart from the ions ^{1,3}A⁺ and (^{1,4}B⁺-2H), the CID- and HCD-mass spectra of the

1 flavanones differ significantly. CID mainly triggers neutral losses directly from the
 2 molecular ion. Losses of water (18 Da) and one or two ketene units (C_2H_2O , 42 Da)
 3 are predominant and afford ions of relatively high masses (Scheme 6.2) [96].

4 Fragment ions from cleavage of the C-ring ($^{1,3}A^+$ and $^{1,4}B^+-2H$) are further de-
 5 composed under the higher energy conditions in HCD experiments. Thus, the
 6 resulting HCD spectra generally display smaller m/z than the CID spectrum (Fig-
 7 ure 6.1). Increasing the normalized collision energy (NCE) from 75 to 100 % in HCD
 8 experiments further increased fragmentation. This is made clear by the increasing
 intensities of smaller fragments upon raising the NCE (Figure 6.1).



Scheme 6.2: Major fragmentation pathways of flavanones. Activation using CID conditions at 45 % NCE mainly results in neutral losses of H_2O and ketene (C_2H_2O) from the molecular ion $[M+H]^+$ (bold frame). These neutral losses are scarcely observed when HCD with a NCE of 75 % or 100 % is used for activation. Here, C-ring cleavages followed by neutral losses from the cleavage fragments are dominant.



Scheme 6.3: Proposed MS^2 fragmentation of ${}^{1,3}\text{A}^+$ after HCD activation. In high energy MS^2 experiments, ${}^{1,3}\text{A}^+$ might loose two CO followed by an unusual C_2H_4 . A single loss of ketene ($\text{C}_2\text{H}_2\text{O}$) to afford $\text{m/z } 111$ is also sensible.

1 Further fragmentation of ion (${}^{1,4}\text{B}^+ - 2\text{H}$) seems to depend on the substituents of
2 the B-ring. Only (${}^{1,4}\text{B}^+ - 2\text{H}$) from eriodictyol (**2**) loses a water, as suggested by a peak
3 at $\text{m/z } 145$. However, the loss of CO is the most prominent decomposition of (${}^{1,4}\text{B}^+ -$
4 2H). The intensities of the peaks corresponding to the (${}^{1,4}\text{B}^+ - 2\text{H}-\text{CO}$) fragment
5 were as high as 36 % in HCD experiments (Figure 6.1). Naringenin (**1**) seems to
6 sequentially lose two CO in HCD mode to afford $\text{m/z } 91$ (intensities at 75 and 100 %
7 NCE at 24 and 100 %, respectively). This m/z is a strong indicator of a benzylum or
8 tropylum cation (Scheme 6.2). Decay of (${}^{1,4}\text{B}^+ - 2\text{H}$) of the other flavanones likely
9 leads to a stable bicyclo[4.1.0]heptatrienyl cation as the high intensity of peak
10 $\text{m/z } 89$ in HCD mode suggests. Methylated flavanones (**3**), (**4**) and (**5**) show a loss
11 of CO followed by a loss of a methyl radical (${}^{1,4}\text{B}^+ - 2\text{H}-\text{CO}-\text{CH}_3\cdot$), as suggested by
12 the respective m/z values of 118 and 134. Another CO loss from this fragment is
13 possible for ponciretin (**3**) to produce an ion $\text{m/z } 90$, which is at 49 % intensity in the
14 HCD spectrum recorded with NCE of 75 %. The evidence suggests, that this ion's
15 structure is best described by a benzylum/tropylum radical cation (Scheme 6.2). It
16 is proposed, that ion ${}^{1,3}\text{A}^+$ can decompose via two different pathways under HCD
17 conditions (Scheme 6.3). A loss of ketene from ${}^{1,3}\text{A}^+$ results in $\text{m/z } 111$. Pyranone
18 (**i**) is suggested as a structure for this ion. Sequential losses of two CO and a C_2H_4
19 could afford ion (**ii**). However, further MS^n experiments are necessary to confirm
20 these proposals.

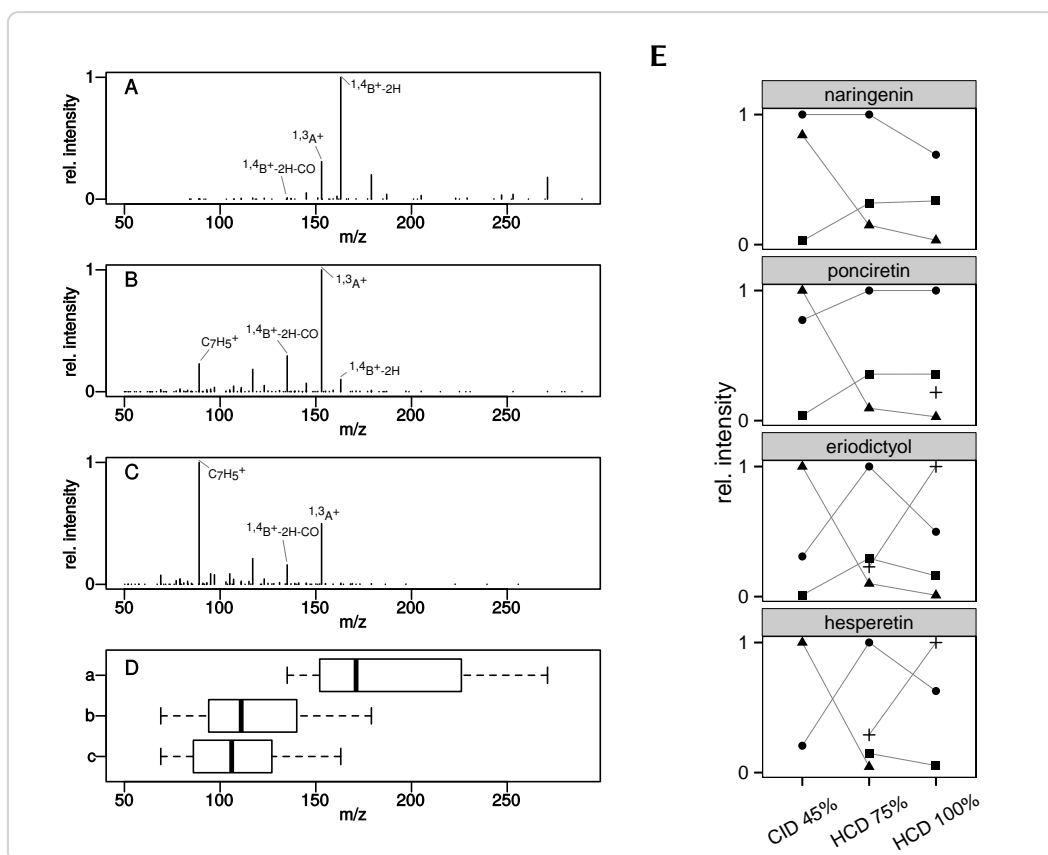
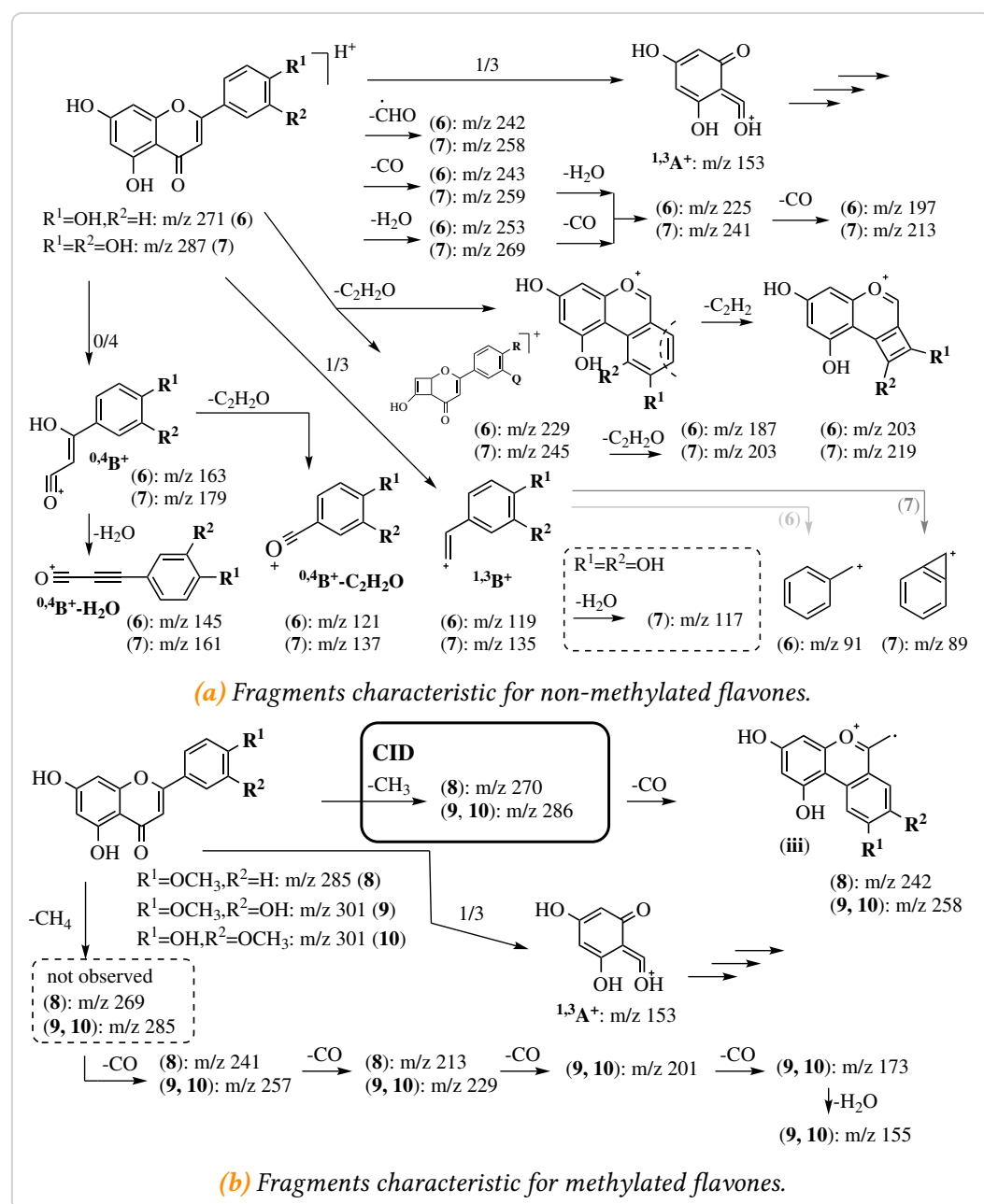


Figure 6.1: Comparison of CID and HCD MS^2 spectra of eriodictyol (2). **A** – CID at 45 % NCE. **B** – HCD at 75 % NCE. **C** – HCD at 100 % NCE. Four different prominent peaks are annotated in each spectrum. **D** – The shift to smaller masses in HCD spectra and with increasing NCE is illustrated by the boxplot of the distribution of peaks with relative intensities above 1 % in each of the above spectra. **E** – Relationship between the activation method and the intensity of four fragments (● $1,3A^+$, ▲ $(^{1,4}B^+-2H)$, ■ $(^{1,4}B^+-2H-CO)$, + $C_7H_5^+$) of different flavanones.

1 6.3 Fragmentation of flavones

2 The principle fragmentation of flavone aglycones apigenin (**6**), luteolin (**7**), acacetin
3 (**8**) and chrysoeriol (**10**) in positive mode CID tandem mass spectrometry was
4 discussed previously [110, 131]. Non-methylated (**6**, **7**) and methylated flavones
5 (**8 – 10**) show significantly different MS² spectra (Table B.2). Apigenin (**6**) and
6 luteolin (**7**) MS² spectra show a characteristic *m/z* 153, corresponding to the ^{1,3}A⁺
7 ion, as a base peak in CID mode and at low activation energies in HCD mode
8 (Scheme 6.4). Contrary to the flavanones, the MS² of non-methylated flavones
9 show the peak corresponding to the molecular ion [M+H]⁺, which is strongest in
10 HCD at NCE of 75 %. Characteristic neutral losses of water, CO and ketene (C₂H₂O)
11 were also observed for (**6**) and (**7**) (Scheme 6.4, Table B.2). MS-peaks corresponding
12 to a loss of a formyl radical, resulting in [M+H-CHO]^{•+} were also observed for
13 (**6**) and (**7**). Loss of ketene is proposed to proceed via two different pathways,
14 such that further neutral losses of another ketene, or C₂H₂ might be explained
15 (Scheme 6.4). Besides the characteristic ^{1,3}A⁺ fragment, apigenin (**6**) and luteolin
16 (**7**) MS² spectra also present peaks corresponding to the B-ring fragments ^{1,3}B⁺
17 (*m/z* 119 and 135) and ^{0,4}B⁺ (*m/z* 163 and 179). From the mass differences of these
18 fragments, the substitution on the B-ring can be deduced. The ^{0,4}B⁺ ion might
19 further degrade by neutral losses of ketene (32 Da) or water (18 Da). The base peaks
20 at a NCE of 100 % in HCD, *m/z* 91 (**6**) and *m/z* 89 (**7**), are most likely due to a further
21 decomposition of ^{1,3}B⁺ in a fashion similar to the flavanones to afford a benzylum
22 or bicycloheptatrienyl cation respectively (Scheme 6.4).

23 The most noteable difference between the methylated and non-methylated rep-
24 resentatives is the almost complete lack of any fragmentation of the methylated
25 flavones other than a methyl loss, in CID experiments (Table B.2, Figure 6.2). A
26 relatively stable radical cation is formed after the loss of a methyl group, due to the
27 fact that the whole system is essentially conjugated (Scheme 6.5). Any other loss
28 would break this conjugation and therefore requires a higher activation energy.
29 HCD experiments at NCE of (75 to 100) % were suitable to fragment the methylated
30 flavones (**8–10**). The base peak in the HCD spectra of (**8**) (*m/z* 242) and (**9**, **10**)
31 (*m/z* 257) at 75 % NCE was attributed to another loss of CO from the [M+H-CH₃]^{•+}



Scheme 6.4: Major fragmentation pathways of non-methylated and methylated flavones. Multiple neutral losses of small molecules (e.g. CO, water or ketene) and 0/4 and 1/3 C ring cleavages are predominant in the MS² spectra of non-methylated flavones. Methylated flavones loose a methyl group in CID experiments, but only in HCD experiments do other fragmentation reaction become obvious.

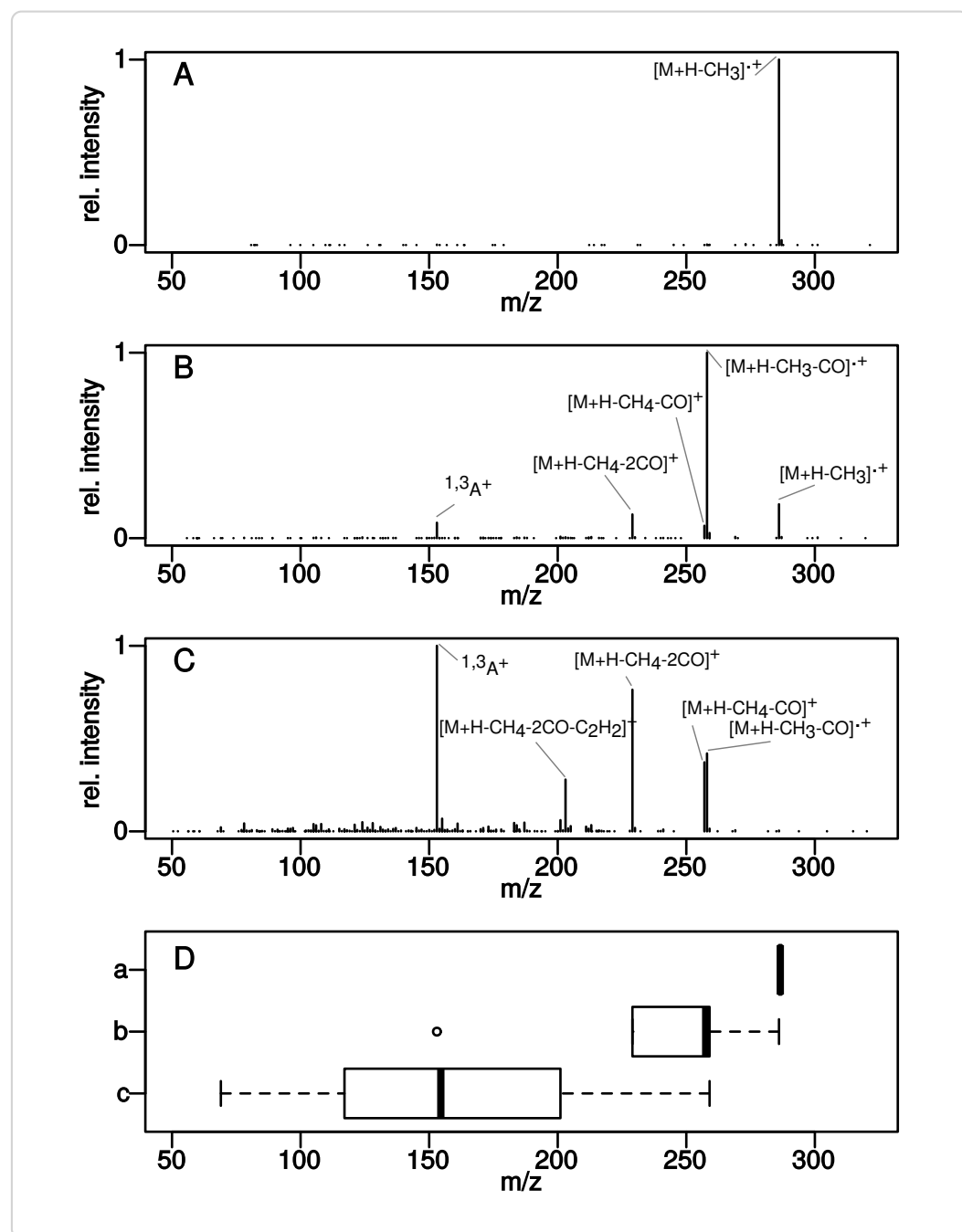
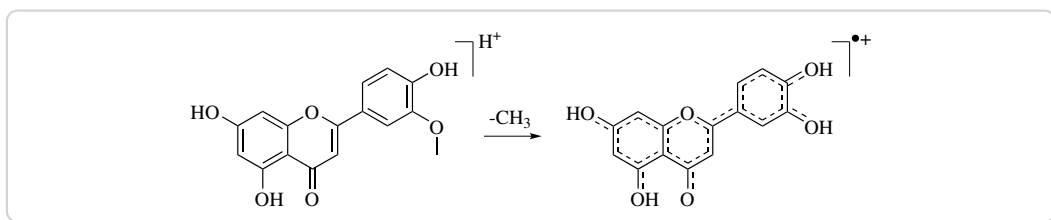


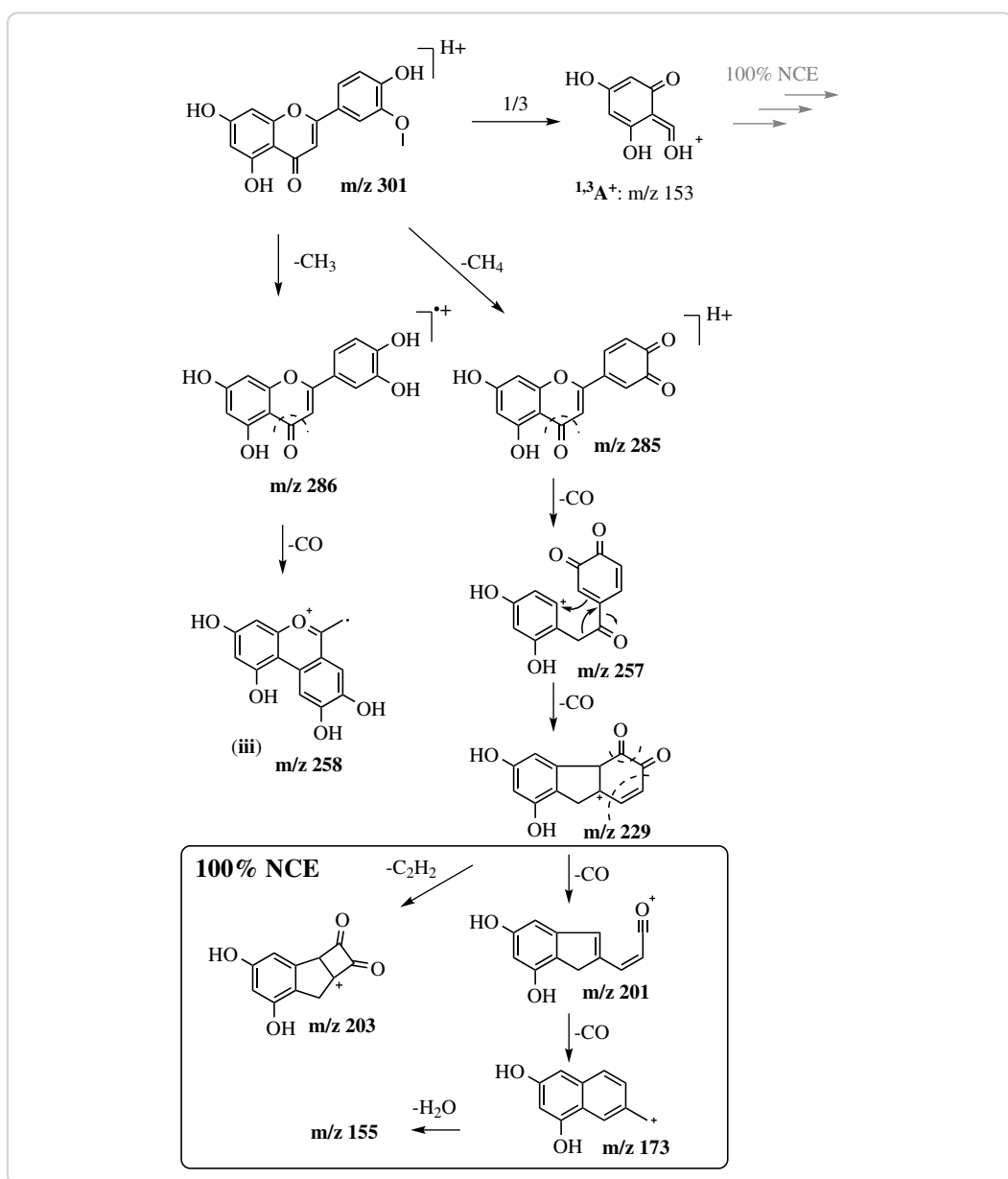
Figure 6.2.: Comparison of CID and HCD MS² spectra of chrysoeriol (10**). **A** – CID at 45 % NCE. **B** – HCD at 75 % NCE. **C** – HCD at 100 % NCE. Four different prominent peaks are annotated in each spectrum. **D** – The shift to smaller masses in HCD spectra and with increasing NCE is illustrated by the boxplot of the distribution of peaks with relative intensities above 1 % in each of the above spectra.**



Scheme 6.5: Stability of the $[M+H-CH_3]^{•+}$ ion of flavones. The $[M+H-CH_3]^{•+}$ ion of methylated flavones like diosmetin is highly stabilized by resonance, explaining the high intensity of the corresponding peak and limiting its fragmentation at low activation energies.

1 ion, while the base peak m/z 153 at 100 % NCE likely corresponds to the $^{1,3}A^+$ ion
 2 (Figure 6.2). Further losses from $[M+H-CH_3-CO]^{•+}$, with the proposed structure of a
 3 benzochromenylium radical cation (**iii**), were not observed (Scheme 6.4, Table B.2).
 4 Mass-to-charge ratios of 241 (**8**) and 257 (**9, 10**) were attributed to a neutral loss of
 5 methane (CH_4), followed by a loss of CO (Scheme 6.4, Scheme 6.6). Interestingly,
 6 the abundance of a peak corresponding to a $[M+H-CH_4]^+$ ion was below 1 % in all
 7 spectra, illustrating its susceptibility for additional losses. The fragment $[M+H-$
 8 $CH_4-CO]^+$ on the other hand might undergo further neutral losses of up to three
 9 CO (compounds **10** and **9**) as is illustrated for chrysoeriol in Scheme 6.6. However,
 10 instead of additional CO losses, fragment $[M+H-CH_3-2CO]^{•+}$ of (**10**) or (**9**) might
 11 as well loose a C_2H_2 (Scheme 6.6), as suggested by the MS^2 spectra (Table B.2). The
 12 only C-ring fragmentation of the methylated flavones (**8–10**) occurs at positions 1/3,
 13 as the observed m/z 153 ($^{1,3}A^+$) suggests. The higher energy MS^2 spectra suggest,
 14 that the $^{1,3}A^+$ fragment might deteriorate further in the same manner as described
 15 for the flavanones (Scheme 6.3). Numerous minor peaks in the MS^2 HCD spectra of
 16 compounds (**8–10**) could not be assigned a fragment or structure, but many even
 17 numbered m/z values suggest quite complex rearrangements.

18 The general trend of smaller sized fragments at higher activation energies is also
 19 true for flavones (Figure 6.2).

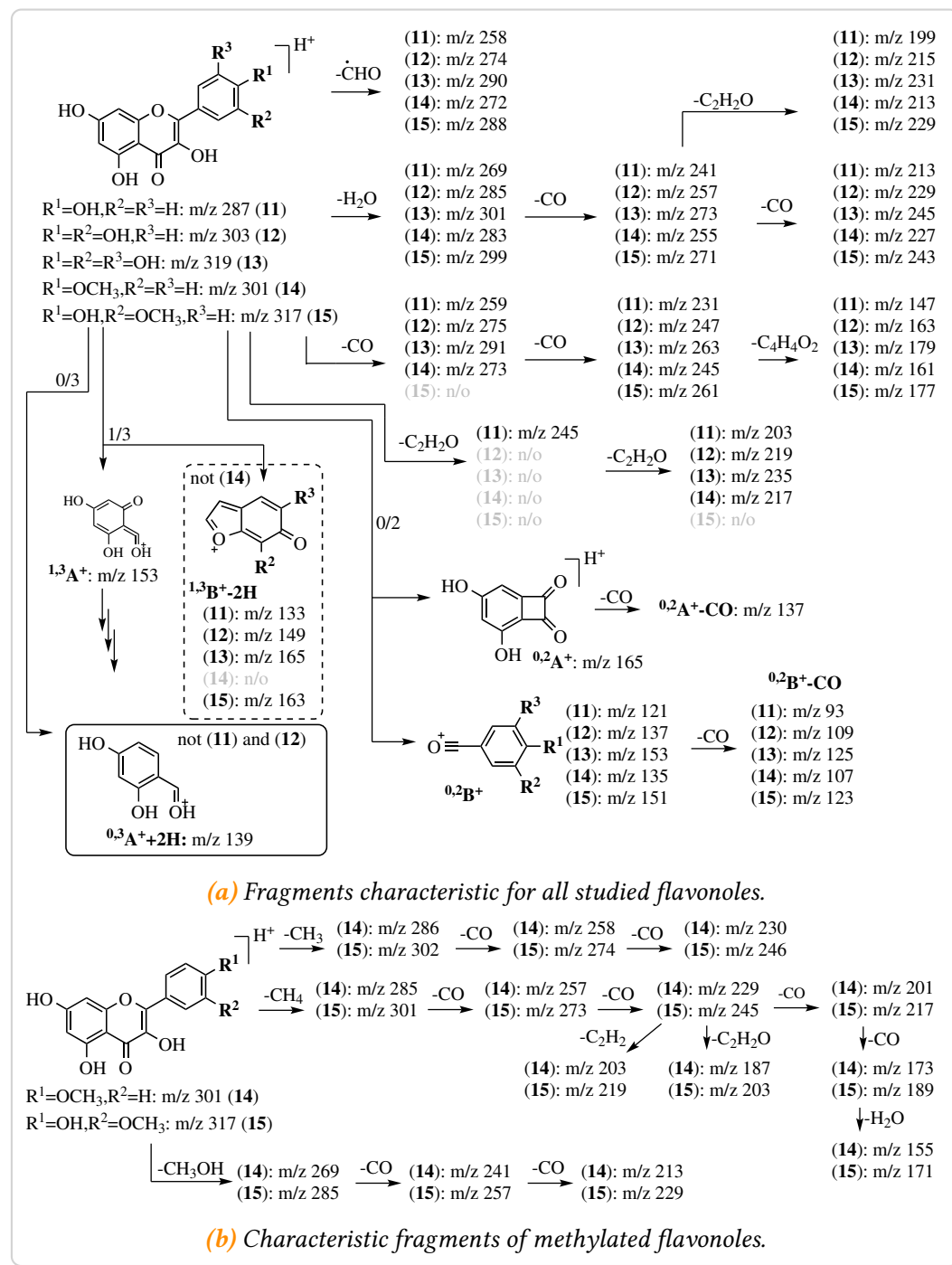


Scheme 6.6: Proposed pathway of fragmentation of (10) after HCD activation. Losses of CH_3^+ and CH_4^+ , followed by loss of CO are the major fragmentations observed in the corresponding MS spectra. However, multiple losses of CO only occur after a loss of methane (CH_4), possibly due to the relative stability of the benzochromenylium radical cation (iii). At 100 % NCE even higher order fragmentations were observed.

1 6.4 Fragmentation of flavonols

2 The principle fragmentation pathways of kaempferol (**11**), quercetin (**12**), myricetin
3 (**13**) and isorhamnetin (**15**) in CID tandem mass spectrometry have been previously
4 reported [131, 136, 220]. Other than flavones, methylated and non-methylated
5 flavonols share similar fragment(ation)s. Whereas in CID methylated flavones
6 hardly showed any fragmentation beyond a methyl loss, methylated flavonoles
7 kaempferide (**14**) and isorhamnetin (**15**) exhibited the same losses as their non-
8 methylated counterparts, albeit at a much lower level (Table B.3, Scheme 6.7 and
9 6.3). These observations are in full agreement with previous reports [131] and hold
10 true in CID as well as HCD measurements. The observed losses from the molecular
11 ion $[M+H]^+$ are essentially the same as those that were described for the flavones
12 (**6**, **7**) (compare Scheme 6.7 and 6.4). Lots of high intensity peaks presented in the
13 MS² spectra of flavonoles and the base peaks changed between compounds. The
14 base peak of (**11**) in the CID spectra was at *m/z* 165, which corresponds to the ^{0,2}A⁺
15 fragment (Scheme 6.7). The signals *m/z* 257 and 273 corresponding to the $[M+H-$
16 $H_2O]^+$ ions were the base peak in the CID-MS² spectra of (**12**) and (**13**) respectively.
17 The $[M+H-CH_3]^{•+}$ ions were highly abundant in the CID experiments of (**14**) and
18 (**15**). The base peak of (**15**) *m/z* 302 corresponds to this fragment. Fragment ^{0,3}A⁺
19 +2H) fits the *m/z* 139, which was the base peak in the CID spectrum of (**14**). The
20 MS signal *m/z* 153 corresponding to fragment ^{1,3}A⁺ was at low abundance in CID
21 spectra, especially for the methylated falvonols (Figure 6.3). However, in HCD
22 experiments *m/z* 153 was the base peak of all flavonols, except kaempferide (**14**)
23 where *m/z* 229 was at 100 % relative intensity.

24 Neutral losses of CO, water or a formyl radical are suggested by the collected
25 spectra (Scheme 6.7, Table B.3). Only for kaempferol (**11**), a neutral loss of 42 Da
26 corresponding ketene was observed. However, MS² spectra of all flavonols, except
27 (**15**), contained signals that could be assigned to the ion $[M+H-2C_2H_2O]^+$, suggest-
28 ing a loss of two ketene units. This advocates the notion that the $[M+H-C_2H_2O]^{•+}$
29 ion of flavonols might be highly unstable. Other than the flavones, flavonoles can
30 loose two sequential CO and another C₄H₄O₂, confirming previously published
31 data [131]. The spectra furthermore suggest, that the $[M+H-H_2O-CO]^+$ fragment of



Scheme 6.7: Major fragmentation pathways of flavonoles. Unlike flavones, methylated and non-methylated flavonoles share common fragmentations, albeit signals corresponding to small molecule losses are typically small for methylated analogues. Ring fragments observed typically correspond to the cleavage along bonds 0/3 or 0/2. Methylated flavonols shared common fragments with the methylated flavones. However, loss of methanol and a couple CO was also observed. n/o – not observed (relative intensity <1 %).

1 flavonols can loose another 42 Da (C_2H_2O), which was not spotted previously. The
2 data also clearly show, that neutral losses off of the molecular ion are most abundant
3 in CID experiments, whereas the shift to smaller masses in HCD experiments is
4 obvious (Table B.3, Figure 6.3).

5 The studied flavonoles all displayed an MS signal at m/z 153 corresponding
6 to the $^{1,3}A^+$ fragment, just as the flavanones and flavones with a 5,7-dihydroxy-
7 substitution of the A-ring did. This further highlights the diagnostic nature of
8 the $^{1,3}A^+$ fragment of flavonoids in MS/MS spectra. At higher energies, $^{1,3}A^+$ can
9 further decompose in a manner discussed in the previous sections (Scheme 6.3).
10 Characteristic ring cleavage fragments of flavonols include $^{0,2}A^+$, $^{0,2}B^+$ and $^{1,3}B^+-2H$
11 [131, 136], all of which were confirmed in the present study. Overall, the intensity of
12 the $^{0,2}A^+$ and $^{1,3}B^+-2H$ fragments decreased in HCD over CID experiments, whereas
13 the intesity of ions $^{0,2}A^+-CO$, $^{0,2}B^+$ and $^{1,3}A^+$ increased (Figure 6.3).

14 Apart from the discussed fragmentations, MS^2 spectra of the methylated flavonols
15 (**14**) and (**15**) also showed fragmentations typical of methyl esters, namely methyl,
16 methane and methanol loss. Methyl and methane loss followed by sequential losses
17 of carbon monoxide were already shown for flavones (**8–10**) and are postulated to
18 proceed in a similar manner in flavonols (**14**) and (**15**) (Scheme 6.8). Because of the
19 extra hydroxyl at the C-ring, methylated flavonols such as isorhamnetin can loose
20 two CO instead of just one after loss of a methyl radical (compare Scheme 6.8 and
21 (Scheme 6.6)). Other than flavones, spectra of methylated flavonols (**14**) and (**15**)
22 also showed signals (m/z 269 and m/z 285) corresponding to a loss of methanol. The
23 data suggests, that these $[M+H-CH_3OH]^+$ fragments can loose up to two CO, similar
24 to the loss of water and CO (Scheme 6.8 and 6.7). The peaks with m/z 301, 273, 245,
25 217 and 189 in the HCD spectra of isorhamnetin (**15**), suggest a loss of up to four
26 CO after the initial loss of methane (Scheme 6.8). As mentioned before, the smaller
27 mass fragments corresponding to multiple neutral losses are more pronounced at
28 higher activation energies and were thus limited to HCD experiments at a NCE of
29 100 % (Figure 6.3, Scheme 6.8).

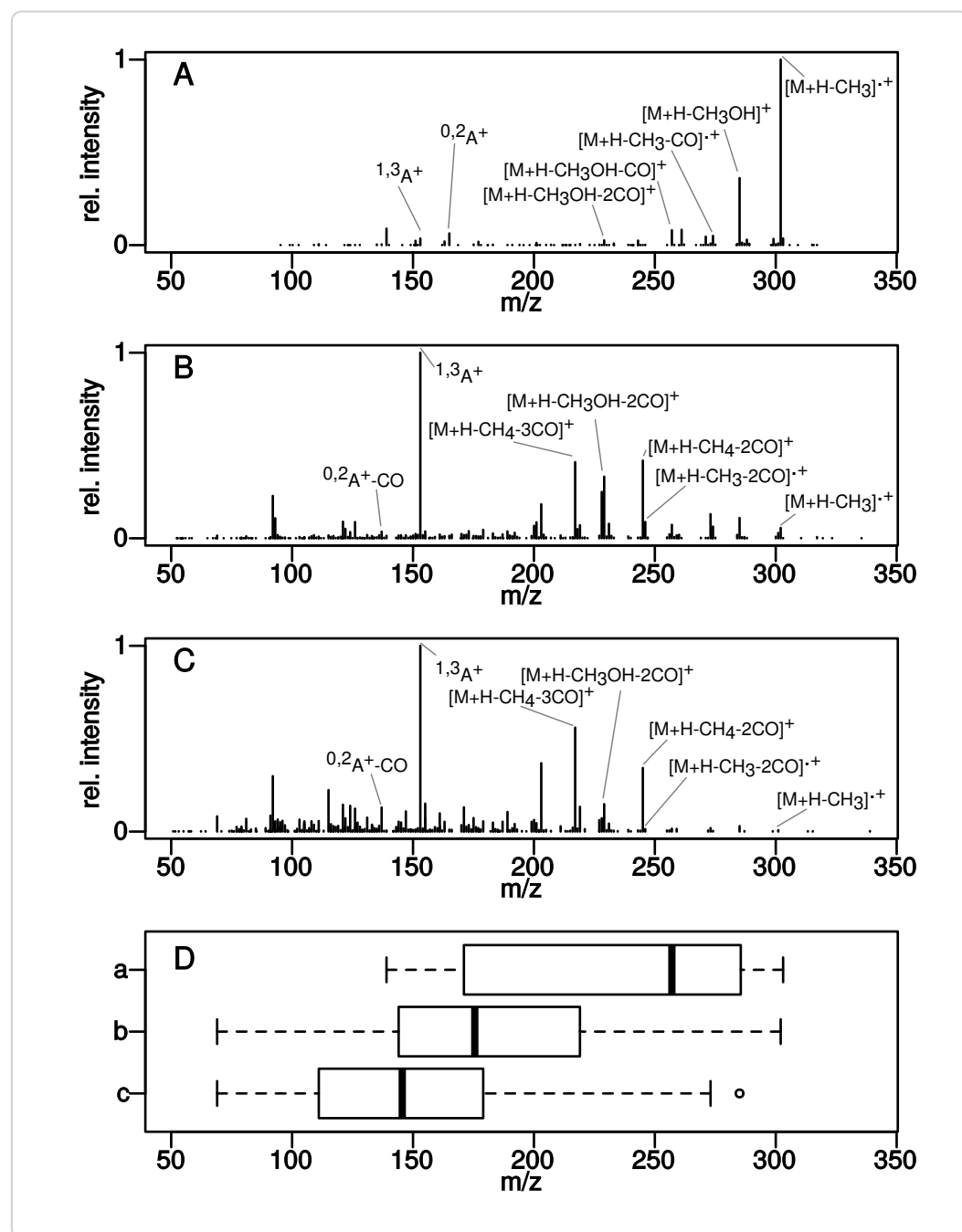
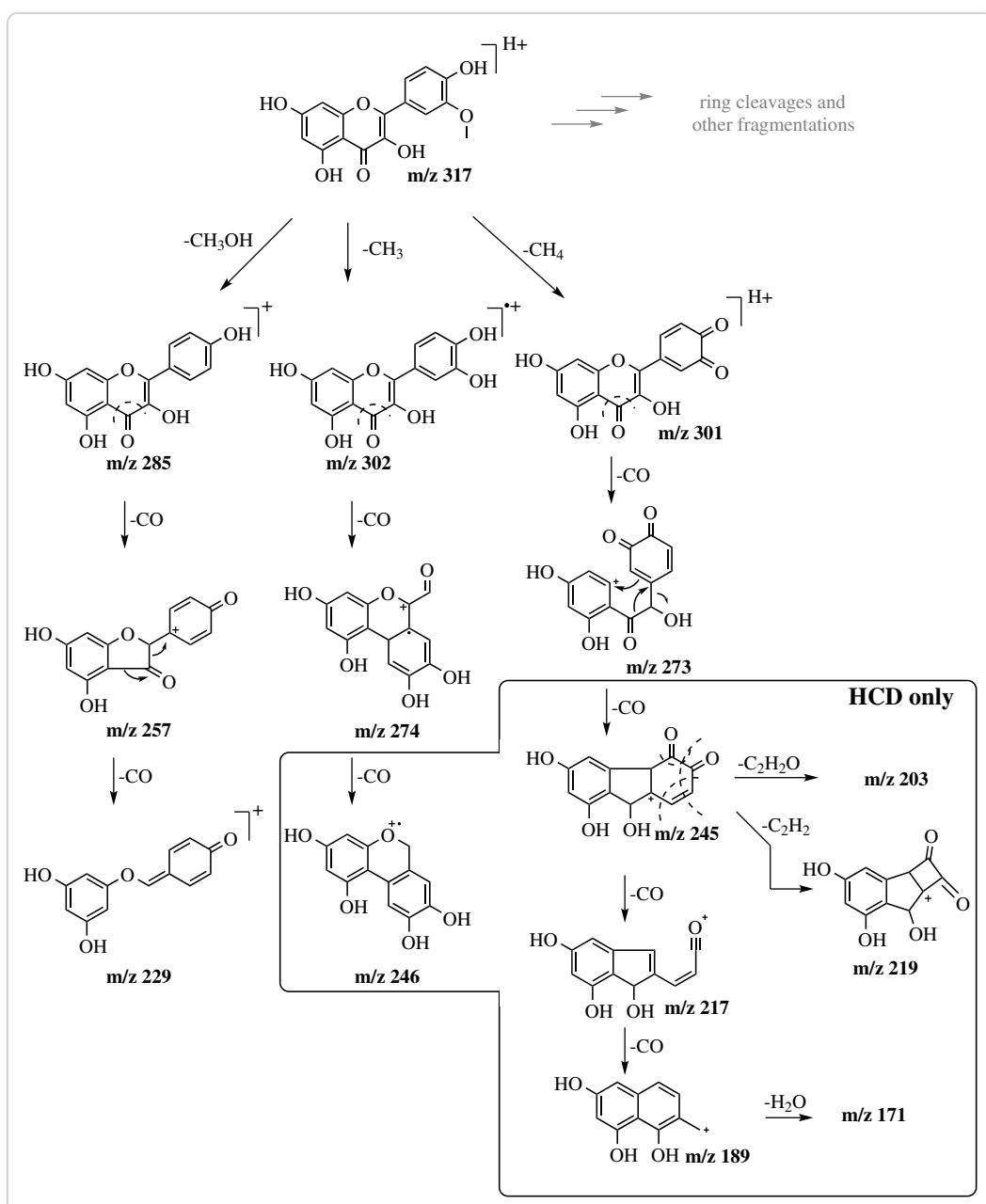


Figure 6.3.: Comparison of CID and HCD MS² spectra of isorhamnetin (15). **A** – CID at 45 % NCE. **B** – HCD at 75 % NCE. **C** – HCD at 100 % NCE. Four different prominent peaks are annotated in each spectrum. **D** – The shift to smaller masses in HCD spectra and with increasing NCE is illustrated by the boxplot of the distribution of peaks with relative intensities above 1 % in each of the above spectra.



Scheme 6.8: Proposed pathways of fragmentation of isorhamnetin (15). Isorhamnetin might lose methyl, methane or methanol upon activation. A similar fragmentation pathway was proposed for the analogous chrysoeriol (Scheme 6.6). Some fragmentations were observed in HCD mode only (box).

1 6.5 Conclusions

2 This comprehensive study shows that, taken together, data from CID and HCD ex-
3 periments can be complementary to give a much deeper understanding of structural
4 features of flavonoids. Mass errors were calculated for each postulated fragment
5 and ranged from (0.4 to 10) ppm, highlighting the accuracy of the instrument which
6 also allowed for the accurate determination of molecular formulas from MS signals.

7 The complementary nature of CID and HCD is especially striking, when com-
8 paring spectra of (9) and (10). CID fragmentation of these B-ring methylated
9 flavones afforded MS spectra, where a methyl loss was by far the dominant frag-
10 mentation. HCD on the other hand provided higher order fragmentations combined
11 with a higher signal-to-noise ratio, for a deeper insight into structural features.
12 These higher order fragmentations were accelerated by increasing the activation
13 energy, but interpretability of the corresponding spectra was limited. However,
14 with the help of *in silico* methods for the interpretation of MS/MS spectra [14, 219]
15 and the computing power available today, the information contained in highly
16 complex spectra might become more easily accessible. Nonetheless, fine-tuning of
17 the activation energy is an option to optimize fragmentation intensities, especially
18 of the C-ring fragmentations.

19 Flavones and flavonols share similar patterns of fragmentation and display a
20 loss of a CHO radical, which distinguishes their MS² spectra from those of the
21 flavanones. Distinguishing characteristics between MS² spectra of flavones and
22 flavonols are the C-ring fragmentations, where the ^{0,4}B⁺ fragment was typically
23 limited to flavones, whereas a (strong) ^{0,2}A⁺ fragment was only observed for (non-
24 methylated) flavonols. While methylated flavanones did not differ in their frag-
25 mentations from their non-methylated analogues, MS spectra of methylated and
26 non-methylated flavones and flavonols showed significant differences. Noticable
27 loss of CH₃[•] or CH₄, followed by losses of CO were typical signs of methylated
28 flavones or flavonols. Loss of methanol was observed in methylated flavonols and
29 in small amounts at 100 % NCE in flavones, not however in the MS² spectra of
30 flavanones. Under the right conditions, all of the studied 5,7-dihydroxy substituted
31 flavonoids presented a ^{1,3}A⁺ ion, with a characteristic *m/z* 153. This information

1 might be of value for studies that want to determine the position of a derivatization
2 of the flavonoid core. To the authors knowledge, a pathway for the decomposition
3 of $^{1,3}\text{A}^+$ at high activation energies was proposed for the first time in this work and
4 is universal for all studied compounds. A signal m/z 91, stemming from the decay
5 of the $^{1,4}\text{B}^+$ or $^{1,3}\text{B}^+$ ion, might be a hint for a *para*-monohydroxylated B-ring on
6 flavanones and flavones respectively. Conversely, a peak m/z 89 can point in the
7 direction of multiple substitutions on the B-ring.

8 In summary, the complementary nature of the studied activation methods CID
9 and HCD provides more thorough data for the study of flavonoids. Key ions
10 might only present themselves in the spectra of either method, and together with
11 differences and similarities in the MS/MS spectra, can be used to gain additional
12 insights into the structural characteristics of a studied compound.

13 **6.6 Contributions**

14 Benjamin Weigel prepared substances, analyzed mass spectral data and prepared
15 manuscript. Annegret Laub and Jürgen Schmidt conducted LC/MS measurement
16 runs. Through helpful discussions, Jürgen Schmidt helped tremendously with the
17 preparation of the manuscript.

¹ 7 Enzymatic methylation of non-
² catechols

1

Enzymatic methylation of non-catecholic aromatic hydroxyls using class I and class II methyl transferases

Benjamin Weigel^{1,a}, Martin Dippe^{2,b}, Annegret Laub^{1,b}, Ludger A. Wessjohann^{1,d}

Contact: bweigel@ipb-halle.de^a, mdippe@ipb-halle.de^b, alaub@ipb-halle.de^c, law@ipb-halle.de^d

Affiliation: Leibniz-Institute of Plant Biochemistry, Department of Bioorganic Chemistry¹

Keywords: methyl transferase, SAM, biocatalysis

3 **Abstract**

4 Phenylpropanoid and flavonoid O-methyl transferase (PFOMT) and soy O-methyl
5 transferase (SOMT-2) are *S*-adenosyl-L-methionine (SAM)-dependent methyl trans-
6 ferases (MTs), belonging to classes I (23–27 kDa, cation-dependent) and II (38–
7 43 kDa, cation-independent) respectively. Methylation of non-catecholic aro-
8 matic hydroxyls (phenolic, 3'-hydroxy-4'-methoxy (3O4M), 4'-hydroxy-3'-methoxy
9 (4O3M)) exemplified by different compound classes was achieved by both enzymes.
10 This is the first time this behavior is described for PFOMT. It is shown, that the
11 activity of PFOMT towards non-catechols is increased at high pH. Adjusting the
12 pH to more basic conditions can also partly remedy the deleterious effect of missing
13 Mg²⁺ for class I enzyme PFOMT. Soluble SOMT-2 enzyme was obtained by opti-
14 mizing *in vitro* refolding conditions using fractional factorial design (FrFD) and
15 design of experiments (DoE). However, the activity of the refolded SOMT-2 was
16 insufficient for *in vitro* experiments.

17

18 7.1 Introduction

19 Phenyl propanoid derived polyphenols are one of the most abundant plant sec-
20 ondary product in nature. Representatives such as flavonoids and anthocyanidins

1 play important roles in plant development, flower color or in the defense systems
2 combating biotic and abiotic stresses. Lignin, the main component of wood, is
3 mostly comprised of phenyl propanoid alcohols and is responsible for the structure
4 and rigidity in (lignified) vascular plants.

5 The properties of flavonoids, lignins and other is largely influenced by their
6 derivatization pattern, and thus so-called tailoring enzymes are widespread in
7 nature. Tailoring enzymes such as methyl-, prenyl- and glycosyl-transferases
8 are responsible for hydroxylations, (*C* and *O*)-methylations, -prenylations and -
9 glycosylations, which are common derivatizations of polyphenols, respectively [42,
10 76, 183, 188, 211, 221].

11 The biosynthetic or biocatalytic production of tailor made natural materials (e.g.
12 lignins) with desireable properties is an important step towards a more ecologi-
13 cal and economical industry and has the potential to greatly impact many areas
14 of modern life [235]. Flavonoids and polyphenols such as resveratrol, that ex-
15 hibit health-beneficial effects (e.g. antioxidative, antimicrobial), are often used in
16 functional foods or to improve the “properties” of food products [36, 120, 227].

17 It is therefore of great importance to evaluate and develop new methods to
18 biocatalytically produce known and new polyphenols with interesting properties.
19 The aim of this study was to assess two plant *O*-methyl transferases (*O*-MTs),
20 PFOMT and SOMT-2, of classes I and II towards their potential for the methylation
21 of structural motifs commonly found in polyphenols. The main interest was to study
22 methylation of so-called non-catecholic moieties, such as phenolic, 3'-hydroxy-4'-
23 methoxy (3O4M) and 4'-hydroxy-3'-methoxy (4O3M) structural motifs and to see
24 whether permethoxylated compounds could be produced by these enzymes.

25 7.2 SOMT-2

26 SOMT-2 is already well characterized in the literature and acts on flavonoids as
27 well as isoflavonoids[99, 102, 103]. However, *in vitro* data of this enzyme has not
28 been published. It was selected as a model candidate as a class II plant *O*-MT, that
29 can already methylate 4'-hydroxyls of non-catecholic flavonoids.

1 7.2.1 *In vivo* biotransformation in *Nicotiana benthamiana*

2 The group of Sylvestre Marillonet (IPB) established an efficient system to clone
 3 and assemble multi enzyme pathways in *Nicotiana benthamiana*, using a modular
 4 cloning toolbox, which has already been used to produce flavonoids [107]. All
 5 the genes required to establish the pathway up to naringenin in *N. benthamiana*
 6 in theory had been cloned previously (Figure 7.1). Only the *SOMT2* gene needed
 7 to be cloned into a suitable vector to be transiently expressed in *N. benthamiana*.
 Infiltrated plants were harvested after 7 days (see section 4.3). The average weight

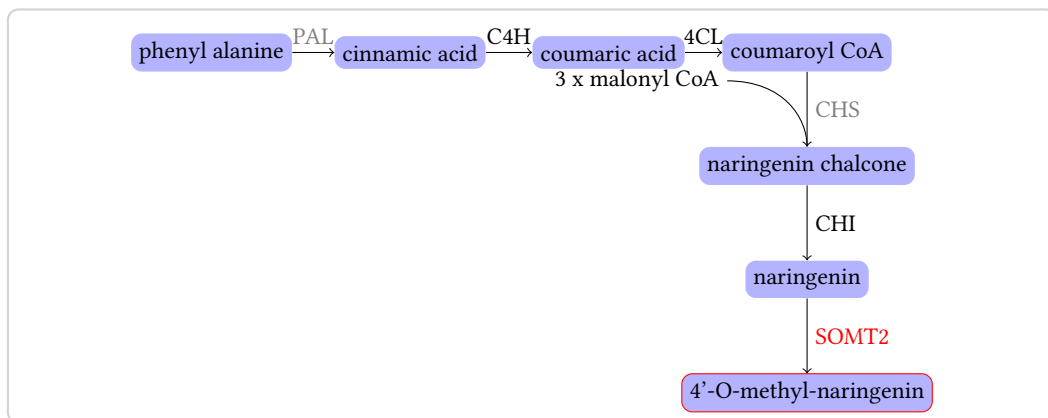
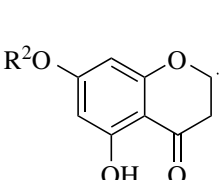
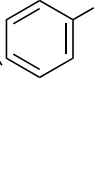


Figure 7.1.: Semi-synthetic pathway to naringenin and 4'-O-methyl naringenin in *N. benthamiana*. Enzymes not endogenous to *N. benthamiana* are in gray. PAL - phenylalanine ammonia lyase, C4H - cinnamic acid 4-hydroxylase, 4CL - 4-coumaric acid:CoA ligase, CHS - chalcone synthase, CHI - chalcone isomerase, SOMT2 - soy O-methyl transferase 2

8 loss after freeze drying was 87.5 %.
 9
 10 The dried material was extracted and analyzed via high-performance liquid
 11 chromatography (HPLC) to determine whether ponciretin or the “down-stream”
 12 glycosylated products (poncirin, didymine) were produced (Table 7.1). However,
 13 through comparison with authentic standards it was apparent, that none of the
 14 expected compounds were detected. This finding suggest, that neither naringenin,
 15 nor any “down-stream” flavonoids (ponciretin, poncirin, didymin) were present in
 16 detectable amounts in the plant tissue at the time of harvest. Although unlikely, it
 17 cannot be excluded that higher amounts of the compounds of interest were present
 18 at some point in the tissue.

Table 7.1.: Naringenin and 4'-methylated derivatives that were inquired for in the plant samples via HPLC. The core structure of the compounds is displayed on the left.

 	R ¹	R ²	name
	H	H	naringenin
	CH ₃	H	ponciretin
	CH ₃	rutinose ¹	poncirin
	CH ₃	neohesperidose ²	didymine

¹ The HPLC chromatograms were analyzed by principal component analysis (PCA) after the data were aligned, centered and scaled, to assess whether the collected plant material samples were different from one another (Figure 7.2 and C.1). The PCA-plot shows that the samples of the different leaf sides do not separate, indicating no difference between infiltration with the *SOMT* gene and vector control between the first two principal components, which account for 80 % of the variance. However, there is a slight separation between top and bottom leaves in the second principal component and between plant 3 and plants (1 and 2) in the first principal component (appendix, Figure C.1). This suggest, that the chemical composition as detected

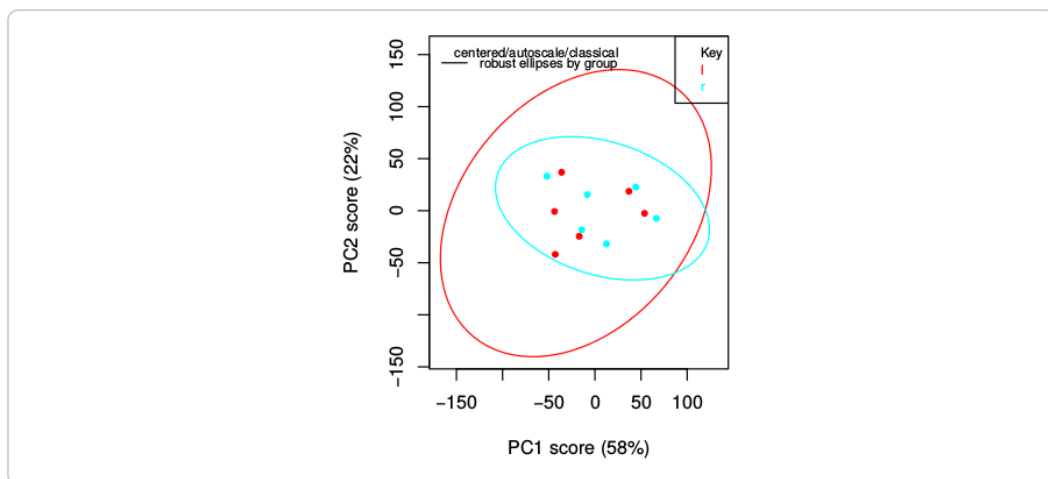


Figure 7.2.: Scatterplot of the first two principal components from the PCA of the HPLC data obtained from leaf material extracts. The samples are colored by leaf side (left/SOMT-2: red, right/vector control: cyan).

- 1 by HPLC is slightly different in the top and bottom leaves, as well as between the
 2 different plants.

3 7.2.2 *In vivo* biotransformation in *E. coli*

4 Kim *et al.* [99, 102, 103] showed, that SOMT-2 could be used for the biotransforma-
 5 tion of different flavonoids in *E. coli* live cultures. The *SOMT-2* gene was cloned into
 6 the pET28a(+) and pET41a(+) vectors, to obtain constructs for the production of
 7 SOMT-2 without and with a N-terminal Glutathion S-transferase (GST)-tag, respec-
 8 tively since both have been used successfully [99, 102, 103]. However, methylated
 9 flavonoids were not detected when biotransformations were prepared according to
 10 the methods of the aforementioned authors (Figure 7.3a). Thus, the biotransfor-
 11 mation medium was changed to auto-induction (AI)-medium with 0.05 % glucose
 [189]. Measured growth curves showed, that the glucose present in the medium

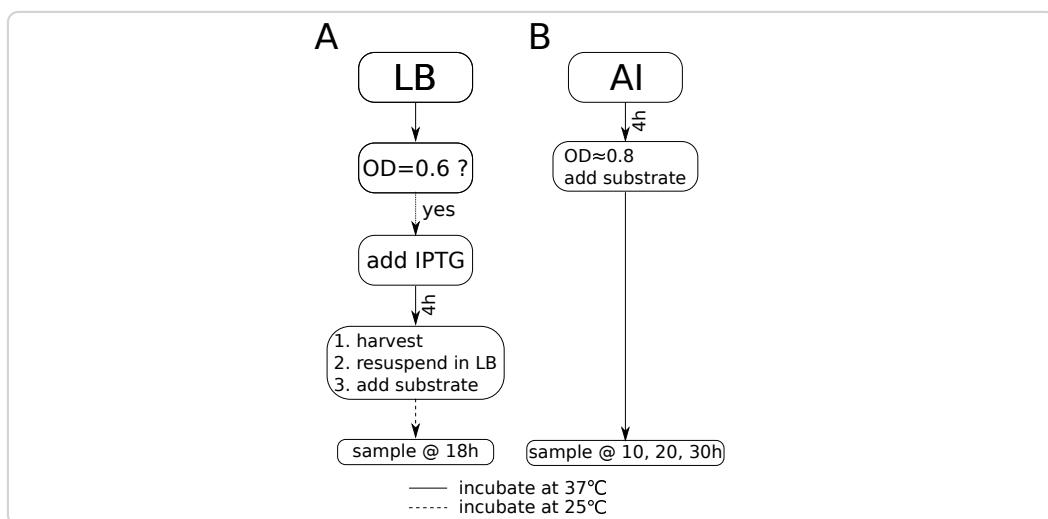


Figure 7.3.: Biotransformation methods as described by Kim *et al.* (A) and developed in this work (B). OD – optiocal density at 600 nm, LB – LB-medium, AI – AI-medium.

- 12
 13 was depleted after about 5 hours into growth (appendix, Figure C.2). Expression of
 14 the *SOMT-2* gene is expected to begin at this time, because the catabolite repression
 15 on the *lac* promoter would be relieved and the promoter would be activated by
 16 the lactose present in the AI-medium. Thus, 0.1 mM of flavonoid substrate were

1 added at 4 hours to minimize its influence on growth and possible degradation.
 2 Although sodium dodecylsulfate (SDS)-polyacrylamide gel electrophoresis (PAGE)
 3 samples were prepared throughout the course of the experiment, accumulating
 4 SOMT-2 could not be clearly distinguished from endogenous *E. coli* protein in the
 5 SDS-PAGE gels (appendix, Figure C.3). Nonetheless, methylation of some of the
 6 tested substrates was observed over a course of 30 hours (Table 7.2). Therefore, the
 sampled medium was extracted using acidified ethyl acetate. Liquid chromatog-

Table 7.2: *In vivo biotransformation of different flavonoids, phenylpropanoids and anthraquinones by SOMT-2 in E. coli. Conversion ratios were calculated for samples taken after 30 hours. Multiple substrates containing a 4'-hydroxyl were methylated. Calculation of conversion percentages are only rough estimates, because of the nature of crude medium extracts. Products were determined by liquid chromatography-tandem mass spectrometry (LC-MS/MS).*

substrate	class	4'-OH conversion product		
alizarin	anthraquinone	✗	✗	–
purpurin	anthraquinone	✗	✗	–
apigenin	flavone	✓	✓(≥54 %)	4'-O-methyl apigenin
chrysins	flavone	✗	✗	–
genistein	isoflavone	✓	✓(<1 %)	Biochanin A
galangin	flavonol	✗	✗	–
kaempferol	flavonol	✓	✓(≥6 %)	kaempferide
naringenin	flavanone	✓	✓(≥55 %)	ponciretin
eriodictyol	flavanone	✓	✓(≥40 %)	hesperetin
homoeriodictyol	flavanone	✓	✓(>6 %)	3',4'-(O,O)-dimethyl eriodictyol
hesperetin	flavanone	✗	✗	–
phloretin	chalcone	✓	✗	–
resveratrol	stilbene	✓	✓(≥86 %)	4'-O-methyl resveratrol
p-coumaric acid	cinnamic acid	✓	✗	–
caffeinic acid	cinnamic acid	✓	✗	–
reosmin	cinnamic acid [†]	✓	✗	–

[†] dihydro cinnamic ketone

7 raphy coupled mass-spectrometry (LC/MS) was employed to determine the site of
 8 methylation, since this method is highly sensitive and numerous structural studies
 9 on flavonoids using tandem-mass spectrometry experiments have highlighted the
 10 feasibility of this approach (see chapter 6) [58, 117]. Collision induced dissociation
 11 (CID) was used to obtain structural information about the target molecules, since

1 soft ionization techniques (e.g. electrospray ionization (ESI)) used in LC/MS instru-
2 ments primarily produce protonated and deprotonated molecular ions, but rarely
3 yield fragments [185]. The CID method collides the precursor ions with a neutral
4 target gas while increasing the energy to induce fragmentation. The produced frag-
5 ments vary depending on the energy chosen for fragmentation. Flavonoids follow
6 certain different fragmentation pathways [58, 117]. The fragmentation of interest
7 in this work, was the one along the C-ring, which produces two fragments (A- and
8 B-ring) (Figure 7.4b). The mass of the A- and B-ring fragments gives strong evidence
9 for the position (ring) at which methylation occurred. Using the CID technique, an
10 energy of 30 eV proved sufficient to fragment most flavonoids along the C-ring as is
11 shown here for the methylated naringenin (Figure 7.4). The molecular ion $[M+H]^+$
12 of the methylated naringenin has a mass-to-charge ratio (m/z) of 287.092. The
13 fragments helping to derive structural information are m/z 133 and m/z 153, which
14 can only be explained if the B-ring was methylated (Figure 7.4b). If the A-ring was
15 methylated, the expected fragment ions of A and B-ring would have m/z -values
16 of 167 and 119 respectively. The LC/MS results suggest, that methylation occurred
17 exclusively at the 4'-hydroxyl, as there was no conversion detected, when the 4'-
18 hydroxyl was absent (Table 7.2). A free 4'-hydroxyl seems therefore necessary for
19 a substance to be a substrate for SOMT-2, which confirms the previous results [99,
20 102]. Conversion was observed for 4'-hydroxylated (iso)flavonoids and the stilbene
21 resveratrol, however conversion rates of the isoflavone genistein were very low. No
22 conversion of anthraquinones, cinnamic acid derivates or chalcones was detected,
23 which is also in accordance with previously published data [99, 102]. SOMT-2 acts
24 on phenolic, catecholic as well as (4-hydroxy-3-methoxy-phenyl)-moieties, as is
25 suggested by the assay results that showed methylation of naringenin, eriodictyol
26 and homoeriodictyol respectively. The methylation of (4-hydroxy-3-methoxy-
27 phenyl)-moieties and of stilbenes are properties of SOMT-2 that have not been
28 described before.

29 The conversion ratios were assessed, but are beset with large errors due to the
30 nature of *E. coli* rich medium extracts. The highest conversions were observed
31 for flavanones and flavones (up to $\geq 55\%$). The tested isoflavones and flavonols
32 showed much lesser conversion ratios (less than 10%). The conversion ratios of

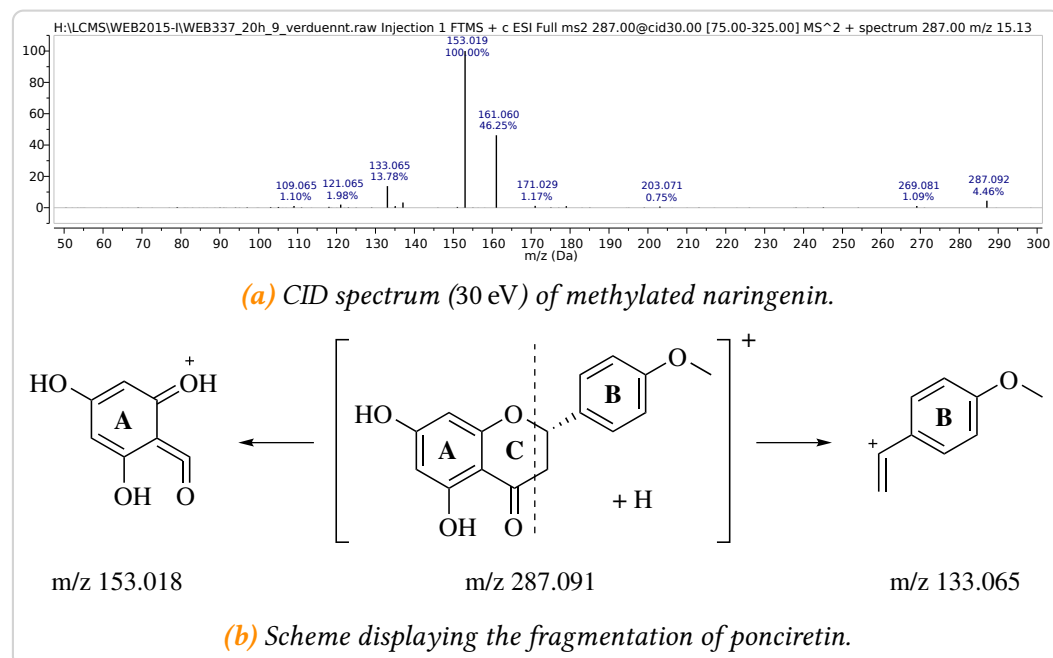


Figure 7.4.: The masses resulting from the fragmentation into A- and B-ring along the C-ring (dashed line, b) are evidence, that the 4'-hydroxyl on the B-ring is methylated by SOMT-2

1 apigenin ($\geq 54\%$) and naringenin ($\geq 55\%$) are comparable to the ones published
 2 previously [99, 102]. However, genistein only showed minute conversions, which
 3 is in disagreement with the data previously published [99, 102]. Conversion of
 4 eriodictyol, homoeriodictyol and kaempferol were not reported before.

5 The biotransformation of resveratrol to 3,5-dihydroxy-4'-methoxy-stilbene
 6 showed a conversion ratio of $\geq 86\%$ in 30 hours. This is roughly double the
 7 conversion which was recently reported for *in vivo* biotransformations using the
 8 specific resveratrol O-MT sbCOM1, which only achieved 42 % conversion in 36
 9 hours [97].

10 7.2.3 **In vitro** studies using recombinantly produced SOMT-2

11 *In vivo* biotransformations are an important tool for the primary characterization
 12 of enzymes. However, because live organisms are used and lots of variables are
 13 unknown, these systems can cause large errors and are not fit to thoroughly

1 characterize an enzyme. Initially, SOMT-2 was to be purified to homogeneity to
 2 be later thoroughly characterized *in vitro*, since the recombinant production of
 3 SOMT-2 in *E. coli* as a fusion protein with an N-terminal T7-tag was previously
 4 shown. However, the recombinant enzyme had not been characterized [99].

5 Protein production test

6 Initial protein production tests were carried out using *SOMT-2* cloned into pET28a(+)
 7 with an N-terminal His₆-tag. However, SOMT-2 was not produced in soluble
 8 form (Figure 7.5). Numerous systems were tested for the expression of *SOMT-2*.
 9 *E. coli* strains used for the trials included BL21(DE3), Rosetta(DE3), Origami(DE3),
 10 C41(DE3), C43(DE3), C41(DE3) pLys, C43(DE3) pLys and DH5 α . The *SOMT-2* gene
 11 was cloned into multiple other vectors, including pET20b for periplasmic protein
 12 production, pET32 for expression with an Trx-tag and vectors that carry promoters
 13 for induction by rhamnose. Multiple media, including terrific broth (TB), lysogeny
 14 broth (LB) and autoinduction media were used along with different inducers (e.g.
 15 lactose, rhamnose, isopropyl-D-thiogalactopyranosid (IPTG)) at different tempera-
 16 tures. Nonetheless SOMT-2 could not be produced in a soluble form and expression
 17 only resulted in inclusion bodies (IBs).

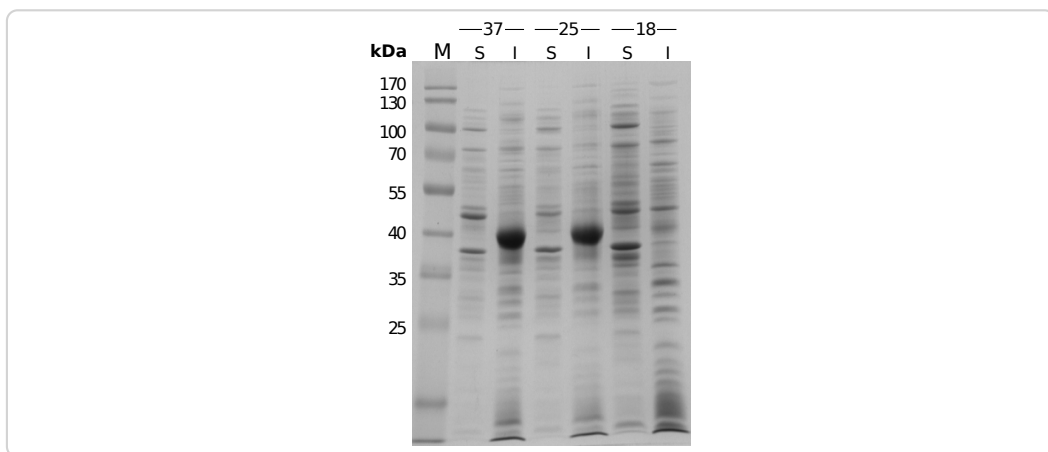


Figure 7.5.: SDS-PAGE of pET28a(+) SOMT-2 expressed in *E. coli* BL21(DE3) in autoinduction medium at different temperatures (shown above). The insoluble fractions show a protein band the same height as the 40 kDa marker band, which corresponds to the SOMT-2 protein (40 425 Da). M – protein size marker, S – soluble fraction, I – insoluble fraction

1 *In vitro* protein refolding

2 Since the SOMT-2 protein could not be obtained in soluble formen, when recom-
3 binantly expressed in *E. coli*, the IBs were prepared [166] and used for *in vitro*
4 refolding studies. For *in vitro* protein refolding, IBs are solubilized using denatu-
5 rants such as GdmCl or urea. The native tertiary structure of the protein is then
6 restored by removal of the denaturant under the “right” conditions (e.g. pH, salt,
7 additives, etc.). However, this is no trivial task since initially the “right” conditions
8 have to be found by trial and error. The refolding process competes with misfolding
9 and aggregation processes and refolding buffers have to be optimized in order to
10 obtain an efficient refolding system with the best possible results [166, 214, 225].
11 Refolding efficiency is best measured via biological activity, but even with adequate
12 assays refolding studies are a time-consuming process. The number of experiments
13 required to even test only four variables, for example pH, salt, temperature and
14 protein concentration with 3 states each (e.g. low, medium, high) in all possible
15 combinations results in $3^4 = 81$. An experimental setup, which accounts for all
16 possible variable (factor) combinations is also called a *full factorial design*. These
17 setups capture main effects, as well as higher level interaction effects [20, 147].
18 However, for screening purposes only a fraction of the experiments can be run.
19 The objective of these fractional factorial design (FrFD) experiments is to identify
20 the variables, which have large effects and are worth expanding the experimental
21 investigation upon. FrFDs have been successfully used for a number of protein
22 refolding trials [196, 205, 214].

23 The following factors were studied for the *in vitro* refolding of SOMT-2: pH,
24 arginine addition, glycerol addition, addition of divalent cations, ionic strength, re-
25 dox system, cyclodextrin addition and effector (*S*-adenosyl-L-homocysteine (SAH))
26 addition. These factors were used, because all have been shown to influence re-
27 folding success [4, 6, 11, 29, 65, 200, 205, 214, 225]. Two factor levels were used
28 in a twelve-run design. This is sufficient to find some main effects, however no
29 statement about interaction effects can be made. For a complete listing of the buffers
30 and conditions the reader is referred to the materials and methods chapter (Tables
31 4.5 and 4.6).

1 Big differences between soluble and insoluble fractions of different refolding
 2 buffers could already be noticed from the SDS-PAGE gels (Figure 7.6, see subsection
 3 4.4.11). Refolding buffers 2,3 and 8–11 mainly produced insoluble protein,
 4 whereas the majority of the protein in refolding buffers 1, 4–7 and 12 was in soluble
 5 form after an overnight refolding reaction (Tables 4.5 and 4.6, Figure 7.6). After
 6 rebuffering the cleared refolding reactions into a unified buffer the protein con-
 7 centrations were estimated by BRADFORD-assays [21]. The protein concentrations
 8 measured by BRADFORD’s method were consistent with the observations from the
 9 SDS-PAGE gels (compare Figure 7.7a and 7.6). Soluble protein was obtained for
 10 buffers 1, 4–7 and 12. The highest amount of soluble protein was present, when the
 refolding reaction took place in buffers 5 or 7. The common denominator of those

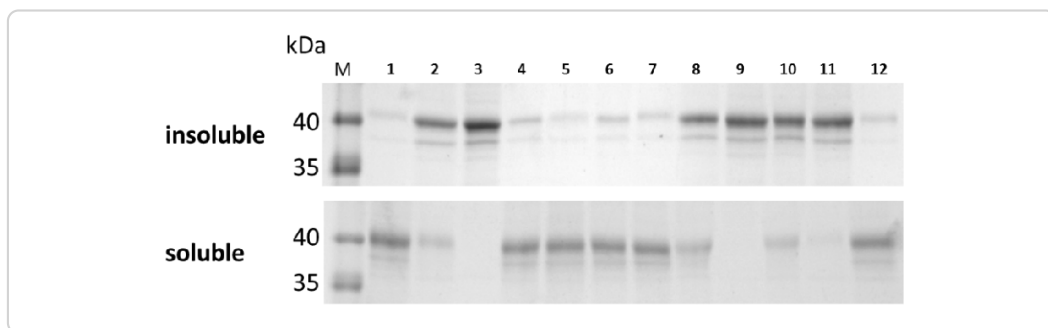


Figure 7.6.: SDS-PAGE of the insoluble and soluble fractions of the refolding reactions. Refolding reactions 2,3,8-11 seem to mainly produce misfolded insoluble protein, while the other refolding buffers (1,4-7,12) produce soluble protein.

11
 12 buffers is that all of them contained arginine, whose addition has proven beneficial
 13 for many refolding applications [29, 65, 200].

14 **Main effects plots (ME-plots)** illustrate the difference between level means for
 15 each factor. Therefore, the mean of the measured property (i.e. protein concentration)
 16 for each level of every factor, described by + or -, of the used refolding buffers is
 17 plotted in relation to the overall mean. For example, the levels of the factor pH are
 18 “low” (-) and “high” (+). When x_i^- is the measured concentration from a refolding
 19 reaction in buffer i with “low” pH and x_j^+ is the measured concentration from a
 20 refolding reaction in buffer j with “high” pH, then the level means \bar{x}^- and \bar{x}^+ are

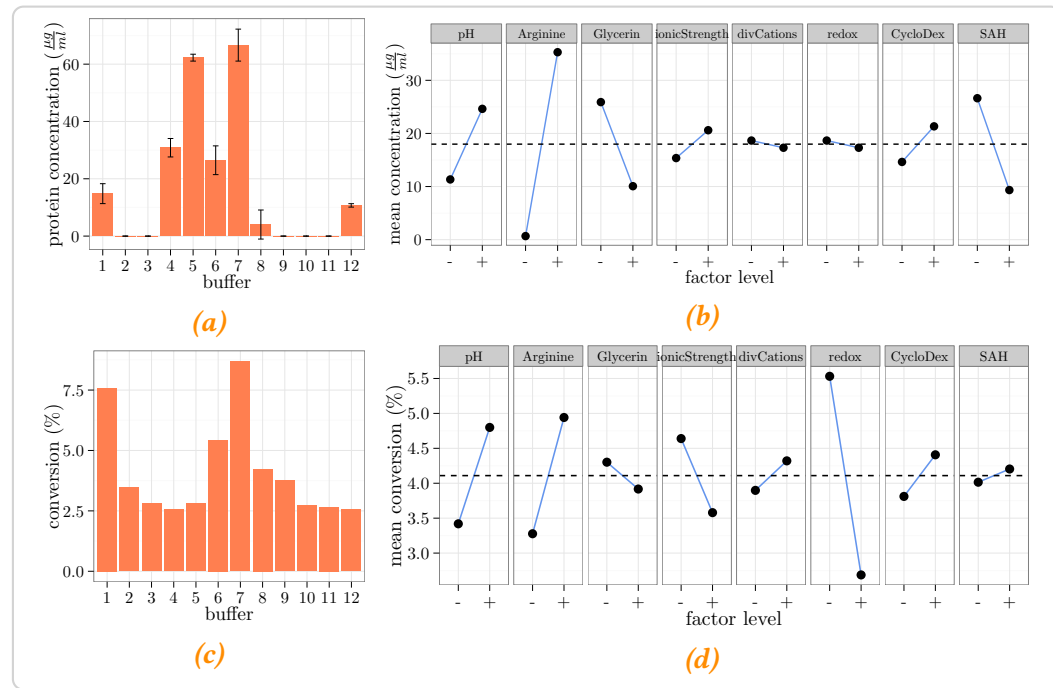


Figure 7.7: Results of *in vitro* protein refolding trials. Measured data (left) is presented alongside the main effects plots (ME-plots) (right). The dashed line through the ME-plots illustrates the overall mean. **a** – Protein concentration after refolding and rebuffering into a universal buffer. The highest yield of soluble protein was achieved in buffers 5 and 7. The ME-plots **(b)** illustrate the connection between a factor and the measured protein concentration, suggesting that high pH and arginine concentration might have been beneficial in the refolding reactions. **c** – Calculated conversion of naringenin to ponciretin by the refolded protein fractions. Protein refolded in buffers 1 and 7 seem to afford the most active protein by conversion (~volume activity). The ME-plots for the conversion **(d)** show that the redox state (reducing) of the refolding environment was important to achieve active protein.

1 calculated as follows:

$$\bar{x}^- = \frac{1}{n} \cdot \sum_{i=1}^n x_i^-$$

$$\bar{x}^+ = \frac{1}{n} \cdot \sum_{j=1}^n x_j^+$$

- 2 In the presented experiment “low” pH buffers were buffers 2, 4, 6, 8, 10 and 12,
 3 whereas “high” pH buffers were buffers 1, 3, 5, 7, 9 and 11, thus the level means

1 were calculated as such:

$$\bar{x}^+ = \frac{x_1^+ + x_3^+ + x_5^+ + x_7^+ + x_9^+ + x_{11}^+}{6} = 24.63$$

$$\bar{x}^- = \frac{x_2^- + x_4^- + x_6^- + x_8^- + x_{10}^- + x_{12}^-}{6} = 11.34$$

2 The ME-plots for protein concentration suggest, that arginine was likely an
 3 important factor for the refolding of SOMT-2 (Figure 7.7b). Furthermore, the
 4 addition of SAH or glycerin and the pH seemed to have an influence, whereas
 5 the other factors seemed to play only minor roles to achieve high concentrations
 6 of soluble protein after refolding. However, the *Analysis of Variance* (ANOVA)
 7 test, which gave a *p*-value of 0.0158 for factor *arginine*, suggests that only arginine
 8 addition had a significant influence on refolding, when the significance level is set
 9 to 5 % (appendix, Table C.1). The other *p*-values are all higher than 0.05, which
 10 suggests the other factors had no influence on the yield of soluble protein. Only
 11 the *p*-value for factor *SAH* (0.0897) would suggest significance, if the significance
 12 level was raised to 10 %.

However, soluble protein is not necessarily active. Therefore activity tests were conducted with the refolded protein samples to check for naringenin conversion (Figure 7.7c). The conversion of naringenin to ponciretin was calculated from the area under the curve (AUC) of the substrate and product peaks as follows:

$$conversion = \frac{AUC_{ponciretin}}{AUC_{naringenin} + AUC_{ponciretin}}$$

13 Although the substrate naringenin was already contaminated with about 2.5 %
 14 ponciretin, this value was not subtracted from the measured conversions to avoid
 15 introduction of unnecessary errors. The protein activity in the refolded samples
 16 was generally very low, as suggested by the low conversions after an overnight
 17 activity assay. The maximum conversion of about 8.7 % (6.2 %) was observed for
 18 the protein sample refolded in buffer 7. The activity of the protein samples did not
 19 correlate well with the amount of soluble protein (Figure 7.7). This becomes clear
 20 from the samples refolded in buffers 4 and 5, where the amount of soluble protein

1 was high but the observed activity was at a baseline level.

2 The ME-plot suggests that the main effects for obtaining high amounts of soluble
3 protein and obtaining active protein after refolding are different (Figure 7.7d). Most
4 notably, the redox state of the refolding reaction seemed to have a big influence on
5 the protein sample's activity. The redox state however had almost no influence on
6 the yield of soluble protein (Figure 7.7b). Indeed, the ANOVA test suggests that using
7 reducing refolding conditions (DTT) over a redox-shuffling system (GSH:GSSG,
8 oxidizing) has a significant influence on methylation activity judged by the *p*-value
9 0.0218 of the factor *redox* (appendix, Table C.2). However, there is the possibility for
10 SOMT-2 to form intramolecular disulfide bridges, as the modelled structure suggests
11 (Figure C.4). There are also reports, which showed that intermolecular disulfide
12 bridges can contribute to the stability of, mainly archeal, MTs and have no influence
13 on the enzymatic activity [68, 75, 90]. Nevertheless most MTs are only active under
14 reducing conditions and literature suggests, that sometimes assays of MTs are
15 explicitly conducted under reducing conditions [85, 236]. Reducing environments
16 reduce the chance of disulfide cross-linked protein mono- and oligomers and allow
17 the enzyme to be more flexible, which might be important for catalysis. When using
18 a significance level of 10 %, the *p*-value for *arginine* is 0.0824, which also suggests
19 a significant influence of this factor on the chance to obtain active protein after
20 refolding. This is plausible, since there cannot be any activity when no soluble
21 protein is present, and refolding reactions without added arginine did not afford
22 any soluble protein. Judging from the ANOVA test, the remaining factors like
23 *glycerin*, *ionic strength* or *divalent cations* had no significant impact on the protein
24 activity after refolding.

25 Due to the promising results obtained from the refolding trials, which impli-
26 cated that the best overall refolding performance (i.e. soluble protein and activity)
27 was achieved in buffer 7 (50 mM borate/NaOH, 0.5 M arginine, 2 mM CaCl₂, 2 mM
28 MgCl₂, 10 mM NaCl, 0.5 mM KCl, 30 mM α -cyclodextrin, 5 mM DTT pH 8.5), this
29 buffer was used to scale up the refolding reaction from a total volume of 1.05 ml to a
30 volume of 50 ml. After concentration of soluble protein from the scaled-up refolding
31 reaction, activity tests were conducted. Unfortunately, the refolded SOMT-2 showed
32 no activity for naringenin methylation, which was evidence that the scaled-up re-

1 folding was unsuccessful. Nonetheless, gel filtration chromatography and circular
 2 dichroism (CD) spectroscopy were used as a tool to study the three-dimensional
 3 structure of the refolded SOMT-2. The retention volume for the major peak eluted
 4 during the gel filtration run was 12.47 ml, but in the chromatogram a shoulder at
 5 14.26 ml was clearly distinguishable (Figure C.5). Molecular masses of the proteins
 6 corresponding to the peaks were estimated from commercial gel filtration protein
 7 standards. The first peak corresponds to a molecular weight of approximately
 8 165 kDa, whereas the shoulder at 14.26 ml corresponds to a globular protein of
 9 approximately 65.5 kDa. 65.5 kDa is roughly the weight of one SOMT-2 monomer
 10 (40 kDa) or a dimer, whereas a mass of 165 kDa would indicate a tetramer. These
 11 results were further indication, that the majority of the refolded protein was not
 12 in the expected native dimeric state. However, the refolded SOMT-2 had adopted
 some kind of fold that allowed for it to be in soluble form. Furthermore, the CD

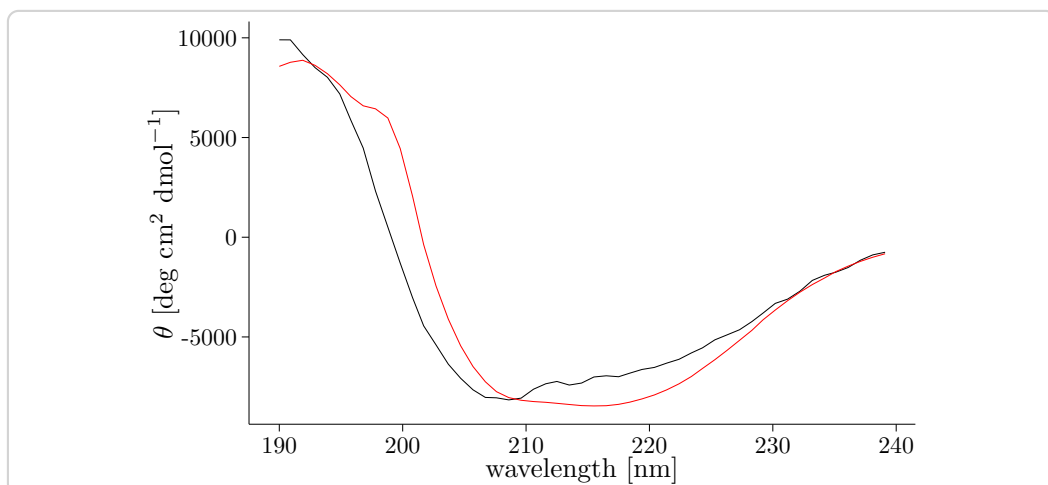


Figure 7.8: CD-spectrum of refolded SOMT-2 (black) compared to the spectrum that was calculated (red) by the K2D3 web service (<http://cbdm-01.zdv.uni-mainz.de/~andrade/k2d3//index.html>) from the SOMT-2 sequence. Secondary structure estimates from the measured spectrum are 12.39 % α -helix and 32.51 % β -sheet.

13 spectrum (Figure 7.8) suggested, that the refolded SOMT-2 possessed a secondary
 14 structure and was not present as an unfolded random coil. The secondary structure
 15 was estimated from the measured CD-spectrum by the K2D3 web service [126].
 16 According to the K2D3 calculations, the secondary structure elements consisted
 17

of 12.39 % α -helix and 32.51 % β -sheet. However, the calculated protein model (Figure C.4) suggests the α -helix content might be much higher (52.3 %), whereas the β -sheet content might accordingly be lower (15.4 %). These findings further indicate, that the refolded protein was not in a native state, which might be the cause of the lack of enzymatic activity. Even over the course of many trials a successful large scale refolding of SOMT-2 yielding active protein could not be achieved.

These results display that DoE combined with FrFD can be a valuable tool for the identification of main factors during protein refolding. However, there still exists a discrepancy between small scale refolding reactions and the process of upscaling, which might not be trivial.

7.3 PFOMT

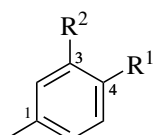
PFOMT is a class I plant *O*-MT, that was thoroughly characterized in previous studies [22, 48, 85, 109, 206]. It is easily obtained by heterologous expression in *E. coli* after which it is fairly active and stable, which is important for *in vitro* experiments. The activity of PFOMT in relation to the pH of the buffer and magnesium addition was the main aim of this part of the study.

7.3.1 Phenolic hydroxyls

Phenolic hydroxyl groups have pK_a -values of around 10 as demonstrated by four *p*-cresole derivatives (Table 7.3). Catecholic systems have two pK_a -values, one for each hydroxyl group. The 3-hydroxyl (R^2) of the displayed example has a much smaller pK_a than the 4-hydroxyl (R^1). This is in part due to the mesomeric (+M) and inductive (+I/-I) properties the substituents exhibit. The M and I-effects let the 3-OH be deprotonated first, which in turn significantly lowers the acidity and thus increases the pK_a of the 4-OH. (4-hydroxy-3-methoxy)- and (3-hydroxy-4-methoxy)-derivatives have a similar pK_a , with the *meta*-position slightly more acidic due to the +I-effect of the methyl substituent. The nucleophilicity of these phenolic groups happens to coincide with their BRØNSTED acidity. Chemically speaking the hydroxyl group with the lower pK_a always reacts first with an electrophile.

However, different enzymes are able to regioselectively methylate the 3- or the 4-OH of such catecholic systems. Enzyme's active sites create a "microclimate", which can selectively raise or lower the effective pK_a of functional groups and allows for the efficient manipulation of the macroscopically observed regioselectivity.

Table 7.3.: pK_a -values of phenolic hydroxyl groups exemplified by *p*-cresole derivatives. Substituent positions on the aromatic ring are arbitrary and do not reflect conventions of the International Union of Pure and Applied Chemistry (IUPAC).

	R ¹	R ²	$pK_a^{-R^1}$	$pK_a^{-R^2}$
	OH	H	10.36	—
	OH	OH	13.1	9.55
	OH	O-Me	10.34	—
	O-Me	OH	—	10.08

Previous studies have established that PFOMT is a 3'-*O*-methyl transferase, which is not able to methylate substrates that bear either phenolic (e.g. naringenin), (3'-hydroxy-4-methoxy)- (e.g. hesperetin) or (4'-hydroxy-3-methoxy)-moieties (e.g. homoeriodictyol) [85]. In these previous studies, the reactions were all run under the same "standard" conditions. However, the reaction buffer can have a tremendous impact on enzymes and their reactions. Therefore reaction conditions require optimization, just as the enzymes themselves, to augment an enzymatic process [17, 105].

Using PFOMT reaction conditions were screened, to assess if any would promote the methylation of non-catecholic substrates. Although enzymes create a specific environment for catalysis, changes in the pH of the medium can still affect said environment and therefore enzymatic activity, especially if charged groups are part of the catalytic mechanism. In the catalytic mechanism of PFOMT a catalytic triad of Lys-Asn-Asp, two of which are charged, is proposed to play a major role [22]. Furthermore, PFOMT is a magnesium dependent enzyme and the activity is affected by altering the concentration of Mg²⁺ or substitution of Mg²⁺ by other divalent cations [85]. Thus, the pH was chosen to be varied along with Mg²⁺ concentration in order to study the influence of those two factors on the methylation reaction.

1 7.3.2 PFOMT pH-profiles are influenced by Mg²⁺

2 PFOMT was dialyzed against 50 mM succinate/sodium phosphate/glycine (SSG)-
 3 buffer pH 7.5 containing 5 mM ethylenediaminetetraacetic acid (EDTA) and again
 4 against the same buffer with the EDTA omitted, to obtain enzyme that was virtually
 5 free of bound divalent cations. pH-profiles (pH 5.5 – 9.5) of three different substrates
 6 (caffeic acid, *iso*-ferulic acid, eriodictyol) were obtained in the same unified buffer
 7 system (succinate/sodium phosphate/glycine, 2:7:7 molar ratio). The pH-profiles
 8 were measured without and with the addition of 10 mM MgCl₂. Maximum methy-
 9 lation activity (\approx 1500 pkat/mg) towards the catecholic substrates (i.e. caffeic acid,
 10 eriodictyol) was observed when magnesium was added and the pH was about 6.5
 11 (Figure 7.9 and Table 7.4). However, the observed maximum activity shifted towards
 12 basic pH values (pH 9.45), when magnesium was omitted from the reaction. The
 13 maximum activity for methylation of *iso*-ferulic acid was measured at pH 9.45,
 regardless of whether magnesium was added. The catecholic substrates caffeic acid

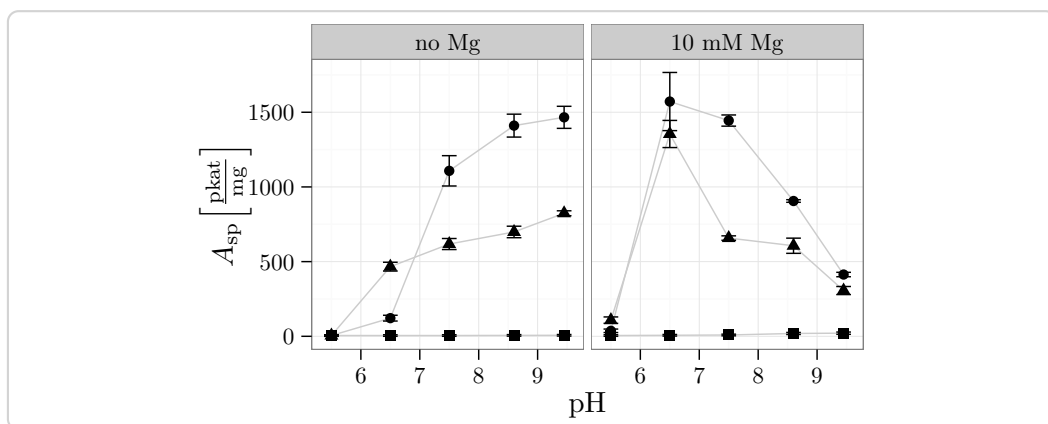


Figure 7.9: Specific activity/pH-profiles for the conversion of three different substrates (● caffeoic acid, ▲ eriodictyol, ■ *iso*-ferulic acid) by PFOMT. The specific activity for the non-catecholic substrate *iso*-ferulic acid was much lower than the specific activity for the catecholic substrates. When magnesium is omitted, the activity is increased by increasing the pH

14 and eriodictyol were converted by PFOMT much more quickly than *iso*-ferulic acid,
 15 which is a (3-hydroxy-4-methoxy)-substituted cinnamic acid (Figure 7.9).

The highest specific activity A_{sp} for *iso*-ferulic acid conversion was two orders of magnitude lower than the highest activity for the conversion of the other two substrates. Nonetheless, conversion was observed for *iso*-ferulic acid with increasing pH and even an influence of magnesium was observed (Figure 7.9 and Table 7.4). *Iso*-ferulic acid was converted rather slowly without the addition of Mg^{2+} ($A_{sp} = 7 \text{ pkat/mg}$). However, addition of 10 mM Mg^{2+} increased the rate of *iso*-ferulic acid conversion by 3-fold, from 7 pkat/mg to 21 pkat/mg at pH 9.45 (Table 7.4).

The specific activities observed for the conversion of caffeic acid are comparable to published data [49]. For the two catecholic substrates, the pH-optimum shifted from neutral to alkaline pHs, when Mg^{2+} was omitted. However, the maximum activity remained roughly the same, even though magnesium addition seemed to have a slight rate increasing effect. Rate enhancements of up to 3-fold were observed at pH 9.45, when Mg^{2+} was omitted compared to when it was present. The maximum activities without magnesium were observed at pH 9.45 with 1466 pkat/mg and 824 pkat/mg for caffeic acid and eriodictyol respectively, while with 10 mM Mg^{2+} the maximum activities were recorded at pH 6.5 and increased to 1572 pkat/mg and 1354 pkat/mg respectively.

Table 7.4.: Maximum specific activity for the conversion of three different substrates with and without addition of magnesium. The pH at which the maximal activity was reached is indicated by the column titled “pH”.

substrate	Mg^{2+}	pH	$A_{sp} \left[\frac{\text{mU}}{\text{mg}} \right]$	$A_{sp} \left[\frac{\text{pkat}}{\text{mg}} \right]$
caffeic acid	FALSE	9.45	88	1466
caffeic acid	TRUE	6.50	94	1572
eriodictyol	FALSE	9.45	49	824
eriodictyol	TRUE	6.50	81	1354
<i>iso</i> -ferulic acid	FALSE	9.45	0.4	7
<i>iso</i> -ferulic acid	TRUE	9.45	1.2	21

During the catalysis of a methyl transferase reaction, the acceptor moiety of the substrate is activated by abstraction of a proton. At high pH-values, the substrates might already be deprotonated, thus increasing the rates of reaction, while the enzyme just acts as a scaffold. High pH-values would also mean that the mainly the 4'-hydroxyl of the catechols would be deprotonated (Table 7.3). However, an

- 1 increasing amount of 4'-methylation was not observed contradicting the notion,
 2 that an already deprotonated substrate entered the active site. It is more likely,
 3 that the external milieu influences the enzymes active site and makes the active
 4 side chains more basic. However, why the addition of magnesium would shift the
 5 pH-optimum back to neutral pH-values is not clear.

To statistically support the presented findings, the collected data were also studied from a statisticians point of view, which is described in the following paragraph in a bit more detail. The shown results are solely included for purposes of making statistics based inferences in the context of domain knowledge. Relationships between independent variables X_1, \dots, p , influencing a system and the outcome Y of such a system can be mathematically described. The simplest relationship between one independent variable X_1 and the dependent variable Y is a linear one and is defined mathematically by a linear equation $Y = \beta_1 X_1 + \beta_0$. The coefficient β_1 describes how much Y is altered by one unit X , while β_0 is the offset. Even seemingly non-linear outcomes of Y might be sufficiently described by multi-term linear equations such as

$$Y = \beta_0 + \beta_1 X_1 + \beta_2 X_2 + \dots + \beta_p X_p + \epsilon,$$

- 6 when the independent variables X_1, \dots, p are known. Linear regression models of this
 7 form can be used to make statistically sound inferences about a studied system and
 8 were thus used to assess the relationship between PFOMT's methylation activity
 9 and pH-modulation as well as Mg²⁺ addition. Two subsets of the activity data were
 10 prepared first. The subsets split the data into substrates with catecholic (i.e. caffeic
 11 acid, eriodictyol) and substrates without catecholic (i.e. iso-ferulic acid) motifs.
 12 This was done to simplify the interpretability of the results, since the activities of
 13 the catecholic and non-catecholic substrates differed greatly. The iso-ferulic acid
 14 data was fit to the linear model

$$\text{activity} = \beta_0 + \beta_1 \times \text{Mg} + \beta_2 \times \text{pH} + \beta_3 \times (\text{Mg} \times \text{pH}), \quad (7.1)$$

- 15 which contains one term, $\beta_3 \times \text{pH} \times \text{Mg}$, to account for an interaction effect between
 16 magnesium and pH besides the main effects terms. This model explains about 93.6 %

1 of the variance ($R^2 = 0.9355$) of the measured data (Table 7.5). Fitting the data
 2 in the R software using the `stats::lm()` function also calculates *p*-values associated
 3 with each parameter estimate. The smallest *p*-value 0.0030 was calculated for

Table 7.5.: Coefficients of the model (Equation 7.1) for activity of iso-ferulic acid methylation. The factor Mg is a categorical variable (addition/no addition) and can therefore only be 0 or 1.

	Estimate	Std. Error	t value	p-value
(Intercept)	-241.4238	420.1485	-0.57	0.5864
pH	38.4239	54.9778	0.70	0.5108
Mg	-2201.3084	594.1797	-3.70	0.0100 *
pH×Mg	373.8131	77.7503	4.81	0.0030 **

significance codes: ** 5 % level; *** 1 % level

3
 4 the interaction factor pH×Mg, and strongly suggests that there is a significant
 5 interaction between methylation activity on iso-ferulic acid and Mg²⁺ addition
 6 combined with pH-modulation. The parameter estimate β_3 for this term is almost
 7 374. Since in this case Mg is categorical and can only be 0 (no magnesium added) or 1
 8 (magnesium added) the interaction term $\beta_3 \times \text{pH} \times \text{Mg}$ resolves to 0, if no magnesium
 9 was added. This means that when Mg²⁺ is added, the activity (in AU min⁻¹) is
 10 increased by 374 for each unit the pH is raised. The *p*-value for pH as a main effect
 11 is rather high, suggesting pH alone has no significant impact on the activity. The
 12 parameter estimate β_1 for factor Mg however has a low *p*-value of 0.010, which
 13 suggest that its impact on activity is significant. Due to the categorical nature of
 14 Mg, this means, that the activity is decreased by 2201 AU min⁻¹ when magnesium
 15 is added. However, this information is only of importance when predicting the
 16 activity outside of the measured pH range, which was not the aim here. Together,
 17 these results illustrate, that neither magnesium addition, nor the pH alone would
 18 have such a strong effect on the activity as both factors combined had.

19 The data of the second subset containing of the catecholic substrates was also
 20 modelled in a similar fashion (see Appendix C.2.1). It was found, that the pH
 21 has a much stronger influence on the methylation activity of PFOMT towards
 22 catechols than iso-ferulic acid. Interaction between magnesium addition and pH-
 23 modulation were also suggested for the catecholic substrates from this data. For a

- more thorough discussion see Appendix C.2.1. In addition to pure inference based modelling, models can also be used to make predictions based on (new) independent variables (Figure 7.10). However, it cannot be stressed enough that models do not reflect the truth, but are rather another tool to gain insight into a system.

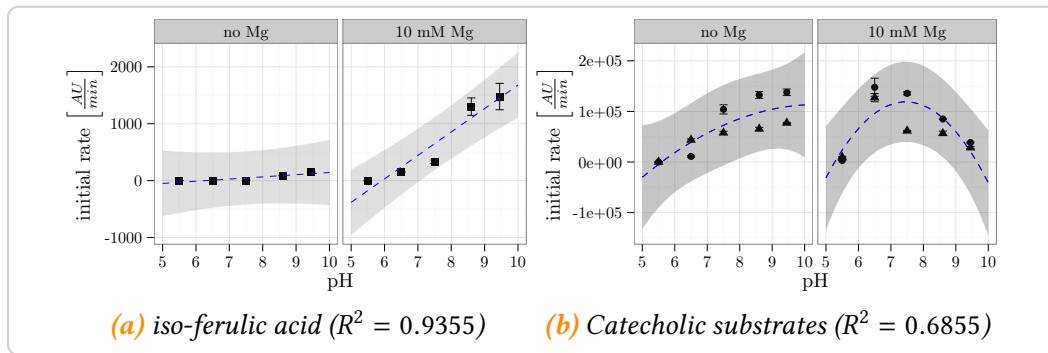


Figure 7.10: pH-profiles of substrate conversion along with predicted data. Predicted data from the linear regression models (blue, dashed lines) grasp the general trend of the data reasonably well to draw inferences. 95 % prediction intervals are displayed as shaded areas.

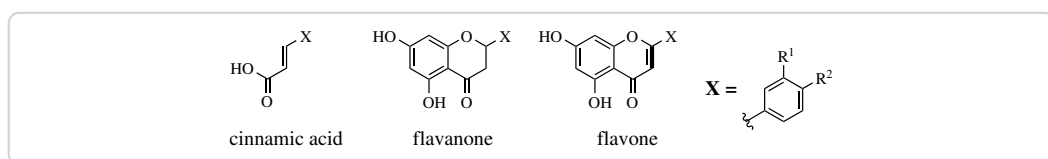
To the knowledge of the author, this is the first time the effects of Mg^{2+} and pH on methyl transferase activity were systematically analyzed. It was shown, that catecholic and non-catecholic substrates could be activated sufficiently by PFOMT at high pHs without the addition of Mg^{2+} . It is improbable that, if the active site retained the same miromilieu under every reaction condition, an influence on the rate of reaction would be observed. This could be a hint, that the enzyme relays the chemical information of the environment directly to the substrate to aid in activation. Furthermore, omission of Mg^{2+} shifts the pH-optimum of the reaction catalyzed by PFOMT to higher pH-values. It would be of interest to analyze this behavior with further systematic studies and multiple levels of Mg^{2+} concentrations.

7.3.3 Methylation of different chemical motifs

The previous section showed the conversion of non-catecholic iso-ferulic acid by PFOMT and prompted additional experiments with other different non-catechols from multiple flavonoid subgroups (Table 7.6). The tested substrates were selected from three different compound groups (cinnamic acids, flavones, flavanones)

and each group contained each of four structural motifs – phenol, catechol, 3'-hydroxy-4'-methoxy (3O4M) and 4'-hydroxy-3'-methoxy (4O3M). Each substrate was assessed for conversion with two enzymes (PFOMT wild-type and 4'-specific variant Y51R N202W) at four different conditions. Magnesium addition and pH were varied for the different conditions (pH/Mg^{2+} : low/no, low/yes, high/no, high/yes). The “low” and “high” pH-values were 7.5 and 8.6, respectively. When Mg^{2+} was added the concentration was 10 mM. The reactions were incubated at 30 °C for 16 h (see section 4.6.3).

Table 7.6: Substrate grid that was tested for methylation with PFOMT. Four different groups of compounds were screened. The groups of flavones, flavanones and cinnamic acids each contained one representative of each motif, phenolic, catecholic, 3'-hydroxy-4'-methoxy (3O4M) and 4'-hydroxy-3'-methoxy (4O3M).



	substrate	group	motif	R ¹	R ²
A.1	p-coumaric acid	cinnamic acid	phenolic	H	OH
A.2	caffeic acid	cinnamic acid	catecholic	OH	OH
A.3	iso-ferulic acid	cinnamic acid	3O4M	OH	OMe
A.4	ferulic acid	cinnamic acid	4O3M	OMe	OH
B.1	naringenin	flavanon	phenolic	H	OH
B.2	eriodictyol	flavanon	catecholic	OH	OH
B.3	hesperetin	flavanon	3O4M	OH	OMe
B.4	homoeriodictyol	flavanon	4O3M	OMe	OH
C.1	apigenin	flavone	phenolic	H	OH
C.2	luteolin	flavone	catecholic	OH	OH
C.2	diosmetin	flavone	3O4M	OH	OMe
C.4	chrysoeriol	flavone	4O3M	OMe	OH

Conversion of all substrates, catecholic and non-catecholic, by the wild-type could be demonstrated. The highest conversion of non-catecholic substrates was shown for 3'-hydroxy-4'-methoxy substituted compounds, especially cinnamic acids and flavanones where conversions of up to 25 % were observed. Conversions of substances with free 4'-hydroxyl groups did not extend beyond 7 % (chrysoeriol).

1 This was to be expected, due to the fact that PFOMT is a 3'-specific MT at physi-
2 ological conditions. However, unexpectedly the 4' specific variant hardly showed
3 any conversion of non-catecholic substrates. High pH favoured the conversion of
4 non-catechols.

5 There was almost complete conversion of the catecholic substrates (eriodictyol,
6 luteolin and caffeic acid) after 16 h of incubation regardless the reaction conditions,
7 at least when the wild-type enzyme was used (Figure 7.11 and Table 7.7). This
8 suggests, that the reaction period was chosen too long for this group of substrates
9 and effects of pH or magnesium addition on this group cannot be distinguished.
10 Conversion was observed for all tested substrates at least under high pH-conditions,
11 when the wild-type was employed (Figure 7.11). The 4'-variant however hardly
12 showed any conversion of non-catecholic substrates (Figure 7.11b). Generally, the
13 highest conversions of non-catecholic substrates were observed at high pH and high
14 Mg²⁺ conditions (Figure 7.11). For example, conversion of iso-ferulic acid was up to
15 25 % at pH 8.6 with 10 mM Mg²⁺ in the reaction. This is a 10-fold increase over the
16 conversion of 2.5 %, which was observed at pH 7.5 with no magnesium added. These
17 findings support the claims from the previous subsection 7.3.2, that PFOMT activity
18 might be modulated enough by pH and magnesium to achieve methylation of non-
19 catecholic phenyl propanoid substrates. Again, the trend in the data suggests, that
20 methylation efficiency of non-catecholic moieties increases with pH, but especially
21 in combination with the addition of magnesium . Overall, methylation of 3O4M
22 motifs was highest apart from the catecholic substrates. Observed conversions of
23 close to 25 % for the cinnamic acid and flavanone substrates (iso-ferulic acid and
24 hesperetin) were observed. For these substrates the conversion increased by almost
25 5-fold upon Mg²⁺ addition, which is close to the observed increase of the initial
26 rate of iso-ferulic acid methylation (subsection 7.3.2). Similar results have been
27 shown for SaOMT5, an O-MT from *Streptomyces avermitilis*, where the enzymatic
28 activity towards quercetin increased by about 5-fold from metal-free conditions
29 to magnesium addition [228]. Conversion of the somewhat more rigid flavone
30 diosmetin (max. conversion 12 %) was lower by at least factor two compared to
31 hespreretin and iso-ferulic acid (Table 7.7, Figure 7.11). At low pH-values and
32 without addition of Mg²⁺ barely any conversion of the non-catecholic substrates

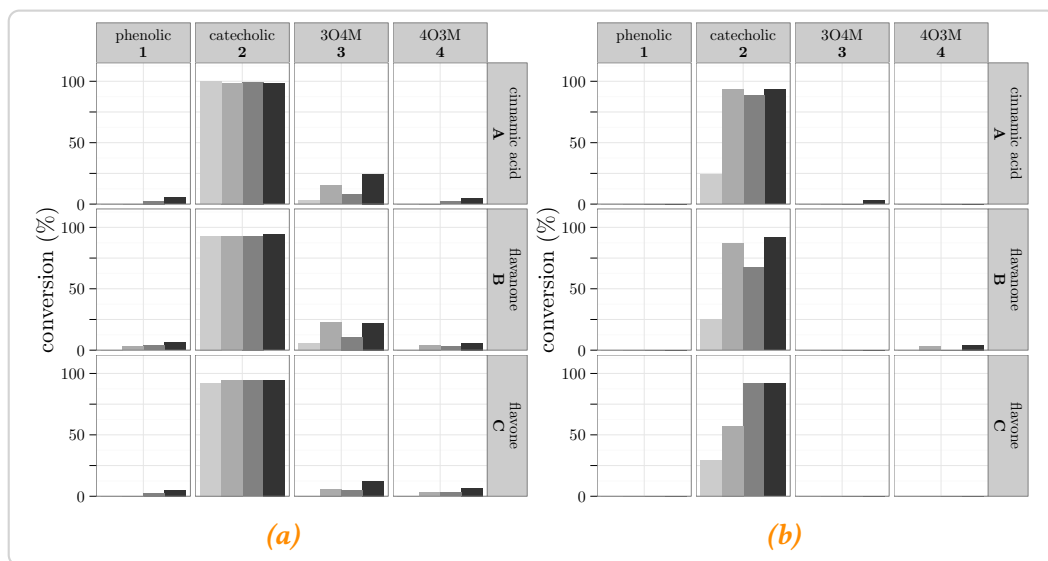


Figure 7.11: Conversion of multiple different substrates, catecholic and non-catecholic, by PFOMT wild-type **(a)** and the 4'-specific variant Y51R N202W **(b)**. Every individual box represents one substrate *p*-coumaric acid (A.1), . . . , chrysoeriol (C.4). pH/Mg²⁺-conditions are color coded from light to dark: $\text{--}/\text{X}$, $\text{--}/\checkmark$, \nearrow/X , \nearrow/\checkmark . — (low pH), \nearrow (high pH), X (no Mg²⁺), \checkmark (yes, Mg²⁺)

1 was observed. The fact, that conversion of 3O4M-moiety bearing substrates is
2 greater than that of the *para*-phenolic and 4O3M substrates could be due to the fact
3 that the wild-type of PFOMT by and large methylates 3'-hydroxyls at physiological
4 conditions.

5 The 4'-specific variant for the most part only showed conversion of the catecholic
6 substrates. Only some conversion of homoeriodictyol ($\approx 4\%$) and *iso*-ferulic acid
7 ($\approx 3\%$) was observed under high pH/Mg²⁺ conditions (Table 7.7, Figure 7.11). How-
8 ever, for the catecholic substrates the same trend – increasing pH/Mg²⁺ increases
9 activity – as before holds true. Control experiments without enzyme at high pH
10 and 10 mM Mg²⁺ revealed, that no substrate conversion took place under these
11 conditions, meaning the enzyme must be involved in the conversion.

12 Products and methylation sites were identified by comparison to authentic stan-
13 dards, or by LC-MS/MS (Table 7.8). As previous studies demonstrated, the products
14 for the conversion of the catecholic substrates by the wild-type and variant were
15 the 3'-methylated and 4'-methylated substrates respectively [48, 85, 109, 206].

Table 7.7.: Conversion of substrates after 16 hours incubation. Only the maximum conversion is displayed, along with the conditions it was achieved under.

substrate	wild-type			4'-specific variant Y51R N202W		
	conversion %	pH	Mg ²⁺	conversion %	pH	Mg ²⁺
A.1 <i>p</i> -coumaric acid	6	↗	✓			
A.2 caffeic acid [†]	100 [‡]		(all)	93		(all)
A.3 iso-ferulic acid	25	↗	✓	3	↗	✓
A.4 ferulic acid	5	↗	✓			
B.1 naringenin	6	↗	✓			
B.2 eriodictyol [†]	94		(all)	92	↗	✓
B.2 hesperetin	22	↘	✓			
B.4 homoeriodictyol	6	↗	✓	4	↗	✓
C.1 apigenin	5	↗	✓			
C.2 luteolin [†]	95		(all)	92	↗	
C.3 diosmetin	12	↗	✓			
C.4 chrysoeriol	7	↗	✓			

[†]wild-type: substrate conversion was maximal for all pH/Mg²⁺ combinations.

[‡]conversion of caffeic acid by the wild-type was set to 100 %.

- 1 As expected, methylation took place on the B-ring of the flavonoids. Ponciretin
 2 and acacetin were produced, when naringenin and apigenin were converted by
 3 PFOMT respectively. However, conversion of the 3O4M and 4O3M flavonoids
 4 (hesperetin/chrysoeriol and homoeriodictyol/diosmetin respectively), afforded the
 5 3',4'-dimethylated compounds. This demonstrates, that even the PFOMT wild-type
 6 is able to methylate the 4'-position of flavonoids, given the right conditions (pro-
 7 longed incubation, high pH, no free 3'-hydroxyl). Furthermore, another type of
 8 product, eluting earlier than the corresponding substrates, was observed for the
 9 flavones apigenin, chrysoeriol and diosmetin after conversion with the wild-type in
 10 the LC/MS runs. Unfortunately, these products could not be identified. Nonetheless
 11 the production of these products seemed favoured over the 3' or 4'-O-methylated
 12 ones, when a free 3'-hydroxyl was absent (Appendix, Figure C.9).

- 13 Enzymatic methylation of the non-catecholic cinnamic acids also afforded two
 14 different types of product, methyl esters and methyl ethers. Methylation of *p*-

- 1 coumaric acid only gave rise to the corresponding *methyl ester* (Appendix C.3).
 2 Two different products were observed for the enzymatic methylation of ferulic
 3 acid and *iso*-ferulic acid. One product was the methyl ester of the corresponding
 4 cinnamic acid, whereas the other product was the di-ether, 3,4-dimethyl caffeic
 acid.

Table 7.8.: Products of the enzymatic methylation of the studied substrates. The products were confirmed by authentic standards or via LCMS.

substrate	product	
	wild-type	4'variant
<i>p</i> -coumaric acid	<i>p</i> -hydroxy methylcinnamate [†] [87]	
caffeic acid	ferulic acid	ferulic acid
<i>iso</i> -ferulic acid	caffeic acid dimethyl ether, <i>iso</i> -ferulic acid methyl ester [†]	n/d
ferulic acid	caffeic acid dimethyl ether, ferulic acid methyl ester [†]	
naringenin	ponciretin	
eriodictyol	homeroeriodictyol	hesperetin
hesperetin	3',4'-dimethyl eriodictyol [†]	
homeroeriodictyol	3',4'-dimethyl eriodictyol [†]	3',4'-dimethyl eriodictyol [†]
apigenin	acacetin	
luteolin	chrysoeriol	n/d
diosmetin	3',4'-dimethyl luteolin [†]	
chrysoeriol	3',4'-dimethyl luteolin [†]	

[†]determined via LCMS; n/d – not determined

- 5
 6 To the authors knowledge, this is the first time that methylation of a diverse
 7 set of non-catecholic substrates was described for a class I magnesium-dependent
 8 methyl transferase. A flavonoid-specific O-MT from *Catharanthus roseus* was de-
 9 scribed to methylate the 4'-position, when the substrates B-ring possessed a 4O3M
 10 substitution [172]. However, said enzyme only showed marginal activities towards
 11 catechols and 3O4M derivatives. A class II O-MT from wheat, named TaOMT2, is
 12 able to sequentially methylate the three hydroxyl-groups on the B-ring of tricetin, in
 13 the proposed order 3'-methyl → 3',5'-dimethyl → 3',4',5'-trimethyl [233]. However,
 14 methylation of dihydroxy-derivatives such as luteolin and eriodictyol by TaOMT2

1 only afforded 3'-mono-methylated products, which is similar to PFOMT. Nonetheless,
2 TaOMT2 can methylate tamarixetin, the 4O3M derivative of quercetin, albeit
3 at low activities.

4 Of the the two PFOMT enzymes, 4'-specific variant and wild-type, only the wild-
5 type showed significant methylation of non-catecholic moieties. These findings
6 support the previous results, that could show a pH and magnesium-dependent
7 rate of methylation of iso-ferulic acid (subsection 7.3.2). Although methylation
8 of 3'-hydroxyl groups was preferred by the wild-type, a tendency to methylate
9 4'-hydroxyls, when these were the only ones present, could be demonstrated.
10 Furthermore, methylation of the acid functionalities of cinnamic acids was demon-
11 strated using PFOMT.

12 The N-terminus of PFOMT is important for the function of the enzyme, as was
13 demonstrated in previous studies, however the role of it *in vivo* is still not fully
14 understood [85, 109, 207]. It cannot be ruled out that it acts as a signal sequence
15 that can direct the enzyme to different compartments. The findings presented here
16 might give some implications as to the regulation of O-MTs, such as PFOMT, since
17 the millieu can be quite different in different cell compartments in plants [139].

18 7.4 Conclusion

19 Enzymatic methylation of non-catecholic moieties, was studied using the two
20 methyl transferases PFOMT and SOMT-2, of classes I and II respectively. Therefore
21 multiple different flavonoid and phenylproanoid substrates, displaying either single
22 phenolic, catecholic, 3'-hydroxy-4'-methoxy or 4'-hydroxy-3'-methoxy moieties,
23 were tested. Furthermore, the influence of pH and magnesium addition on PFOMT
24 was systematically studied.

25 In *in vivo* biotransformation experiments it could be shown, that the class II
26 O-methyl transferase SOMT-2 is able to methylate flavonoids and stilbenes at the
27 4'-OH of the B-ring, regardless the exact moiety (phenolic, catecholic, 4'-hydroxy-
28 3'-methoxy). Although overall the conversions were very low, the conversion of the
29 stilbene resveratrol was superior over all other tested substrates ($\geq 86\%$ vs. $\geq 55\%$).
30 SOMT-2 showed methylating activity exclusively when a free 4'-OH was present,

1 suggesting it only acts on 4'-hydroxyl groups. Unfortunately, these results are
2 purely based on *in vivo* bitransformations carried out in *E. coli*. SOMT-2 could not
3 be obtained in pure, soluble form for *in vitro* characterization. Nonetheless, using
4 SOMT-2 it was shown that design of experiments (DoE) and fractional factorial
5 design (FrFD) can be valuable tools for the systematic determination of factors that
6 influence refolding of O-MTs.

7 *In vitro* experiments using the class I O-methyl transferase PFOMT, showed that
8 non-catecholic substrates could be methylated. These findings are contrary to the
9 belief, that PFOMT only acted on vicinal aromatic dihydroxyls that are present
10 in compounds such as eriodictyol or caffeic acid. The best conversion of non-
11 catechols was achieved for substrates with 3'-hydroxy-4'-methoxy-moieties (e.g.
12 hesperetin, *iso*-ferulic acid), even though conversion was observed for phenolic
13 (e.g. naringenin) and 4'-hydroxy-3'-methoxy-substrates (e.g. homoeriodictyol),
14 thus demonstrating the ability of PFOMT to methylate both 3'- and 4'-hydroxyls.
15 The best conversions were obtained using the PFOMT wild-type at elevated pH
16 and after Mg²⁺ addition. Magnesium addition and pH displayed synergistic effects,
17 meaning the effects of both are not just additive. pH optimum of PFOMT shifted
18 from around pH 7 to more basic conditions (pH >8), when Mg²⁺ was omitted.
19 Although no magnesium was present under these high pH conditions, it seemed
20 as though the chemical environment surrounding the enzyme was relayed into the
21 active site. Thus, non-catecholic substrates were methylated at high pH without
22 magnesium, whereas they were hardly methylated at low pH without the addition
23 of magnesium. These findings also show, that the linear stepwise optimization of
24 reaction conditions might not always yield the best overall results, when it comes to
25 such complex systems as enzymes and that synergistic effects need to be considered
26 when looking for the best working conditions.

8 Summary

Plant secondary metabolites comprise a vast collection of compounds with a myriad of biological activities and functions, that include defense against biotic and abiotic stresses, communication as well as gene regulation. These biological activities are largely determined by the compounds substitution patterns. Phenyl propanoid derived phenolic compounds such as flavonoids make up a major part of the secondary metabolites in plants and tailoring enzymes such as methyl-, prenyl- and glycosyl-transferases are responsible of putting a finish on their molecular structure. This work aimed to study the ability of two plant O-methyl transferases (*O*-MTs), phenylpropanoid and flavonoid O-methyl transferase (PFOMT) and soy O-methyl transferase (SOMT-2), for the alkylation of common structural motifs in polyphenols.

In the first part PFOMT was characterized by biophysical methods, which showed that the enzyme is able to bind the non-natural ethylated *S*-adenosyl-L-methionine (SAM) analogue *S*-adenosyl-L-ethionine (SAE). Conversion of SAE was however not observed. In addition a novel crystal structure of the *apo*-form of PFOMT was solved that gave insights into the movements associated with substrate binding.

The second part comprised of a tandem mass-spectrometry (MS/MS)-study of 15 flavonoids of different classes (i.e. flavanones, flavones and flavonoles). Two activation methods, collision induced dissociation (CID) and higher-energy collisional dissociation (HCD), were shown to produce complementary information that enables a fast and reliable structural characterization of the studied substances.

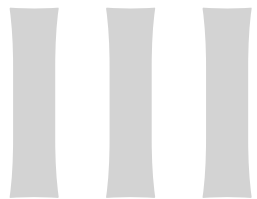
Finally, a comprehensive study showed the methylation of several non-catecholic flavonoids, stilbenes and cinnamic acids by the enzymes SOMT-2 and PFOMT *in vivo* and *in vitro*. For the first time methylation of phenolic, 3'-hydroxy-4'-methoxy and

1 4'-hydroxy-3'-methoxy, which was achieved through the modulation of the reaction
2 conditions (e.g. pH, magnesium concentration), by PFOMT could be demonstrated.
3 Together, the results presented herein show that both class I and II plant *O*-
4 MTs can be used to methylate non-catecholic moieties of polyphenolic compounds.
5 Modulation of the reaction conditions is a worthwhile study and might bring
6 to light new activities, that were not to be expected. This is of specific interest
7 for biocatalytic reactions, where the naturally observed reaction might not be
8 the desired behavior of an enzyme. Furthermore these results might spark new
9 discussions about the regulation and function of enzymes in different compartments
10 (i.e. reaction milieus).

¹ 9 Acknowledgements

10 Affidavit

- 2 I hereby declare that this document has been written only by the undersigned and
3 without any assistance from third parties. Furthermore, I confirm that no sources
4 have been used in the preparation of this document other than those indicated in
5 the thesis itself.
- 6 Date:....., Location:....., Signature:.....



1

2

Appendix

¹ A Engineering of PFOMT

Table A.1: Crystallographic data, phasing and refinement statistics.

140519_PFOMT	
<i>data collection</i>	
resolution (Å)	1.95
total reflections	392 368
unique reflections	125 822
completeness (%)	99.12
$I/\sigma(I)$	9.9
space group	$P2_12_12_1$
cell dimensions (Å)	
<i>a</i>	86.16
<i>b</i>	128
<i>c</i>	129.3
<i>refinement</i>	
$R_{\text{work}}/R_{\text{free}}$	0.21369 / 0.24700
rmsd bond lengths (Å)	0.0199
rmsd bond angles (°)	2.0568
B-values (Å ²)	21.593
<i>Ramachandran plot (%)</i>	
favoured	96.82
allowed	2.38
outliers	0.8

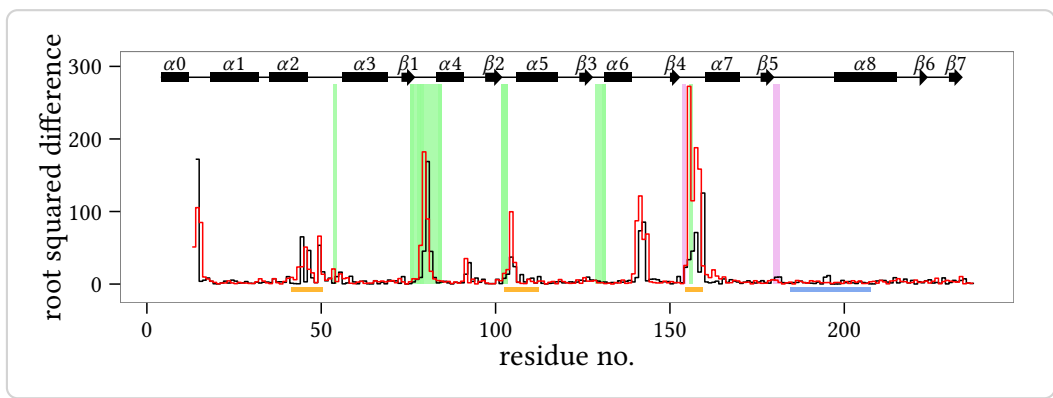


Figure A.1: Differences in the dihedrals ψ (red) and ϕ (black) of the solved apo-PFOMT and the structure with bound S-adenosyl-L-homocysteine (SAH) (pdb: 3C3Y). The secondary structure is displayed at the top. Helices are displayed as rectangles and sheets are shown as arrows. Graphical background annotations are used to display the binding sites of SAH (green) and the metal ion (plum). The orange bars indicate regions, where much movement seems to happen upon binding or release of the co-substrate. The blue bar shows the region that was annotated as "insertion loop" in previous studies.

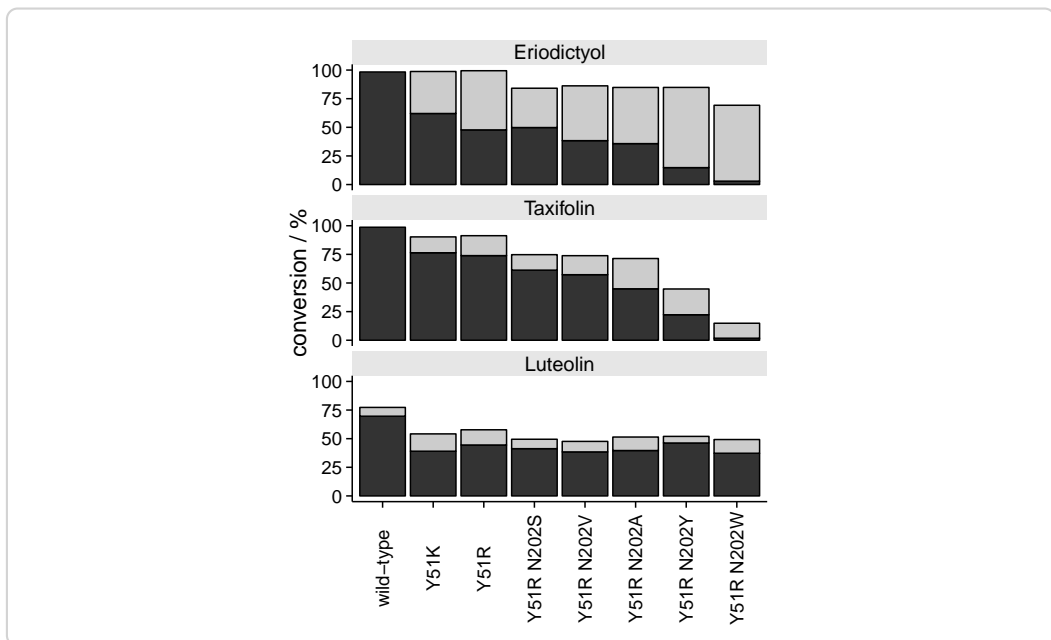


Figure A.2.: Differences in the regioselectivity of some phenylpropanoid and flavonoid O-methyl transferase (PFOMT) variants. The products observed in high-performance liquid chromatography (HPLC) and liquid chromatography coupled mass-spectrometry (LC/MS) measurements switched from 3'-methylated (dark grey) to 4'-methylated (light grey) for the displayed variants. The height of the bars corresponds to the total conversion of substrate.

¹ **B Tandem mass-spectrometry stud-**
² **ies of flavonoids**

Table B.1: Key ions in the positive mode CID and HCD ESI- MS^2 spectra of flavanones.

fragment	CID, 45 % NCE					HCD, 75 % NCE					HCD, 100 % NCE				
	(1)	(2)	(3)	(4)	(5)	(1)	(2)	(3)	(4)	(5)	(1)	(2)	(3)	(4)	(5)
2 [M+H-H ₂ O] ⁺	255(1)	271(18)	269(1)	285(10)	285(4)										
4 [M+H-C ₂ H ₂ O] ⁺	231(4)	247(3)	245(3)	261(2)	261(2)										
5 [M+H-2C ₂ H ₂ O] ⁺	189(5)	205(3)	203(4)	219(2)	219(1)										
8 AC ⁺	179(4)	179(20)	179(5)	179(28)	179(30)	179(1)	179(1)	179(2)	179(2)	179(2)	179(2)	179(2)	179(2)	179(2)	179(1)
11 1,3A ⁺	153(100)	153(31)	153(77)	153(21)	153(57)	153(100)	153(100)	153(100)	153(100)	153(100)	153(69)	153(50)	153(100)	153(63)	153(58)
12 1,3A ⁺ -CO											125(1)	125(1)	125(1)	125(1)	125(1)
13 1,3A ⁺ -C ₂ H ₂ O											111(2)	111(1)	111(1)	111(2)	111(2)
14 1,3A ⁺ -2CO						97(3)	97(4)	97(3)	97(4)	97(4)	97(10)	97(8)	97(15)	97(9)	97(9)
15 1,3A ⁺ -2CO-C ₂ H ₄						69(2)	69(2)	69(2)	69(2)	69(2)	69(9)	69(8)	69(13)	69(9)	69(8)
17 1,4B ⁺ -2H	147(84)	163(100)	161(100)	177(100)	177(100)	147(15)	163(10)	161(10)	177(4)	177(2)	147(3)	163(1)	161(3)		
18 1,4B ⁺ -2H-H ₂ O		145(5)				145(7)									
19 1,4B ⁺ -2H-CO	119(3)	135(1)	133(4)			119(32)	135(29)	133(36)	149(15)	149(11)	119(34)	135(16)	133(36)	149(5)	149(3)
20 1,4B ⁺ -2H-CO-CH ₃							118(11)	134(11)	134(7)		91(100)		118(57)	134(20)	134(13)
22 1,4B ⁺ -2H-2CO						91(24)		90(3)				90(49)			
23 1,4B ⁺ -2H-2CO-CH ₃															
24 1,4B ⁺ -2H-C ₂ H ₂ O-H ₂ O															
25 1,4B ⁺ -2H-H ₂ O-CO							117(18)					117(21)			
26 C ₇ H ₇ ⁺							91(24)	91(1)	91(3)	91(2)	91(100)		91(5)	91(7)	91(5)
27 C ₇ H ₅ ⁺							89(23)		89(29)	89(24)	89(100)	89(22)	89(100)	89(100)	

Table B.2: Key ions in the positive mode CID and HCD ESI-MS² spectra of flavones.

fragment	CID, 45 % NCE				HCD, 75 % NCE				HCD, 100 % NCE			
	(6)	(7)	(8)	(9)	(10)	(6)	(7)	(8)	(9)	(10)	(6)	(7)
1 [M+H] ⁺	271(2)				271(84)	287(66)	285(4)				271(2)	287(2)
2 [M+H-CH ₃] ^{•+}	253(1)	269(9)	270(100)	286(100)	253(3)	269(6)	270(9)	286(20)	286(18)			
3 [M+H-H ₂ O] ⁺	243(7)	259(9)			243(7)					243(2)		
4 [M+H-CO] ⁺	242(14)	258(47)			242(1)	258(3)				242(2)	258(2)	
5 [M+H-CHO] ^{•+}	229(21)	245(13)	243(1)		229(4)		242(100)	258(100)	258(100)			
6 [M+H-C ₂ H ₂ O] ⁺			242(7)				241(1)	257(7)	257(7)			
7 [M+H-CH ₃ -CO] ^{•+}							225(4)	241(16)				
8 [M+H-CH ₄ -CO] ⁺								197(4)	213(7)			
9 [M+H-H ₂ O-CO] ⁺	225(13)	241(13)						187(2)	203(2)			
14 [M+H-CH ₄ -2CO] ⁺								199(1)				
15 [M+H-H ₂ O-2CO] ⁺												
16 [M+H-2C ₂ H ₂ O] ⁺	187(3)	203(4)										
17 [M+H-CH ₃ OH-2CO] ^{•+}												
18 [M+H-CH ₄ -2CO-C ₂ H ₂] ⁺												
20 [M+H-CH ₄ -3CO] ⁺												
23 [M+H-CH ₄ -4CO] ⁺												
24 [M+H-2CO-2C ₂ H ₂ O] ⁺												
27 0,4B ⁺	163(6)	179(7)			131(2)	147(1)				143(1)		
28 0,4B ⁺ -H ₂ O	145(13)	161(12)			163(8)	179(3)				131(5)	147(3)	
25 0,4B ⁺ -C ₂ H ₂ O	121(6)	137(7)			145(17)	161(16)				163(2)		
29 1,3A ⁺	153(100)	153(100)	153(5)		121(16)	137(12)				145(41)	161(29)	
30 1,3A ⁺ -CO					153(100)	153(100)	153(11)	153(8)	153(8)	121(25)	137(16)	
31 1,3A ⁺ -C ₂ H ₂ O					125(1)	125(2)				125(3)	125(2)	
32 1,3A ⁺ -2CO					111(2)	111(2)				111(4)	111(3)	
33 1,3A ⁺ -2CO-C ₂ H ₄					97(2)	97(2)				97(9)	97(1)	
34 1,3B ⁺	119(12)	135(11)	133(2)		69(4)	69(5)				69(24)	69(22)	
35 1,4A ⁺ +2H					119(49)	135(40)	133(3)			69(1)	69(2)	
39 C ₇ H ₇ ⁺	91(1)				91(26)	127(1)				119(35)	127(2)	
40 C ₇ H ₅ ⁺						89(17)				91(100)	89(100)	89(3)
										89(7)	89(100)	89(1)

Table B.3.: Key ions in the positive mode CID and HCD ESI-MS² spectra of flavonoids.

fragment	CID, 45% NCE					HCD, 75% NCE					HCD, 100% NCE				
	(11)	(12)	(13)	(14)	(15)	(11)	(12)	(13)	(14)	(15)	(11)	(12)	(13)	(14)	(15)
1 [M+H] ⁺						287(25)	303(8)	319(1)	301(9)	286(12)	302(6)				
2 [M+H-CH ₃] ^{•+}						286(62)	302(100)			285(5)	301(3)				285(1)
3 [M+H-CH ₄] ⁺						269(32)	285(63)	301(40)	283(2)	299(3)	269(2)	285(3)			
4 [M+H-H ₂ O] ⁺						259(24)	275(14)	291(6)	273(3)	259(3)	259(2)	285(3)			
5 [M+H-CO] ⁺						258(46)	274(20)	290(22)	272(20)	288(3)	258(10)	274(4)	272(2)		
6 [M+H-CHO] ^{•+}											269(11)	285(36)	269(11)	285(11)	
7 [M+H-CH ₃ OH] ^{•+}						245(4)									
9 [M+H-C ₂ H ₅ O] ⁺															
10 [M+H-CH ₃ -CO] ^{•+}															
12 [M+H-CH ₄ -CO] ⁺															
13 [M+H-H ₂ O-CO] ⁺						241(99)	257(100)	273(100)	255(3)	271(5)	241(5)	257(13)	273(6)		
14 [M+H-2CO] ⁺						231(40)	247(37)	263(25)	245(17)	261(8)	231(5)	247(2)	241(2)	257(7)	
15 [M+H-CH ₃ OH-CO] ^{•+}															
17 [M+H-CH ₃ -2CO] ^{•+}															
19 [M+H-CH ₄ -2CO] ⁺															
20 [M+H-H ₂ O-2CO] ⁺						213(77)	229(70)	245(32)	227(2)	243(2)	213(20)	229(49)	245(22)	227(2)	213(12)
21 [M+H-3CO] ⁺															
22 [M+H-2C ₂ H ₂ O] ⁺						203(7)	219(4)	235(4)	217(2)	219(1)	231(1)	213(11)	229(33)	203(1)	219(2)
23 [M+H-H ₂ O-CO-C ₂ H ₂ O] ^{•+}						199(3)	215(2)	231(2)	213(4)	229(3)	213(11)	229(33)	203(3)	219(7)	213(10)
23 [M+H-CH ₃ OH-2CO] ^{•+}															
24 [M+H-CH ₄ -2CO-C ₂ H ₂] ⁺															
25 [M+H-H ₂ O-2CO-C ₂ H ₂] ⁺															
26 [M+H-CH ₄ -3CO] ⁺															
27 [M+H-CH ₄ -2CO-C ₂ H ₂ O] ⁺															
28 [M+H-CH ₄ -4CO] ⁺															
29 [M+H-2CO-C ₂ H ₂ O] ⁺						147(13)	163(7)	179(7)	161(13)	177(2)	147(9)	163(7)	179(9)	147(8)	163(5)
31 0,2A ⁺						165(100)	165(59)	165(41)	165(31)	165(6)	165(11)	165(9)	165(6)	165(1)	165(2)
32 0,2A ⁺ -CO						137(11)	137(23)	137(6)	137(4)	137(47)	137(14)	137(7)	137(15)	137(4)	137(12)
33 0,2B ⁺						121(36)	137(23)	153(35)	135(18)	151(2)	137(47)	153(100)	135(14)	151(2)	121(69)
35 0,3A ⁺ +2H															
37 1,3A ⁺						153(61)	153(20)	153(35)	153(28)	153(4)	153(100)	153(100)	153(65)	153(100)	153(100)
38 1,3A ⁺ -CO															
39 1,3A ⁺ -C ₂ H ₂ O						111(19)	111(7)	111(4)			111(5)	111(6)	111(1)	111(4)	111(5)
40 1,3A ⁺ -2CO											97(2)	97(3)	97(3)	97(14)	97(3)
41 1,3A ⁺ -2CO-C ₂ H ₄						133(25)	149(10)	165(41)			69(7)	69(8)	69(3)	69(33)	69(31)
42 1,3B ⁺ -2H															
49 C ₇ H ₇ ⁺															
50 C ₇ H ₅ ⁺															

¹ C Enzymatic methylation of non-
² catechols

³ C.1 SOMT expression studies

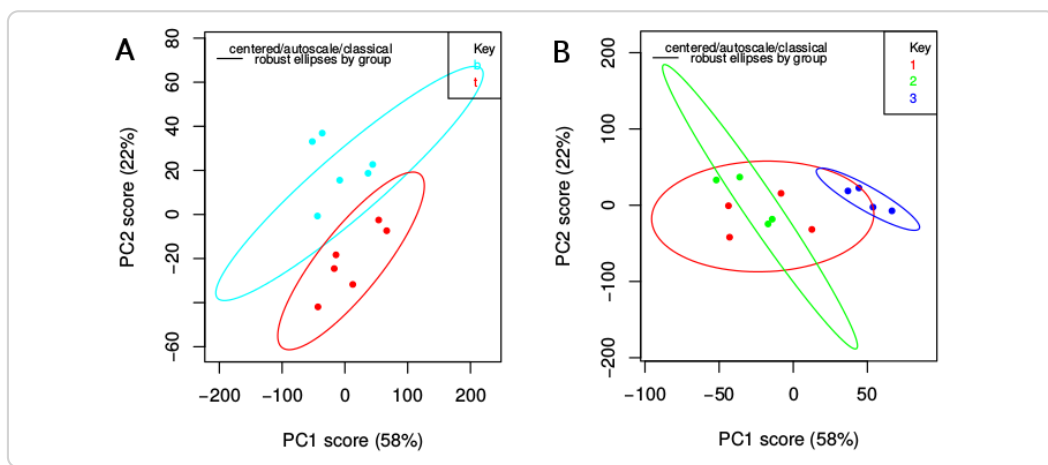


Figure C.1.: Additional scatterplots of the principal component analysis (PCA) of high-performance liquid chromatography (HPLC) data obtained from *N. benthamiana* leaves infiltrated by *A. tumefaciens* harbouring different constructs. **A** – samples colored by leaf position (top: red; bottom: cyan), **B** – samples colored by plant (plant 1: red; plant 2: green; plant 3: blue)

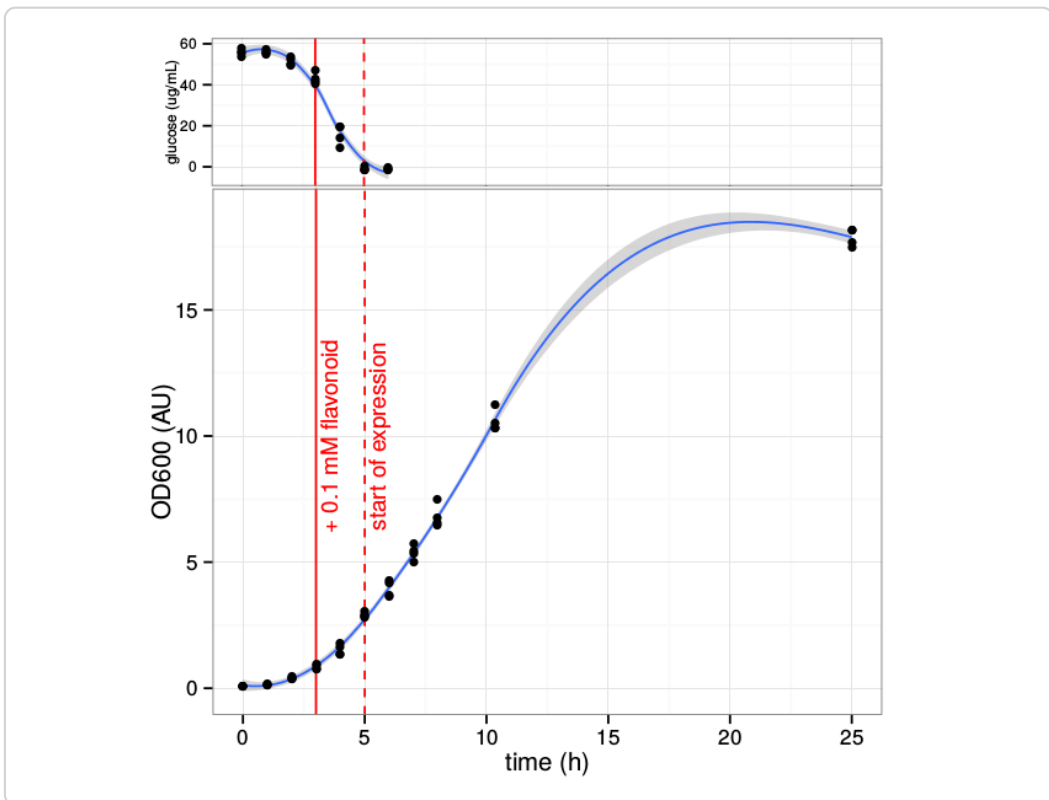


Figure C.2.: Growth curve of *E. coli* BL21(DE3) expressing soy O-methyl transferase (SOMT-2) at 37 °C. Glucose is depleted about 5 hours into growth, at which point the start of SOMT-2 expression is expected. The OD₆₀₀ after inoculation was about 0.1.

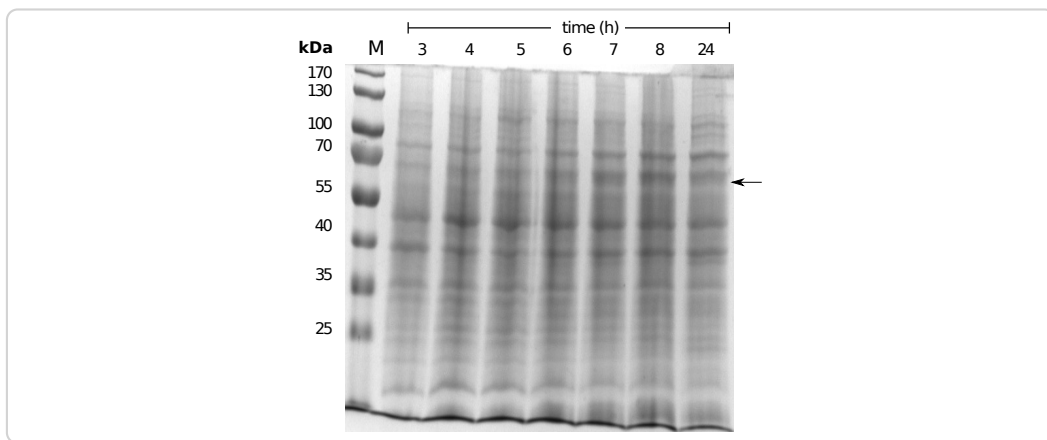


Figure C.3.: sodium dodecylsulfate (SDS)-polyacrylamide gel electrophoresis (PAGE) gel of samples aquired during growth curve measurements. The arrow indicates the band that could correspond to the GST-tagged SOMT-2 protein.

Table C.1.: Results for the Analysis of Variance (ANOVA) of the main effects model describing soluble protein obtained after refolding.

	df	Sum Sq	Mean Sq	F value	Pr(>F)	
Arginine	1	3595.63	3595.63	24.56	0.0158	*
pH	1	529.87	529.87	3.62	0.1533	
Glycerin	1	752.08	752.08	5.14	0.1083	
ionicStrength	1	82.37	82.37	0.56	0.5077	
divCations	1	5.49	5.49	0.04	0.8588	
redox	1	5.52	5.52	0.04	0.8584	
CycloDex	1	134.67	134.67	0.92	0.4083	
SAH	1	896.83	896.83	6.13	0.0897	•
Residuals	3	439.26	146.42			

significance codes: '•' 10 % level; '**' 5 % level

Table C.2.: Results for the ANOVA of the main effects model describing protein activity after refolding.

	df	Sum Sq	Mean Sq	F value	Pr(>F)	
Arginine	1	8.31	8.31	6.62	0.0824	•
pH	1	5.71	5.71	4.55	0.1227	
Glycerin	1	0.44	0.44	0.35	0.5945	
ionicStrength	1	3.38	3.38	2.69	0.1997	
divCations	1	0.54	0.54	0.43	0.5605	
redox	1	24.26	24.26	19.31	0.0218	*
CycloDex	1	1.07	1.07	0.85	0.4250	
SAH	1	0.11	0.11	0.09	0.7893	
Residuals	3	3.77	1.26			

significance codes: '•' 10 % level; '*' 5 % level

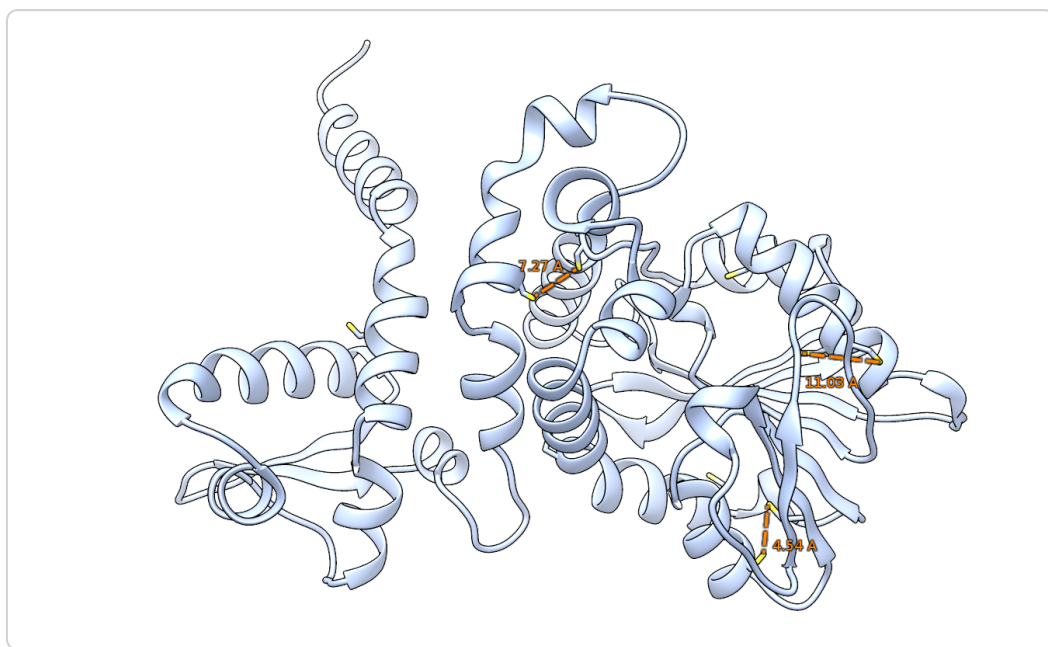


Figure C.4.: Graphical representation of a soy O-methyl transferase (SOMT-2) model obtained from the PHYRE2 web portal (<http://www.sbg.bio.ic.ac.uk/phyre2/html/page.cgi?id=index>) [98]. Cysteines are shown as sticks. The distance between neighboring cysteines that could be oxidized to disulfide bridges is shown in orange.

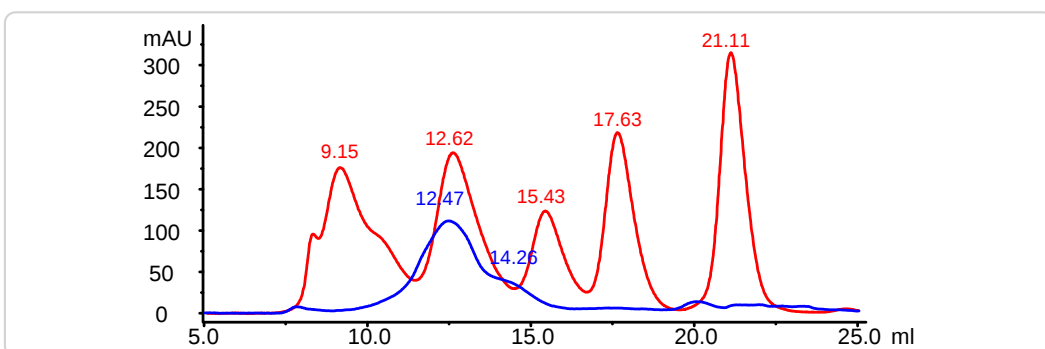


Figure C.5.: Chromatogram of the gel filtration analysis of refolded SOMT-2 (blue). Gel filtrations standards (red) were used to assess the size of the SOMT-2 protein. The estimated molecular weights for the eluting peaks were 165 kDa (12.47 ml) and 65.5 kDa (14.26 ml). Protein standard: 9.15 ml – thyroglobulin (670 kDa), 12.62 ml – γ -globulin (158 kDa), 15.43 ml – ovalbumin (44 kDa), 17.63 ml – myoglobin (17 kDa), 21.11 ml – vitamin B12 (1.35 kDa)

1 C.2 Conversion of non-catechols by PFOMT

2 C.2.1 Modelling and shrinkage of catechols subset (pH pro- 3 file)

4 The bell-shaped pH profile for the catecholic substrates showed, that there might
 5 be a quadratic relationship between pH and activity. A bell-shaped pH profile is
 6 common for most enzymatic reactions, where ionizable groups are involved the
 7 reaction [35]. A quadratic term was thus included into the linear model to capture
 8 this relationship:

$$activity = \beta_0 + \beta_1 \times Mg + \beta_2 \times pH + \beta_3 \times (Mg \times pH) + \beta_4 \times pH^2 + \beta_5 \times (pH^2 \times Mg). \quad (C.1)$$

The model describes the actual data reasonable well, with about 68.6 % of the

Table C.3.: Coefficients of the model (C.1) for activity of catechol methylation by PFOMT. The factor Mg is a categorical variable (addition/no addition) and can therefore only be 0 or 1.

	Estimate	Std. Error	t value	p-value
(Intercept)	-421929.9946	356063.7085	-1.18	0.2557
Mg	-839999.8874	503550.1257	-1.67	0.1175
pH	103271.3345	97739.1728	1.06	0.3086
pH ²	-4977.7406	6512.6996	-0.76	0.4574
Mg × pH	266920.7964	138224.0638	1.93	0.0740 •
Mg × pH ²	-19830.2264	9210.3481	-2.15	0.0492 *

significance codes: '•' 10 % level; '** 5 % level

variance explained ($R^2 = 0.6855$)(Figure 7.10). Also here the p-values for the coefficients β_3 (0.074) and β_4 (0.0492) suggest an interaction between Mg^{2+} and pH (Table C.3), at significant levels of 10 and 5 % respectively. The coefficient estimate of 266920 for β_3 illustrates, that for the catecholic substrates the effect of the pH is much larger than for the methylation of iso-ferulic acid. In addition to the simplified

linear model (Equation C.1) a more complex linear model,

$$\text{activity} = \beta_0 + \beta_1 \times \text{Mg} + \beta_2 \times \text{pH} + \beta_3 \times \text{pH}^2 + \beta_4 \times (\text{Mg} \times \text{pH}) + \beta_5 \times (\text{pH}^2 \times \text{Mg}) + \beta_6 \times (\text{pH} \times \text{pH}^2) + \beta_7 \times (\text{Mg} \times \text{pH} \times \text{pH}^2), \quad (\text{C.2})$$

1 was prepared and shrunken via the LASSO method and 5-fold cross validation
 2 (Table C.4) [195]. The LASSO is a shrinkage method that can shrink coefficients
 3 to exactly zero and thus make a complex model less complex and therefore more
 4 interpretable [195]. The shrunken model only contained the factors pH , $\text{pH} \times \text{Mg}$,
 5 $\text{pH} \times \text{pH}^2$ and $\text{pH} \times \text{Mg} \times \text{pH}^2$. The large coefficient estimate for parameter β_2 (pH)
 6 suggests, that in fact the pH has a large influence on the activity. This is contrary
 7 to the linear model (Equation C.1), which, judged by the p -value for this coefficient,
 8 suggested otherwise. However, the shrunken model also shows that the activity is
 9 dependent on the interaction of pH and magnesium, which supports the implica-
 10 tions of the linear model (Equation C.1). The results of the the shrunken model and
 11 the results obtained by linear modelling are further statistical evidence that pH and
 12 Mg^{2+} show main effects and also interaction effects which seem to be associated
 13 with the enzyme's activity towards catecholic substrates (i.e eriodictyol, caffeic
 14 acid). Nonetheless, all of these rather simple models can not reflect the reality of
 such complex systems as enzymes where lots of factors play important roles.

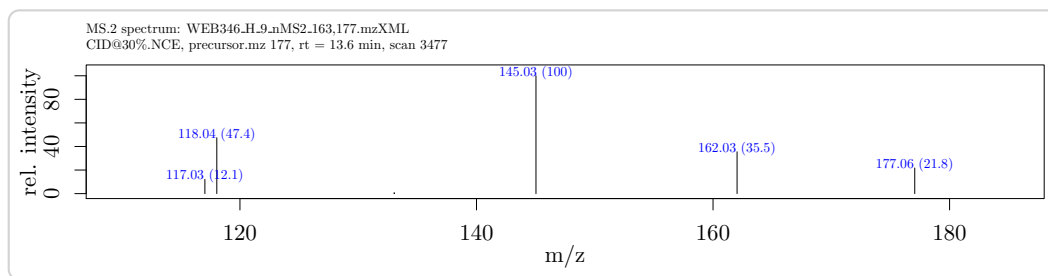
Table C.4: Coefficients obtained for linear regression model using the catechols subset after shrinkage using the Lasso method and 5-fold cross validation. Only non-zero coefficients (variables actually do have an effect) are retained during the Lasso. Seed was set to 1336.

variable	coefficient
(Intercept)	-467632.3821
pH	94469.8366
$\text{pH} \times \text{Mg}$	19068.9540
$\text{pH} \times \text{pH}^2$	-381.5863
$\text{pH} \times \text{Mg} \times \text{pH}^2$	-292.3608

C.3 Identification of products from conversion of non-catechols by PFOMT

C.3.1 *p*-Coumaric acid methylester

The product obtained by conversion of *p*-coumaric acid by phenylpropanoid and flavonoid O-methyl transferase (PFOMT) was determined as 4-hydroxy cinnamic acid methyl ester. The negative mode MS² spectrum showed four prominent peaks *m/z* 177 (21) [M-H]⁻, 162(35), 145(100) and 118(47). If the enzymatic product was the methyl ether, one would expect a strong *m/z* 133, corresponding to [M-H-CO₂]⁻ [186]. However *m/z* 133 was not observed, strongly suggesting the methyl ester. Comparison of the obtained data with literature data confirmed the methyl ester as sole product [87].



C.3.2 *iso*-Ferulic acid esters and caffeic acid dimethylether

Methylation of *iso*-ferulic acid and ferulic acid afforded two methylated products with retention times of 12.9 and 13.7 min. The compound eluting at 12.9 min was identified as caffeic acid dimethylether (**1**) through comparison to an authentic standard, whereas the compounds eluting about one minute later were identified as the ferulic (**2**) and *iso*-ferulic acid methyl esters (**3**). Since the the retention time is an indicator for the polarity of an eluting compound and the methyl ester is much more unpolar than the dimethyl ether, it comes as no surprise that the latter elutes earlier on a reversed-phase column. Ionization of the enzymatic products was difficult in negative mode, but easily achieved in positive mode. The only

1 peaks in the positive mode MS² spectra of (**1**) and (**2,3**) were *m/z* 191 and *m/z* 177
 2 respectively. This indicates a loss of water and methanol from the dimethylether
 3 and methyl ester respectively.

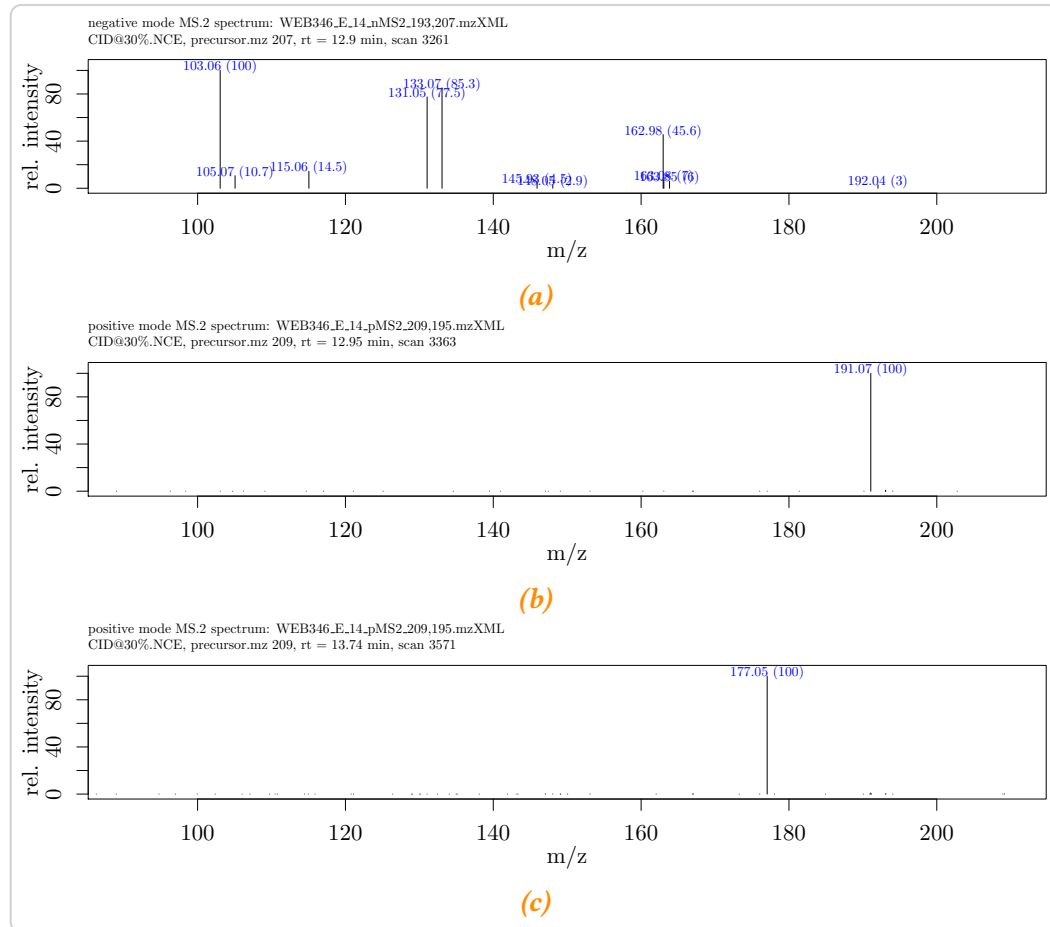


Figure C.6.: MS² spectra of (**1**) and (**3**). (a) negative mode MS² of (**1**). (b) positive mode MS² of (**1**). (c) positive mode MS² of (**3**).

4 C.3.3 3',4'-dimethyl eriodictyol

5 Conversion of homoeriodictyol or hesperetin by PFOMT afforded 3',4'-dimethyl
 6 eriodictyol (**4**). The product was identified by liquid chromatography-tandem mass
 7 spectrometry (LC-MS/MS). Products from both conversions possessed the same
 8 retention times of 14.54 min. The collision induced dissociation (CID) spectra of

these products showed five distinct signals at m/z 299 (14), 191(100), 179(62), 165(17) and 153(67) (Figure C.7). The m/z 299 corresponds to the ion $[M+H-H_2O]^+$, showing that both, homoeriodictyol as well as hesperetin were methylated. The m/z 153 corresponds to the $^{1,3}A^+$ fragment, which is characteristic for 3,7-dihydroxy substituted flavonoids. This indicates a methylation of the B-ring. Further evidence of a dimethoxylated B-ring is the fragment $^{1,4}B^+-2H$ with m/z 191. The fragmentation pattern of 3',4'-dimethyl eriodictyol agrees with the general fragmentation of flavanones described in chapter 6.

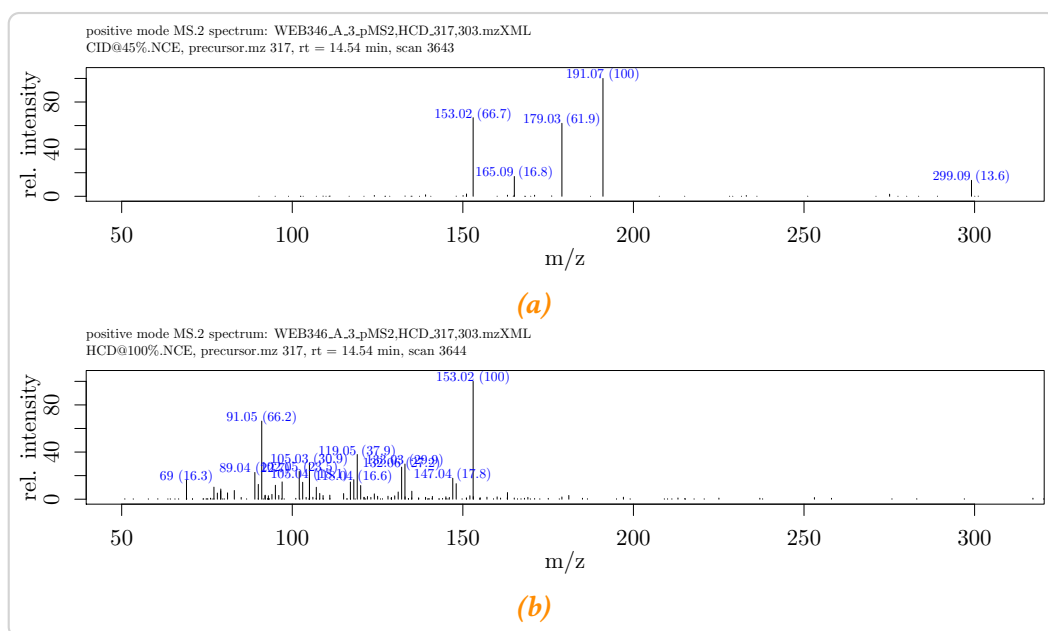


Figure C.7: MS^2 spectra of 3',4'-dimethyl eriodictyol (4). (a) positive mode MS^2 CID spectrum of (4). (b) positive mode MS^2 HCD spectrum of (4).

C.3.4 3',4'-dimethyl luteolin

Conversion of diosmetin and chrysoeriol by PFOMT afforded 3',4'-dimethyl luteolin (5) and an unidentified product. (5) eluted after 14.53 min. The CID spectrum of (5) shows three signals, m/z 300 (100), 299(87) and 271(17) (Figure C.8). These signals correspond to the $[M+H-CH_3]^{+}$, $[M+H-CH_4]^{+}$ and $[M+H-CH_4-CO]^{+}$ ions respectively. The higher-energy collisional dissociation (HCD) spectrum of (5)

- 1 clearly shows a peak with m/z 153 amongst other masses. Again, this is spectro-
 2 metric evidence of a 3,7-dihydroxylated flavonoid (fragment $^{1,3}\text{A}^+$) demonstrating
 a 3',4'-dimethylation. The unidentified products of the conversions of apigenin,

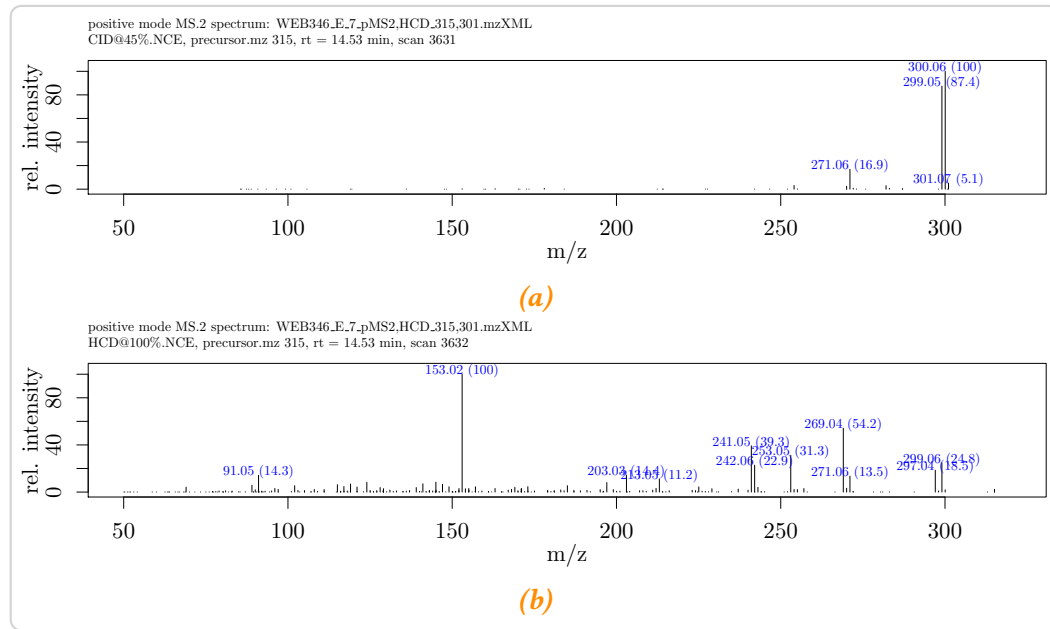


Figure C.8.: MS^2 spectra of 3',4'-dimethyl luteolin (**5**). **(a)** positive mode MS^2 CID spectrum of (**5**). **(b)** positive mode MS^2 HCD spectrum of (**5**).

- 3
 4 diosmetin and chrysoeriol eluted after 12.59, 12.77 and 12.69 min respectively.

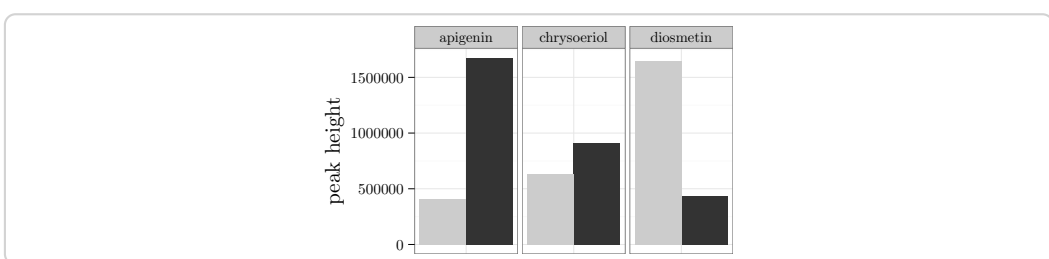


Figure C.9.: Product composition after conversion of flavones with PFOMT. Bar chart of the peak heights of the unidentified (black) and (3' or 4')-O-methylated products (gray) in the selected ion chromatograms (HCD at 100 % NCE). The conversion experiments were conducted with the wild-type PFOMT at pH 8.6 with 10 mM Mg²⁺ added.

¹ D Additional information

Table D.2.: SAM analogues that have been used with MTs. Targets: P – peptide/protein, D – DNA, R – RNA, S – small molecule.

analogue	enzyme	target	references
<i>SAM</i>			
–CH ₂ –CH ₃	PRMT1, M.TaqI, M.HhaI, M.BcnIB, RebM, RapM	S,P,D	[44, 114, 184, 194] ¹
–CH ₂ –CH ₂ –CH ₃	PRMT1, M.TaqI, M.HhaI, M.BcnIB	P,D	[44, 194]
–CH ₂ –CH ₂ –CH ₂ –CH ₃	PRMT1	P	[194]
–CH ₂ –C ₆ H ₅	NovO, CouO,	S,P	[187, 194]
–CH ₂ –C(=O)–CH ₃	PRMT1 COMT, TPMT, CazF	S	[116, 217]

¹Singh *et al.* (2014) published a series of 44 biocatalytically synthesized SAM and *Se*-adenosyl selenomethionine (*Se*AM) derivatives, most of which were not tested towards their alkyl donation potential in MT reactions.

analogue	enzyme	target	references
$-\text{CH}_2-\text{CH}=\text{CH}_2$	NovO, CouO, RapM, PRMT1, M.TaqI, M.HhaI, M.BcnIB, RebM, Tgs	P,S,D	[44, 114, 175, 184, 187, 192, 194, 208, 209]
$-\text{CH}_2-\text{CH}=\text{CH}-\text{CH}_3$	NovO, CouO	S	[187]
$-\text{CH}_2-\text{C}\equiv\text{CH}$	Dim-5, HsMLL, TRM1, NovO, CouO, PRMT1	P,R,S	[86, 187, 208, 209, 215]
$-\text{CH}_2-\text{C}\equiv\text{N}$	RebM	S	[184]
$-\text{CH}_2-\text{CH}_2-\text{C}\equiv\text{CH}$	PKMT	P	[86]
$-\text{CH}_2-\text{CH}_2-\text{CH}_2-\text{C}\equiv\text{CH}$	PKMT	P	[86]
$-\text{CH}_2-\text{C}\equiv\text{C}-\text{CH}_3$	NovO, CouO, M.HhaI, M.TaqI, M.BcnIB	S,D	[44, 129, 187]
$-\text{CH}_2-\text{C}\equiv\text{C}-\text{CH}_2-\text{CH}_3$	M.HhaI	D	[129]
$-\text{CH}_2-\text{C}\equiv\text{C}-\text{CH}_2-\text{NH}_2$	M.HhaI	D	[129]
$-\text{CH}_2-\text{C}\equiv\text{C}-\text{CH}_2-\text{NH}-\text{C}(=\text{O})(-\text{CH}_2-)_3-\text{NH}_2$	M.HhaI	D	[129]
$-\text{CH}_2-\text{C}\equiv\text{C}(-\text{CH}_2-)_3-\text{NH}_2$	M.HhaI	D	[129]
$-\text{CH}_2-\text{C}\equiv\text{C}(-\text{CH}_2-)_3-\text{NH}-\text{C}(=\text{O})(-\text{CH}_2-)_3-\text{NH}_2$	M.HhaI	D	[129]
$-\text{CH}_2-\text{C}\equiv\text{C}(-\text{CH}_2-)_3-\text{C}\equiv\text{CH}$	M.HhaI	D	[129]
$-\text{CH}_2-\text{C}\equiv\text{C}(-\text{CH}_2-)_3-\text{N}_3$	M.HhaI	D	[129]
$-\text{CH}_2-\text{CH}=\text{CH}-\text{C}\equiv\text{CH}$	Dim-5, HsMLL, TRM1, PRMT1, Tgs	P,R	[86, 150, 158, 175, 208, 209, 215]
$-\text{CH}_2-\text{CH}=\text{CH}-\text{CH}_2-\text{C}\equiv\text{CH}$			[86, 208]

Appendix D. Additional information

analogue	enzyme	target	references
$-\text{CH}_2-\text{CH}=\text{CH}-\text{CH}_2-\text{O}-\text{CH}_2-\text{C}\equiv\text{CH}$	PRMT1	P	[208, 209]
<i>SeAM</i>			
$-\text{CH}_3$			
$-\text{CH}_2-\text{C}\equiv\text{CH}$	Dim-5, <i>HsMLL</i> , TRM1, RebM, CazF	P,R,S	[19, 184, 215, 217]
<i>N</i> -mustard derivatives			
$-\text{CH}_2-\text{CH}_2-\text{I}$	RebM	S	[229]

Table D.1: Overview over the constructs produced for the present thesis. Each step during the production of the construct is given in the workflow steps column. Primers (*italic font*) or restriction sites used during each step are displayed in parenthesis.

construct name	description	entry constructs	con-	destination	workflow steps (primers/cloning sites)
pBEW103	pBEW102 with BamHI cloning site	pBEW102		pBEW103	amplification (<i>pRhal,fw/rv</i>), cloning (BglII, BamHI)
pBEW104	rhalPBAD promoter	pBEW4b		pICH413038	amplification (<i>somt1/2/3/4</i> , golden gate cloning (BpuI))
pBEW106	pICH413038-somt	pET28MC-somt		pICH75044	golden gate cloning (Bsal)
pBEW107		pICH51266,			
		pBEW106,			
		pICH41421			
pET28-pfomt	<i>pfromt</i> gene in pET-28a(+), endogenous NdeI site removed	pQE30-pfomt	pET-28a(+)	<i>(pfromt,fw/rv)</i> , mutagenesis	amplification (<i>pfromt,fw/rv</i>), cloning (NdeI, EcoRI)
	N-terminal pfB-tag fusion for periplasmic expression			<i>(pfromt,fw/rv)</i> , mutagenesis	amplification
pET20-somt			pET20-b(+)		
pET28-somt				pET28-a(+)	
pET32-somt				pET-32a(+)	
pET41-somt				pET-41a(+)	
pUC19*	added BpuI site	pUC19		-	mutagenesis (<i>pUC1,fw/rv</i>)
pUCB1	pUC19 derivative with <i>lsrA</i> promoter	<i>lsr</i> -XX-DAS	pUC19*	pUC19*	cloning (NdeI, BglII)

¹ Bibliography

- 2 [1] Paul D. Adams et al. “PHENIX: A comprehensive Python-based system for
3 macromolecular structure solution”. en. In: *Acta Crystallographica Section*
4 *D: Biological Crystallography* 66.2 (Feb. 2010), pp. 213–221.
- 5 [2] Giovanni Agati et al. “Flavonoids as antioxidants in plants: location and
6 functional significance.” In: *Plant science : an international journal of exper-*
7 *imental plant biology* 196 (Nov. 2012), pp. 67–76.
- 8 [3] Agilent Technologies. *QuikChange II Site-Directed Mutagenesis Kit: Instruc-*
9 *tion Manual*. 2011.
- 10 [4] Neda Akbari et al. “Efficient refolding of recombinant lipase from Es-
11 cherichia coli inclusion bodies by response surface methodology”. In: *Protein*
12 *Expression and Purification* 70.2 (Apr. 2010), pp. 254–259.
- 13 [5] Martin Alexander and B. K. Lustigman. “Effect of Chemical Structure on
14 Microbial Degradation of Substituted Benzenes”. In: *Journal of Agricultural*
15 *and Food Chemistry* 14.4 (July 1966), pp. 410–413.
- 16 [6] Bernd Anselment et al. “Experimental optimization of protein refolding
17 with a genetic algorithm”. In: *Protein Science* 19.11 (2010), pp. 2085–2095.
- 18 [7] F Ausubel et al. “Current Protocols in Molecular Biology”. In: (2008), p. 23.
- 19 [8] Peter Ball et al. “Kinetic Properties of a Soluble Catechol 0-Methyltransferase
20 of Human Liver”. In: *Eur J Biochem* 26 (1972), pp. 560–569.
- 21 [9] R V Banerjee and R G Matthews. “Cobalamin-dependent methionine syn-
22 thase.” In: *The FASEB journal : official publication of the Federation of Amer-*
23 *ican Societies for Experimental Biology* 4.5 (1990), pp. 1450–1459.
- 24 [10] G.M. Barton. “New C-methylflavanones from Douglas-fir”. In: *Phytochem-*
25 *istry* 11.1 (Jan. 1972), pp. 426–429.

Bibliography

- 1 [11] Isabelle Benoit et al. “Expression in Escherichia coli, refolding and crys-
2 tallization of Aspergillus niger feruloyl esterase A using a serial factorial
3 approach”. In: *Protein Expression and Purification* 55.1 (Sept. 2007), pp. 166–
4 174.
- 5 [12] Sanjoy K. Bhattacharya and Ashok K. Dubey. “Kinetic mechanism of cy-
6 tosine DNA methyltransferase MspI”. In: *Journal of Biological Chemistry*
7 274.21 (1999), pp. 14743–14749.
- 8 [13] Amie K Boal et al. “Structural basis for methyl transfer by a radical SAM
9 enzyme.” In: *Science (New York, N.Y.)* 332.6033 (2011), pp. 1089–1092.
- 10 [14] S. Bocker and F. Rasche. “Towards de novo identification of metabolites by
11 analyzing tandem mass spectra”. In: *Bioinformatics* 24.16 (2008), pp. i49–i55.
- 12 [15] Gyu Kim Bong et al. “Synthesis of ermanin, 5,7-dihydroxy-3,4'-dimethoxyflavone
13 from kaempferol, 3,5,7,4'-tetrahydroxyflavone with two O-methyltransferases
14 expressed in E. coli”. In: *Bulletin of the Korean Chemical Society* 27.3 (2006),
15 pp. 357–358.
- 16 [16] Ronald T. Borchardt. “Mechanism of alkaline hydrolysis of S-adenosyl-L-
17 methionine and related sulfonium nucleosides”. In: *Journal of the American
18 Chemical Society* 101.2 (1979), pp. 458–463.
- 19 [17] U. T. Bornscheuer et al. “Engineering the third wave of biocatalysis”. In:
20 *Nature* 485.7397 (May 2012), pp. 185–194.
- 21 [18] Ian R. Bothwell and Minkui Luo. “Large-scale, protection-free synthesis of
22 Se-adenosyl-l-selenomethionine analogues and their application as cofactor
23 surrogates of methyltransferases”. In: *Organic Letters* 16.11 (2014), pp. 3056–
24 3059.
- 25 [19] Ian R. Bothwell et al. “Se-adenosyl-L-selenomethionine cofactor analogue
26 as a reporter of protein methylation”. In: *Journal of the American Chemical
27 Society* 134.36 (2012), pp. 14905–14912.
- 28 [20] George E. P. Box, J. Stuart Hunter, and William G. Hunter. *Statistics for
29 Experimenters: Design, Innovation, and Discovery*. 2nd ed. New York: Wiley-
30 Interscience, 2005.
- 31 [21] M M Bradford. “A rapid and sensitive method for the quantitation of micro-
32 gram quantities of protein utilizing the principle of protein-dye binding.”
33 In: *Analytical biochemistry* 72.1-2 (May 1976), pp. 248–254.

Bibliography

- 1 [22] Wolfgang Brandt, Kerstin Manke, and Thomas Vogt. "A catalytic triad
2 – Lys-Asn-Asp – Is essential for the catalysis of the methyl transfer in
3 plant cation-dependent O-methyltransferases". In: *Phytochemistry* 113 (May
4 2015), pp. 130–139.
- 5 [23] W Brandt et al. "Molecular and structural basis of metabolic diversity medi-
6 ated by prenyldiphosphate converting enzymes". In: *Phytochemistry* 70.15-
7 16 (Oct. 2009), pp. 1758–1775.
- 8 [24] Joan B Broderick et al. "Radical S - Adenosylmethionine Enzymes". In:
9 (2014).
- 10 [25] W. Butte. "Rapid method for the determination of fatty acid profiles from
11 fats and oils using trimethylsulphonium hydroxide for transesterification".
12 In: *Journal of Chromatography A* 261 (1983), pp. 142–145.
- 13 [26] G. L. Cantoni. "S-Adenosylmethionine; Anew intermediate formed enzy-
14 matically from L-methionine and adenosinetriphosphate". In: *The Journal
15 of Biological Chemistry* 204 (1953), pp. 403–416.
- 16 [27] Guohua Cao, Emin Sofic, and Ronald L. Prior. "Antioxidant and Prooxidant
17 Behavior of Flavonoids: Structure-Activity Relationships". In: *Free Radical
18 Biology and Medicine* 22.5 (Jan. 1997), pp. 749–760.
- 19 [28] Hung Ju Chen, Baskaran Stephen Inbaraj, and Bing Huei Chen. "Determi-
20 nation of phenolic acids and flavonoids in Taraxacum formosanum kitam
21 by liquid chromatography-tandem mass spectrometry coupled with a post-
22 column derivatization technique". In: *International Journal of Molecular
23 Sciences* 13.1 (2012), pp. 260–285.
- 24 [29] Jing Chen et al. "Different Effects of L -Arginine on Protein Refolding :
25 Suppressing Aggregates of Hydrophobic Interaction, Not Covalent Binding".
26 In: (2008), pp. 1365–1372.
- 27 [30] Vincent B. Chen et al. "MolProbity: All-atom structure validation for macro-
28 molecular crystallography". In: *Acta Crystallographica Section D: Biological
29 Crystallography* 66.1 (Jan. 2010), pp. 12–21.
- 30 [31] a Claiborne and Irwin Fridovich. "of of of". In: *Society* 18 (1979), pp. 2324–
31 2329.
- 32 [32] Heather Coiner et al. "Methylation of sulfhydryl groups: a new function
33 for a family of small molecule plant O-methyltransferases." In: *The Plant
34 journal : for cell and molecular biology* 46.2 (Apr. 2006), pp. 193–205.
- 35 [33] Austria Computing, R Foundation for Statistical Vienna. *R: A language and
36 environment for statistical computing*. Vienna, Austria, 2008.

Bibliography

- 1 [34] Robert a. Copeland. "Molecular pathways: Protein methyltransferases in
2 cancer". In: *Clinical Cancer Research* 19.23 (2013), pp. 6344–6350.
- 3 [35] Athel Cornish-Bowden. *Fundamentals of Enzyme Kinetics*. 3rd ed. London:
4 Portland Press Ltd, 2004.
- 5 [36] Marjorie Murphy Cowan. "Plant Products as Antimicrobial Agents". In:
6 *Clin. Microbiol. Rev.* 12.4 (1999), pp. 564–582.
- 7 [37] J K Coward, E P Slixz, and F Y Wu. "Kinetic studies on catechol O-
8 methyltransferase. Product inhibition and the nature of the catechol
9 binding site." In: *Biochemistry* 12.12 (1973), pp. 2291–2297.
- 10 [38] Ivana Crnovčić, Roderich Süssmuth, and Ullrich Keller. "Aromatic C-
11 Methyltransferases with Antipodal Stereoselectivity for Structurally
12 Diverse Phenolic Amino Acids Catalyze the Methylation Step in the
13 Biosynthesis of the Actinomycin Chromophore". In: *Biochemistry* 49.45
14 (Nov. 2010), pp. 9698–9705.
- 15 [39] Rodney Croteau, Toni M Kutchan, and Norman G Lewis. "Secondary
16 Metabolites". In: *Biochemistry Molecular Biology of Plants*. Ed. by B.
17 Buchanan, W. Gruissem, and R. Jones. Vol. 7. 7. 2000, pp. 1250–1318.
- 18 [40] T.P. Tim Cushnie and Andrew J. Lamb. "Antimicrobial activity of
19 flavonoids". In: *International Journal of Antimicrobial Agents* 26.5 (Nov.
20 2005), pp. 343–356.
- 21 [41] Filip Cuyckens and Magda Claeys. "Mass spectrometry in the structural
22 analysis of flavonoids". In: *Journal of Mass Spectrometry* 39.1 (2004), pp. 1–
23 15.
- 24 [42] Ermias Dagne et al. "O-Geranylated and O-prenylated flavonoids from
25 Millettia ferruginea". In: *Phytochemistry* 29.8 (1990), pp. 2671–2673.
- 26 [43] Yuntao Dai et al. "Natural deep eutectic solvents as new potential media for
27 green technology". In: *Analytica Chimica Acta* 766 (Mar. 2013), pp. 61–68.
- 28 [44] Christian Dalhoff et al. "Direct transfer of extended groups from syn-
29 synthetic cofactors by DNA methyltransferases." In: *Nature chemical biology*
30 2.1 (2006), pp. 31–32.
- 31 [45] Christian Dalhoff et al. "Synthesis of S-adenosyl-L-methionine analogs and
32 their use for sequence-specific transalkylation of DNA by methyltrans-
33 ferases." In: *Nature protocols* 1.4 (2006), pp. 1879–1886.
- 34 [46] Daresbury Laboratory. "No Title". In: *Newsletter on protein crystallography*
35 33 (1997), pp. 25–30.

Bibliography

- 1 [47] Bettina E. Deavours et al. “Functional analysis of members of the isoflavone
2 and isoflavanone O-methyltransferase enzyme families from the model
3 legume *Medicago truncatula*”. In: *Plant Molecular Biology* 62.4-5 (2006),
4 pp. 715–733.
- 5 [48] Martin Dippe et al. “Engineering of a Mg²⁺-dependent O-methyltransferase
6 towards novel regiospecificity”. In: *manuscript submitted* (2015).
- 7 [49] M. Dippe et al. “Rationally engineered variants of Sadenosylmethionine
8 (SAM) synthase: reduced product inhibition and synthesis of artificial co-
9 factor homologues”. en. In: *Chem. Commun.* 51.17 (Feb. 2015), pp. 3637–
10 3640.
- 11 [50] M M Dixon et al. “The structure of the C-terminal domain of methionine
12 synthase: presenting Sadenosylmethionine for reductive methylation of
13 B12.” In: *Structure (London, England : 1993)* 4.11 (1996), pp. 1263–1275.
- 14 [51] J D Dunitz. “The entropic cost of bound water in crystals and biomolecules.”
15 In: *Science (New York, N.Y.)* 264.5159 (Apr. 1994), p. 670.
- 16 [52] J D Dunitz. “Win some, lose some: enthalpy-entropy compensation in
17 weak intermolecular interactions.” In: *Chemistry & biology* 2.11 (Nov. 1995),
18 pp. 709–712.
- 19 [53] Elsevier. *Reaxys, version 2.19790.2*.
- 20 [54] P. Emsley et al. “Features and development of Coot”. In: *Acta Crystallo-*
21 *graphica Section D: Biological Crystallography* 66.4 (2010), pp. 486–501.
- 22 [55] Carola Engler, Romy Kandzia, and Sylvestre Marillonnet. “A one pot, one
23 step, precision cloning method with high throughput capability”. In: *PLoS ONE* 3.11 (Jan. 2008), e3647.
- 24 [56] Madeleine Ernst et al. “Mass spectrometry in plant metabolomics strategies:
25 from analytical platforms to data acquisition and processing.” en. In: *Natural
26 product reports* 31.6 (June 2014), pp. 784–806.
- 27 [57] Philip Evans. “Scaling and assessment of data quality”. In: *Acta Crystallo-*
28 *graphica Section D: Biological Crystallography* 62.1 (Jan. 2006), pp. 72–82.
29 arXiv: S0907444905036693 [doi: 10.1107].
- 30 [58] Nicolas Fabre et al. “Determination of flavone, flavonol, and flavanone
31 aglycones by negative ion liquid chromatography electrospray ion trap mass
32 spectrometry”. In: *Journal of the American Society for Mass Spectrometry*
33 12.6 (2001), pp. 707–715.

Bibliography

- 1 [59] J L Ferrer et al. “Structure of chalcone synthase and the molecular basis
2 of plant polyketide biosynthesis.” In: *Nature structural biology* 6.8 (1999),
3 pp. 775–784.
- 4 [60] Alan Fersht. *Structure and mechanism in protein science*. Ed. by Michelle R.
5 Julet and Georgia L. Hadler. New York: W.H. Freeman and Company, 1999.
- 6 [61] H G Floss and M D Tsai. “Chiral methyl groups.” In: *Advances in enzymology*
7 and related areas of molecular biology
- 8 [62] Heinz G. Floss and Sungsook Lee. “Chiral Methyl Groups: Small is Beautiful”.
9 In: *Acc. Chem. Res.* 26.3 (1993), pp. 116–122.
- 10 [63] Matthew W. Freyer and Edwin a. Lewis. “Isothermal Titration Calorimetry:
11 Experimental Design, Data Analysis, and Probing Macromolecule/Ligand
12 Binding and Kinetic Interactions”. In: *Methods in Cell Biology* 84.07 (Jan.
13 2008), pp. 79–113.
- 14 [64] Mendel Friedman et al. “Antimicrobial activities of tea catechins and
15 theaflavins and tea extracts against *Bacillus cereus*.” In: *Journal of food*
16 *protection* 69.2 (2006), pp. 354–361.
- 17 [65] Akiko Fujimoto, Atsushi Hirano, and Kentaro Shiraki. “Ternary system of
18 solution additives with Arginine and salt for refolding of beta-galactosidase”.
19 In: *Protein Journal* 29.3 (2010), pp. 161–166.
- 20 [66] Gasteiger E. et al. “Protein Identification and Analysis Tools on the ExPASy
21 Server”. In: *The Proteomics Protocols Handbook*, Humana Press. Ed. by John
22 M. Walker. Humana Press, 2005, pp. 571–607.
- 23 [67] Paul J. Gates and Norberto P. Lopes. “Characterisation of Flavonoid Agly-
24 cones by Negative Ion Chip-Based Nanospray Tandem Mass Spectrometry”.
25 In: *International Journal of Analytical Chemistry* 2012 (2012), pp. 1–7.
- 26 [68] Christine L. Gee et al. “Disulfide-linked dimers of human adrenaline synthe-
27 sizing enzyme PNMT are catalytically active”. In: *Biochimica et Biophysica*
28 *Acta - Proteins and Proteomics* 1750.1 (June 2005), pp. 82–92.
- 29 [69] Azra Gholami et al. “Natural product biosynthesis in *Medicago* species.” In:
30 *Natural product reports* 31.3 (2014), pp. 356–80.
- 31 [70] S C Gill and P H von Hippel. “Calculation of protein extinction coefficients
32 from amino acid sequence data.” In: *Analytical biochemistry* 182.2 (Nov.
33 1989), pp. 319–326.
- 34 [71] Paola Gilli et al. “Enthalpy-Entropy Compensation in Drug-Receptor Bind-
35 ing”. In: *Journal of Physical Chemistry* 98.5 (Feb. 1994), pp. 1515–1518.

Bibliography

- 1 [72] R M Goodrich and R J Braddock. "Major By-Products of the Florida Citrus
2 Processing". In: *Processing* (2006), pp. 1–4.
- 3 [73] Carmen H. Gray et al. ".alpha.-Deuterium and carbon-13 isotope effects
4 for a simple, intermolecular sulfur-to-oxygen methyl-transfer reaction.
5 Transition-state structures and isotope effects in transmethylation and
6 transalkylation". In: *Journal of the American Chemical Society* 101.15 (1979),
7 pp. 4351–4358.
- 8 [74] Erich Grotewold. *The Science of Flavonoids The Science of Flavonoids*. Ed. by
9 Erich Grotewold. 1st ed. New York: Springer, 2006, pp. 1–274.
- 10 [75] Amandine Guelorget et al. "Insights into the hyperthermostability and
11 unusual region-specificity of archaeal Pyrococcus abyssi tRNA m1A57/58
12 methyltransferase". In: *Nucleic Acids Research* 38.18 (2010), pp. 6206–6218.
- 13 [76] R. Hegnauer. *The Flavonoids*. Ed. by J. B. Harborne. 1st ed. Vol. 15. 2. Chap-
14 man and Hall, 1976, p. 357.
- 15 [77] J L Hoffman. "Chromatographic analysis of the chiral and covalent instabil-
16 ity of S-adenosyl-L-methionine." In: *Biochemistry* 25.15 (1986), pp. 4444–
17 4449.
- 18 [78] Albert Hofmann. *Die Mutterkornalkaloide*. Solothurn: Nachtschatten Verlag,
19 2000.
- 20 [79] E.C. Horning et al. "Liquid chromatograph—mass spectrometer—computer
21 analytical systems". In: *Journal of Chromatography A* 99 (Jan. 1974), pp. 13–
22 21.
- 23 [80] Yonglin Hu et al. "Crystal structures of a *Populus tomentosa* 4-coumarate:CoA
24 ligase shed light on its enzymatic mechanisms." In: *The Plant cell* 22.9
25 (2010), pp. 3093–3104.
- 26 [81] Ze Lin Huang et al. "Deep eutectic solvents can be viable enzyme activa-
27 tors and stabilizers". In: *Journal of Chemical Technology and Biotechnology*
28 October 2013 (2014).
- 29 [82] Ruth Huey et al. "Software news and update a semiempirical free energy
30 force field with charge-based desolvation". In: *Journal of Computational
31 Chemistry* 28.6 (Apr. 2007), pp. 1145–1152.
- 32 [83] Richard J. Hughes et al. "A tandem mass spectrometric study of selected
33 characteristic flavonoids". In: *International Journal of Mass Spectrometry*
34 210-211 (2001), pp. 371–385.

Bibliography

- 1 [84] Sarah C Hunter and Edgar B Cahoon. “Enhancing vitamin E in oilseeds:
2 unraveling tocopherol and tocotrienol biosynthesis.” In: *Lipids* 42.2 (Mar.
3 2007), pp. 97–108.
- 4 [85] Mwafaq Ibdah et al. “A Novel Mg²⁺-dependent O-Methyltransferase in the
5 Phenylpropanoid Metabolism of *Mesembryanthemum crystallinum*”. In:
6 *Journal of Biological Chemistry* 278.45 (Nov. 2003), pp. 43961–43972.
- 7 [86] Kabirul Islam et al. “Expanding cofactor repertoire of protein lysine methyl-
8 transferase for substrate labeling”. In: *ACS Chemical Biology* 6.7 (2011),
9 pp. 679–684.
- 10 [87] Tiffany M. Jarrell et al. “Characterization of organosolv switchgrass lignin
11 by using high performance liquid chromatography/high resolution tandem
12 mass spectrometry using hydroxide-doped negative-ion mode electrospray
13 ionization”. In: *Green Chemistry* 16.5 (2014), p. 2713.
- 14 [88] J M Jez et al. “Structure and mechanism of the evolutionarily unique plant en-
15 zyme chalcone isomerase.” In: *Nature structural biology* 7.9 (2000), pp. 786–
16 791.
- 17 [89] Eun Ji Joe et al. “Engineering of flavonoid O-methyltransferase for a novel
18 regioselectivity.” In: *Molecules and cells* 30.2 (Aug. 2010), pp. 137–41.
- 19 [90] Julien Jorda and Todd O. Yeates. “Widespread disulfide bonding in proteins
20 from thermophilic archaea”. In: *Archaea* 2011 (2011).
- 21 [91] P.D. Josephy, Thomas Eling, and R.P. Mason. “The horseradish peroxidase-
22 catalyzed oxidation of 3, 5, 3', 5'-tetramethylbenzidine. Free radical and
23 charge-transfer complex intermediates.” In: *Journal of Biological Chemistry*
24 257.7 (1982), pp. 3669–3675.
- 25 [92] Chandrashekhar P. Joshi and Vincent L. Chiang. “Conserved sequence
26 motifs in plant S-adenosyl-L-methionine-dependent methyltransferases”.
27 In: *Plant Molecular Biology* 37.4 (1998), pp. 663–674.
- 28 [93] Wolfgang Kabsch. “Automatic processing of rotation diffraction data from
29 crystals of initially unknown symmetry land cell constants”. In: *Journal of
30 Applied Crystallography* 26.pt 6 (Dec. 1993), pp. 795–800.
- 31 [94] Wolfgang Kabsch. “Integration, scaling, space-group assignment and post-
32 refinement”. In: *Acta Crystallographica Section D: Biological Crystallogra-
33 phy* 66.2 (Feb. 2010), pp. 133–144.
- 34 [95] Wolfgang Kabsch. “Xds”. In: *Acta Crystallographica Section D: Biological
35 Crystallography* 66.2 (Feb. 2010), pp. 125–132.

Bibliography

- 1 [96] Jinguo Kang, Larry a Hick, and William E Price. “A fragmentation study
2 of isoflavones in negative electrospray ionization by MS n ion trap mass
3 spectrometry and triple quadrupole mass spectrometry”. In: *Rapid Commu-*
4 *nications in Mass Spectrometry* 21.6 (2007), pp. 857–868.
- 5 [97] Sun-Young Kang et al. “Biosynthesis of methylated resveratrol analogs
6 through the construction of an artificial biosynthetic pathway in *E. coli*.”
7 In: *BMC biotechnology* 14.1 (2014), p. 67.
- 8 [98] Lawrence a Kelley et al. “The Phyre2 web portal for protein modeling,
9 prediction and analysis.” In: *Nature protocols* 10.6 (June 2015), pp. 845–858.
- 10 [99] Bong Gyu Kim et al. “Multiple regiospecific methylations of a flavonoid by
11 plant O-methyltransferases expressed in *E. coli*”. In: *Biotechnology Letters*
12 27.23-24 (Dec. 2005), pp. 1861–1864.
- 13 [100] Bong Gyu Kim et al. “Plant Flavonoid O-Methyltransferases: Substrate
14 Specificity and Application”. In: *Journal of Plant Biology* 53.5 (Sept. 2010),
15 pp. 321–329.
- 16 [101] Bong-Gyu Kim, Eun Ji Joe, and Joong-Hoon Ahn. “Molecular characteriza-
17 tion of flavonol synthase from poplar and its application to the synthesis of
18 3-O-methylkaempferol.” In: *Biotechnology letters* 32.4 (Apr. 2010), pp. 579–
19 84.
- 20 [102] Dae Hwan Kim et al. “Regiospecific methylation of naringenin to ponciretin
21 by soybean O-methyltransferase expressed in *Escherichia coli*”. In: *Journal*
22 *of Biotechnology* 119.2 (Sept. 2005), pp. 155–162.
- 23 [103] Min Ji Kim, Bong Gyu Kim, and Joong Hoon Ahn. “Biosynthesis of bioactive
24 O-methylated flavonoids in *Escherichia coli*”. In: *Applied Microbiology and*
25 *Biotechnology* 97.16 (2013), pp. 7195–7204.
- 26 [104] Saulius Klimasauskas et al. “Hhal methyltransferase flips its target base out
27 of the DNA helix”. In: *Cell* 76.2 (1994), pp. 357–369.
- 28 [105] K M Koeller and C H Wong. “Enzymes for chemical synthesis.” In: *Nature*
29 409.6817 (Jan. 2001), pp. 232–240.
- 30 [106] Youichi Kondou et al. “cDNA Libraries”. In: *Methods* 729 (2011), pp. 183–197.
- 31 [107] Kristin König. “Engineering of the Anthocyanin Biosynthetic Pathway
32 in *Nicotiana benthamiana*”. Master. Martin-Luther-Universität Halle-
33 Wittenberg, 2014.
- 34 [108] Frank Koopman et al. “De novo production of the flavonoid naringenin in
35 engineered *Saccharomyces cerevisiae*.” In: *Microbial cell factories* 11 (2012),
36 p. 155.

Bibliography

- 1 [109] Jakub G. Kopycki et al. “Biochemical and Structural Analysis of Substrate
2 Promiscuity in Plant Mg²⁺-Dependent O-Methyltransferases”. In: *Journal*
3 *of Molecular Biology* 378.1 (Apr. 2008), pp. 154–164.
- 4 [110] Fabian Kuhn et al. “Differentiation of isomeric flavone/isoflavone aglycones
5 by MS2 ion trap mass spectrometry and a double neutral loss of CO”. In:
6 *Rapid Communications in Mass Spectrometry* 17.17 (2003), pp. 1941–1949.
- 7 [111] Shashank Kumar and Abhay K. Pandey. “Chemistry and Biological Activities
8 of Flavonoids: An Overview”. In: *The Scientific World Journal* 2013.7 (2013),
9 pp. 1–16.
- 10 [112] U K Laemmli. “Cleavage of structural proteins during the assembly of the
11 head of bacteriophage T4.” In: *Nature* 227.5259 (1970), pp. 680–685.
- 12 [113] L L Lairson et al. “Glycosyltransferases: structures, functions, and mecha-
13 nisms.” In: *Annual review of biochemistry* 77 (2008), pp. 521–555.
- 14 [114] Brian J. C. Law et al. “Site-specific bioalkylation of rapamycin by the RapM
15 16-O-methyltransferase”. In: *Chem. Sci.* (2015), pp. 2885–2892.
- 16 [115] Gunhild Layer et al. “Crystal structure of coproporphyrinogen III oxidase
17 reveals cofactor geometry of Radical SAM enzymes”. In: *EMBO Journal*
18 22.23 (2003), pp. 6214–6224.
- 19 [116] Bobby W K Lee et al. “Enzyme-catalyzed transfer of a ketone group from
20 an S-adenosylmethionine analogue: A tool for the functional analysis of
21 methyltransferases”. In: *Journal of the American Chemical Society* 132.11
22 (2010), pp. 3642–3643.
- 23 [117] Jong Suk Lee et al. “Identification of flavonoids using liquid chromatography
24 with electrospray ionization and ion trap tandem mass spectrometry with
25 an MS/MS library”. In: *Rapid Communications in Mass Spectrometry* 19.23
26 (2005), pp. 3539–3548.
- 27 [118] Effendi Leonard et al. “Expression of a soluble flavone synthase allows the
28 biosynthesis of phytoestrogen derivatives in *Escherichia coli*.” In: *Applied*
29 *microbiology and biotechnology* 70.1 (Mar. 2006), pp. 85–91.
- 30 [119] Monica Leopoldini et al. “Iron chelation by the powerful antioxidant
31 flavonoid quercetin”. In: *Journal of Agricultural and Food Chemistry* 54.17
32 (2006), pp. 6343–6351.
- 33 [120] Jakob P. Ley et al. “Evaluation of bitter masking flavanones from Herba
34 Santa (*Eriodictyon californicum* (H. & A.) Torr., Hydrophyllaceae)”. In:
35 *Journal of Agricultural and Food Chemistry* 53.15 (2005), pp. 6061–6066.

Bibliography

- 1 [121] Chen Li et al. “Tandem mass spectrometric fragmentation behavior of lignans, flavonoids and triterpenoids in *< i>Streblus asper</i>*”. In: *Rapid Communications in Mass Spectrometry* 28.21 (2014), pp. 2363–2370.
- 2 [122] Kai Li and J W Frost. “Synthesis of Vanillin from Glucose”. In: 7863.Table 1
5 (1998), pp. 10545–10546.
- 6 [123] Liwei Li et al. “PDBcal: A comprehensive dataset for receptor-ligand interactions with three-dimensional structures and binding thermodynamics from isothermal titration calorimetry”. In: *Chemical Biology and Drug Design* 71.6
9 (June 2008), pp. 529–532.
- 10 [124] Manuel Liebeke et al. “Metabolome Analysis of Gram-Positive Bacteria such
11 as *Staphylococcus aureus* by GC-MS and LC-MS”. In: *Methods in Molecular
12 Biology* 815 (Jan. 2012), pp. 377–398.
- 13 [125] Gordon V. Louie et al. “Structural Determinants and Modulation of Substrate
14 Specificity in Phenylalanine-Tyrosine Ammonia-Lyases”. In: *Chemistry and
15 Biology* 13.12 (2006), pp. 1327–1338.
- 16 [126] Caroline Louis-Jeune, Miguel a. Andrade-Navarro, and Carol Perez-Iratxeta.
17 “Prediction of protein secondary structure from circular dichroism using
18 theoretically derived spectra”. In: *Proteins: Structure, Function and Bioinformatics* 80.2 (Feb. 2012), pp. 374–381.
- 20 [127] J D Lozada-Ramírez et al. “Cloning, overexpression, purification, and char-
21 acterization of S-adenosylhomocysteine hydrolase from *Corynebacterium
22 efficiens* YS-314.” In: *Biotechnology progress* 24.1 (2008), pp. 120–7.
- 23 [128] Liang Lu et al. “A High-Resolution LC-MS-Based Secondary Metabolite
24 Fingerprint Database of Marine Bacteria”. en. In: *Scientific Reports* 4 (Jan.
25 2014), p. 6537.
- 26 [129] Gražvydas Lukinavičius et al. “Enhanced chemical stability of AdoMet
27 analogues for improved methyltransferase-directed labeling of DNA”. In:
28 *ACS Chemical Biology* 8.6 (2013), pp. 1134–1139.
- 29 [130] Y L Ma, H V Heuvel, and M Claeyns. “Characterization of 3-methoxyflavones
30 using fast-atom bombardment and collision-induced dissociation tandem
31 mass spectrometry.” In: *Rapid communications in mass spectrometry : RCM*
32 13.19 (1999), pp. 1932–42.
- 33 [131] Y. L. Ma et al. “Characterization of flavone and flavonol aglycones by
34 collision-induced dissociation tandem mass spectrometry”. In: *Rapid Com-
35 munications in Mass Spectrometry* 11.12 (1997), pp. 1357–1364.

Bibliography

- 1 [132] Tom J. Mabry, K. R. Markham, and M. B. Thomas. *The Systematic Identification of Flavonoids*. Berlin, Heidelberg: Springer Berlin Heidelberg, 1970.
- 2
- 3 [133] Savvas C Makrides and Savvas C Makrides. “Strategies for Achieving High-
4 Level Expression of Genes in *Escherichia coli*”. In: *Microbiological reviews*
5 60.3 (1996), pp. 512–538.
- 6 [134] Sailesh Malla et al. “Production of 7-O-methyl aromadendrin, a medici-
7 nally valuable flavonoid, in *Escherichia coli*.” In: *Applied and environmental
8 microbiology* 78.3 (Feb. 2012), pp. 684–94.
- 9 [135] S. V. Mani, D. W. Connell, and R. D. Braddock. “Structure activity relation-
10 ships for the prediction of biodegradability of environmental pollutants”. en.
11 In: *Critical Reviews in Environmental Control* 21.3-4 (Jan. 1991), pp. 217–236.
- 12 [136] Raymond E. March and Xiu Sheng Miao. “A fragmentation study of
13 kaempferol using electrospray quadrupole time-of-flight mass spectrome-
14 try at high mass resolution”. In: *International Journal of Mass Spectrometry*
15 231.2-3 (2004), pp. 157–167.
- 16 [137] Raymond March and Jennifer Brodbelt. “Analysis of flavonoids: Tandem
17 mass spectrometry, computational methods, and NMR”. In: *Journal of Mass
18 Spectrometry* 43.12 (Dec. 2008), pp. 1581–1617.
- 19 [138] Nektaria Markoglou and Irving W Wainer. “Biosynthesis in an on-
20 line immobilized-enzyme reactor containing phenylethanolamine N-
21 methyltransferase in single-enzyme and coupled-enzyme formats.” In:
22 *Journal of chromatography. A* 948.1-2 (Mar. 2002), pp. 249–56.
- 23 [139] Alexandre Martinière et al. “Development and properties of genetically
24 encoded pH sensors in plants.” In: *Frontiers in plant science* 4. December
25 (2013), p. 523.
- 26 [140] M McClelland, M Nelson, and E Raschke. “Effect of site-specific modification
27 on restriction endonucleases and DNA modification methyltransferases.”
28 In: *Nucleic acids research* 22.17 (1994), pp. 3640–3659.
- 29 [141] Airlie J. McCoy. “Solving structures of protein complexes by molecular
30 replacement with Phaser”. In: *Acta Crystallographica Section D: Biological
31 Crystallography* 63.1 (Jan. 2006), pp. 32–41.
- 32 [142] Airlie J. McCoy et al. “Phaser crystallographic software”. In: *Journal of
33 Applied Crystallography* 40.4 (Aug. 2007), pp. 658–674.

Bibliography

- 1 [143] Edoardo Mentasti, Ezio Pelizzetti, and Guido Saini. “Reactions between
2 iron(III) and catechol (o-dihydroxybenzene). Part II. Equilibria and kinet-
3 ics of the redox reaction in aqueous acid solution”. en. In: *Journal of the*
4 *Chemical Society, Dalton Transactions* 23 (Jan. 1973), p. 2609.
- 5 [144] Diana Metodiewa et al. “Quercetin may act as a cytotoxic prooxidant after
6 its metabolic activation to semiquinone and quinoidal product”. In: *Free*
7 *Radical Biology and Medicine* 26.1-2 (Jan. 1999), pp. 107–116.
- 8 [145] Gurvan Michel et al. “The structure of the RlmB 23S rRNA methyltransferase
9 reveals a new methyltransferase fold with a unique knot”. In: *Structure* 10.10
10 (2002), pp. 1303–1315.
- 11 [146] Ivan Mihel et al. “.alpha.-Deuterium isotope effects and transition-state
12 structure in an intramolecular model system for methyl-transfer enzymes”.
13 In: *Journal of the American Chemical Society* 101.15 (July 1979), pp. 4349–
14 4351.
- 15 [147] Douglas Montgomery. *Design and Analysis of Experiments*. 5th ed. New
16 York: John Wiley & Sons, 2008, p. 680.
- 17 [148] Takashi MORISHIGE, Kum-Boo CHOI, and Fumihiko SATO. “In Vivo
18 Bioconversion of Tetrahydroisoquinoline by Recombinant Coclaurine N
19 -Methyltransferase”. In: *Bioscience, Biotechnology and Biochemistry* 68.4
20 (May 2014), pp. 939–941.
- 21 [149] Garrett M. Morris et al. “Software news and updates AutoDock4 and
22 AutoDockTools4: Automated docking with selective receptor flexibility”.
23 In: *Journal of Computational Chemistry* 30.16 (Dec. 2009), pp. 2785–2791.
- 24 [150] Yuri Motorin et al. “Expanding the chemical scope of RNA:methyltransferases
25 to site-specific alkynylation of RNA for click labeling”. In: *Nucleic Acids*
26 *Research* 39.5 (2011), pp. 1943–1952.
- 27 [151] N. Mulinacci et al. “Polyphenolic content in olive oil waste waters and
28 related olive samples”. In: *Journal of Agricultural and Food Chemistry* 49.8
29 (2001), pp. 3509–3514.
- 30 [152] Garib N. Murshudov, Alexei a. Vagin, and Eleanor J. Dodson. “Refine-
31 ment of macromolecular structures by the maximum-likelihood method”.
32 In: *Acta Crystallographica Section D: Biological Crystallography* 53.3 (May
33 1997), pp. 240–255.
- 34 [153] Janet Newman. “Novel buffer systems for macromolecular crystallization”.
35 In: *Acta Crystallographica Section D: Biological Crystallography* 60.3 (2004),
36 pp. 610–612.

Bibliography

- 1 [154] Novagen. *pET System Manual*. 11th ed. Vol. 123. 2 Pt 1. Darmstadt: EMD
2 Chemicals, 2014, p. 369. arXiv: 1007.2303v3.
- 3 [155] Zouhaier B Ouallagui et al. "Valorization of Olive Processing By-Products :
4 Characterization , Investigation of Chemico-Biological Activities and Iden-
5 tification of Active Compounds". In: 64 (2012), pp. 61–64.
- 6 [156] Javier Palazón et al. "Application of metabolic engineering to the production
7 of scopolamine." In: *Molecules (Basel, Switzerland)* 13.8 (Jan. 2008), pp. 1722–
8 42.
- 9 [157] Ira Palmer and Paul T. Wingfield. "Preparation and extraction of insoluble
10 (Inclusion-body) proteins from Escherichia coli". In: *Current Protocols in*
11 *Protein Science* 1.SUPPL.70 (Nov. 2012), Unit6.3.
- 12 [158] Wibke Peters et al. "Enzymatic site-specific functionalization of protein
13 methyltransferase substrates with alkynes for click labeling". In: *Angewandte Chemie - International Edition* 49.30 (2010), pp. 5170–5173.
- 15 [159] Eric F. Pettersen et al. "UCSF Chimera - A visualization system for ex-
16 ploratory research and analysis". In: *Journal of Computational Chemistry*
17 25.13 (2004), pp. 1605–1612.
- 18 [160] Harold R. Powell. "The Rossmann Fourier autoindexing algorithm in MOS-
19 FLM". In: *Acta Crystallographica Section D: Biological Crystallography* 55.10
20 (1999), pp. 1690–1695.
- 21 [161] O. Rigbers and S.-M. Li. "Ergot Alkaloid Biosynthesis in Aspergillus fumi-
22 gatus: OVERPRODUCTION AND BIOCHEMICAL CHARACTERIZATION
23 OF A 4-DIMETHYLALLYLTRYPTOPHAN N-METHYLTRANSFERASE". In:
24 *Journal of Biological Chemistry* 283.40 (Aug. 2008), pp. 26859–26868.
- 25 [162] K D Robertson. "DNA methylation, methyltransferases, and cancer." In:
26 *Oncogene* 20.24 (2001), pp. 3139–3155.
- 27 [163] Keith D Robertson. "DNA methylation and human disease." In: *Nature*
28 *reviews. Genetics* 6.8 (2005), pp. 597–610.
- 29 [164] M. G. Rossmann and D. M. Blow. "The detection of sub-units within the crys-
30 tallographic asymmetric unit". In: *Acta Crystallographica* 15.1 (Jan. 1962),
31 pp. 24–31.
- 32 [165] Michael G. Rossmann. "Molecular replacement - Historical background". In:
33 *Acta Crystallographica - Section D Biological Crystallography* 57.10 (Sept.
34 2001), pp. 1360–1366.
- 35 [166] Rainer Rudolph and Hauke Lilie. "In vitro folding of inclusion body pro-
36 teins". In: *The FASEB Journal* 10.1 (1996), pp. 49–56.

Bibliography

- 1 [167] J Sambrook and D W Russell. *Molecular Cloning: A Laboratory Manual*.
2 3rd ed. Cold Spring Harbor (NY, USA): Cold Spring Harbor Laboratory
3 Press, 2001.
- 4 [168] Cleydson Breno R Santos et al. “A SAR and QSAR study of new artemisinin
5 compounds with antimalarial activity”. In: *Molecules* 19.1 (2014), pp. 367–
6 399.
- 7 [169] Yuji Sawada and Masami Yokota Hirai. *Integrated LC-MS / MS system for*
8 *plant metabolomics*. en. May 2013.
- 9 [170] Artur Sawicki and Robert D Willows. “S-adenosyl-L-methionine:magnesium-
10 protoporphyrin IX O-methyltransferase from Rhodobacter capsulatus:
11 mechanistic insights and stimulation with phospholipids.” In: *The Biochemical*
12 *journal* 406.3 (2007), pp. 469–478.
- 13 [171] Jason W. Schmidberger et al. “Halomethane biosynthesis: Structure of a
14 SAM-dependent halide methyltransferase from arabidopsis thaliana”. In:
15 *Angewandte Chemie - International Edition* 49.21 (2010), pp. 3646–3648.
- 16 [172] Gudrun Schröder et al. “Flavonoid methylation: A novel 4’-O-methyltransferase
17 from Catharanthus roseus, and evidence that partially methylated fla-
18 vanones are substrates of four different flavonoid dioxygenases”. In:
19 *Phytochemistry* 65.8 (2004), pp. 1085–1094.
- 20 [173] H L Schubert et al. “The X-ray structure of a cobalamin biosynthetic en-
21 zyme, cobalt-precorrin-4 methyltransferase.” In: *Nature structural biology*
22 5.7 (1998), pp. 585–592.
- 23 [174] Heidi L. Schubert, Robert M. Blumenthal, and Xiaodong Cheng. “Many paths
24 to methyltransfer: A chronicle of convergence”. In: *Trends in Biochemical*
25 *Sciences* 28.6 (2003), pp. 329–335.
- 26 [175] Daniela Schulz, Josephin Marie Holstein, and Andrea Rentmeister. “A
27 chemo-enzymatic approach for site-specific modification of the RNA cap”.
28 In: *Angewandte Chemie - International Edition* 52.30 (2013), pp. 7874–7878.
- 29 [176] N. Schweigert, a. J B Zehnder, and R. I L Eggen. “Chemical properties of
30 catechols and their molecular modes of toxic action in cells, from microor-
31 ganisms to mammals”. In: *Environmental Microbiology* 3.2 (2001), pp. 81–
32 91.
- 33 [177] Mark S. Searle, Martin S. Westwell, and Dudley H. Williams. “Application
34 of a generalised enthalpy-entropy relationship to binding co-operativity
35 and weak associations in solution”. en. In: *Journal of the Chemical Society,*
36 *Perkin Transactions 2* 1 (Jan. 1995), p. 141.

Bibliography

- 1 [178] S K Shapiro and D J Ehninger. "Methods for the analysis and preparation of
2 adenosylmethionine and adenosylhomocysteine." In: *Analytical biochemistry* 15.2 (May 1966), pp. 323–333.
- 4 [179] Y. Q. Shi and R. R. Rando. "Kinetic mechanism of isoprenylated protein
5 methyltransferase". In: *Journal of Biological Chemistry* 267.14 (1992),
6 pp. 9547–9551.
- 7 [180] Alexander Ann Shulgin. *Tihkal: The Continuation*. Ed. by Dan Joy. 1st ed.
8 Berkeley: Transform Press, 1997, p. 804.
- 9 [181] Sigma-Aldrich. *Technical Bulletin no. 2003-03: freezing of microbial samples
10 prior to testing. Parenteral Drug Association*. 2003.
- 11 [182] Simon A. Simms and Kotha Subbaramaiah. "Kinetic Mechanism of the
12 CheR Methyltransferase". In: *Journal of Biological Chemistry* 266.19 (1991),
13 pp. 12741–12746.
- 14 [183] Henrik T. Simonsen et al. "Methylenedioxy- and methoxyflavones from
15 Melicope coodeana syn. Euodia simplex". In: *Phytochemistry* 60.8 (Aug.
16 2002), pp. 817–820.
- 17 [184] Shanteri Singh et al. "Facile chemoenzymatic strategies for the synthesis and
18 utilization of S-adenosyl-L-methionine analogues". In: *Angewandte Chemie
19 - International Edition* 53.15 (2014), pp. 3965–3969.
- 20 [185] Lekha Sleno and Dietrich a. Volmer. "Ion activation methods for tandem
21 mass spectrometry". In: *Journal of Mass Spectrometry* 39.10 (2004), pp. 1091–
22 1112.
- 23 [186] Qingqing Song et al. "Potential of hyphenated ultra-high performance liquid
24 chromatography-scheduled multiple reaction monitoring algorithm for
25 large-scale quantitative analysis of traditional Chinese medicines". In: *RSC
26 Adv.* 5.71 (2015), pp. 57372–57382.
- 27 [187] Harald Stecher et al. "Biocatalytic Friedel-Crafts alkylation using non-
28 natural cofactors". In: *Angewandte Chemie - International Edition* 48.50 (Jan.
29 2009), pp. 9546–9548.
- 30 [188] Anna Winona Struck et al. "S-Adenosyl-Methionine-Dependent Methyl-
31 transferases: Highly Versatile Enzymes in Biocatalysis, Biosynthesis and
32 Other Biotechnological Applications". In: *ChemBioChem* 13.18 (Nov. 2012),
33 pp. 2642–2655.
- 34 [189] F William Studier. "Protein production by auto-induction in high density
35 shaking cultures." In: *Protein expression and purification* 41.1 (May 2005),
36 pp. 207–234. arXiv: NIHMS150003.

Bibliography

- 1 [190] Fusao Takusagawa et al. "Crystal Structure of S -Adenosylmethionine Syn-
2 thetase *". In: 271.1 (1996), pp. 136–147.
- 3 [191] Loverine P Taylor and Erich Grotewold. "Flavonoids as developmental
4 regulators." In: *Current opinion in plant biology* 8.3 (June 2005), pp. 317–23.
- 5 [192] Martin Tengg et al. "Molecular characterization of the C-methyltransferase
6 NovO of Streptomyces sphaeroides, a valuable enzyme for performing
7 Friedel-Crafts alkylation". In: *Journal of Molecular Catalysis B: Enzymatic*
8 84 (Dec. 2012), pp. 2–8.
- 9 [193] David J Thomas et al. "Arsenic (+3 Oxidation State) Methyltransferase
10 and the Methylation of Arsenicals". In: *Experimental biology and medicine*
11 (Maywood, N.J.) 232.1 (Jan. 2007), pp. 3–13.
- 12 [194] Marie Thomsen et al. "Chemoenzymatic synthesis and in situ application
13 of S-adenosyl-L-methionine analogs." In: *Organic & biomolecular chemistry*
14 11.43 (2013), pp. 7606–10.
- 15 [195] Robert Tibshirani. *Regression Selection and Shrinkage via the Lasso*. 1994.
- 16 [196] Dominique a Tobbell et al. "Identification of in vitro folding conditions
17 for procathepsin S and cathepsin S using fractional factorial screens." In:
18 *Protein expression and purification* 24.2 (Mar. 2002), pp. 242–254.
- 19 [197] Jaime Torres-Corzo, Roberto Rodríguez-Della Vecchia, and Leonardo
20 Rangel-Castilla. *Observation of the ventricular system and subarachnoid*
21 *space in the skull base by flexible neuroendoscopy: normal structures*. 1st ed.
22 Vol. 141. 2. New York: Garland Science, 2009, pp. 165–168.
- 23 [198] Emmanouil a. Trantas et al. "When plants produce not enough or at all: metabolic engineering of flavonoids in microbial hosts". In: *Frontiers in Plant Science* 6.January (2015), pp. 1–16.
- 26 [199] Oleg Trott and Arthur J. Olson. "Software news and update AutoDock Vina:
27 Improving the speed and accuracy of docking with a new scoring function,
28 efficient optimization, and multithreading". In: *Journal of Computational Chemistry* 31.2 (Jan. 2010), pp. 455–461.
- 30 [200] Kouhei Tsumoto et al. "Role of arginine in protein refolding, solubilization,
31 and purification." In: *Biotechnology progress* 20.5 (2004), pp. 1301–1308.
- 32 [201] P. Urban et al. "Characterization of recombinant plant cinnamate 4-
33 hydroxylase produced in yeast - Kinetic and spectral properties of the
34 major plant P450 of the phenylpropanoid pathway". In: *European Journal of Biochemistry* 222.3 (1994), pp. 843–850.

Bibliography

- 1 [202] Alexei a. Vagin et al. “REFMAC5 dictionary: Organization of prior chemical
2 knowledge and guidelines for its use”. en. In: *Acta Crystallographica Section*
3 *D: Biological Crystallography* 60.12 I (Nov. 2004), pp. 2184–2195.
- 4 [203] Jacob L. Venzie et al. “Electron-impact and glow-discharge ionization LC-MS
5 analysis of green tea tincture”. In: *Analytical and Bioanalytical Chemistry*
6 387.1 (2007), pp. 321–333.
- 7 [204] J Vidgren, L a Svensson, and a Liljas. “Crystal structure of catechol O-
8 methyltransferase.” In: *Nature* 368.6469 (1994), pp. 354–358.
- 9 [205] Renaud Vincentelli et al. “High-throughput automated refolding screening
10 of inclusion bodies.” In: *Protein science : a publication of the Protein Society*
11 13.10 (2004), pp. 2782–2792.
- 12 [206] Thomas Vogt. “Regiospecificity and kinetic properties of a plant natural
13 product O-methyltransferase are determined by its N-terminal domain”. In:
14 *FEBS Letters* 561.1-3 (Mar. 2004), pp. 159–162.
- 15 [207] Thomas Vogt. “Regiospecificity and kinetic properties of a plant natural
16 product O-methyltransferase are determined by its N-terminal domain”. In:
17 *FEBS Letters* 561.1-3 (Mar. 2004), pp. 159–162.
- 18 [208] Rui Wang et al. “Formulating a fluorogenic assay to evaluate S-adenosyl-L-
19 methionine analogues as protein methyltransferase cofactors”. In: *Molecular*
20 *BioSystems* 7.11 (2011), p. 2970.
- 21 [209] Rui Wang et al. “Labeling substrates of protein arginine methyltransferase
22 with engineered enzymes and matched S-adenosyl-l-methionine analogues”.
23 In: *Journal of the American Chemical Society* 133.20 (2011), pp. 7648–7651.
- 24 [210] Williard J. Werner et al. “In vitro phosphinate methylation by PhpK from
25 *Kitasatospora phosalacinea*”. In: *Biochemistry* 50.42 (2011), pp. 8986–8988.
- 26 [211] Ludger a. Wessjohann et al. “Alkylating enzymes”. In: *Current Opinion in*
27 *Chemical Biology* 17.2 (Mar. 2013), pp. 229–235.
- 28 [212] C M Whitehouse et al. “Electrospray interface for liquid chromatographs
29 and mass spectrometers.” In: *Analytical chemistry* 57.3 (Mar. 1985), pp. 675–
30 679.
- 31 [213] Christine a Williams and Renee J Grayer. “Anthocyanins and other
32 flavonoids.” In: *Natural product reports* 21.4 (2004), pp. 539–573.
- 33 [214] Melissa Swope Willis et al. “Investigation of protein refolding using a frac-
34 tional factorial screen: a study of reagent effects and interactions.” In: *Protein*
35 *science : a publication of the Protein Society* 14.7 (2005), pp. 1818–1826.

Bibliography

- 1 [215] Sophie Willnow et al. “A Selenium-Based Click AdoMet Analogue for Ver-
2 satile Substrate Labeling with Wild-Type Protein Methyltransferases”. In:
3 *ChemBioChem* 13.8 (2012), pp. 1167–1173.
- 4 [216] Martyn D. Winn et al. “Overview of the CCP4 suite and current devel-
5 opments”. In: *Acta Crystallographica Section D: Biological Crystallography*
6 67.4 (Apr. 2011), pp. 235–242.
- 7 [217] Jaclyn M. Winter et al. “Expanding the structural diversity of polyketides
8 by exploring the cofactor tolerance of an inline methyltransferase domain”.
9 In: *Organic Letters* 15.14 (2013), pp. 3774–3777.
- 10 [218] Tomasz Włodarski et al. “Comprehensive structural and substrate specificity
11 classification of the *Saccharomyces cerevisiae* methyltransferome”. In: *PLoS ONE* 6.8 (2011).
- 13 [219] Sebastian Wolf et al. “In silico fragmentation for computer assisted iden-
14 tification of metabolite mass spectra.” In: *BMC Bioinformatics* 11 (2010),
15 p. 148.
- 16 [220] J.-L. Wolfender et al. “Evaluation of Q-TOF-MS/MS and multiple stage IT-
17 MSn for the Dereplication of Flavonoids and Related Compounds in Crude
18 Plant Extracts”. In: *Analisis* 28.10 (Dec. 2000), pp. 895–906.
- 19 [221] Eckhard Wollenweber. “On the occurrence of acylated flavonoid aglycones”.
20 In: *Phytochemistry* 24.7 (1985), pp. 1493–1494.
- 21 [222] R W Woodard et al. “Stereochemical Course of the Transmethylation
22 Catalyzed by Catechol O-Methyltransferase”. In: *The Journal of Biological
23 Chemistry* 255.19 (1980), pp. 9124–9127.
- 24 [223] Ronald W Woodard et al. “Stereochemistry of Indolmycin Biosynthesis.
25 Steric Course of C- and N-Methylation Reactionsa”. In: *Journal of the Amer-
26 ican Chemical Society* 102.20 (1980), pp. 6314–6318.
- 27 [224] B. Xiao et al. “Structure and catalytic mechanism of the human histone
28 methyltransferase SET7/9”. In: 421.February (2003).
- 29 [225] Hiroshi Yamaguchi and Masaya Miyazaki. “Refolding techniques for recov-
30 ering biologically active recombinant proteins from inclusion bodies.” In:
31 *Biomolecules* 4.1 (2014), pp. 235–51.
- 32 [226] William C Yee, Susan J Eglsær, and William R Richards. “Confirmation of a
33 ping-pong mechanism for S-adenosyl-L-methionine:magnesium protopor-
34 phyrin methyltransferase of etiolated wheat by an exchange reaction.” In:
35 *Biochemical and biophysical research communications* 162.1 (1989), pp. 483–
36 490.

Bibliography

- 1 [227] E. G. Yordi et al. "Antioxidant and Pro-Oxidant Effects of Polyphenolic
2 Compounds and Structure-Activity Relationship Evidence". In: *Nutrition,*
3 *Well-Being and Health* (2012), pp. 23–48.
- 4 [228] Yoon Youngdae et al. "Characterization of an O-methyltransferase from
5 Streptomyces avermitilis MA-4680". In: *Journal of Microbiology and Biotechnology*
6 20.9 (2010), pp. 1359–1366.
- 7 [229] Changsheng Zhang et al. "Natural product diversification using a non-
8 natural cofactor analogue of S-adenosyl-L-methionine". In: *Journal of the*
9 *American Chemical Society* 128.9 (2006), pp. 2760–2761.
- 10 [230] Qi Zhang and Wilfred A van der Donk. "Catalytic promiscuity of a bacterial
11 α -N-methyltransferase." In: *FEBS letters* 586.19 (Sept. 2012), pp. 3391–7.
- 12 [231] Qi Zhang, Wilfred A. van der Donk, and Wen Liu. "Radical-Mediated Enzy-
13 matic Methylation: A Tale of Two SAMS". In: *Accounts of Chemical Research*
14 45.4 (Apr. 2012), pp. 555–564.
- 15 [232] Xing-Hai Zhang and C. C. Chinnappa. "Molecular characterization of a
16 cDNA encoding caffeoyl-coenzyme A 3-O-methyltransferase of *Stellaria*
17 *longipes*". In: *Journal of Biosciences* 22.2 (Mar. 1997), pp. 161–175.
- 18 [233] Jian Min Zhou et al. "Sequential O-methylation of tricetin by a single
19 gene product in wheat". In: *Biochimica et Biophysica Acta - General Subjects*
20 1760.7 (2006), pp. 1115–1124.
- 21 [234] Saijie Zhu et al. "Efficient synthesis of eriodictyol from l-tyrosine in es-
22 cherichia coli". In: *Applied and Environmental Microbiology* 80.10 (2014),
23 pp. 3072–3080.
- 24 [235] Chloe Zubieta et al. "Structural Basis for the Modulation of Lignin
25 Monomer Methylation by Caffeic Acid / 5-Hydroxyferulic Acid 3 / 5- O
26 -Methyltransferase". In: *The Plant Cell* 14.June (2002), pp. 1265–1277.
- 27 [236] C Zubieta et al. "Structures of two natural product methyltransferases reveal
28 the basis for substrate specificity in plant O-methyltransferases." In: *Nature*
29 *structural biology* 8.3 (Mar. 2001), pp. 271–279.

1 Acronyms

- 2 **Å** Ångström, 0.1 nm
- 3 **3O4M** 3'-hydroxy-4'-methoxy
- 4 **4CL** 4-coumarate:CoA ligase
- 5 **4O3M** 4'-hydroxy-3'-methoxy
- 6 **ABPP** activity based protein profiling
- 7 **AC-9** anthracene-9-carboxylic acid
- 8 **AI** auto-induction 96, *see* ZYP-5052
- 9 **ANOVA** Analysis of Variance
- 10 **APCI** atmospheric pressure chemical ionisation
- 11 **ATP** adenosine triphosphate
- 12 **AUC** area under the curve
- 13 **BisTris** 2-[Bis(2-hydroxyethyl)amino]-2-(hydroxymethyl)propane-1,3-diol
- 14 **B-PER** bacterial protein extraction reagent
- 15 **C4H** cinnamate-4-hydroxylase
- 16 **CBD** cobalamin binding domain
- 17 **CCoAOMT** caffeoyl CoA dependent O-methyltransferase
- 18 **CCP4** Collaborative Computational Project No. 4
- 19 **CD** circulary dichroism
- 20 **CHI** chalcone isomerase
- 21 **CHS** chalcone synthase
- 22 **CID** collision induced dissociation
- 23 **C-MT** C-methyl transferase
- 24 **CoA** coenzyme A
- 25 **COMT** catechol O-methyl transferase

Acronyms

- 1 **Coot** Crystallographic Object-Oriented Toolkit
- 2 **CV** column volumes
- 3 **dAdo** 5'-deoxyadenosyl
- 4 **DMSO** dimethyl sulfoxide
- 5 **DNA** desoxyribonucleic acid
- 6 **DNA-MT** DNA methyl transferase
- 7 **DoE** design of experiments
- 8 **DTT** dithiothreitol; (2*S*,3*S*)-1,4-bis(sulfanyl)butane-2,3-diol
- 9 **EDTA** ethylenediaminetetraacetic acid
- 10 **EEC** enthalpy-entropy compensation
- 11 **EI** electron ionization
- 12 **ESI** electrospray ionization
- 13 **F3H** flavanone-3-hydroxylase
- 14 **FNS** flavone synthase
- 15 **FPLC** fast protein liquid chromatography
- 16 **FrFD** fractional factorial design
- 17 **FT** Fourier transformation
- 18 **FTMS** Fourier transform mass spectrometry
- 19 **GdmCl** guanidinium hydrochloride
- 20 **GFP** green fluorescent protein
- 21 **GOD** glucose oxidase
- 22 **GSH** glutathione, γ -L-glutamyl-L-cysteinylglycine
- 23 **GSSG** glutathione disulfide
- 24 **GST** Glutathion S-transferase
- 25 **HCD** higher-energy collisional dissociation
- 26 **HEPES** 2-[4-(2-hydroxyethyl)piperazin-1-yl]ethanesulfonic acid
- 27 **H-ESI** heated-electrospray ionization
- 28 **HIC** hydrophobic interaction chromatography
- 29 **HPLC** high-performance liquid chromatography
- 30 **HRP** horseradish peroxidase
- 31 **IB** inclusion body

Acronyms

- 1 **IEX** ion exchange chromatography
- 2 **IFS** isoflavone synthase
- 3 **IMAC** immobilized metal affinity chromatography
- 4 **IPB** Leibniz-Institute of Plant Biochemistry
- 5 **IPTG** isopropyl- β -D-thiogalactopyranosid
- 6 **ITC** Isothermal Titration Calorimetry
- 7 **LB** lysogeny broth
- 8 **LC** liquid chromatography
- 9 **LC/MS** liquid chromatography coupled mass-spectrometry
- 10 **LC-MS/MS** liquid chromatography-tandem mass spectrometry
- 11 **m/z** mass-to-charge ratio
- 12 **ME-plot** main effects plot
- 13 **MES** 2-(*N*-morpholino)ethanesulfonic acid
- 14 **MLU** Martin-Luther-Universität
- 15 **MMT** L-malic acid/MES/Tris
- 16 **MR** molecular replacement
- 17 **MS/MS** tandem mass-spectrometry
- 18 **MT** methyl transferase
- 19 **MTP** micro-titer plate
- 20 **MW** molecular weight
- 21 **MWCO** molecular weight cut-off
- 22 **NADES** natural deep eutectic solvent
- 23 **NCE** normalized collision energy
- 24 **N-MT** *N*-methyl transferase
- 25 **nos** nopaline synthase
- 26 **NPS** nitrogen, phosphate, sulfate buffer
- 27 **NRPS** non-ribosomal peptide synthase
- 28 **NTA** nitrilo triacetic acid
- 29 **O-MT** *O*-methyl transferase
- 30 **PAGE** polyacrylamide gel electrophoresis
- 31 **PAL** phenylalanine ammonia-lyase

Acronyms

- 1 **PBS** phosphate buffered saline
- 2 **PCA** principal component analysis
- 3 **PCH** propane-1,2-diol/choline chloride,natural deep eutectic solvent (NADES)-mixture
- 4 **PCR** polymerase chain reaction
- 5 **PDA** photo diode array
- 6 **PDB** Protein Data Base 47, 48
- 7 **PFOMT** phenylpropanoid and flavonoid O-methyl transferase
- 8 **PHENIX** Phyton-based Hierarchial Environment for Integrated Xtallography
- 9 **PKS** poly ketide synthase
- 10 **PMSF** phenylmethylsulfonylfluoride
- 11 **P-MT** protein methyl transferase
- 12 **QSAR** quantitative structure activity relationship
- 13 **rmsd** root mean squared deviation
- 14 **RNA-MT** RNA methyl transferase
- 15 **ROS** reactive oxygen species
- 16 **RP** resolving power
- 17 **rRNA** ribosomal ribonucleic acid
- 18 **RSMT** radical SAM methyl transferase
- 19 **RT** room temperature
- 20 **SAE** *S*-adenosyl-L-ethionine, (2*S*)-2-amino-4-[[*(2S,3S,4R,5R)*-5-(6-aminopurin-9-yl)-3,4-dihydroxyoxolan-2-yl]methyl-ethylsulfonio]butanoat
- 21 **SAH** *S*-adenosyl-L-homocysteine
- 22 **SAM** *S*-adenosyl-L-methionine
- 23 **SAMS** *S*-adenosylmethionine synthase
- 25 **SAR** structure activity relationship
- 26 **SDS** sodium dodecylsulfate
- 27 **SeAM** *Se*-adenosyl selenomethionine
- 28 **SET** suvar3-9, enhancer-of-zeste, trithorax
- 29 **SID** surface-induced dissociation
- 30 **smMT** small molecule methyl transferase
- 31 **S-MT** S-methyl transferase
- 32 **SOMT-2** soy O-methyl transferase
- 33 **SPOUT** *SpoU-TrmD*

Acronyms

- 1 **SSG** succinate/sodium phosphate/glycine
- 2 **TB** terrific broth
- 3 **TCA** trichloro acetic acid
- 4 **Ti-plasmid** tumor inducing plasmid
- 5 **Tris** tris(hydroxymethyl)-aminomethane
- 6 **U** enzyme unit; measure for enzymatic activity ($1\text{ U} = 1\text{ }\mu\text{mole/min} = 1/60\text{ }\mu\text{kat}$)
- 7 **UDP** uridine diphosphate
- 8 **UHPLC** ultra-high performance liquid chromatography
- 9 **UV** ultra violet
- 10 **UV/VIS** ultra violet/visible (light spectrum)
- 11 **V** volume
- 12 **ZYP** N-Z-amino, yeast extract, phosphate 39, 173, 174, *see ZYP-5052*

1 Glossary

- 2 **His₆-tag** Hexa-histidine tag commonly used for recombinant protein production.
- 3 **PFOMT** Phenylpropanoid and flavonoid O-methyl transferase from *Mesembryanthemum*
4 *crystallinum*, which was first described by Ibdah et al. in 2003 [85]
- 5 **T7-tag** Initial 11 amino acids of the T7 gene *10* protein.
- 6 **Ti-plasmid** Commonly found plasmids in *A. tumefaciens* and *A. rhizogenes* that confer
7 virulence
- 8 **Trx-tag** Thioredoxin tag used to increase solubility and stability of recombinantly ex-
9 pressed proteins.
- 10 **ZYP-5052** Autoinduction medium developed by Studier [189]. The naming stems from
11 the components N-Z-amine, yeast extract and phosphate. The numbering designates
12 the composition; e.g. 5052 refers to 0.5 % glycerol, 0.05 % glucose and 0.2 % lactose. 173